AN ABSTRACT OF THE THESIS OF

Gabrielle Dunkle for the degree of Master of Science in Civil Engineering presented on September 2, 2021

Title: Wave Resource Assessments: Spacio-Temporal Effect of Wave Energy Converter Scale and Blue Economy Opportunities

Abstract approved:

_____

Bryson Robertson

Wave energy has the potential to power large and small factions of economies around the world alike. Current methods for determining the amount of wave energy resource available to wave energy converter (WEC) devices entail capturing the look of the sea state at large by presenting characteristic wave heights, periods, and directions for the simplest of assessments. This method is proven to suffice in estimating the power available to large-scale WECs, operating to convert megawatts (MW) of power at a time, since WECs operate optimally when moving at the same scale as the surrounding ocean environment. However, large devices are costly and must possess a high survivability factor since their deployment locations are extremely energetic. Small-scale WECs (operating on the scale of a few 100 to a few 1000s of kW) on the other hand, typically operate in moderate motion, decreasing the amount of design and funds that must go toward survivability measures. In addition, smaller devices equate to less investment expenditures required for the build. This notion has driven research and industry in the direction of designing and testing small WECs for less demanding power applications. Some barriers to progress are created when

attempting to quantify the power available to these small devices using the current standard methods for wave resource assessment. Devices that do not operate on the MW scale would not be able to function in an extreme sea state. Thus, it is essential to devise new methods for wave resource assessment in respect to small WECs and their capture abilities. In this study, instead of using only gross wave power (which typically overestimates power available for small devices), power limits for small WEC bodies were applied to determine devices' power capture abilities in five study locations. Budal's upper bound, P_b, was utilized, which describes the power available to a small WEC based on its volume stroke. Budal's upper bound was used with the radiated power limit, P_a, a power limit that describes the maximum amount of wave power a WEC can absorb according to its radiation pattern, to filter the wave power available in the sea for the "baseline case." The "expanded case" utilized these two power limits along with gross power, P_{gross}, to determine the amount of absorbable power available, also known as net power, P_{net}. These two cases were explored and compared to the current standardized wave resource assessment methods. The baseline and expanded cases for power available to small WECs demonstrated significantly less resource than International Electrotechnical Commission (IEC) methods, which overestimated the absorbable power for the devices. Further, the expanded case yielded a more realistic analysis of absorbable power than the baseline case since it included gross power in its filtering process. This helps bring further understanding to where and when wave power is available to small WECs. Determining the spacio-temporal effects of WEC scale expands the potential applications of wave energy by focusing not just on less frequent, large waves, but also on more common, less energetic high frequency ocean waves. These findings also support development of blue economy applications for wave energy converters, including harnessing wave power for ocean observation buoys, aquaculture farms, and other standalone applications.

Wave Resource Assessments: Spacio-Temporal Effect of Wave Energy Converter Scale and Blue Economy Opportunities

by
Gabrielle Dunkle

A THESIS

submitted to

Oregon State University

in partial fulfillment of
the requirements for the
degree of

Master of Science

Presented September 2, 2021
Commencement June 2022

Master of Science thesis of Gabrielle Dunkle presented on September 2, 2021

APPROVED:

Major Professor, representing Civil Engineering

Head of the School of Civil and Construction Engineering

Dean of the Graduate School

I understand that my thesis will become part of the permanent collection of Oregon State University libraries. My signature below authorizes release of my thesis to any reader upon request.

Gabrielle Dunkle, Author

ACKNOWLEDGEMENTS

When anxious, uneasy and bad thoughts come, I go to the sea,
and the sea drowns them out with its great wide sounds,
cleanses me with its noise, and imposes a rhythm upon
everything in me that is bewildered and confused.

Rainer Maria Rilke

I would like to thank the Universe for all the wonder it has bestowed upon us, from impossibly beautiful earth to wild yet tranquil seas. For plotted coincidences and simple pleasures, for the majesty of all creatures and the mystery of the human experience. I am endlessly grateful to exist.

To my family, I cannot begin to describe how much I love and appreciate you. Mom and Dad, thank you for loving me, picking me up at my worst, and for instilling in me values of empathy, justice, and integrity. Allison, Sam, and Chelsey, thank you for inspiring me to consistently be my best.

I express my love and gratitude for my family passed. Grandpa Bill, thank you for supporting us in our dreams and for teaching us that "it's your America, kid." Thank you to Grandmas Gayle and Susan, Grandpa Pete, and all my ancestors for embarking on their own journeys that somehow, bewitchingly lead to this. I vow to forever explore and learn.

I want to thank my advisor Dr. Bryson Robertson for consistently encouraging me and being a wonderful teacher. Thank you to Dr. Shangyan Zou for acting as my sounding board, and for exercising patience and understanding. I would like to thank my committee members Dr. Meagan Wengrove, Dr. Merrick Haller, and Dr. Edward Dever for their support and insightful critique of my work. Thank you to all the faculty and teachers I have learned from previously, who helped me along the way.

Finally, a HUGE thank you to my fellow students and friends. Thank you to my virtual “officemates” Matt Leary, Courtney Berringer, Jonah Gadasi, Timma Flanagan, and Nicholas May-Varas for always giving sound advice and comments. Thank you especially to Tyler Inkley, Austin Berrier, Jake and Jill Light, Aeron and Mel Roach, Micahel Devin, Caroline Furcolo, Jacquelyn Potvin, Carrie Hall, Rabbi Phil Bresseler, and many more for being there for me always.

TABLE OF CONTENTS

Page

LIST OF FIGURES

Figure Page

LIST OF FIGURES (continued)

LIST OF FIGURES (continued)

LIST OF FIGURES (continued)

LIST OF FIGURES (continued)

LIST OF TABLES

1. Introduction

Opportunities for the ocean renewable energy field are becoming increasingly abundant, especially given the global motivation for decreased dependence on fossil fuels. Inclusion of ocean renewable energy sources in the makeup of power production is a valuable addition to the decarbonization of the energy sector. With international goals to reduce emissions in the coming decades, every possible avenue of reduction must be explored to create a comprehensive energy plan. Within ocean renewables, wave energy holds particular interest due to its consistency, magnitude, and great amount of power per area.

To determine the best locations for wave energy converters (WECs), researchers conduct wave energy resource assessments. Wave energy resource has been quantified globally during the past two decades [1]–[18], with methodology recently converging under a set of guidelines published by the International Electrotechnical Commission (IEC) in 2015, to standardize the technical specifications for resource assessments. Current methods for determining the amount of wave energy resource available to wave energy converter (WEC) devices involve capturing the state of the ocean and presenting characteristic wave heights, periods, and directions for the simplest of assessments. This method is proven to suffice in estimating the power available to large-scale WECs, operating to convert megawatts (MW) of power at a time. WECs operate optimally when moving at the same scale as the surrounding ocean environment, for example: large WECs require proportional excitation forces, best operating in large wave heights rather than small ones.

However, such large devices are extremely costly and must possess a high survivability factor, since their deployment locations are in highly energetic oceanic waters for them to match the surrounding sea state [19]. Small scale

WECs (operating on the scale of a few 100 W to a few 1000s kW) on the other hand, require less energetic sea states for operation, decreasing the amount of design efforts and funds dedicated to survivability measures. Small WECs that do not operate on the MW scale cannot function in highly energetic sea states with great amounts of available wave power, leading to the question, do small WECs require different methods for wave energy resource assessments? The research questions that inspired this study are listed below:

- *How does wave power available to WECs change as device is scaled down, and is it possible to evaluate this with current methods in place?*
- *What is the difference between using current methods to assess wave resource for small WECs and using power limits to determine the power available to the devices?*
- *Where can small WECs be used? What time of year? In other words, how do space and time domains for WEC application change with size?*

To characterize a small WEC's capture ability, power limits based on the body must be established. The three power limits that will be explored and implemented in this study are:

- Radiated power limit P_a
- Budal's upper bound P_b
- Gross power P_{gross}

These limits will be utilized to filter the incident wave power and quantify the net power, P_{net}, available for conversion by each WEC at each study location.

The radiated power limit, P_a, describes the maximum amount of wave power a WEC can absorb based on its optimum radiation pattern. Budal's upper bound, P_b, describes the power available to a small WEC based on its maximum

stroke, and relies on the assumption that the WEC body is so small that it doesn't significantly disturb the surrounding ocean environment. Both the radiated power limit and Budal's upper bound have been used in tandem to quantify the absorbable power to a small WEC device using experimental and numerical data [20]. This process is defined as the baseline case in this study.

These two limits have yet to be applied to observed or modeled wave data. This novel study applies the radiated power limit and Budal's upper bound to SWAN-modeled data, acting as the first piece of research to use the two limits to filter absorbable wave power to WEC devices from a wave hindcast.

In addition to the radiated power limit and Budal's upper bound, the gross wave power, P_{gross}, acted as a power limitation for an expanded methodology. Realistically, gross power is the maximum amount of power available in the ocean. At times, the radiated power limit and Budal's upper bound indicate there is absorbable power beyond the gross power [21], reflecting the caveat of the baseline case. This research's results emphasize the importance of including gross power as a limit when assessing absorbable power available to small WEC devices.

Overall, this novel study assumes that small WECs require a different approach to wave energy resource assessment compared to large WECs intended for grid power integration. Small devices could be used for power applications in coastal regions, potentially those with less energetic seas, opening previously dismissed regions of the globe for this type of renewable energy application.

Specifically, small WECs have great potential to power the Blue Economies (BEs) of coastal communities worldwide [22]. BE activities pose good candidates for decarbonization by way of ocean wave energy due to the sector's rapid growth and subsequent increasing power needs. A popular concept of the BE was conceived at the United Nations (UN) Conference on Sustainable Development in 2012. The definition of the BE in this study encompasses the

responsible utilization of ocean resources for sustainable development, equitable resource distribution, and improved livelihood of people and environment.

BE activities include anything from microgrid battery charging to aquaculture monitoring and powering of Autonomous Underwater Vehicles (AUVs), and they do not require large, utility-scaled wave energy conversion. Rather, small or micro scale WECs hold interest for stand-alone BE power applications, which is beneficial due in part to their dependence on less energetic sea states.

In this study, the WECs are assumed to be deployed in deep water, which allows for the use of deep water linear wave simplifications. Further, assuming the sea state was comprised of only regular waves allowed linear wave theory to be used. To delve further into linear wave theory and its corresponding simplifications, readers are encouraged to see Holthuijsen [23] and Dean and Dalrymple [24]. The WEC devices are assumed to have optimum oscillation and operation. Realistically, WECs in the ocean would not operate under such ideal conditions. This study does not explore explicit WEC mechanics and behavior, and readers are encouraged to read Todalshaug [25] for a more in-depth analysis.

In this thesis, Section 2. **Background** provides background for wave energy resource assessments, current WEC technology, small WEC power absorption limits, and more. Section 3. **Methods** lays out the methods necessary for current wave resource assessments and the novel methods for small WEC resource assessments. In Section 4. **Study data and method validation** the data used in the study along with the small WEC resource assessment methods are validated. Results are presented in Section 5. **Results** and are discussed in Section 7. **Conclusions** followed by conclusions in Section 7. **Conclusions**.

2. Background

Wave energy has the capacity to supplement the global mix of power supply, filling in gaps that cannot be filled by other renewable energy technologies like terrestrial wind and solar. Ocean renewable energy technologies are generally untapped and represent a new frontier of renewable energy development. Some benefits of wave energy include temporal consistency, spatial concentration of resource, and large magnitudes of power.

Various types of renewable energy currently are under development, optimization, and implementation around the globe. The technology behind wind and solar energy are well established and mature, and fairly accepted by the public. Terrestrial wind and solar energy have been commercialized and are growing fast, with energy costs comparable to that of thermal power plants [19], [26]. At the same time, terrestrial wind and solar energy have significant limitations that inhibit their growth. Solar energy is intermittent, meaning that it may only be harnessed at certain times and in certain climate conditions: during the daytime in sunny locations. Additionally, large plots of land are needed for solar farms in order to produce large-scale solar energy, and exposure to air pollution can decrease the effectiveness of the technology [27]. Terrestrial wind faces similar barriers to broad implementation, including intermittency and availability only in certain areas [28].

In contrast, the ocean provides a wide range of renewable energy solutions available constantly and at a greater magnitude. Therefore, harvesting marine renewable energy (including offshore wind, thermal energy, wave, current, and tidal) attracts increasing attention from the research community. According to Neil and Hashemi [9], the use of ocean renewables continues to consistently increase and is projected to contribute 748 gigawatts (GW) to the global energy supply by 2050. In this vein, there is potential for marine renewable energy

technology development and applications globally. However, the marine renewable energy technologies are relatively underdeveloped. Comparing to other marine renewable energy technologies (e.g., offshore wind which currently contributes to largest amount of power generation), the development of wave energy conversion technology is still at its infancy. There are various documented barriers to wave energy, including narrow funding support avenues and device scaling-up issues [29]. At the same time, there has been no convergence by the field to one single device or even technology concept for wave energy [30]–[32]. Additionally, commercial wave energy converter devices have not been thoroughly tested at smaller scales, where a large portion of wave energy application lies [33].

Yet, instead of viewing these issues as barriers, they may be seen as opportunities. There is room for potential size and applications of wave energy conversion as its development continues. And, since areas of deployment vary vastly depending on desired amount of power conversion, wave energy devices may need to have different modes of operation to function optimally.

Presently, wave energy converters (WECs) are aimed at converting large amounts of wave power for useful energy. To understand where, when, and how much wave energy is available, researchers must conduct wave resource assessments. The International Electrotechnical Commission (IEC) has created standardized methods for quantifying wave resource, allowing for uniformity in assessments across the globe. According to their website, the IEC is comprised of member countries and their national committees, representing governmental agencies, professionals, and industry among others [34]. It is an international organization that "prepares and publishes international standards for all electrical, electronic, and related technologies" [34]. IEC guidelines have been created and passed for wave energy converter technology, ensuring that member countries utilize the same standards when creating WECs.

2.1 Wave resource assessment methods

Wave energy resource has been characterized around the globe in the past half-century, demonstrating a wide range of not only locations but parameters to represent the resource [4], [5], [7], [9]–[11], [13], [16], [35]–[38]. Wave energy is desirable to quantify as WECs increasingly become viable devices for power conversion and the push for renewable sources gains traction. For analyzing the overall global wave energy resource available, Cornett's global assessment of wave energy transport, or wave power, is a useful tool [4]. Cornett was the among the first to globally characterize wave energy, providing a broad look at the global distribution of the resource.

Cornett's assessment was based on a 10-year hindcast generated by the National Oceanic and Atmospheric Administration's (NOAA's) wave model WAVEWATCH III (WWIII), aimed at predicting waves on a global level [4]. WWIII is a wave model developed at the NOAA and the National Centers for Environmental Prediction (NCEP), built off previous WAVEWATCH models from Delft University of Technology and NASA.

WWIII is widely accepted and utilized for wave resource assessments around the world, and is often coupled with the Simulating WAves Nearshore (SWAN) model to resolve the nearshore, shallow water regions of the ocean [2], [17], [35], [39]–[42]. SWAN was developed at the Delft University of Technology in The Netherlands, and has been validated and utilized for wave modeling since its conception [9]. Cornett's wave modeling methods remain in use to this day, and the resource assessments cited in this study tend to use WWIII-SWAN for hindcast simulations.

According to Cornett's assessment, as proved by subsequent resource assessments, wave energy in the United States is most prominent in the northwest coastal regions [4], [12]. Various resource assessments have been conducted in the past decade, all aiming to quantify the wave energy available in the region [2],

[10], [43], [44]. In 2011, Lenee-Bluhm et al. [44] quantified the resource in the Pacific Northwest, specifically off the coasts of Washington, Oregon, and Northern California. In this case, physically observed data was utilized to complete the assessment instead of modeled data.

The six quantities used to quantify wave energy by Lenee-Bluhm et al. [44] would later be seen in the IEC's Technical Specification (TS) 62600-101 [45], requirements for wave energy resource assessments and characteristics, published in 2015. The IEC TS 62600-101 aims to standardize the wave energy resource assessment process, promoting a convergence in the process of classifying sea states and associated energy availability around the globe. A detailed methodology involved for completing a wave energy resource assessment using the IEC specification is described the Methodology section.

The IEC TS 62600-101 guidelines should be applied throughout the entire resource assessment project, including site assessment, wave model development and implementation, defining, recording, and processing parameters, and subsequent reporting of results. According to the IEC, a 10-year dataset is the required length of dataset from which wave resource should be analyzed, as the dataset is thought to be long enough to capture seasonal trends, producing less uncertainty [45]. The energy quantified using the IEC guidelines is aimed at powering utility-sized WECs, which are designed to achieve resonance at the same frequency as surrounding ocean waves, meaning that the WEC must be sufficiently large in size in very energetic wave climates [38].

Many researchers have utilized the IEC's TS 62600-101 for wave resource assessments, particularly in the Pacific Northwest of the US and Canada in terms of the Northern Hemisphere [2], [6], [46]. Additionally, researchers increasingly have developed wave hindcast models to help them complete with assessments. Specifically, engineering and scientists at the Pacific Northwest National Lab (PNNL) and the National Renewable Energy Lab (NREL) in the U.S. have

created high-resolution wave hindcast models for the coastlines of the U.S., both continental and contiguous states and territories [11], [47]. Modeled wave data can be used to complete IEC wave resource assessments [45].

Despite the existence of the IEC standards, Yang et al. [48] point out that wave resource assessments in the field do not always follow the established IEC standards. For example, some countries of the world are not members of the IEC and therefore do not need to abide by the guidelines set forth by the IEC [30]. Global adherence to the IEC standards is important to cohesively produce consistent quality of WECs and other ocean energy devices.

There are other limitations induced by the IEC guidelines. For starters, environmental conditions are not always adequately considered in wave resource assessments, according to Robertson et al. whom investigated the impact of including detailed wave and environmental conditions to a standard IEC wave resource assessment [49]. Robertson et al. found that the inclusion of wind and current speed along with wave "groupiness" in wave power estimates increases maximum power predictions by 328% compared to a base IEC assessment [49].

Many regions around the globe see significant changes in wave energy available interannually [50]. Yang et al. suggest that a longer time period of than the 10 years of data required by the IEC may be necessary to accurately determine the effect of climate variability [48]. Nevertheless, the IEC wave resource assessment procedure proves to be substantive [50].

As noted, in the United States, wave energy has been quantified on all coasts and in most territories. Entities like NREL, PNNL, and the Bureau of Ocean Energy Management (BOEM) have consistently generated updated wave hindcasts, resource assessment literature and toolboxes, and products for the research and larger communities (e.g., the Marine Energy Atlas [51]). In terms of the coastal locations with the most wave power in the United States, the Pacific

Northwest possesses the most, followed by Hawaii, the California coasts, the Northeast coasts, the Mid-Atlantic, Southeast, Gulf states, and Puerto Rico [12].

Areas outside of the Pacific Northwest and Hawaii are less likely to be considered for wave energy projects due to their lower magnitudes of incident wave power. In fact, in an analysis by Kilcher and Thresher [52] that identified and ranked all potential wave energy sites in the United States and its territories, locations with a wave power density less than 5 kW/m were excluded from the analysis. This threshold was implemented based on industry feedback that deemed 10-15 kW/m as the minimum power threshold for sites. The ranking of locations in Kilcher and Thresher 2016 [52] resulted in Oregon, California, Washington, and Hawaii placing in the top four best wave energy locations in the United States (ignoring energy cost); Puerto Rico, East coast states, Pacific Islands, and Alaskan communities follow respectively. Kilcher and Thresher determined the wave energy contribution to each location based on the amount of power required by the load of the local electric, meaning grid the wave energy assessed was to be used for utility grid purposes.

A breakdown of different WEC technologies is presented in the following section, along with a review of WEC size classification as it stands presently.

2.2 Current wave energy technology

WEC devices can be categorized in several different ways, including by mode of motion for energy harvesting, type of mechanical process for conversion, etc. Perhaps most generally, WECs are broken into category by deployment location [32]. Different WECs will operate optimally in different bathymetries, and some devices are tethered to the seabed. Alternatively, WECs can be mounted to the shore via breakwaters or other coastal structures. The WECs described are optimized to convert power at relatively large scales, with the aim for grid power integration.

A common classification of WECs is given by comparing the WEC body extension relative to wavelength and wave direction. Kofoed explores this classification in the “Handbook of Ocean Energy” [32]: attenuator devices have large horizontal extensions orthogonal to the direction of wave propagation, terminators have large horizontal extensions parallel to the direction of wave propagation, and point absorbers have small horizontal extensions compared to incident wavelength.

Kofoed [32] also offers a more detailed classification of WEC types, sorting bodies by the hydrodynamics of device. The categories include oscillating water columns (OWC), overtopping devices, and wave activated bodies.

OWCs are considered to be the first WECs, invented by Yoshio Masuda in Japan in the 1940s [53]. For conversion in these devices, air is trapped inside the hollow structure of the device by sea water, whose elevation changes force the change in air volume to power a turbine (see Figure 1). OWCs are generally simple devices, with the turbine operating above the water to convert energy [53].

This WEC type has been thoroughly modeled and studied, and is thought to have the most deployed prototypes in the ocean [53]. Two examples of OWCs are shown in Figure 1.

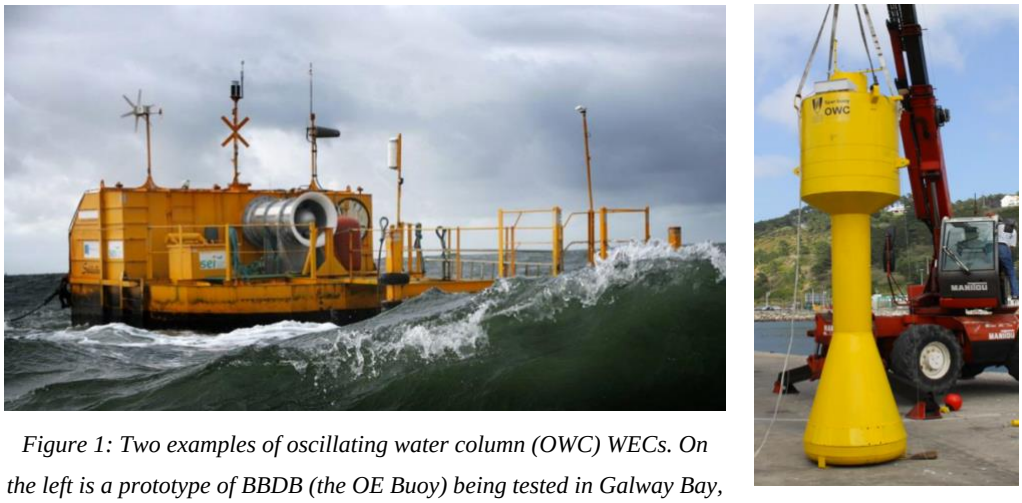

Figure 1: Two examples of oscillating water column (OWC) WECs. On the left is a prototype of BBDB (the OE Buoy) being tested in Galway Bay, Ireland. On the right, a scaled, spar buoyed OWC. Images from Falcão and Henriques, 2016.

Overtopping devices are dependent on incident waves running up a sloping wall, filling the reservoir of the device; here, the water is stored higher than the surrounding sea and potential energy can be converted to useful power [54]. These WECs may be fixed structures or floating, or integrated into shoreline structures like breakwaters [55]. An example of an overtopping device is shown in Figure 2.

Figure 2: The world's first offshore wave energy converter, the Wave Dragon, is an overtopping device. Waves flow over the top of the device into a reservoir, after which they are funneled through a vertical turbine, creating energy. After the absorption process, the water flows back into the ocean. Image from Wave Dragon.

Wave activated bodies are classified by Kofoed as buoys that extract energy via WEC body interaction with the incident wave field. The incident wave field induces an oscillatory motion by the body, which is why this WEC type is also referred to as an oscillating body system [56]. These bodies absorb wave energy by displacing water through an oscillatory motion in phase with the surrounding sea state. In other words, wave activated bodies move with the sea's motion, and attempt to "catch" the power in incoming waves. This category is made up of a wide variety of WEC device concepts, like the heaving point absorber called *Wavebob*, submerged oscillating flap device called the *Oyster*, and semi-submerged *Pelamis* WEC. For more examples, readers are referred to Kofoed [32] and Babarit [57].

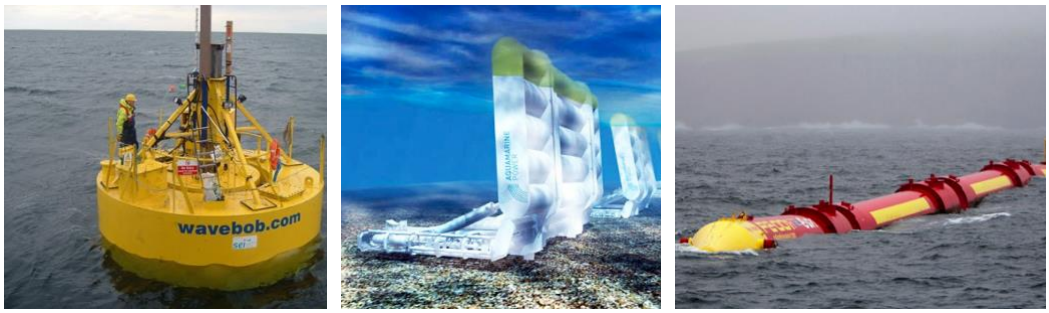

Figure 3: Examples of type WECs. Far left is the Wavebob, a heaving point absorber that moves vertically in the water column. Center is the Oyster, an oscillating flap device that moves perpendicular to shore in the water column. Far right is the Pelamis WEC, which is semi-submerged and generates electricity by flexing and bending as waves pass the device. Images from Marine Renewables Canada and Oleo International.

For those interested in detailed WEC specifications, performance, and applications, readers are directed to Babarit [57]. The wave energy field has not converged on a device design or energy harnessing mode, accounting for the wide variation of WEC devices being researched, tested, and designed. This may prove to be useful, since ocean environments are incredibly diverse depending on latitude, local bathymetric terrain and depth, and climate patterns among other phenomena. Therefore, convergence to any one device may prove to be more difficult than the current approach.

2.3 WEC modeling

Physical records of sea states are spatially sparse and expensive to undertake; wave measurement buoys record data at the one point they are deployed in and must possess high survivability to withstand sea states. Wave modeling and WEC modeling allows researchers to conduct wave resource assessments with little to no physically measured data, at a fraction of the cost. Wave models, like WWIII or SWAN, may simulate wave conditions at great spatial and temporal variability, with outputs compared to existing physical records to complete validation and calibration. This process is known as wave

hindcasting when estimating sea state conditions in the past. If computed for predicting future sea states, the term wave prediction suffices.

On the technology side, modeling WECs is a necessary step in understanding the effect of the sea state on devices, risk reduction, power capture ability, and necessity of optimization pre-physical modeling phases. Researchers at universities and institutions like the United States Department of Energy (US DOE) have spent years developing numerical modeling tools to simulate WEC bodies and their interactions with the ocean environment.

Some of these models are open-source, or publicly accessible, like the US DOE's WEC-Sim or Proteus. Other software like the École Centrale de Nantes's NEMOH or WAMIT use boundary element method (BEM) solvers and are commercially available, requiring users to purchase software packages. These models and software programs allow the user to simulate anything from WEC body motion to mooring dynamics to power conversion and are operated primarily through MATLAB or Python computing.

2.4 Small scale WECs

Some WEC applications do not necessarily require large-scale devices converting power on the MW scale. Already, the US DOE acknowledges that navigation markers and ocean observation systems could make particular use of small WECs, decreasing funding needs and allowing for expansion of the market for ocean observation [58]. Recently, some focus has been diverted from developing utility-scale wave energy conversion to smaller, more targeted applications like oceanographic sensing or underwater vehicle charging [58]. By innovating and testing WECs at a small scale, a path may be paved for eventual upscaling of devices.

Researchers are finding that small WECs, while unable to convert objectively high amounts of power, have the capability to convert wave energy to

useful power more steadily throughout the year [59]. This is due to small WECs that reach resonance at small wave periods (high wave frequencies) [59], corresponding to sea states that are present in most coastal locations in the U.S. throughout the entire year. In fact, WECs that operate in smaller wave periods may extract more energy on average than WECs in more energetic sea states, due to temporal consistency and steady operation [59].

Economic viability of WEC development presents perhaps one of the largest barriers to the increased reliance on wave energy. Coe et al. [59] has published a review of wave resource metrics, including cost and efficiency, including reasoning supporting the notion that small WEC devices deserve further investigation. Current wave resource assessment methods have directed policymakers and WEC developers to aim for deployment in the most energetic of seas; vast amounts of gross wave energy tend to draw people in, brimming with high energy extraction potential [59]. However, this approach fundamentally neglects the effect of WEC size on monetary cost. This has led to design and WEC test siting decisions to favor large WECs operational in very energetic sea states [59]. Increasing power generation capabilities necessarily leads to an increase in the size of the WEC, which raises the need for structural reinforcements, larger power conversion mechanics/electronics, and more intensive mooring capabilities [59]. On the economic side, smaller WECs are thought to potentially have better average annual energy capture, capacity factor, and overall costs [59]. And since funding is such an essential factor in renewable energy development, Coe et al. [59] along with other proponents of small wave energy conversion merit further investigation of small WECs and their development.

Recent research in wave energy conversion has delved into various scaled operation applications. Mundon [33] considered a scale for WEC power capacity (rated power) and subsequent purposes, emphasizing that the “archetypes

currently developed for WEC have all been developed with a focus on larger scales for grid power." The scale is broken down accordingly:

- Utility (large) scale: WECs designed for large scale grid operation with individual rated powers from 100s of kW to MW. Intended for array deployment.
- Community/Facility scale: devices designed for connection to microgrids or weak grid applications with individual rated powers $\leq$ 100 kW. May be deployed in array or individually.
- Small scale: designed for individual use and rated powers between a few hundred W and a few kW
- Micro scale: intended for deployment to oceanographic devices with a mean power output $<$100 W

Aderinto et al. points out, however, that power capacity categorization for small scale energy are varied in general, let alone in the world of wave energy conversion [60]. They categorize small devices as having power ratings between 5 kW and 5 MW. A classification system for WEC volume has yet to be proposed in literature. This disparity speaks to the lack of representation and documentation of any WEC classification scale beyond utility purposes.

There is various literature similar to Mundon [33] that aims to forge a path in the field, focusing on small- and micro-scale WEC classification and experimentation. For instance, de Abreu D'Aquino et al. [61] examined the specific example of the implementation of a small-scale oscillating-water-column (OWC) WEC for nearshore applications, integrated into structures like piers or breakwaters. Johnson et al. [62] investigated the ability of a small scale rotating mass WEC integrated in a Gorlov helical turbine to convert subsea ocean current and surface wave energy into useful power. They found that the Gorlov turbine-rotating mass integration in the WEC allowed for "multimethod energy" conversion and was most feasible at a small scale.

Such studies prove potential success of small WEC devices for various purposes based on what is generally understood about resource assessment for ocean energy. However, the current standards for wave energy resource assessment depend on gross oceanic-scale properties, such as significant wave height H_{m0}, energy period T_e, omnidirectional wave power J (all discussed in Section 3.1 **Traditional wave energy resource assessments**. As referenced previously, large-scale WEC devices are optimal for absorbing power from highly energetic seas, theoretically [38]. However, from practical and economical points of view, large scale WECs may not outperform smaller devices since their required sea states occur less often and pose increased probability of failure due to survivability.

As scaled wave power absorption systems become more prevalent in solving pieces of the economic decarbonization puzzle, there is an increasing need for a reconciliation of resource assessment with WEC size. This study aims to suggest an avenue for scaled wave energy resource assessment, based on the power capture limits established and discussed in this research.

2.5 Limits for WEC power capture

An important piece of WEC development and application is fundamentally understanding the limits of the technology. Such understanding rides on knowledge of deployment location and conditions the WEC will face as well as the maximum threshold of power the WEC is rated to absorb and convert. According to the law of conservation of energy, no energy may be created nor destroyed, and therefore WECs must be able to take energy from the sea, reducing the amount of energy present in the surrounding ocean [63].

In this study, exploring the limits of power capture for WECs is a main objective. Gross power available in the sea is not equal to the net power that is absorbable by a WEC, regardless of device size. Todalshaug [25] points out that

there are a couple of different manners in which absorbable power may be estimated, including using measured data to calculate capture width ratio and theoretical upper bounds, the latter of which will be explored below.

Upper bounds for WEC power capture were previously defined, first by Budal and Falnes [64] and explored thereafter by many others [20], [63], [65]–[67]. A basic power limit that applies to WECs depends on their radiation patterns of the waves generated by the WEC itself. This power limit is the product of the incident wave power and the maximum absorption width of the WEC device. It changes based on body shape, where the absorption width of the device changes if it is an axisymmetric body (symmetric about the vertical axis) or a terminator body, which is large in width comparative to wavelength. In this study, this power limit is called the radiation power limit and is referred to as P_a.

The radiated power limit is known as the power limit dependent on WEC radiation pattern corresponding to maximum power absorption. It is dependent on the assumption that the interaction between the WEC and wave is optimal, i.e., the WEC oscillates optimally according to the surrounding sea state. In this manner, the WEC must adjust its oscillation pattern as the wave height increases, making the overall power generated by the wave and absorbed by the WEC larger. In other words, the radiated power limit assumes that the WEC body is in resonance with the incident waves, and therefore will increase in magnitude as wave height and period increase.

Another power limit used to estimate absorbable power, for small WECs specifically, is based on the swept volume of the WEC body during oscillation [68]. This limit is called Budal's upper bound, designated P_b. Kjell Budal and Johannes Falnes from the Norwegian University of Science and Technology found that small resonance-tuned point absorber WECs are effective wave energy converter devices [69]. The two researchers derived a condition that limits the

amount of power the point absorber WEC can absorb, which was granted the name Budal's upper bound.

Budal's upper bound focuses on the maximum utilization of the wave excitation force, under the assumption that the oscillations of the body are optimal [20]. It depends on the volume of the body in excitation and is more restrictive at higher wave periods. This contrasts with the radiated power limit, which is more restrictive at lower wave periods.

While Budal's upper bound increases with wave height, it gets smaller as wave period increases. This is because Budal's upper bound mathematically depends on the ratio between wave height and period. Physically, Budal's upper bound assumes the maximum utilization of the wave's excitation force and the WEC's body volume. As waves get smaller and more frequent (shorter wave periods), the WEC has more opportunity for excursion, meaning the body's oscillations increase with wave occurrence. Smaller devices have higher natural frequencies, so the smaller the device, the better will oscillate in high frequency sea states.

Budal's upper bound states that the absorbable wave power by a small point absorber is equal to the excitation power from the wave onto the device, ignoring all viscous forces. The excitation power is equal to

$$P_e = \frac{1}{2}\left|\widehat{F_e}\hat{u}\right| \cos\gamma \tag{1}$$

where $\widehat{F_e}$ is the complex amplitude of the heaving body's excitation force, $\hat{u}$ is the complex amplitude of the body's velocity, and γ is the phase angle between the two [65]. In the ideal oscillation case, the optimum phase $\gamma = 0$. Additionally, the following inequalities apply [20]:

$$\left|\widehat{F_e}\right| < \rho g S_w A \tag{2}$$

and

$$|\hat{u}| < \frac{\omega V}{2S_w} \tag{3}$$

where ρ is the density of sea water, g is gravitational acceleration, S_w is the cross-sectional area of the device crossing the water plane, A is the amplitude of the wave, ω is the angular wave frequency, and V is the swept volume of the device. These inequalities were found via small body approximation, relevant since Budal's upper bound assumes the WEC is much smaller than the wavelength [64], [70].

Substituting inequalities from Eqs. (2) and (3) for $\left|\widehat{F_e}\right|$ and $|\hat{u}|$, the excitation force becomes

$$P_e < \frac{\rho g A \omega V}{4} \tag{4}$$

According to linear wave theory, regular waves $H = 2A$ and $\omega = \frac{2\pi}{T}$, rendering:

$$P_e < \frac{\rho g \pi}{4} V \frac{H}{T} \tag{5}$$

At ideal volume utilization in wave conditions, the final form of Budal's upper bound is

$$P_b = \frac{\rho g \pi}{4} V \frac{H}{T} \tag{6}$$

Falnes and Budal used this form of Budal's upper bound, and strove to explore how WEC size, mode of oscillation, and stroke affect a device's power absorption. Eq. (6) is Budal's upper bound for power extraction for small, heaving WECs, and is used in a wealth of research [25], [32], [63], [65], [68], [71][20]. Budal's upper bound is valid assuming ideal WEC oscillation, small body volume, and maximum body amplitude are achieved. Additionally, the swept volume V is equal to the body volume since ideal oscillation is assumed.

Using the radiated power limit and Budal's upper bound, a Budal diagram can be created, displaying the range of absorbable power available to a WEC based on wave period, wave height, and WEC volume. An example of this is shown in Figure 4:

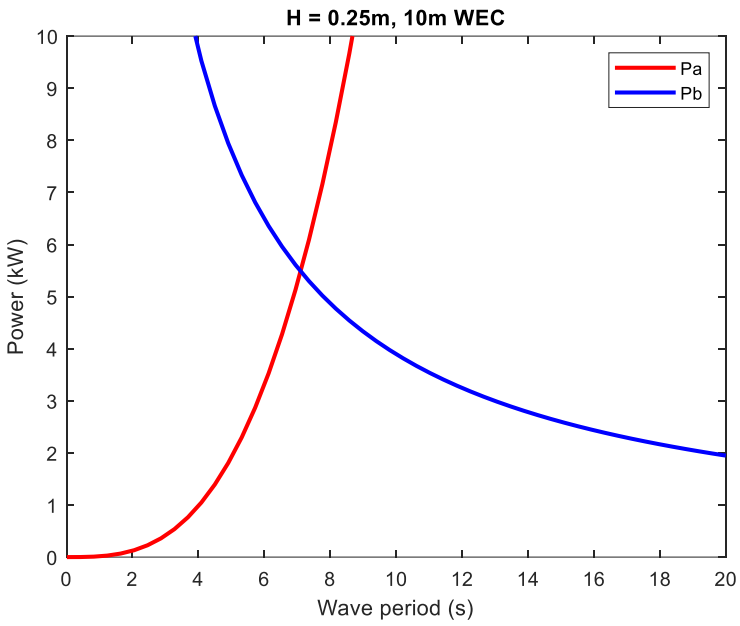

Figure 4: Budal diagram for 10m WEC device and unit wave height of 0.25 m

Figure 4 illustrates the restrictive nature of both power limits; the radiated power limit restricts the power at lower wave periods while Budal's upper bound limits at higher wave periods. The power underneath the curves and their intersection is theoretically absorbable, according to the power limits. So far in published research, the radiated power limit and Budal's upper bound have dictated the theoretical amount of power absorbable for a given WEC [20], [21], [63], [65], [68].

Beatty et al. [20] conducted an experiment finding the theoretical power limitations for small two-body heaving WECs using an extension of Budal's upper bound and the radiated power limit. While focused more on device control and power take-off control schemes, the research proves valuable when understanding the effect of the limits on available absorbable powe for small WECs.

Beatty et al. [20] utilized an extension of Budal's upper bound, which allows for constraint of the maximum stroke of the device. In their research, Beatty et al.

limits the stroke of the two-body WEC to 13% of the device's diameter, incorporating some practicality [20]. Doing so ensures that the body will not emerge completely out of the water or submerge itself completely under the sea surface.

The theoretical radiated power limit and Budal's upper bound values found in Beatty et al. [20] accurately reflect the nature of these power limits. The radiated power limit and Budal's upper bound rely on assumptions regarding the surrounding sea state and the WEC bodies themselves, resulting in theoretical, mathematical maximum power absorption limits. The theoretical absorbable power is necessarily attainable; actual power absorption is closer to the experimental and modeled data in [20], which was expected.

The limits used assume that the devices function optimally, operating at and in ideal conditions, e.g., maximum stroke, perfect power conversion, and ability to achieve the mathematical maximum of power absorbable. Due to this perfect nature, the actual realistic absorbable power is understandably less than what is predicted by a Budal diagram.

3. Methods

The following sections provide methodologies for the IEC wave resource assessments and both cases of small WEC wave resource assessments.

3.1 Traditional wave energy resource assessments

When assessing the wave energy resources for a potential project, the IEC TS 62600-101 [45] is used to "promote international cooperation on all questions concerning standardization." In other words, IEC guidelines are utilized to ensure consistency and accuracy in wave resource assessments. Required wave parameters for assessment include significant wave height H_{m0}, energy period T_e, omni-directional wave power J, the directionally resolved wave power and its

direction (J_θ and $\theta_{J\theta max}$), directionality coefficient (d), and spectral width (ϵ_0). Such parameters are calculated from the directional wave spectrum, which may be obtained via numerical modeling or physically observed measurements. To calculate omni-directional parameters, the two-dimensional frequency-directional variance density spectrum are transformed into one-dimensional frequency-domain spectrum via Eq. (7):

$$S_i = \sum_j S_{ij} \Delta\theta_j \tag{7}$$

where S_{ij} is the variance density in the i^{th} frequency and j^{th} directional bin and $\Delta\theta_j$ is the directional bin spacing. Spectral moments of the n^{th} order, m_n, are calculated from frequency variance density by:

$$m_n = \Sigma_i f_i^n S_i \Delta f_i \tag{8}$$

where f_i is frequency. Using the moments of the spectrum, the significant wave height is calculated using the zeroth spectral moment:

$$H_{m0} = 4\sqrt{m_0} \tag{9}$$

which is generically referred to as the significant wave height calculated from the wave spectrum. The preferred characteristic wave period for wave resource assessments is the energy period – Eq. (16).

$$T_e = \frac{m_{-1}}{m_o} \tag{10}$$

Omni-directional, or directionally unresolved, wave power, J, is the time averaged energy flux through a vertical cross section of unit diameter that extends from the seafloor to the surface, calculated by:

$$J = \rho g \sum_{i,j} c_{g,i} S_{ij} \Delta f_i \Delta\theta_j \tag{11}$$

where $c_{g,i}$ is the group celerity, ρ is the water density, and g is the gravitational constant. The time-averaged energy flux across a plane normalized to direction θ is defined as the directionally resolved wave power. This directionally resolved

wave energy transport is the sum of the contributions of each component with a positive component in direction θ, calculated by:

$$J_\theta = \rho g \sum_{i,j} c_{g,i} S_{ij} \Delta f_i \Delta\theta_j \cos(\theta - \theta_j)\, \delta \qquad \begin{cases} \delta = 1, & \cos(\theta - \theta_j) \geq 0 \\ \delta = 0, & \cos(\theta - \theta_j) < 0 \end{cases} \tag{12}$$

The maximum value of J_θ represents the maximum time averaged wave power propagating in a single direction and is denoted by $J_{\theta_{Jmax}}$. The directionality coefficient is a characteristic measure of the directional spreading of wave power. It is the ratio of the maximum directionally resolved wave energy transport to the omni-directional wave energy transport:

$$d = \frac{J_{\theta_{Jmax}}}{J} \tag{13}$$

Spectral width, ϵ_0, characterizes the frequency-domain spreading of variance density [72]. This parameter is defined using:

$$\epsilon_0 = \sqrt{\frac{m_0 m_{-2}}{m_{-1}^2} - 1} \tag{14}$$

The specification identifies three classes of resource assessment and associated project application: Class 1 – Reconnaissance, Class 2 – Feasibility, and Class 3 – Design. The spatial and temporal fidelity of the required data increases with Class; Class 1 has the lowest allowable resolution and Class 3 the highest resolution [45]. A Class 1 assessment may be conducted by analyzing existing, archived sea state parameters, or analyzing directional spectra generated via a numerical wave propagation model, while Class 2 and 3 data should be based on either directly measured directional wave spectra or an Measure-Correlate-Predict method [45].

Mean bivariate histograms are required by the IEC specifications, along with annual monthly means, standard deviations, percentiles, and variations of all wave parameters. Monthly averages over the study period, variations of the mean,

variation of one standard deviation above and below the mean, and 10th, 50th, and 90th percentiles are plotted to show the statistical monthly variations. The percentile analysis is completed to show the limits of the datasets and identify the median. The 10^{th} and 90^{th} percentiles are used to show the upper and lower limits of the data, and the 50^{th} percentile is equivalent to the median of the dataset.

In a normal distribution, the curve of a dataset is symmetric about the mean, earning the reference "bell curve." If a dataset is skewed, the shape of the distribution has asymmetric qualities. Figure 5 offers a visual perspective of skewness in a dataset by comparing variously skewed distributions. By comparing the mean and the median of the distribution, it is possible to assess the degree of skewness. If the mean value is greater than the median, the dataset is positively skewed, meaning that the distribution has the most occurrences on the lower end of the curve. This is typical of sea state distributions, as more extreme events are less frequent [73].

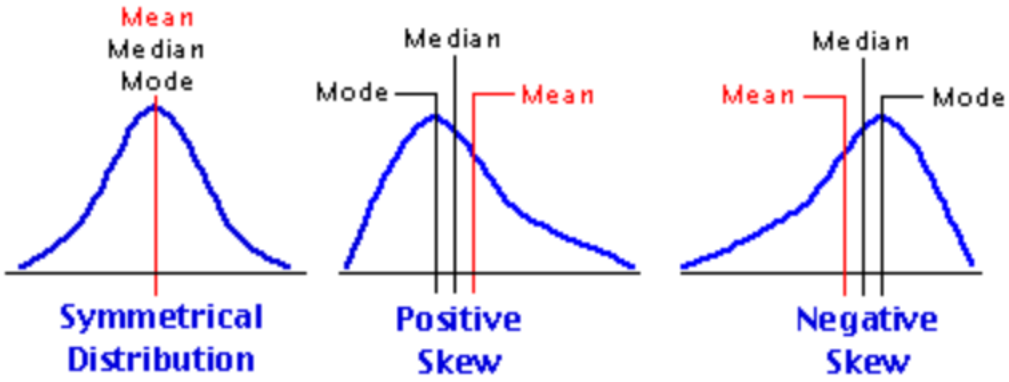

Figure 5: Skewness is indicated by the difference of the median (50th percentile) and the mean. Larger differences between percentiles and the mean determine the degree to which the distribution is skewed (CFA, 2020)

The bivariate histogram shows the annual frequency of occurrence of sea states, parameterized in terms of significant wave height and energy period with a resolution of 0.5 m and 1 s respectively. The wave rose shows the joint

distribution of maximum directionally resolved wave power and its direction is also required for inclusion in Class 2 and 3 assessments.

The IEC standards require a minimum of 10 years of sea state data for assessments, and acknowledge that a longer period of data may be necessary to quantify the low frequency climate variability, pertaining to events like the El Niño-Southern Oscillation [45].

As discussed previously in the Introduction, IEC methods for wave energy resource assessments are sound processes in capturing the bulk wave resource present at a given location. The IEC parameters detailed in this section aim to distinguish the wave climate on a general, gross scale. And, to capture bulk ocean energy, WECs must be significantly large if they aim to resonate at long periods associated with the most energetic sea states. When examining small WECs and their capabilities for capturing ocean energy, it is essential to think about the process in an altered manner. New methods for analyzing capturable power by small WECs are proposed and outlined below.

3.2 Novel small scale wave energy resource assessments

The incident wave power that interacts with the devices P_{gross}, the maximum power absorbable by the WEC due to its radiation pattern P_a, and Budal's upper bound P_b were calculated for this study.

3.2.1 Power Limits

The maximum wave power available for conversion is given by Falnes [74]:

$$P_a = J d_{max} \tag{15}$$

where J is the wave energy transport in W/m and d_{MAX} is the maximum absorption width of the WEC. d_{MAX} is dependent on the mode of oscillation of the WEC; this study is concerned with isotropically radiating WECs, or WECs that operate as a point source of radiation, in which case $d_{MAX} = \frac{\lambda}{2\pi} = \frac{1}{k}$ [67]. Therefore,

$$P_a = \frac{J}{k} \tag{16}$$

The first power limit, denoted as the radiated power limit, describes the total incident wave power available to the heaving WEC according to its radiation pattern. In [63], Falnes assumes deep water, and linear wave theory allows for the substitution of $\lambda = \frac{gT^2}{2\pi}$, rendering $\frac{\lambda}{2\pi} = \frac{gT^2}{4\pi^2}$. Additionally, in deep water, $J = \frac{\rho g^2}{32\pi} H^2 T$ [23]. With these substitutions, Falnes arrives at

$$P_a = \frac{\rho\left(\frac{\pi}{g}\right)^3}{128} H^2 T^3 \tag{17}$$

This limit is completely dependent on the regular sea state rather than WEC device specifications, and results in units of Watts (W) [63]. The radiated power limit was used to calculate the power limit based on incident wave conditions and does not change as the WECs are scaled up and down in size. To calculate P_a using sea state parameters H and T, the variance density of the frequency spectrum was used to find the wave amplitude A, or the elevation of the sea state (or η). Wave spectra can be transformed to frequency spectra using Eq. (7) described previously for the IEC Resource Assessments. If the timeseries for wave elevation is in possession, the spectra may also be transformed using the following relation [23]:

$$S_i = \frac{1}{2}\left(\frac{A^2}{\Delta f}\right) \rightarrow A = \sqrt{2S_i \Delta f} \rightarrow H = 2\sqrt{2S_i \Delta f} \tag{18}$$

where Δf is frequency spacing.

In Todalshaug [21], the radiated power limit was compared to the incident wave power available to a 100m WEC device. Todalshaug shows that, at longer wave periods, the radiated power limit gets larger than the incident power available [21], indicating that the radiation power limit is valid at relatively small and mid-range wave periods.

The second power limit used to estimate absorbable power is based on the swept volume of the WEC body during oscillation [68]. For this study, the volumes of the WEC bodies are assumed to be so small such that viscous forces like diffraction are negligible. Therefore, the net absorbable power from waves for the WEC bodies is equal to the excitation power of the waves. Excitation power is

$$P_e = \frac{1}{2}\left|\widehat{F_e}\hat{u}\right| \cos\gamma \tag{19}$$

where $\widehat{F_e}$ is the complex amplitude of the heaving body's excitation force, $\hat{u}$ is the complex amplitude of the body's velocity, and γ is the phase angle between the two [65]. In the ideal oscillation case, the optimum phase $\gamma = 0$. Additionally, the following inequalities apply [20]:

$$\left|\widehat{F_e}\right| < \rho g S_w A \tag{20}$$

and

$$|\hat{u}| < \omega s_{max} \tag{21}$$

where S_w is the area of the device crossing the water plane, A is the wave amplitude, ω is angular frequency, and s_{max} is the maximum allowable stroke of the WEC device. Utilizing Eqs 6 and 7, Budal's upper bound equates to:

$$P_b = \rho g S_w A \omega s_{max} \tag{22}$$

Beatty et al. [20] utilized this form of Budal's upper bound, which allows for practical constraint of the maximum stroke of the device. In their research, Beatty et al. limits the stroke of their two-body WEC to 13% of the device's diameter [20]. Doing so ensures that the body will not emerge completely out of the water or submerge itself completely under the sea surface.

Beatty et al. [20] obtained excitation force, $\left|\widehat{F_e}\right|$, via Boundary Element Method (BEM) analysis, but this value also can be estimated from small-body approximations [20]. Beatty et al. set a static $|\hat{u}|$ equal to 4m for the full-scale model, aimed at applying practicality to Budal's upper bound.

The theoretical P_a and P_b values found in Beatty et al. [20] accurately reflect the nature of these power limits. The radiated power limit and Budal's upper bound rely on extensive assumptions regarding the surrounding sea state and the WEC bodies themselves, resulting in theoretical, mathematical maximum power absorption limits, not necessarily attainable power capture bounds. Actual power absorption is closer to the experimental and modeled data in Beatty et al. [20], which was expected. The example from Beatty et al. [20] is the baseline scenario, which utilizes P_a and P_b to filter the wave power available to the device.

Attempting to validate these power limits, modeled data from the RM3 WEC was used for excitation force and set the same stroke limitations as Beatty et al. [20], resulting in Figure 6.

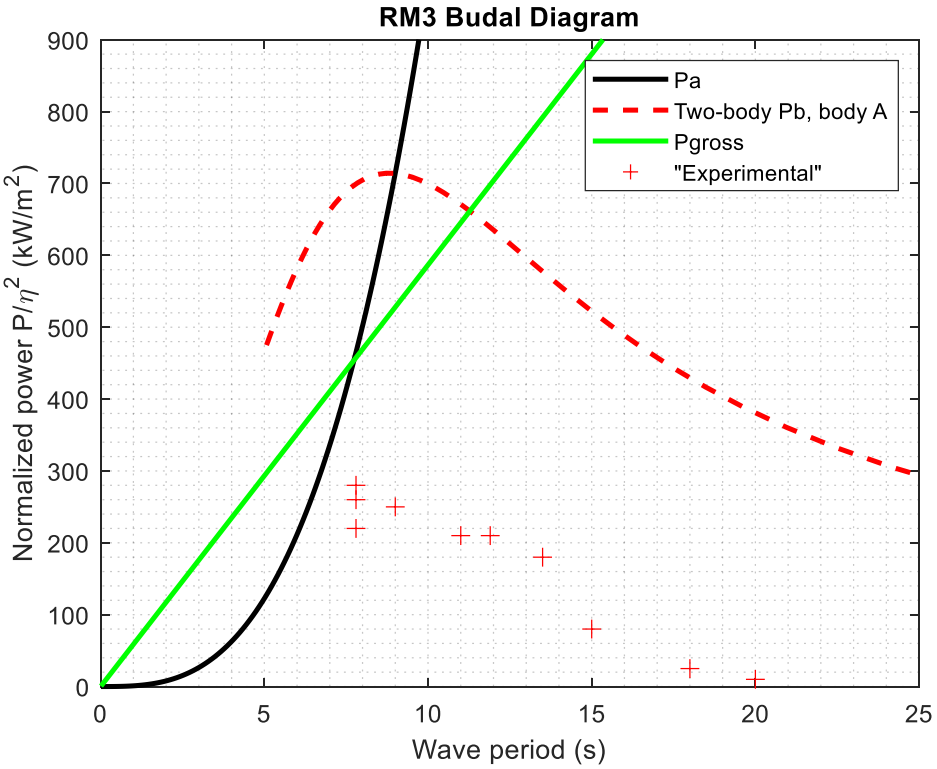

Figure 6: Recreation of Beatty et al. using RM3 WEC data. Black solid line is the radiation power limit, dashed red line is Budal's upper bound for [20] *body A, red crosses are experimental data points from* [20]*, and the solid green line is the gross incident wave power that interacts with the device*

The black solid line in Figure 6 shows the P_a power limit while the red dashed line shows Budal's upper bound. In addition to the radiated power limit and Budal's upper bound used in Beatty et al. [20], gross wave power P_{gross} available in the sea was implemented as a limitation. Realistically, no wave power greater than gross power exists in the ocean, it is essential to include as an upper limit for absorbable wave power. This process is a novelty implemented in this study that has not been enacted in previous works.

In Figure 6, at wave periods 8s through 11s, the total theoretical power is limited by gross power, i.e., the radiated power limit and Budal's upper bond are greater than gross power at these periods. Therefore, including gross power P_{gross} is essential in understanding the practical limitations of absorbable power for small WECs. When observing the upper limits for power absorption in terms of all three power limits, some reality is imposed to otherwise absolute perfect, maximum capture limits.

Two scenarios were explored in this study, explained in Table 1. The baseline case represents the status quo, or currently what metrics have been used to quantify absorbable power for small WECs in published research thus far. At the same time, the power limits used in baseline case have not yet been applied to real sea state data, neither observed nor hindcasted. Therefore, applying the radiated power limit and Budal's upper bound to the 10-year SWAN model data used in this study is a novelty in and of itself.

The expanded case corresponds to the expanded methods presented in this thesis, where gross power is also used to filter absorbable power along with the radiated power limit and Budal's upper bound. Inclusion of gross power is essential, as seen in Figure 6. Additionally, wave amplitude A is used as a bound for the dynamic stroke limitation instead of wave height H for the expanded case.

Table 1: Description of case scenarios analyzed in this study

	Baseline Case	Expanded Case
Filters	P_a, P_b	P_a, P_b, P_{gross}
Maximum stroke	$s_{max} = \begin{cases} 25\%\ of\ D & H > 0.25D \\ H & H < 0.25D \end{cases}$	$s_{max} = \begin{cases} 25\%\ of\ D & H > 0.25D \\ A & H < 0.25D \end{cases}$

For the baseline and expanded cases, for all H greater than 25% of the body's diameter, the maximum stroke is set equal to $0.25D$. If H is smaller than 25% of the body's diameter, s_{max} is set equal to H for the baseline and A for the expanded case. Both cases' constraints are based on existing research that limits the maximum stroke to a percentage of the body's characteristic dimension, from Beatty et al. [20]. For the expanded case, the stroke limitation is set to A if $H < 0.25D$. WEC devices without control mechanisms are said to have passive damping control, in that the devices simply follow the motion of the waves [32]. Since it can be challenging for small WECs to extend their bodies for the entire length of H, s_{max} was set equal to A, or $\frac{1}{2}H$, in the baseline case [33].

3.2.2 Modeled wave data application

The radiated power limit and Budal's upper bound were calculated for each wave height – wave period combination throughout the time period for five study locations near coasts in the United States. P_b was calculated for each of the five WECs, whereas P_a remained constant despite device geometry changing, as expected due to the function of its equation. The resulting limits were compared for each period/frequency, and the minimum value at each prevailed. The result was the net power denoted P_{net}, corresponding to the power extractable by the WEC device.

Net power was analyzed on daily, monthly, annual scaled. Statistics including the mean, coefficient of variation (COV), percent reduction, and maximum values were calculated.

This methodology was completed for wave frequency spectra from the five different locations where classic resource assessments were previously completed:

PacWave (Central Oregon), Los Angeles, California, WETS (Oahu, Hawaii), Cape Cod, MA, and Miami, Florida. At each location, four different sized WECs with heave mode operation were considered: 1m, 2m, 5m, and 10m.

4. Study data and method validation

Wave data from five different coastal locations in the United States was analyzed for both the IEC and small WEC resource assessments. The details and motivation for selection pertaining to the locations can be found in the following subsection.

Prior to applying the small WEC resource assessment methods to the study data, they were applied to a generic Pierson-Moskowitz spectrum. The results of this application were observed and used for method validation.

4.1 Study data

This thesis aims to provide a Class 1 IEC and small WEC resource assessment for five different locations: PacWave (Central Oregon), Los Angeles (California), WETS (Oahu, Hawaii), Cape Cod (Massachusetts) and Miami (Florida).

For IEC methods, Class 1 assessments were completed since the IEC-required wave data is publicly available. Class 2 and Class 3 assessments require high spatial and temporal resolution of sea state data, including wave, tidal, current, and wind data, and modeling these parameters is significantly computationally expensive. Also, Class 2 and 3 data is not accessible by the public.

The five locations for resource assessments were chosen for specific reasons, as explained in Table 2.

Table 2: Locations for wave resource assessments and reasoning for selection for the study

Location	Lat/Lon	Depth (m)	Reason for selection
PacWave, OR	44.557°, -124.229°	68	Existing wave energy test site infrastructure; aimed at utility-scale resource
Los Angeles, CA	33.854°, -118.633°	350	Less energetic site; close to major city; stable resource
WETS, Oahu, HI	21.466°, -157.751°	34	Goals for 100% renewable energy powered; island state; very stable resource
Miami, FL	25.460°, -80.030°	318	Classified as unusable for classic WEC deployment; physically vulnerable to increased storms due to climate change; close to major population hubs
Cape Cod, MA	41.140°, -70.690°	38	Proximity to Vineyard Wind, new offshore wind turbine location; physically vulnerable to increased storms due to climate change

Three sites in the Pacific and two in the Atlantic oceans were chosen for analysis to provide a varied perspective of small WEC possibilities in the United States. The depth for the five sites varies between 34 m and 350 m. If there was more time for this study to be completed, each site would have been evaluated for depth classification: shallow, intermediate, or deep water. Depending on the

results, different sites would have different applications of the linear dispersion relationship, either employing shallow water assumptions, use of the full linear dispersion equation, or deep water assumptions accordingly. The linear dispersion equation affects the wave power equation used in all relevant calculations. In this study, each location is assumed to be in deep water for simplicity and uniformity, therefore rendering deep water assumptions applicable. For more information regarding linear dispersion and relevant simplifications, readers are directed to Dean and Dalrymple [24].

Spectral wave data for the locations analyzed in this study was obtained from PNNL, which operates within the United States DOE, and from the Sandia National Laboratory. The hindcast model constructed by PNNL used nested-grid WWIII on both global and regional scales [47]. Their WWIII model was paired with a high-resolution, unstructured-grid SWAN model [47]. The output files included project title, latitude and longitude of model run locations, frequencies in Hz, spectral nautical directions in degrees, date and time stamps, and variance density in $m^2/Hz/deg.$ S_{ij} was measured at a range of frequencies and directions depending on the location. Data from 2000-2010 was analyzed to account for potential seasonality for both the IEC and small WEC assessments.

The hindcast model from the Sandia National Lab was constructed using an unstructured mesh with a coastal resolution of 200m, utilizing the SWAN model and forcing from the Climate Forecast System Reanalysis and WWIII [37], [75], [76]. Output files from SWAN contained project title, latitude and longitude of model run locations, frequencies in hertz, nautical directions in degrees, date and time stamps, and variance density (S_{ij}) in $m^2/Hz/deg.$ S_{ij} was measured at a range of frequencies and directions depending on the location.

This study does not aim to provide thorough information and assessment of the wave models, or any wave modeling software for that matter. For further

information regarding wave modeling for this specific hindcast, readers are directed to Wu et al. [47].

4.2 Method validation

An example scenario was created to observe the effects of the power limits on a known wave spectrum. A generic Pierson-Moskowitz (PM) spectrum with significant wave height H_s = 3m and peak period T_p = 10s was created, seen in Figure 7. To see the power limit behavior, three wave periods and associated wave heights were selected. With the three combinations, the radiated power limit and Budal's upper bound were applied to a 2m WEC for both the baseline and expanded cases. The PM spectrum was generated using the Waves Analysis for Fatigue and Oceanography (WAFO) Matlab toolbox [77].

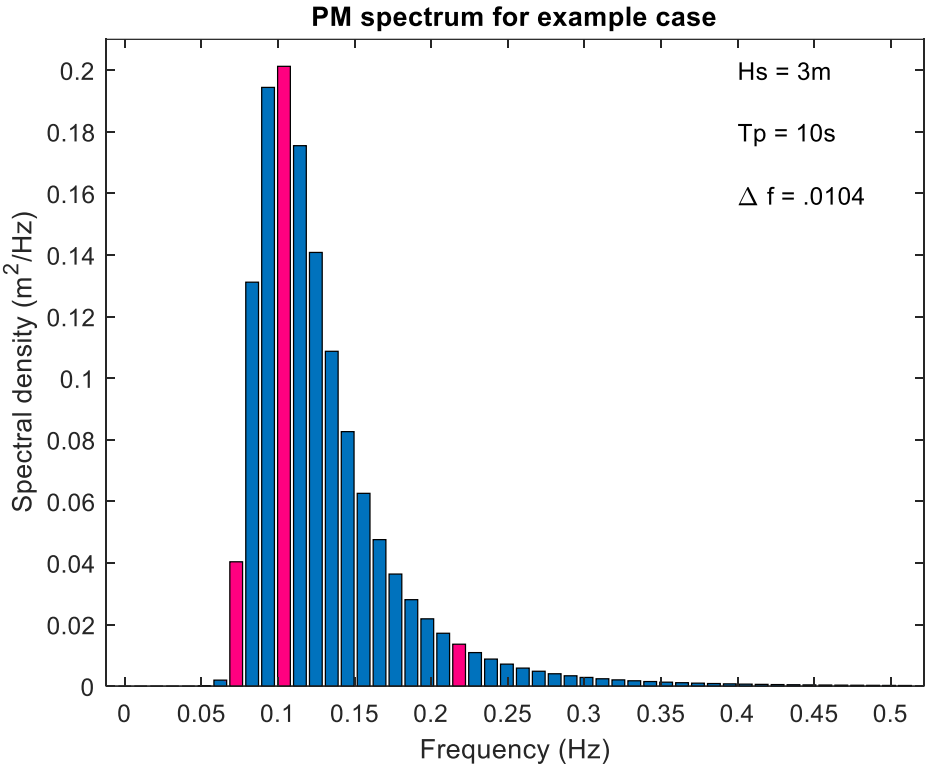

Figure 7: Pierson-Moskowitz spectrum created for example case and method validation. Pink bars correspond to the data selected for further analysis.

The three pink bars in Figure 7 highlight the data used for the example case. The wave height and period from each of the pink bars was used to calculate radiated power, Budal's upper bound, and gross power depending on case. For the baseline case, all the power beneath the radiated power and Budal's upper bound is considered absorbable. However, for the expanded case, with implementation of gross power as a limitation, all the power underneath the three curves is considered absorbable.

Figure 8 shows the Budal diagrams for the baseline and expanded cases associated with the data taken from the first pink bar in Figure 7. This set of data has the second-most amount of energy in out of the three bars.

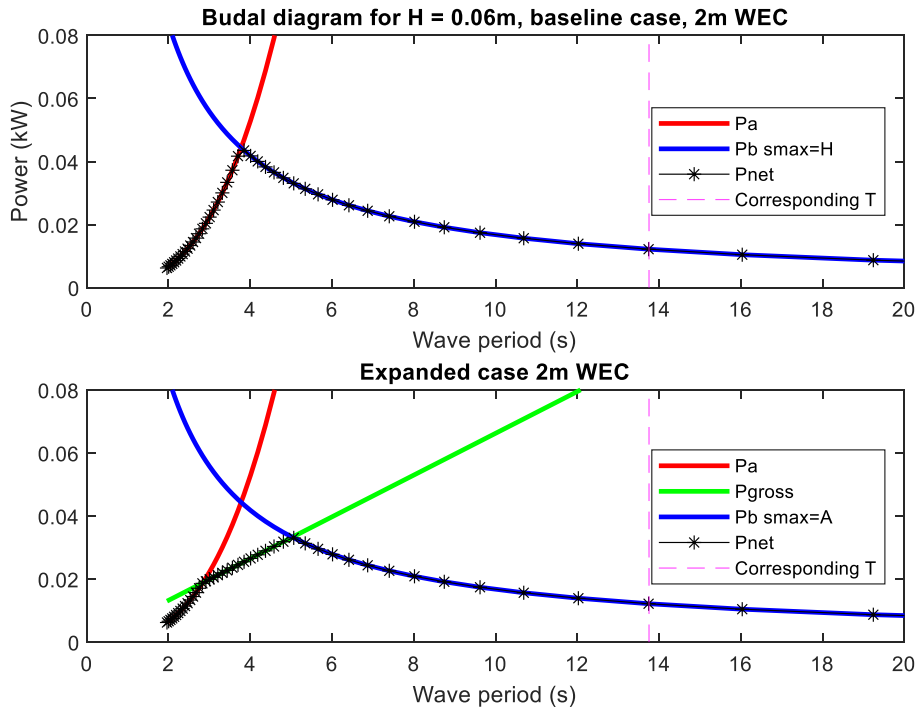

Figure 8: Budal diagrams for the baseline case and expanded case for a 2m WEC in wave height of 0.06m. The black star line corresponds to the net power extractable by the device and the dashed pink line is the wave period at which the wave height was measured.

The Budal diagram for the baseline case in Figure 8 was measured at a 13.8s wave period, highlighted in the plots. The area underneath the curves

represents the total power available for conversion by the 2m WEC. The expanded case yields less power for conversion compared to the baseline because of the implementation of gross power as a limit. Gross power is a necessary limit for determining the power available to small WECs, since power does not exist beyond the gross power available in the sea. Therefore, the Budal diagrams for the expanded case is a more accurate reflection of absorbable power.

Figure 9 shows the Budal diagram for both the baseline and expanded cases for a wave height of 0.09m, corresponding to a wave period of 9.6s. This dataset represents the peak of the spectrum, seen as the middle pink bar in Figure 7.

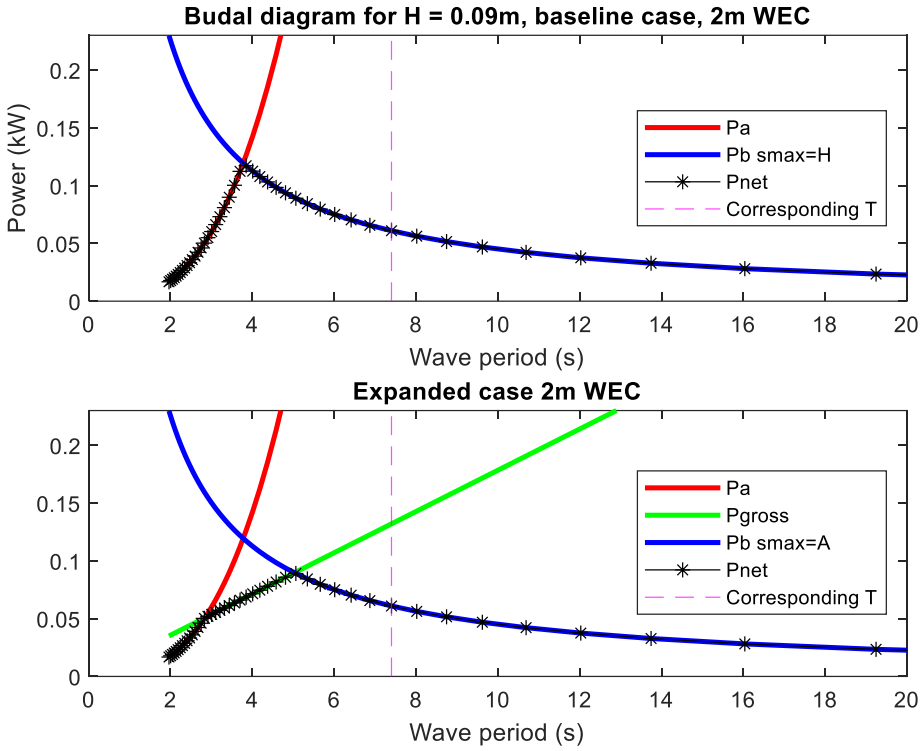

Figure 9: Budal diagrams for the baseline case and expanded case for a 2m WEC in wave height of 0.09m. The black star line corresponds to the net power extractable by the device and the dashed pink line is the wave period at which the wave height was measured.

Again, the expanded case presents less available wave power for conversion compared to the baseline case, a reflection of the imposed reality of the gross power.

Finally, the data from the last combination yields the Budal diagram in Figure 10. The relevant wave height and period are 0.03m and 4.6s respectively.

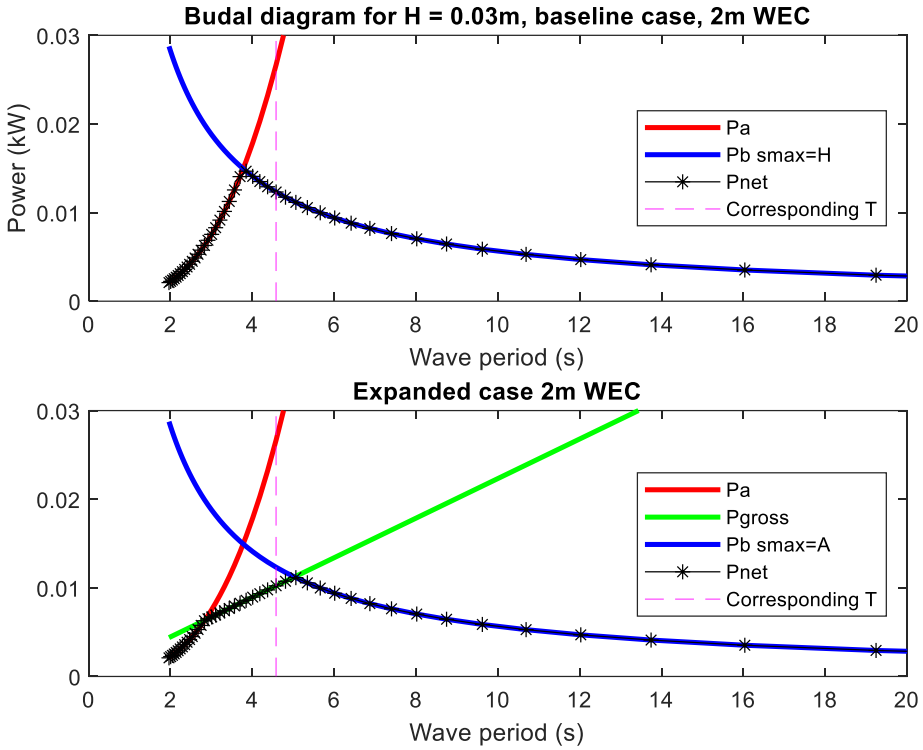

Figure 10: Budal diagrams for the baseline case and expanded case for a 2m WEC in wave height of 0.03m. The black star line corresponds to the net power extractable by the device and the dashed pink line is the wave period at which the wave height was measured.

In Figure 10, the gross power directly limits the absorbable power at the relevant wave period for the expanded case. These example cases for small resource assessments using the PM spectrum allowed for observation of the expected behavior of a spectrum with known shape and behavior when applying the radiation power limit and Budal's upper bound.

Intuitively, it is not clear why gross power is smaller than the radiated power limit and Budal's upper bound, since the latter two are "power limits" and would necessarily limit the gross amount of power absorbable. This issue became present when cementing the methods for the analysis. However, Todalshaug, [21] compared the radiated power limit to gross power available to their WEC of interest. In the analysis, the radiated power limit is in fact larger than the gross power at certain wave periods, however the literature does not explicitly account for this. Future derivations and more intensive work should be explored regarding this relationship.

5. Results

The results pertaining to the IEC Class 1 and the small WEC wave resource assessments. IEC results are presented by location first, followed by small WEC results.

5.1 Traditional wave resource assessments

Bivariate histograms and monthly statistics for significant wave height, energy period, and wave power were found for each location from 2000-2010 using hindcast data modeled by PNNL and Sandia. These results may be classified as a Class 1 – Reconnaissance assessment according to the IEC TS 62600-101 [45]. Table 3 describes the mean and maximum significant wave height, energy period, and wave power per location.

Table 3: Mean and maximum values for significant wave height, energy period, and omnidirectional wave power at each study location from 2000-2010

	Max H_{mo}	Mean H_{mo}	Max T_e	Mean T_e	Max J	Mean J
PacWave	9.70 m	2.30 m	19.80 s	9.70 s	719 kW	36.8 kW
Los Angeles	4.03 m	1.07 m	16.5 s	9.38 s	80.3 kW	5.81 kW
WETS	4.46 m	1.66 m	15.4 s	7.59 s	145 kW	12.6 kW

Cape Cod	7.33 m	1.55 m	16.6 s	6.78 s	344 kW	12.4 kW
Miami	7.44 m	0.857 m	12.9 s	5.49 s	256 kW	3.24 kW

In the following results are the bivariate histograms and variation of wave power throughout the time period. Remaining results for the variation of significant wave height and energy period can be found in Appendix A**: Wave resource assessment results**.

5.1.1 PacWave, Oregon

Figure 11 shows the bivariate histogram of significant wave height and energy period. The numbers in each cell represent the mean annual hours recorded per sea state combination while the shading of the cells reflects the corresponding weighted energy flux, found by $0.5H_{mo}^2T_e$ multiplied by hours of occurrence.

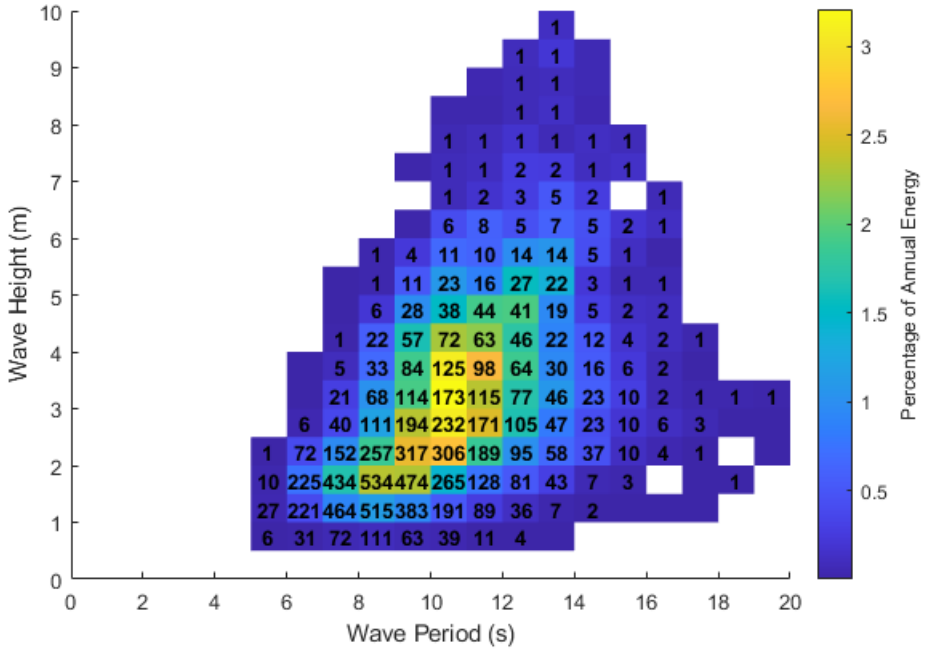

Figure 11: Bivariate histogram for the PacWave South site off the coast of Newport, OR from 2000-2010 (mean annual conditions)

The most commonly occurring sea state at PacWave has a significant wave height of 1.75m and an energy period of 8.5s for an average of 534 hours per year. The sea state contributing to the highest energy flux occurs on average 173 hours per year (~ 2% per year) with a significant wave height of 3.25m and an energy period of 10.5s. A wide variation of sea states is observed at PacWave, and is indicated by the spread of mean hours of H_{mo}-T_e combinations apparent in Figure 11.

Figure 12 presents the monthly mean, mean + standard deviation, mean – standard deviation, 10th, 50th (median), and 90th percentiles of omnidirectional wave power from 2000-2010 at PacWave, per IEC requirements for a Class 1 assessment.

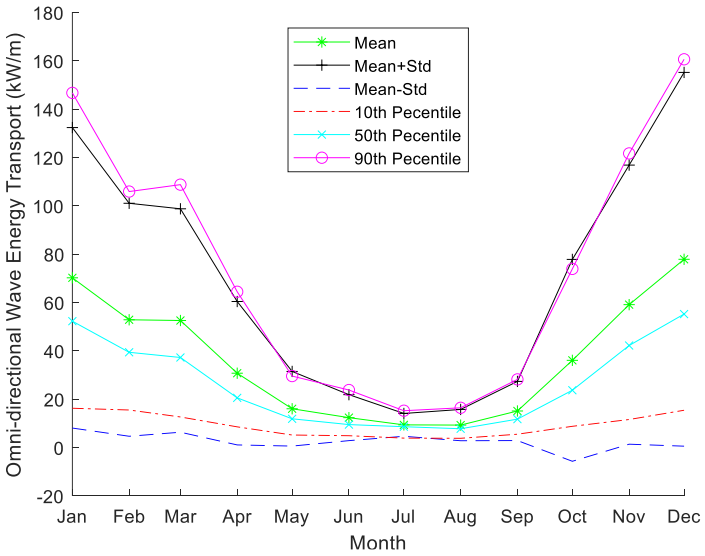

Figure 12: Monthly statistics for omnidirectional wave power at PacWave South from 2000-2010

Seasonality is reflected in Figure 12. Mean winter measurements of omnidirectional wave power fluctuate between 53 kW/m and 77 kW/m while summer values range between 9 kW/m and 16 kW/m. Skewness is apparent in the dataset since the average J is greater than the median in most months.

5.1.2 Los Angeles, California

Figure 13 presents the bivariate histogram off the coast of Los Angeles from 2000-2010. The most commonly occurring sea state also corresponds to the most energetic sea state, accounting for an average of 955 hours per year (~ 11% per year). This sea state has a significant wave height of 1.25m and an energy period of 8.5s. Less variation of sea states are apparent in Los Angeles, indicated in Figure 13 by the relatively small range of significant wave height and energy period values

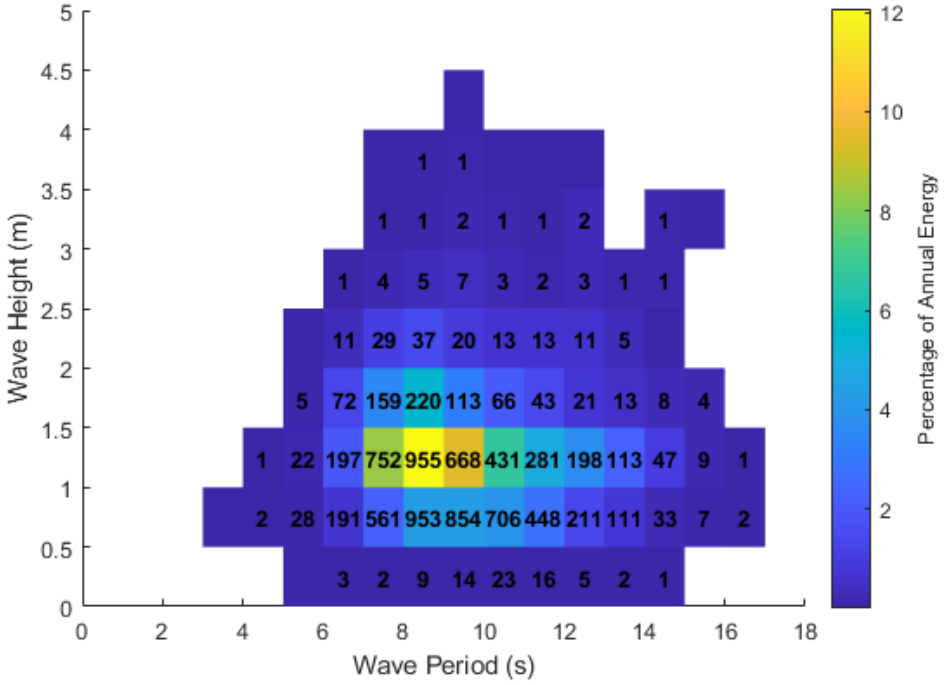

Figure 13: Bivariate histogram for Los Angeles from 2000-2010 (mean annual conditions)

. Figure 14 shows the monthly statistics for omnidirectional wave power for the Class 1 assessment requirements [45].

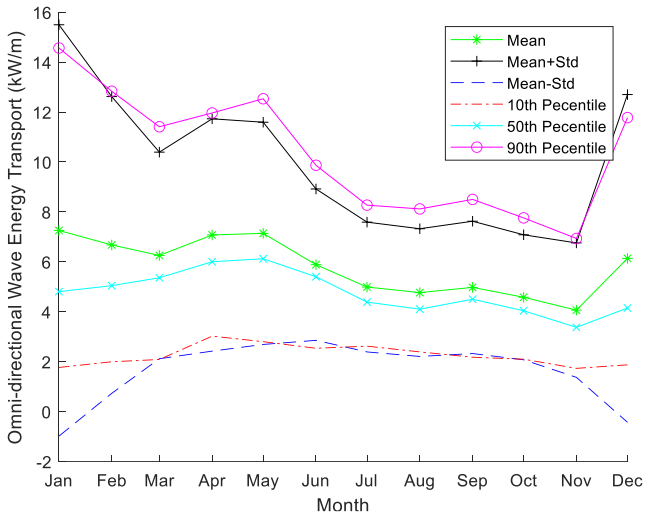

Figure 14: Monthly statistics for omni-directional wave power at Los Angeles from 2000-2010

Average wave power ranges from 4 kW/m to 7.2 kW/m throughout the year. Slight skewness is apparent in the winter months when the mean is greater than the median value.

5.1.3 WETS, Oahu, Hawaii

The most energetic and most frequently occurring sea states are one in the same at the Wave Energy Test Site (WETS) off the coast of Oahu, Hawaii. This significant wave height – energy period combination accounts for 1448 hours per year (~ 16.5% per year). Again, a less varied makeup of sea states is present at WETS indicated by the small spread of average hours of occurrence shown in Figure 15.

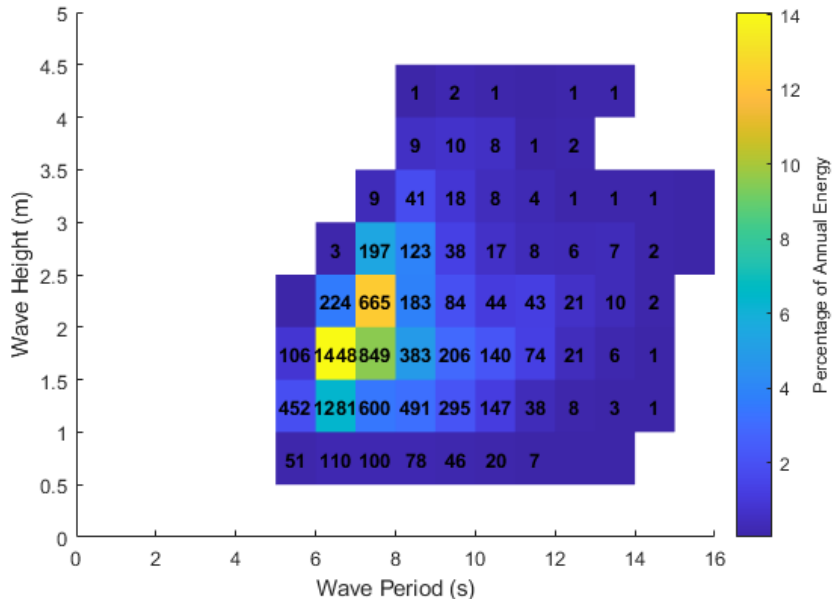

Figure 15: Bivariate histogram for WETS from 2000-2010 (mean annual conditions)

Figure 16 shows the monthly statistics for omnidirectional wave power at WETS from 2000-2010. Winter months see greater values on average throughout the time period, varying between 15.5 kW/m and 18.5 kW/m. Summer months average between 7.5 kW/m and 8.5 kW/m.

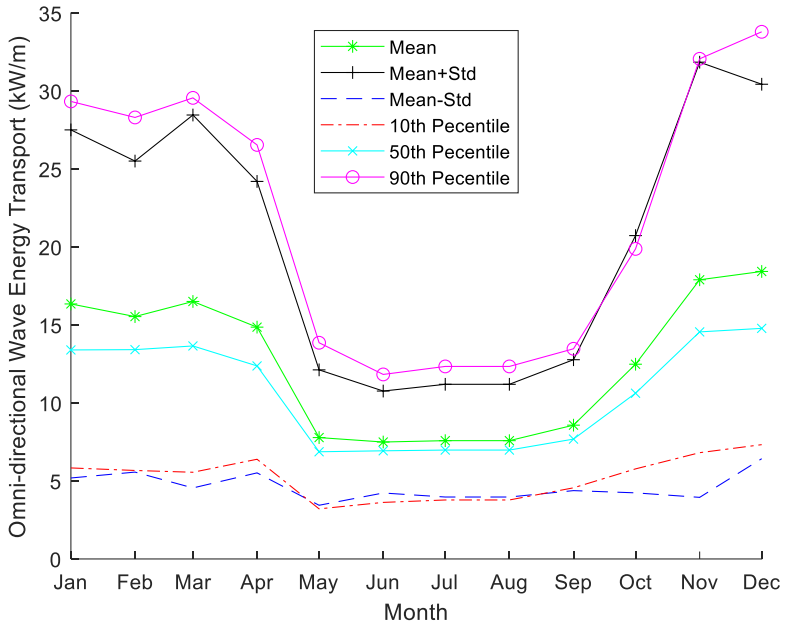

Figure 16: Monthly statistics for omni-directional wave power at WETS from 2000-2010

5.1.4 Cape Cod, Massachusetts

Offshore of Martha's Vineyard and Cape Cod, Massachusetts, the wave energy resource is fairly varied with the most energetic sea states concentrating between 4.5s-9.5s T_e and 1.25m and 4.5m significant wave height as seen in Figure 17. The most frequently occurring sea state on average takes place at 1.25m significant wave height and 6.5s energy period for 915 hours per year (~10.5% per year) on average. The most energetic sea state occurs at 2.25m significant wave height and 6.5s T_e for 324 hours per year (~4% per year) on average.

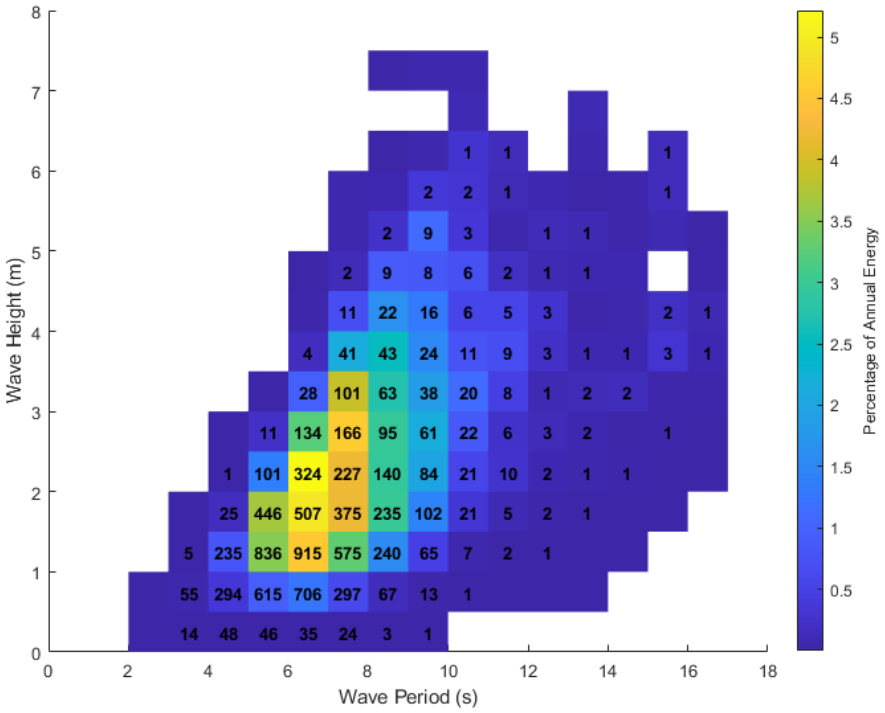

Figure 17: Bivariate histogram for Cape Cod from 2000-2010 (mean annual conditions)

In Figure 18, omnidirectional wave power varies seasonally on average throughout the year, with maximum power occurring in winter months and minimums in summer months. Peak average wave power occurs in December at 20 kW/m while minimum is in August at 6.5 kW/m. This was expected due to storm frequency in the fall and winter.

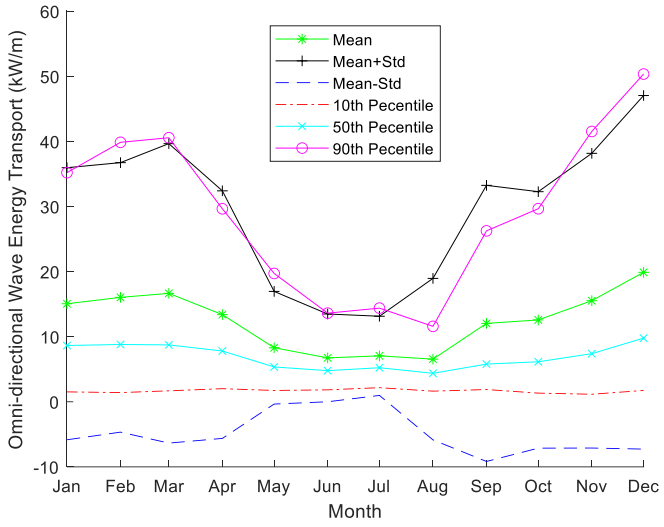

Figure 18: Monthly statistics for omni-directional wave power at Cape Cod from 2000-2010

5.1.5 Miami, Florida

The last site used to complete an IEC wave energy resource assessment is offshore southeast of Miami, Florida. As shown in Figure 19, most significant wave heights range between 0.25m and 5.25m, with outliers between 5.75m and 7.25m. Energy period ranges between 2.5s and 12.5s. The most frequently occurring sea state is composed of a 0.75m significant wave height and 4.5s energy period for 1420 hours per year (~16% per year) on average. The most energetic sea state is slightly larger overall, with a significant wave height equal to 1.25m and energy period equal to 5.5s for 714 hours per year (~8% per year) on average.

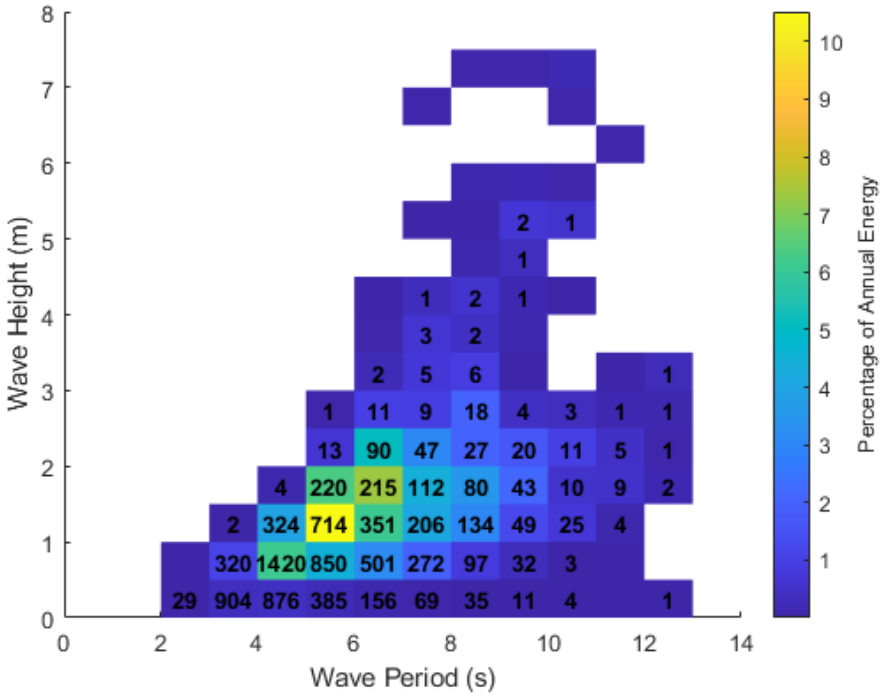

Figure 19: Bivariate histogram for Miami from 2000-2010 (mean annual conditions)

Figure 20 shows the monthly statistics for omnidirectional wave power by month from 2000-2010. Wave power varies seasonally with a maximum average of 5 kW/m in Jan. and minimum of 0.9 kW/m in July. Positive skewness is evident in the fall and winter months where the mean is larger than the median, due to storms during these time periods [78].

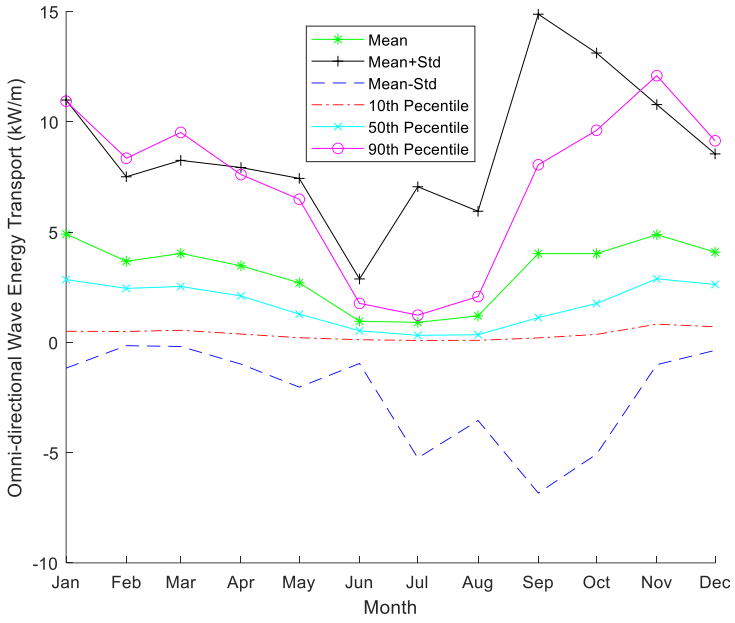

Figure 20: Monthly statistics for omni-directional wave power at Miami from 2000-2010

5.2 Small WEC Resource Assessments

The annual net power production for the baseline and expanded cases were found and compared to the annual power found from the IEC analysis. For comparison purposes, the gross wave power from the IEC assessment was normalized by device size and the y-axis in Figure 21 is on a logarithmic scale.

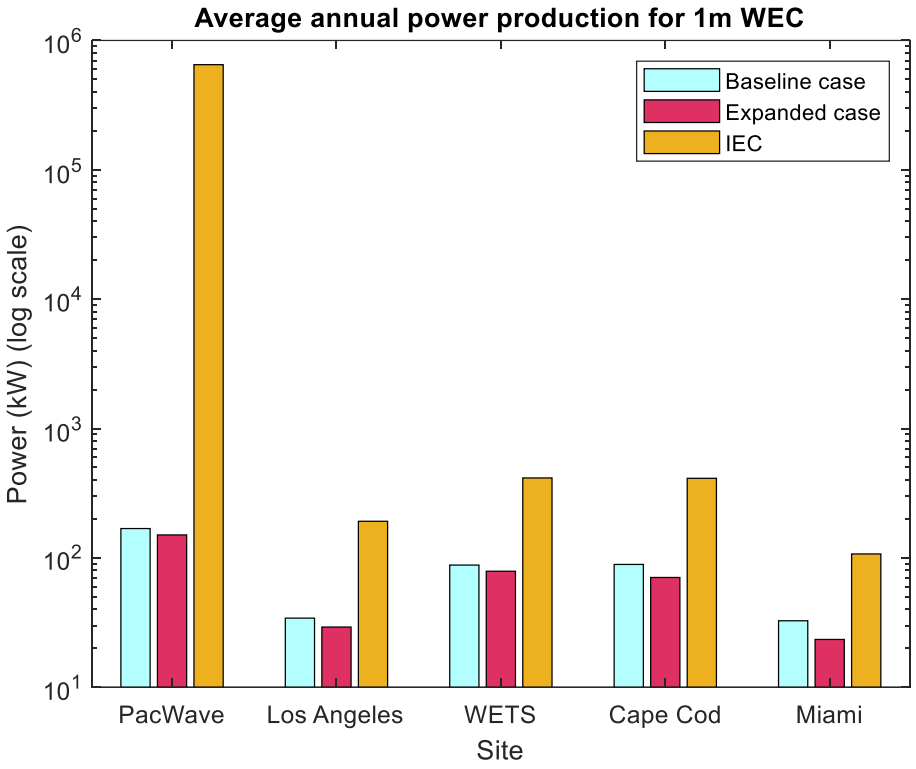

Figure 21: Total average annual power production for a 1m WEC from 2000-2010 for the baseline case and expanded case compared to the average annual gross power available according to the IEC assessment (y-axis is in logarithmic scale)

Figure 21 shows the average annual power production for a 1m WEC. As expected, the power found through the IEC assessment is much greater than both the baseline and expanded cases for net power filtration. The gross power available for absorption according to the IEC assessment is about four orders of magnitude greater than both the baseline and expanded cases at PacWave. At the remaining locations, the IEC power is about 0.5 magnitudes greater than the net power found in the baseline and expanded cases for the 1m device. The baseline case is at the same scale of power as the expanded case, but overall produces greater average annual net power.

Consistently, the IEC calculated wave power was much larger than the baseline and expanded cases. Results for the 2m, 5m, and 10m WECs and can be found in Appendix A**: Wave resource assessment results**.

The average annual power production for each site is detailed in Appendix A**: Wave resource assessment results**. Figure 22 shows the results for PacWave, OR. For each WEC size, the baseline case yields a greater amount of average power per year than the expanded case. This was expected, since the baseline case only utilized the radiated power limit and Budal's upper bound to filter out absorbable power, while the expanded case utilizes gross power along with the remaining power limits.

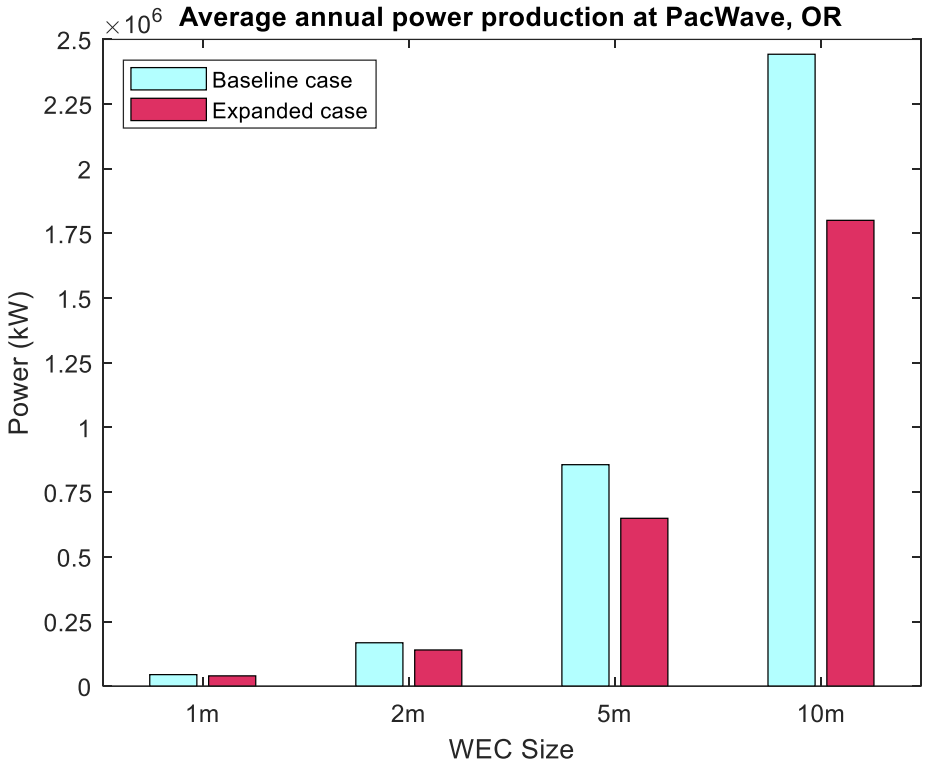

Figure 22: Total average annual power production for the WECs from 2000-2010 for the baseline case and expanded case at PacWave, OR

As WEC sizes increases, the disparity between the two cases grows larger. Again, this is due to the use of the gross power, radiated power limit, and Budal's upper bound by the expanded case. While gross power increases with WEC size, it only does so linearly compared to the exponential increase of Budal's upper bound with size. The same results were found for the remaining sites and can be found in Appendix A**: Wave resource assessment results**.

The percent reduction between the two cases for each site is detailed in Table 4. Percent reduction is the difference between the total power production from 2000-2010 for the baseline and expanded cases in percentage form.

Table 4: Percent reduction between baseline and expanded cases of power limit applications for all WEC sizes and study locations from 2000-2010

	1m WEC	**2m WEC**	**5m WEC**	**10m WEC**
PacWave	11%	17%	24%	26%
Los Angeles	15%	19%	22%	22%
WETS	10%	18%	27%	23%
Cape Cod	21%	25%	25%	20%
Miami	28%	30%	24%	16%

For the 1m device, WETS had the smallest decrease between power production for the baseline and expanded cases over the course of the time period followed by PacWave, Los Angeles, Cape Cod, and Miami. Interestingly, the reverse is true for the 10m device: Miami has the smallest difference between the two cases, followed by Cape Cod, Los Angeles, WETS, then PacWave.

Next, the power filters were applied to the gross power in the spectra at each location. WECs of sizes 1m, 2m, 5m, and 10m were evaluated for the small WEC resource assessments. In Figure 23 are the mean net power and COV for the baseline case and the expanded case (see Table 1 for details per case scenario).

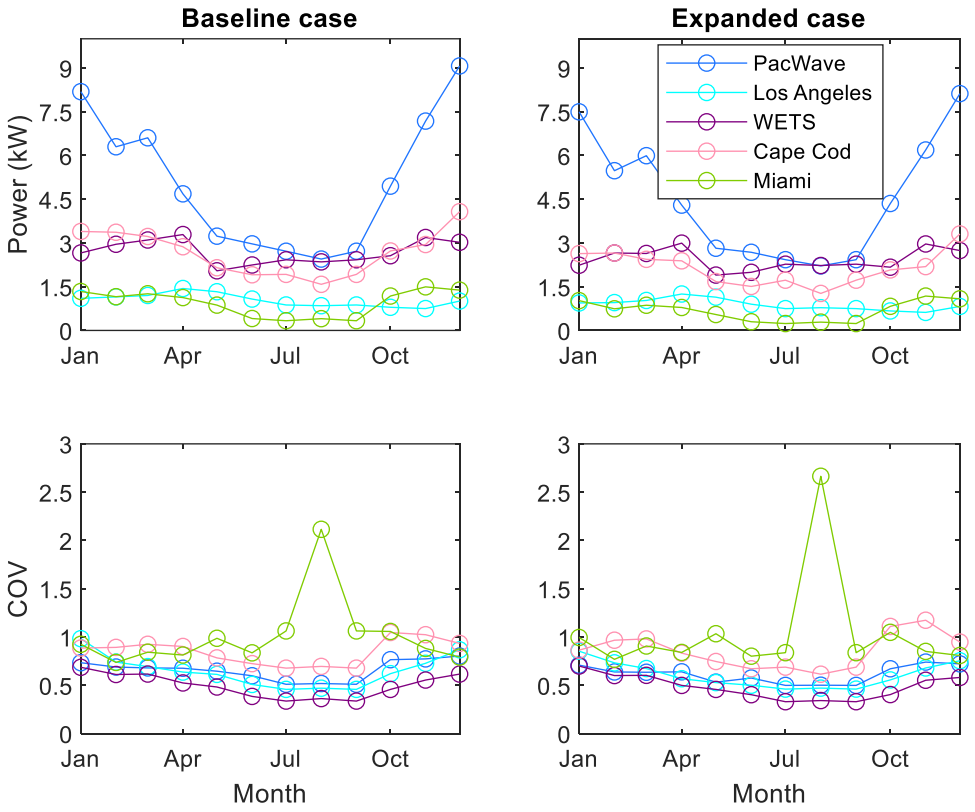

Figure 23: Monthly average power and COV for the baseline and expanded cases applied to a 1m WEC from 2000-2010

Figure 23 shows that all average net power is less than 10 kW at all study locations for a 1m WEC. PacWave sees the greatest amount of P_{net} on average throughout the year, while Miami and Los Angeles see the least. The baseline case sees more power throughout the average year at all sites; PacWave has a maximum mean P_{net} of 9 kW in December, the maximum for Los Angeles is 1.4 kW in April, for WETS is 3.3 kW in April, for Cape Cod is 4 kW in December, and for Miami is 1.5 kW in November. The expanded case has maximum P_{net} of 8 kW at PacWave in December, 1.2 kW at Los Angeles in April, 3 kW at WETS in April, 3.3 kW at Cape Cod in December, and 1.2 kW at Miami in November.

The COV of net power for the different sites varies throughout an average year as well. For both the baseline and expanded case have maximum COVs greater than 2 at Miami in the month of August. The lowest COV for the entire year on average is found at WETS, staying below 0.7 for both cases. Los Angeles and PacWave have comparable COVs, while Cape Cod and Miami are the two sites with the largest values throughout an average year.

The same pattern of monthly average power and COV are seen for the remaining WEC sizes, results for which can be found in Appendix A**: Wave resource assessment results**.

Annual maximums were found for all five locations and WEC sizes throughout 2000-2010 for both the baseline and expanded cases. The maximum net power at all five locations for each size for the expanded case are shown in **Error! Reference source not found.** through **Error! Reference source not found.**.

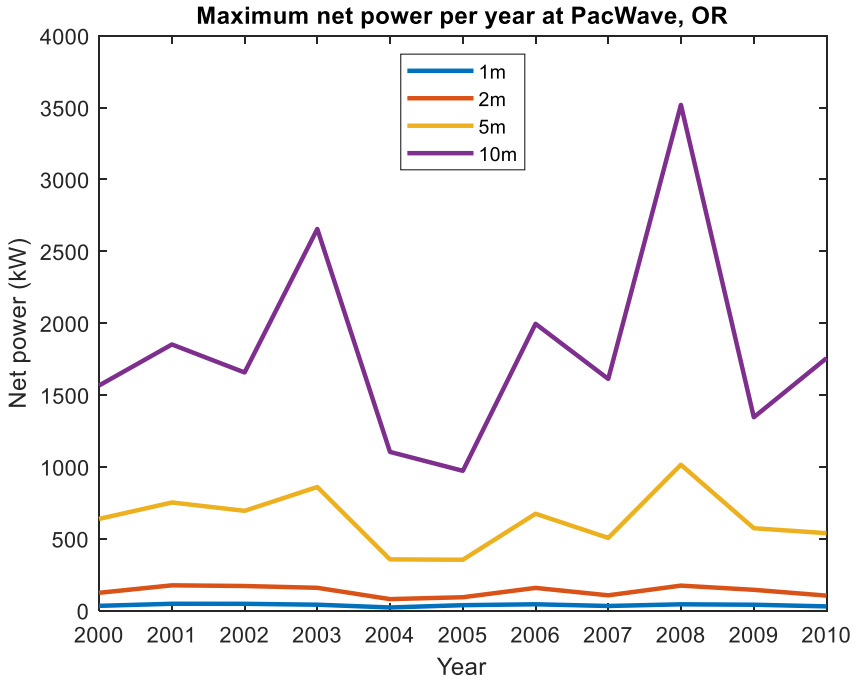

Figure 24: Annual maximum net power for the expanded case at PacWave from 2000-2010

Error! Reference source not found. gives an idea of the most power that the devices will encounter at PacWave for the expanded case. The 1m and 2m devices consistently have maximum power measurements under 300 kW while the 5m and 10m WECs encounter more incident waves, and therefore will see a greater range of wave power. PacWave sees the largest amount of wave power for any device, with maximums for the 10m WEC between 1000 kW and 3600 kW.

For the 5m and 10m devices on the West Coast, maximums spike in 2002, 2003, 2006, and 2008. All of these years pertain to El Niño events, which cause increased wave heights and wave periods due to storm activity induced by warmer-than-average temperatures [79]. During these years, the 1m and 2m maximums either slightly increase, stay the same, or decrease; large wave periods are not conducive to power absorption for the 1m and 2m WECs, as they resonate at lower frequencies. Therefore, these devices did not see a spike in maximum power absorption.

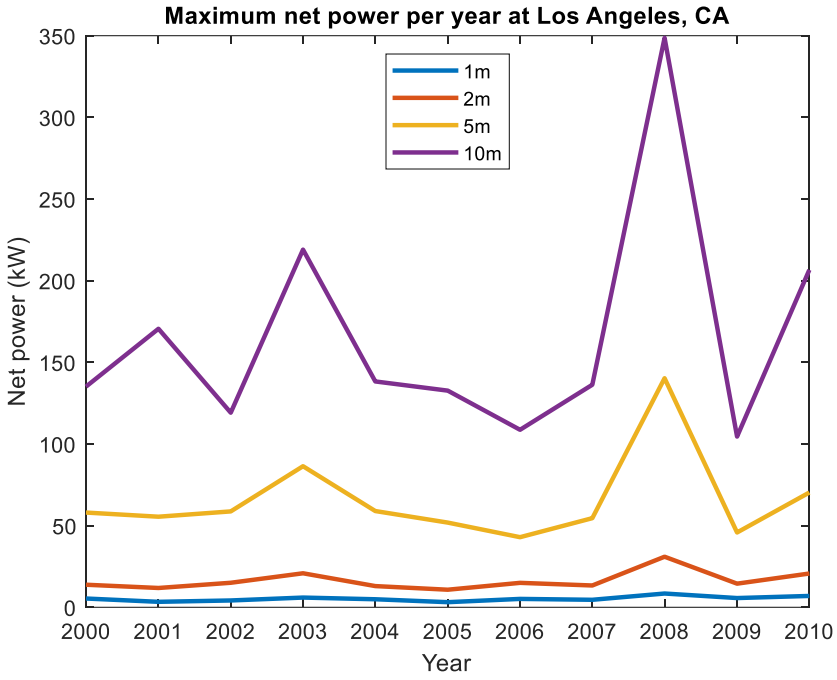

Figure 25: Annual maximum net power for the expanded case at Los Angeles from 2000-2010

Figure 25 shows the maximum net power per year for the expanded case at Los Angeles from 2000-2010. 1m and 2m device maximums stay well below 50 kW each year while the 5m and 10m devices have maximums ranging from 50 kW to 350 kW. Again, spikes in the maximum net power for 5m and 10m devices occur in El Niño years at Los Angeles, while smaller spikes or decreases occur in these years for the 1m and 2m WECs.

Figure 26 shows the maximum net power per year for the baseline case at WETS for the given time period. Maximums for the 1m and 2m devices are slightly larger than those seen at Los Angeles but remain under 10 kW for years 2000-2010. The maximums for the 5m and 10m devices are almost double those for Los Angeles, ranging between 100 kW and 860 kW. Relatively smaller spikes occur in years 2002 and 2008 for WETS compared to Los Angeles and PacWave, with larger spikes occurring in 2003 and 2008. The spike in 2003 is due to Hurricane Jimena, which skimmed by Oahu leading to high surf [80]. The 1m and

2m devices are unable to capture power from such waves, with large heights and periods, and therefore do not have as large of spikes. The maximum net power seen by these devices remains relatively consistent throughout the time period.

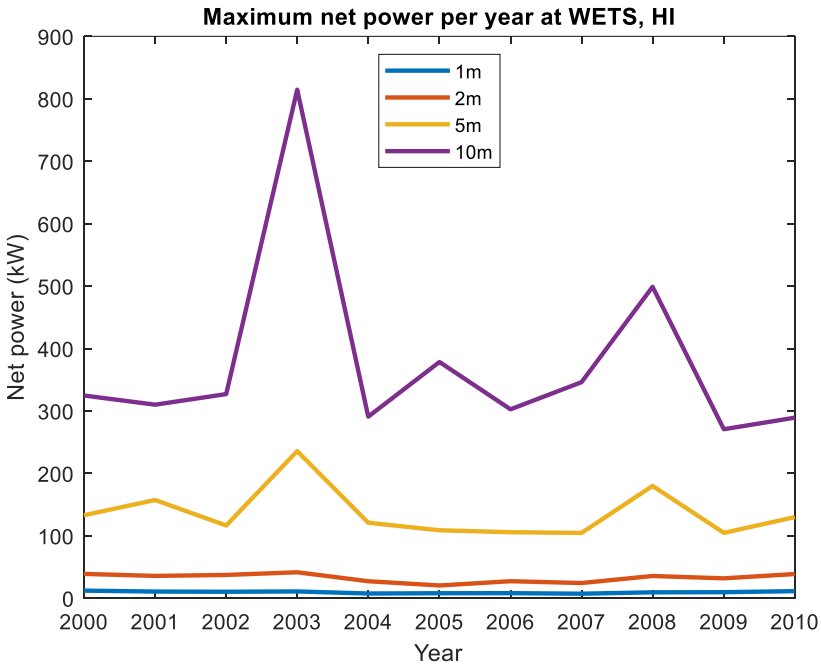

Figure 26: Annual maximum net power for the expanded case at WETS from 2000-2010

Figure 27 describes the maximum net power measurements for the baseline case at Cape Cod for years 2000-2010. The scale of the net power available for conversion at Cape Cod is about comparable to that of WETS, but with a few years possessing greater maximums. The 10m device sees the largest maximums in select years since it is the WEC that interacts with the most incident wave power. Spikes in the maximums occur in 2003, 2006, and 2008, all of which correspond to abnormally active storm seasons, which include hurricanes, tropical depressions, and tropical storms. Again, 1m and 2m WECs are less able to capture the wave power from large wave heights and periods that occur with storm events. Therefore, these two devices do not see the same spikes in maximum net power as their larger counterparts do.

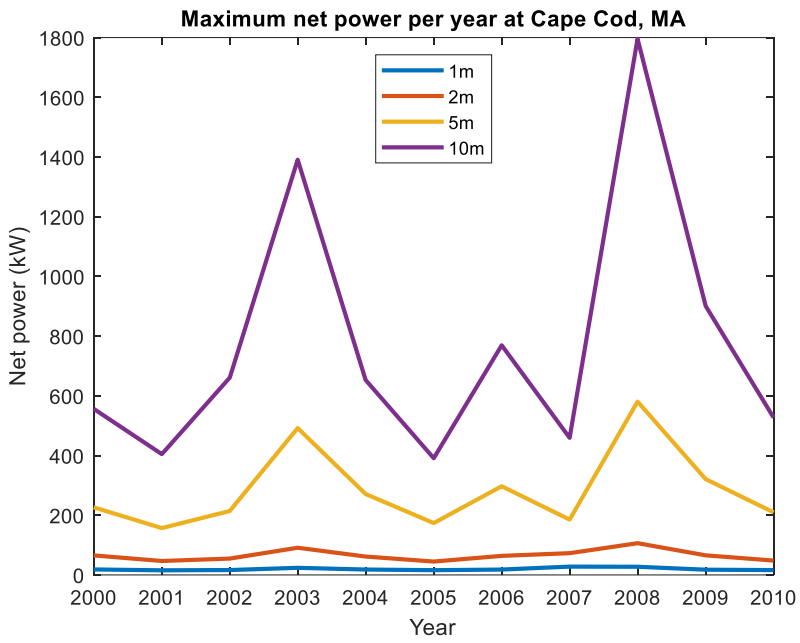

Figure 27: Annual maximum net power for the expanded case at Cape Cod from 2000-2010

Annual maximum measurements for net power for the expanded case for Miami are shown in **Error! Reference source not found.**. The maximums for all years and device sizes stay below 300 kW until 2008 when all devices saw a spike in maximum net power available. Again, 2008 corresponds to a very active storm season on the southern Atlantic coast, whereas 2003 and 2006 were not as impactful in the region as they were in Cape Cod.

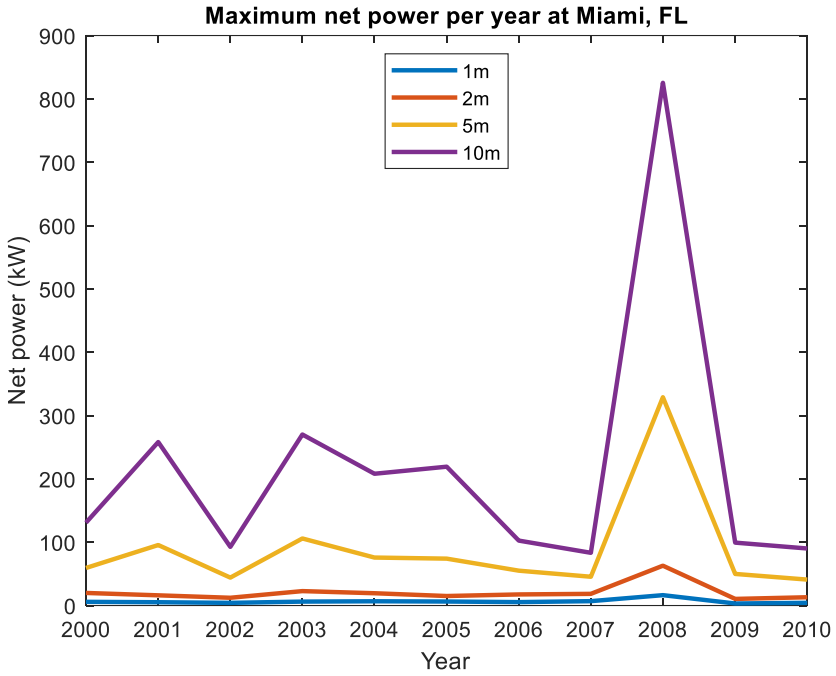

Figure 28: Annual maximum net power for the expanded case at Miami from 2000-2010

Resolving years' worth of wave power data to averages and maximums can understandably downplay the difference between individual net power measurements. To illustrate the difference between the baseline and expanded case at a higher resolution, an excerpt of the time series of P_{net} for both cases was plotted in Figure 29.

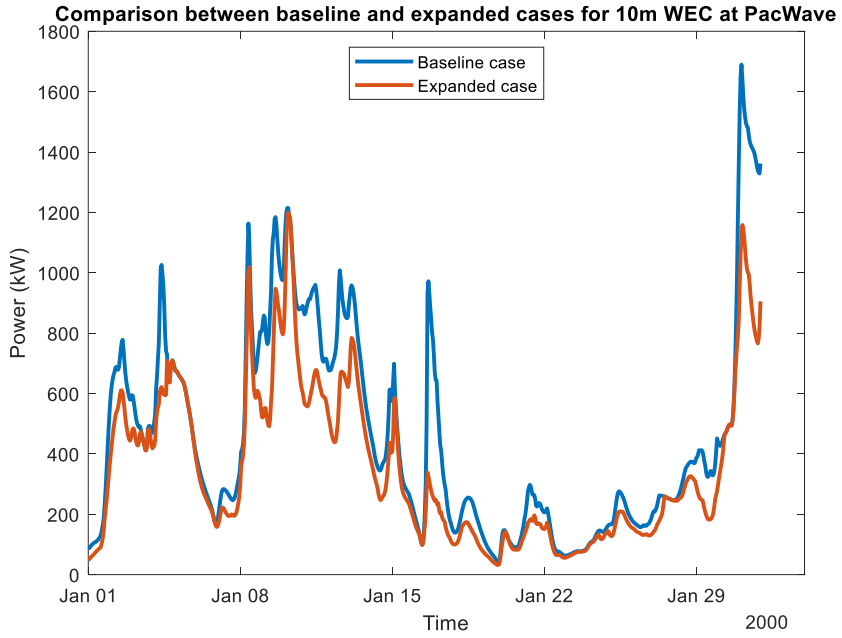

Figure 29: Time series of net power measurements for the baseline and expanded cases of a 10m WEC at PacWave, OR. This excerpt is from the month of January in 2000.

While most measurements have negligible differences between the baseline and expanded cases, certain timesteps vary greatly. For instance, on January 17th, the expanded case measured 375 kW and the baseline case measured 1100 kW. On January 30th the expanded case measured a net power of 1200 kW while the baseline case measured 1750 kW. While these differences may not be blatantly apparent through statistical analyses, they are noteworthy and demonstrate the contrast between the baseline and expanded cases.

Table 5 through Table 8 give values for the mean hourly, max hourly, and total differences between the baseline and expanded case for all study locations and device sizes from 2000-2010.

Table 5: Summary of discrete differences between the baseline and expanded cases at all study locations for 1m WEC from 2000-2010

1m WEC	**Mean hourly difference**	**Max hourly difference**	**Total difference from 2000-2010**

PacWave	0.548 kW	36.4 kW	52.8 MW
Los Angeles	0.152 kW	7.16 kW	14.7 MW
WETS	0.276 kW	6.09 kW	2.67 MW
Cape Cod	0.557 kW	22.1 kW	5.38 MW
Miami	0.279 kW	18.0 kW	2.70 MW

Table 6: Summary of discrete differences between the baseline and expanded cases at all study locations for 2m WEC from 2000-2010

2m WEC	**Mean hourly difference**	**Max hourly difference**	**Total difference from 2000-2010**
PacWave	3.18 kW	165 kW	306 MW
Los Angeles	0.699 kW	26.8 kW	67.4 MW
WETS	1.74 kW	26.5 kW	168 MW
Cape Cod	2.31 kW	72.7 kW	223 MW
Miami	0.877 kW	35.8 kW	84.7 MW

Table 7: Summary of discrete differences between the baseline and expanded cases at all study locations for 5m WEC from 2000-2010

5m WEC	**Mean hourly difference**	**Max hourly difference**	**Total difference from 2000-2010**
PacWave	23.6 kW	755 kW	2.28 GW
Los Angeles	3.31 kW	108 kW	320 MW
WETS	11.5 kW	169 kW	1.11 GW
Cape Cod	8.96 kW	369 kW	865 MW
Miami	2.14 kW	74.9 kW	207 MW

Table 8: Summary of discrete differences between the baseline and expanded cases at all study locations for 10m WEC from 2000-2010

10m WEC	**Mean hourly difference**	**Max hourly difference**	**Total difference from 2000-2010**
PacWave	73.3 kW	2.32 MW	7.06 GW
Los Angeles	8.50 kW	196 kW	820 MW
WETS	23.3 kW	254 kW	2.15 GW
Cape Cod	15.5 kW	429 kW	1.50 GW
Miami	2.71 kW	298 kW	262 MW

As expected, as the device size increases, the mean, max, and total differences between the two cases increase as well. Notably, the total difference in power increases with WEC size from MW-scale at the 1m device to GW levels of power at the 10m device. Therefore, as device size increases, the gap between the two cases expands accordingly.

6. Discussion

Overall, there are some noteworthy disparities in this work. One disparity is the sizable difference in WEC power deemed available for absorption by the IEC specification versus the small WEC resource assessments. Another is the considerable difference between the baseline case for net power quantification and the expanded case. The results of the comparisons are in the subsequent discussions.

6.1 IEC Resource assessments

The traditional resource assessments conducted according to the IEC TS 62600-101 provide a comprehensive look at the gross wave energy available in the sea at each location. At PacWave, the histogram in Figure 11 displays a great variety of sea states, from significant wave height between 0.75 m and 9.75 m and energy period between 5.5s and 19.5s. The positively skewed significant wave

height in the winter month datasets indicate that storm conditions are present in this time period.

Further down the coast, Los Angeles wave conditions are much more concentrated in terms of significant wave height and energy period. Figure 13 shows that significant wave height and energy period combinations range between 0.25m-4.25m and 3.5s-16.5s respectively, a much narrower and smaller band than PacWave. Additionally, the monthly variations of omnidirectional wave power are much smaller than PacWave, seen in Figure 14. This indicates that the gross wave resource is steadier throughout the year rather than increasing only in the winter months due to storms, like PacWave. These results are expected as PacWave is at a higher latitude than Los Angeles, and more susceptible to energetic wave conditions due to increased storm activity [73].

WETS in Hawaii possesses an even smaller range of energetic sea states than Los Angeles, with significant wave height between 0.75m and 4.25m and energy period between 5.5s and 15.5s according to Figure 15. There is slight skewness in the omnidirectional wave power dataset in the winter months due to storms, but overall, the average monthly statistics for WETS are quite normally distributed. Increased power in the winter months is due to storm activity. And, although WETS has a smaller range of sea states present than Los Angeles, the site possesses a greater amount of omni-directional wave power on average. WETS is at a lower latitude than Los Angeles, but is subject to distant storms and sea states generated by the trade winds that affect the islands [13].

The resource assessments for the Pacific locations reinforce that gross wave energy is greatest at higher latitudes in continental sites like PacWave, however the greatest magnitude of energy is present in the winter months only. WETS and Los Angeles present the opportunity to convert a steadier amount of resource throughout the entire year; less energetic sea states on average additionally mean less issues with WEC survivability. For non-grid related WEC

deployment applications, WETS and Los Angeles prove to be more attractive locations for these reasons.

Offshore of Cape Cod on the East Coast of the United States, there are greatly varied wave conditions as shown by Figure 17. There is some positive skewness in the dataset as demonstrated by the variation of the omnidirectional wave power monthly statistics. Like the Pacific, this is due to increased storms present in the winter months [73].

Off the coast of Miami, Florida, there is less variation in the sea states exemplified by the bivariate histogram in Figure 19. There is greater variation of wave parameters significant wave height and energy period at this location, due to its increased susceptibility to storms from the north and south Atlantic ocean compared to Cape Cod [78]. Slight positive skewness is evident in the dataset throughout the year due to fall and winter storms correlating with hurricane and nor'easter events.

Both Cape Cod and Miami present minimal variation of wave power on average throughout the year, indicating that these sites would provide a steady amount of wave power regardless of season. Additionally, along with WETS and Los Angeles, less energetic seas overall may increase the chances of WEC survivability.

6.2 Small WEC resource assessments

For the small WEC assessment, 1m, 2m, 5m, and 10m diameter WECs were evaluated. To integrate some practicality to the assessment, a dynamic stroke limit for both the status quo and novel small WEC resource assessments was applied (see Table 1 for details). Implementing a dynamic stroke limit based on body diameter has previously been researched with the purpose of implementing restrictions to WEC power absorption [20].

This goes one step further in this study, where another limitation is added: the gross wave power itself, P_{gross}. As explained in the previously, the radiated power limit and Budal's upper bound can sometimes, mathematically, be larger than the gross power due to the perfect absorption nature of the power limits. Yet, any wave power limit that is greater than the gross power available to a device is not real, and therefore must be ignored. By utilizing all three as power limits, unrealistic parts of the power limits are ignored, and realistic restrictions are imposed.

Applying the power limits to actual wave hindcast data, the average annual power production, or available power, was calculated for each study location and WEC size. Both the baseline and expanded cases were examined along with the IEC-calculated power available for conversion. Figure 21 shows this for a 1m WEC at all five sites, while the remaining sizes' results can be found in Appendix A**: Wave resource assessment results**.

Overall, PacWave has the greatest amount of annual power available for wave energy conversion for all WEC sizes and locations. In each analysis, the IEC assessment methods overestimated the available power for wave energy conversion. The baseline and expanded cases both seriously limit the amount of power available, as they are orders of magnitude less than what is available according to the IEC power. This occurs since the methods from the IEC TS 62600-101 calculate gross wave power and consider the resulting value entirely extractable. Additionally, the WEC devices aimed at extracting this gross power are geared toward utility use and are extremely large in comparison to the small WECs studied in this thesis. These results go to show that small devices may absorb much less power, in some cases four orders of magnitude less, than the IEC specification deems possible, and highlights the need for altered resource assessments for small devices.

Between the baseline and expanded cases, there are also sizable differences. Table 4 describes the percent reduction (difference) between the baseline and expanded cases for each WEC size and location. For the 1m device, discrepancies between the cases range between 10% and 28% depending on location; the 2m device sees percent reductions between 17% and 30%; the 5m device sees reductions between 22% and 27%; and the 10m WEC sees percent reductions between 16% and 26%.

These discrepancies highlight the effect the small WEC resource methods have on the total power available for conversion. The baseline case overestimated the available power for conversion. Without inclusion of the inherent limit gross power, the baseline case yields an impossible amount of wave power, as gross power restricts both the radiated power limit and Budal's upper bound at times, as predicted by Figure 6.

When the percentage reduction between the two cases is small, the radiated power limit and Budal's upper bound are the dominating restrictions for the net absorbable power. This is because the expanded case-calculated net power approaches that of the baseline, which only employs the radiated power limit and Budal's upper bound. When the percentage reduction between the two cases gets larger, the net power values between the two become further apart, indicating that the gross power is more restrictive for the expanded case. Therefore, when the percent reduction is low for a specific device and location, there is an opportunity to get net power absorption close to the theoretical maximum presented by the baseline case.

Specifically, the 1m WEC extracts the most relatively available net power at PacWave, Los Angeles, and WETS, while the 10m device extracts the most relatively available net power for Cape Cod and Miami. This finding was not anticipated, as PacWave has the most gross wave power and Miami has the least. At PacWave, there are an abundance of high-frequency waves in the summer

months, which the 1m device may resonate frequently with [8]. Similarly in Cape Cod and Miami, storm seasons in the fall and winter induce long period waves [78], [81], which can induce motion in the relatively larger small WECs like the 10m device. These storm events also skew the data by relatively increasing the mean and other statistics, as discussed in Section 3.1 **Traditional wave energy resource assessments**.

Locations like WETS and Los Angeles have more steady sources of wave power compared to the other study locations and have the smallest percentage reduction for the 1m WEC. For the 1m device at these locations, the radiated power limit and Budal's upper bound restrict the net power more than the gross power.

To further investigate the difference between the baseline and expanded cases, monthly means and COVs for an average year were computed for the net power available to each device at all study locations. Figure 23 along with the remaining figures in Appendix A**: Wave resource assessment results** display these results.

The average net power is greater in the baseline cases for all WEC sizes and locations compared to the expanded cases. This was expected, given the annual power production analysis consistently showed the baseline case as having greater absorbable wave power than the expanded case.

The monthly COV describes the variation of the dataset from the mean values. A larger COV means that the calculated net power varies greatly, therefore indicating that the wave resource is less steady. The COV does not vary a notable amount between the baseline and expanded case, meaning that both cases have similar variation from the mean.

For each WEC size, WETS has the lowest COV throughout the year, only reaching a maximum of 0.73 for the 10m WEC baseline case. Therefore, WETS is deemed to have the most consistent wave resource of the study locations. This is

reinforced by the low variation of the monthly mean wave power available for the different WEC sizes at the site. Los Angeles has only slightly higher COV values throughout the year for all sizes and has a remarkably steady monthly mean net power, indicating another location with steady resource.

The COV values for Miami are noticeably high in the month of August for each case. This is due to the presence of hurricanes in the late summer, along with an above average storm season in 2008 [81]. 2008 saw 16 tropical storms, five of which were major hurricanes equal to a Category 3 or above storm [81]. In a location like Miami which is home to very active hurricane seasons, large storm events cause high wave heights and long periods, making for very energetic wave power events. This all leads to an unsteady and generally unpredictable long term wave resource, a consideration to take into account for both small WEC deployment and design. Less steady resources, or those with larger COVs, can present challenges for small WEC design and implementation.

At each location for each size, the mean monthly power calculated by the baseline case exceeds that calculated by the expanded case. The baseline case's failure to include gross power in its methods wrongly identifies some amounts of power available for conversion. Therefore, the expanded case, while slightly more limiting, should be used for a realistic analysis of wave power available to a small WEC.

The annual maximums of net power for the expanded case are shown in Figure 24Figure 28. As explained in Results, certain years have significant spikes in maximum net power. For instance, on the West Coast of the continental US, the biggest spike in maximum net power was in 2008 for the 2m, 5m, and 10m devices. This date pertains to an El Niño event, which increases wave heights and periods due to increased storm activity [79]. At the same time, the maximum power for the 1m did not spike but rather remained steady. Large wave heights

and periods are not conducive to power absorption for the 1m device in this year since it finds resonance at lower frequencies.

On the Atlantic Coast of the continental US, the largest spike in maximum power also occurred in 2008, but was due to an irregularly active tropical storm season [81]. Again, large maximum net powers for certain devices may not translate across device size. For WECs like the 1m and 2m devices, shorter wave periods harbor better conditions for power extraction since the devices are more easily excited by high frequencies. In contrast, bigger small WECs like the 5m and 10m devices need bigger wave periods for excitation and subsequent power absorption, so they require different sea states.

The baseline cases consistently have greater maximum power measurements compared to the expanded case, again due to the case's reduced stroke restriction and inclusion of inherent power limit P_{gross}. As WEC size increases, maximum power seen by the devices increases as well since larger WECs encounter more waves.

To illustrate the differences between the baseline and expanded cases, the two were compared at the finest resolution available. Power was measured hourly in the dataset, so one month's worth of net power was presented and compared in Figure 29. At most measurements, the baseline and expanded P_{net} do not vary greatly. However, for certain instances, like January 17th or January 30th described previously, demonstrate the contrast between the implementation of the baseline methods versus the expanded methods. This example highlights just how much the difference between the two cases can be, and why it is essential to include P_{gross} when assessing the wave power available to a small WEC.

Mean and maximum hourly differences between the baseline and expanded cases along with the total difference throughout the time period are presented in Table 5 through Table 8. As expected, all difference metrics for the

two cases increase with WEC size. Budal's upper bound increases quadratically with device size while gross power increases linearly; as WEC size increases, the expanded case restricts absorbable power in a more confining manner than the baseline case since it depends on gross power.

Again, the hourly and total difference results conclude that the expanded case is much more restrictive than the baseline case in terms of absorbable power estimates. The inclusion of gross power in the limitations imposes some reality to the otherwise mathematically maximum power absorption dictated by the radiated power limit and Budal's upper bound alone. Actual absorbable power differs by MW and GW in some cases between the baseline and expanded cases. This highlights the overestimation of absorbable power by the baseline case, and reinforces the justification for using the expanded case for small WEC resource assessment methods.

Throughout the results in general, despite WEC size, PacWave possesses the most net power available to the devices, followed by WETS and Cape Cod, and Los Angeles and Miami. This was expected since PacWave lies in a region with some of the most gross wave power available in the world [4]. At each size, WETS and Cape Cod sites offer comparable amounts of net power, as do Los Angeles and Miami. Spatially, this method suggests that small devices have the potential for deployment in previously dismissed locations for wave energy conversion, like Cape Cod or Miami. Other sites that are already expected to contribute maximum ocean power are still able to host smaller WECs, as demonstrated by the PacWave analysis.

Temporally, the average net power absorbable does not change significantly with the seasons, regardless of WEC size or location. This indicates that small WECs may be used for power applications throughout the entire year, operating independent of seasonally available maximum wave power. And since

small WEC applications would require consistent power, a temporally steady energy source is not only ideal but possible.

Depending on intended WEC application, the different size devices may be utilized. For instance, an ocean observation buoy could be a 1m or 2m device, whereas a community backup battery for the electric grid may be closer to 10m in diameter. The larger the device, the more incident wave power it will meet. That being said, relatively larger small WEC devices require longer and more energetic waves to initiate excitation [59].

6.3 Small WEC applications for the BE

Small WECs have the potential to transform the blue economies (BEs) of the United States. Small WECs will operate in the physical domain of the BE, making them an obvious choice for utilization. Existing BE operations ranging from ocean agriculture to remote underwater vehicle charging to ocean observation require smaller power-loads than what is available in the gross wave energy at site locations. One or two W- to kW-level WECs working to supply energy to a large aquaculture farm can provide more than enough power. Small WECs can help "green" these existing operations. Investigated BE applications for small WECs are listed in Table 9.

Table 9: Blue Economy activities and subsequent power needs

Service	**Power needs**
Food and water [58], [82]	• Ocean agriculture *Aquaculture and fish farms*: compressed air production, nutrient and waste disbursement, monitoring, refrigeration, feeders, lights, heat *Algae and Seaweed*: harvesting, drying, monitoring, maintenance, maneuvering, buoyancy control

	• Seawater desalination: water pumping, filtration, pressurization of system, distribution of water to main systems
Energy	• Community microgrid powering: battery charging • Emergency power: backup power (reserved battery charging)
Ocean observation and navigation	• Wave buoy powering • Wave monitoring buoys with data communication capabilities • Ferries, shipping barges, other maritime vessels

According to the resource assessments, small WECs seem best suited for deployment at all locations, depending on desired application and resource size. A closer look at BE activities and possible small WEC opportunities in each of these locations are explored below.

PacWave is located off the coast of Newport, Oregon and consists of two wave energy test sites: North and South. The North site is geared toward supporting small-scale, prototype, and maritime market technologies with permit access in less than one year [83]. PacWave North is shallower than the South site and is closer to the shore as well [8]. PacWave South, currently under construction at the time of this publication, is a grid-connected test site with pre-permitted berths [83]. The northern site is better designed for testing small-scale devices, like the WECS in this study, while the southern site allows for up to four berths with dedicated 5 MW power outputs, rendering the site better suited for large WECs [83].

Examples of potential blue economy services in the PacWave region include marine agriculture, energy capture, and ocean observation and navigation, all detailed further in Table 9 [84]. Since small WECs on the bigger end of the scale, like a 10m device, would best function at this site, with the potential in battery charging for community grids or marine vessels.

The Los Angeles County Economic Development Corporation (LAEDC) states that, currently, 90% of the county's ocean economy employment is made up of tourism and marine transportation [85]. LAEDC expects that, while these two sectors will remain important, economic activity will be spurred by growth in emerging sectors like surveillance and safety, marine aquaculture, and marine biotechnology [85]. With the local government in the city looking to expand their BE, small WECs could prove essential to aiding in the growing economy. Already, small WECs are being investigated for US DOD and other robotic, surveillance initiatives [58]. Integrating the devices into the expansion of BE activities is a great opportunity not only to test small WEC abilities but also to develop sustainably in Los Angeles.

Further into the Pacific, WETS offshore the island of Oahu, Hawaii provides a location for testing WECs both in their technical abilities and environmental impacts. In addition to a strong BE, Hawaii also possesses an element of sustainability in its development plans. The Hawaiian Islands have a 100% renewable energy goal set for 2045 and integrating small wave energy conversion into the power mix offers a path to achieve this. WETS (and Hawaii in general [13]) has consistent wave energy resources, promising a reliable energy source all year-long. At WETS, this resource is located close to shore and in an already existing permitted wave energy site, offering a prime location for small WEC testing and deployment. Hawaii's BE is made up of a range of ocean-related activities, from tourism and beach-going to small-scale fisheries and ocean observation.

According to Conservation International, 75% of Hawaii's small-scale fisheries are depleted or in critical condition; prior to European and American colonization, Hawaiians maintained fishery systems that yielded up to 2 million pounds of seafood per year [86]. Currently, aquaculture efforts in Hawaii supply just 623,000 pounds yearly [86]. This is due to the loss of traditional fishing practices and basically nonexistent resource management, resulting in little supply of local seafood in Hawaii. Hawaii is essentially reliant on imported food sources" 80%-90% of food consumed in Hawaii is imported, while 63% of seafood sold is imported due to depleted local fisheries [86]. Climate change and depletion of worldwide fisheries only add to the challenges that Hawaii faces with its food systems and BE.

Small scale WECs could be considered to aid in the re-implementation of small, local fisheries in Hawaii, under the framework of combining Western technology with Indigenous practices and traditions. Small WECs can be used to power equipment like feeders, lights, and heat if necessary. Additionally, via modelling efforts, WECs have been proven to help protect aquaculture projects either operating in arrays or co-located with wind farms [29], [87]. More specific power applications for aquaculture are listed in Table 9 further discussing BE impact on climate justice, to which this example is directly related. It is essential to understand the impact of WEC technology on the surrounding environment before deployment, which is why WETS makes a good testing ground for small WECs in the Hawaiian Islands.

On top of aquaculture and re-integration of small fisheries for local food supply in Hawaii, small WECs have the potential to supply power to other standalone BE operations that can improve the lives of local citizens. WECs have been considered for seawater desalination by means of reverse osmosis, a practice that has already been tested in Hawaii and is being considered a possible potable water source on Oahu [88]. Realistically, any BE activity described previously

could be implemented in the Hawaiian Islands, since the barrier to possibility lies in the wave energy resource, which is abundant in the location. Serious considerations that must be considered are environmental impact and potential to integrate new technology with Indigenous knowledge and participation in implementation (co-design, stakeholder input, etc.).

As for Cape Cod, small WECs are of particular interest because they have the potential to be integrated with the upcoming installation of Vineyard Wind, an 800 MW offshore wind farm currently under construction [89]. Benefits of co-located offshore wind and WEC devices are numerous; co-location offers maximum spatial utilization in limited marine environments, and can reduce overall costs by sharing expensive infrastructure like cables and moorings [6].

In terms of its BE, Cape Cod already has mechanisms in place to help grow its BE sustainably. In 2015, the Cape Cod Chamber of Commerce developed "The Blue Economy Project," which is a "regional initiative to promote and sustain a maritime-focused economy on Cape Cod, the islands of Martha's Vineyard and Nantucket, and southern Plymouth County" [90]. Existing BE framework allows for easier implementation of renewable energy systems.

Further down the East Coast, Florida residents rely heavily on their BEs for their livelihoods. Florida's coastal counties are home to more than 15 million people, and contribute more than $797 billion to the state's economy every year [91]. Miami-Dade county specifically has the highest amount of BE-related jobs, with most employees working in ocean tourism, recreation, and transportation [91].

Although Miami's (and Florida's in general) BEs are well-developed, they still lack a certain element of sustainability. The Florida Ocean Alliance (FOA) is an organization whose goal is to "protect and enhance Florida's coastal and ocean resources for continued social and economic benefits" by uniting private, academic, and nonprofit sectors [92]. The FOA has published a policy plan for

Florida's BEs, dissecting the makeup of the BEs economically and emphasizing the need for a strategic policy plan moving forward. In the FOA's 2020 Strategic Policy Plan for Florida's Oceans and Coasts [91], the organization also pushes for the need of sustainability and improved resilience in Florida's BE continuation and future development.

Just 50 miles north of Miami in Boca Raton, Florida Atlantic University (FAU) is home to the Southeast National Marine Renewable Energy Center (SNMREC); researchers at SNMREC are working to capture the energy of ocean currents and ocean thermal energy since these types of ocean renewable energy are abundant. By integrating a small WEC test site into SNMREC, the door to consistent and small wave energy could open in the Miami, FL to help support the abundant energy requirements for the region's BEs. The FOA is focused on marine agriculture, engineering, and water quality, among other initiatives, whose energy needs are outlined in Table 9. These applications can be powered by small WEC devices, helping sustainably grow the Miami region and Florida's BEs.

At all locations, BEs are essential components of the local economies, with residents relying on jobs and income. Most BEs in the study do not possess the sustainability component just yet, but all locations have goals to integrate elements of environmentally friendly practices into their initiatives. The island of Oahu in Hawaii may just be the most likely location for small WEC implementation, given its economy's sustainable development goals and willingness to try using wave power.

6.4 Future work

This study relied on numerous assumptions, many of which are not conducive to representing realistic sea states when applied. It would be useful to extrapolate the radiated power limit and Budal's upper bound such that they could

be used to quantify absorbable power for small WECs in irregular sea states (i.e., free of linear wave theory assumptions).

Given that gross power restricts the radiated power limit and Budal's upper bound, not the other way around, in different cases within this study, it may be necessary to further refine the bounds P_a and P_b for small WECs. Intuitively, it seems that P_a and P_b should limit the amount of P_{gross} available to the devices since they are deemed "power limits." Further studies investigating the application of these limits to real sea states may further confirm this suggestion.

7. Conclusions

Small WECs require an alternative approach to design due to their smaller sizes and subsequent power needs, introducing the need for a novel approach to quantifying wave energy resource available. Published research exploring absorbable power limits for small WECs has been introduced in the past half century but have not yet been applied to actual measured wave spectra. This gap was filled by applying the maximum absorbable power limit based on radiation pattern P_a and the Budal's upper bound for power capture P_b to the incident wave power for a baseline case. An expanded case was presented which used these two power limits along with the gross wave power P_{gross} to find absorbable power for the small WECs.

An example case with a generic Pierson-Moskowitz (PM) spectrum was created for the purpose of establishing some expectations as to how the power limits would perform, since PM spectrums have a well-known shape and behavior. However, the evaluation of the sample case revealed that the radiated power limit and Budal's upper bound did not limit gross power, but rather, the opposite reigned true for the expanded case.

IEC standardized wave resource assessments were completed at all five study locations for the purpose of comparing the absorbable power by small

WECs to the gross power deemed available for extraction according to the standards. PacWave, Oregon had the most energetic sea states in the context of gross wave power, followed by WETS, Oahu, Hawaii; Cape Cod, Massachusetts; Los Angeles, California; and finally, Miami, Florida. When comparing the gross wave resource available to the net power extractable by the small devices, it was found that the IEC-calculated absorbable power greatly overestimated what is extractable by the small WEC devices.

The results of the small WEC resource assessment show that, using Budal's upper bound, radiation power limit, and the gross wave power as filters, the average absorbable wave power by small WECs differs greatly from the baseline case, whose method has previously been explored.

The study found that temporally, small WECs in differing locations can absorb comparable amounts of power. For instance, a 1m WEC in Miami absorbs only marginally less average power than the same device deployed in Los Angeles. Therefore, spatially, there is potential to use small WECs in locations previously dismissed for wave energy conversion sites, like Miami, Florida.

Temporally, average power absorbable does not change significantly with the seasons, unlike gross wave power. This finding indicates that small WECs could be used for power applications throughout the entire year, independent of seasonally changing gross power. Since applications for small WECs require consistent power, this finding supports the argument for increased development and usage of the devices.

Overall, the IEC specification was found to oversimplify the makeup of wave power available. Additionally, the baseline case for finding net power absorbable incorrectly assesses the realistic amount of power available to the small WECs. The expanded case incorporates the radiated power limit and Budal's upper bound, and also includes the essential limit of gross power available in the ocean.

Each of the study locations has a unique BE that small WECs have the potential to decarbonize. Common BE applications for small WEC powering at each site include ocean observation buoys, aquaculture, fisheries, and sea water desalination, to name a few. Since WECs operate in the ocean and/or nearshore, and are themselves a faction of the BE, the devices prove to be extremely well suited for providing power needs to BE applications.

The results from this thesis fill a wide gap in the realm of small WEC research. Small devices naturally operate differently in the ocean than their more developed, larger counterparts. To account for this difference, it is important to quantify the resource available to small WECs in a proportional way, thus introducing the need for our small WEC resource assessments. Methods for small WEC resource assessments were investigated along with how they alter the total net power available to the devices. To do so, two previously researched power limits were applied, Budal's upper bound P_b and the WEC radiated power limit P_a, and limited the gross power in two different scenarios, the baseline and expanded cases. By filtering the gross wave power available in the spectra according to the power limits, the actual amount of energy available to the WECs, i.e., the net power P_{net}, becomes apparent. Utilizing the most realistic of the two cases' methods, the IEC specification along with the baseline case were found to overestimate the wave power available to a small WEC device. The expanded case methods prove necessary and functional for a small WEC wave resource assessment.

8. References

[1] L. Kilcher, M. Fogarty, M. Lawson, L. Kilcher, M. Fogarty, and M. Lawson, "Marine Energy in the United States : An Overview of Opportunities Marine Energy in the United States : An Overview of Opportunities," *NREL Rep.*, no. February, 2021.

[2] G. García-Medina, H. T. Özkan-Haller, and P. Ruggiero, "Wave resource assessment in Oregon and southwest Washington, USA," *Renew. Energy*, vol. 64, 2014, doi: 10.1016/j.renene.2013.11.014.

[3] C. Guedes Soares, A. R. Bento, M. Gonçalves, D. Silva, and P. Martinho, "Numerical evaluation of the wave energy resource along the Atlantic European coast," *Comput. Geosci.*, vol. 71, pp. 37–49, 2014, doi: 10.1016/j.cageo.2014.03.008.

[4] A. Cornett, "A global wave energy resource assessment," *Sea Technol.*, vol. 50, no. 4, pp. 59–64, 2008.

[5] J. Morim, N. Cartwright, A. Etemad-Shahidi, D. Strauss, and M. Hemer, "Wave energy resource assessment along the Southeast coast of Australia on the basis of a 31-year hindcast," *Appl. Energy*, vol. 184, pp. 276–297, 2016, doi: 10.1016/j.apenergy.2016.09.064.

[6] B. Robertson, G. Dunkle, J. Gadasi, G. Garcia-medina, and Z. Yang, "Holistic marine energy resource assessments : A wave and offshore wind perspective of metocean conditions," *Renew. Energy*, vol. 170, pp. 286–301, 2021, doi: 10.1016/j.renene.2021.01.136.

[7] G. Lavidas and V. Venugopal, "Prospects and applicability of wave energy for South Africa," *Int. J. Sustain. Energy*, vol. 37, no. 3, pp. 230–248, 2018, doi: 10.1080/14786451.2016.1254216.

[8] G. Dunkle, B. Robertson, G. Garcia-Medina, and Z. Yang, "PacWave Wave Resource Assessment," 2020, [Online]. Available: https://ir.library.oregonstate.edu/concern/technical_reports/hm50tz68v.

[9] S. P. Neill and M. R. Hashemi, "Wave power variability over the northwest European shelf seas," *Appl. Energy*, vol. 106, pp. 31–46, 2013, doi: 10.1016/j.apenergy.2013.01.026.

[10] B. R. D. Robertson, C. E. Hiles, and B. J. Buckham, "Characterizing the near shore wave energy resource on the west coast of Vancouver Island, Canada," *Renew. Energy*, vol. 71, 2014, doi: 10.1016/j.renene.2014.06.006.

[11] G. García-Medina, Z. Yang, W. C. Wu, and T. Wang, "Wave resource characterization at regional and nearshore scales for the U.S. Alaska coast based on a 32-year high-resolution hindcast," *Renew. Energy*, vol. 170, pp. 595–612, 2021, doi: 10.1016/j.renene.2021.02.005.

[12] S. Ahn, K. A. Haas, and V. S. Neary, "Wave energy resource characterization and assessment for coastal waters of the United States," *Appl. Energy*, vol. 267, no. June, p. 114922, 2020, doi:

10.1016/j.apenergy.2020.114922.
[13] J. E. Stopa, K. F. Cheung, and Y. L. Chen, “Assessment of wave energy resources in Hawaii,” *Renew. Energy*, vol. 36, no. 2, pp. 554–567, 2011, doi: 10.1016/j.renene.2010.07.014.
[14] C. V. C. Weiss, R. Guanche, B. Ondiviela, O. F. Castellanos, and J. Juanes, “Marine renewable energy potential: A global perspective for offshore wind and wave exploitation,” *Energy Convers. Manag.*, vol. 177, no. September, pp. 43–54, 2018, doi: 10.1016/j.enconman.2018.09.059.
[15] F. Ferrari, G. Besio, F. Cassola, and A. Mazzino, “Optimized wind and wave energy resource assessment and offshore exploitability in the Mediterranean Sea,” *Energy*, vol. 190, p. 116447, 2020, doi: 10.1016/j.energy.2019.116447.
[16] Electric Power Research Institute, “Mapping and Assessment of the United States Ocean Wave Energy Resource,” *Tech. Rep.*, p. 176, 2011.
[17] K. Gunn and C. Stock-Williams, “Quantifying the global wave power resource,” *Renew. Energy*, vol. 44, pp. 296–304, 2012, doi: 10.1016/j.renene.2012.01.101.
[18] M. G. Hughes and A. D. Heap, “National-scale wave energy resource assessment for Australia,” *Renew. Energy*, vol. 35, no. 8, pp. 1783–1791, Aug. 2010, doi: 10.1016/j.renene.2009.11.001.
[19] M. R. Hashemi and S. P. Neill, *Fundamentals of Ocean Renewable Energy*, 1st ed. Joe Hayton, 2018.
[20] S. J. Beatty, M. Hall, B. J. Buckham, P. Wild, and B. Bocking, “Experimental and numerical comparisons of self-reacting point absorber wave energy converters in regular waves,” *Ocean Eng.*, vol. 104, pp. 370–386, 2015, doi: 10.1016/j.oceaneng.2015.05.027.
[21] J. H. Todalshaug, “Practical limits to the power that can be captured from ocean waves by oscillating bodies,” *Int. J. Mar. Energy*, vol. 3–4, no. 0314, pp. 70–81, 2013, doi: 10.1016/j.ijome.2013.11.012.
[22] UNCSD *et al.*, “Blue Economy Concept Paper,” *Mar. Policy*, vol. 194, no. 1, pp. 1–15, 2016, doi: 10.1057/s41301-016-0046-9.
[23] L. H. Holthuijsen, *Waves in Oceanic and Coastal Waters*. New York: Cambridge University Press, 2007.
[24] R. G. Dean and R. A. Dalrymple, *Water wave mechanics for engineers and scientists*. Englewood Cliffs, New Jersey: Prentice-Hall, 1984.
[25] J. H. Todalshaug, “Hydrodynamics of WECs,” in *Handbook of Ocean Wave Energy*, 2017, pp. 139–158.
[26] Y. Chu, “Review and Comparison of Different Solar Energy Technologies, Global Energy Network Institute (GENI), 2011,” no. August, p. 22, 2011.
[27] E. Kabir, P. Kumar, S. Kumar, A. A. Adelodun, and K. H. Kim, “Solar energy: Potential and future prospects,” *Renew. Sustain. Energy Rev.*, vol.

82, no. October 2017, pp. 894–900, 2018, doi: 10.1016/j.rser.2017.09.094.
[28] P. Kiss and I. M. Jánosi, “Limitations of wind power availability over Europe: A conceptual study,” *Nonlinear Process. Geophys.*, vol. 15, no. 6, pp. 803–813, 2008, doi: 10.5194/npg-15-803-2008.
[29] D. Clemente, P. Rosa-Santos, and F. Taveira-Pinto, “On the potential synergies and applications of wave energy converters: A review,” *Renew. Sustain. Energy Rev.*, vol. 135, no. January 2020, p. 110162, 2021, doi: 10.1016/j.rser.2020.110162.
[30] M. A. Hemer, R. Manasseh, K. L. McInnes, I. Penesis, and T. Pitman, “Perspectives on a way forward for ocean renewable energy in Australia,” *Renew. Energy*, vol. 127, pp. 733–745, 2018, doi: 10.1016/j.renene.2018.05.036.
[31] I. Fairley *et al.*, “A classification system for global wave energy resources based on multivariate clustering,” *Appl. Energy*, vol. 262, no. January, p. 114515, 2020, doi: 10.1016/j.apenergy.2020.114515.
[32] J. P. Kofoed, *Handbook of Ocean Wave Energy*. Springer, 2017.
[33] T. R. Mundon, “Performance evaluation and analysis of a micro-scale wave energy system,” pp. 1–8, 2019.
[34] IEC, “The International Electrotechnical Commission,” 2021. .
[35] C. Guedes Soares, A. R. Bento, M. Gonçalves, D. Silva, and P. Martinho, “Numerical evaluation of the wave energy resource along the Atlantic European coast,” *Comput. Geosci.*, vol. 71, pp. 37–49, 2014, doi: 10.1016/j.cageo.2014.03.008.
[36] B. Robertson, H. Bailey, M. Leary, and B. Buckham, “A methodology for architecture agnostic and time flexible representations of wave energy converter performance,” *Appl. Energy*, vol. 287, no. February, p. 116588, 2021, doi: 10.1016/j.apenergy.2021.116588.
[37] M. N. Allahdadi, B. Gunawan, J. Lai, R. He, and V. S. Neary, “Development and validation of a regional-scale high-resolution unstructured model for wave energy resource characterization along the US East Coast,” *Renew. Energy*, vol. 136, pp. 500–511, 2019, doi: 10.1016/j.renene.2019.01.020.
[38] S. Ahn, K. A. Haas, and V. S. Neary, “Wave energy resource classification system for US coastal waters,” *Renew. Sustain. Energy Rev.*, vol. 104, no. January 2018, pp. 54–68, 2019, doi: 10.1016/j.rser.2019.01.017.
[39] C. W. Zheng, J. Pan, and J. X. Li, “Assessing the China Sea wind energy and wave energy resources from 1988 to 2009,” *Ocean Eng.*, vol. 65, pp. 39–48, 2013, doi: 10.1016/j.oceaneng.2013.03.006.
[40] S. Behrens, J. Hayward, M. Hemer, and P. Osman, “Assessing the wave energy converter potential for Australian coastal regions,” *Renew. Energy*, vol. 43, pp. 210–217, 2012, doi: 10.1016/j.renene.2011.11.031.

[41] M. A. Hemer and D. A. Griffin, “The wave energy resource along Australia’s Southern margin,” *J. Renew. Sustain. Energy*, vol. 2, no. 4, 2010, doi: 10.1063/1.3464753.
[42] M. Gonçalves, P. Martinho, and C. Guedes Soares, “Wave energy conditions in the western French coast,” *Renew. Energy*, vol. 62, pp. 155–163, 2014, doi: 10.1016/j.renene.2013.06.028.
[43] P. Lenee-Bluhm, “The Wave Energy Resource of the US Pacific Northwest,” Oregon State University, 2010.
[44] P. Lenee-Bluhm, R. Paasch, and H. T. Özkan-Haller, “Characterizing the wave energy resource of the US Pacific Northwest,” *Renew. Energy*, vol. 36, no. 8, pp. 2106–2119, 2011, doi: 10.1016/j.renene.2011.01.016.
[45] International Electrotechnical Commission, *Marine energy : wave, tidal and other water current converters. Part 101, Wave energy resource assessment and characterization.* .
[46] B. R. D. Robertson, C. E. Hiles, and B. J. Buckham, “Characterizing the near shore wave energy resource on the west coast of Vancouver Island, Canada,” *Renew. Energy*, vol. 71, 2014, doi: 10.1016/j.renene.2014.06.006.
[47] W. C. Wu, T. Wang, Z. Yang, and G. García-Medina, “Development and validation of a high-resolution regional wave hindcast model for U.S. West Coast wave resource characterization,” *Renew. Energy*, vol. 152, pp. 736–753, 2020, doi: 10.1016/j.renene.2020.01.077.
[48] Z. Yang, G. García-Medina, W.-C. Wu, and T. Wang, “Characteristics and variability of the nearshore wave resource on the U.S. West Coast,” *Energy*, vol. 203, p. 117818, 2020, doi: 10.1016/j.energy.2020.117818.
[49] B. Robertson, H. Bailey, and B. Buckham, “Resource assessment parameterization impact on wave energy converter power production and mooring loads,” *Appl. Energy*, vol. 244, 2019, doi: 10.1016/j.apenergy.2019.03.208.
[50] V. Ramos and J. V. Ringwood, “Exploring the utility and effectiveness of the IEC (International Electrotechnical Commission) wave energy resource assessment and characterisation standard: A case study,” *Energy*, vol. 107, pp. 668–682, 2016, doi: 10.1016/j.energy.2016.04.053.
[51] NREL, “Marine Energy Atlas.” .
[52] L. Kilcher and R. Thresher, “Marine Hydrokinetic Energy Site Identification and Ranking Methodology Part I: Wave Energy,” no. October, 2016, doi: 10.2172/1330619.
[53] A. F. O. Falcão and J. C. C. Henriques, “Oscillating-water-column wave energy converters and air turbines: A review,” *Renew. Energy*, vol. 85, pp. 1391–1424, 2016, doi: 10.1016/j.renene.2015.07.086.
[54] A. F. d. O. Falcão, “Wave energy utilization: A review of the technologies,” *Renew. Sustain. Energy Rev.*, vol. 14, no. 3, pp. 899–918,

2010, doi: 10.1016/j.rser.2009.11.003.
[55] Bevilacqua.G and Zanuttigh.B, “Overtopping Wave Energy Converters : general aspects and stage of development,” *Int. Coast. Eng. Proc.*, no. 1, p. 21, 2011.
[56] T. Aderinto and H. Li, “Review on power performance and efficiency of wave energy converters,” *Energies*, vol. 12, no. 22, pp. 1–24, 2019, doi: 10.3390/en12224329.
[57] A. Babarit, J. Hals, M. J. Muliawan, A. Kurniawan, T. Moan, and J. Krokstad, “Numerical benchmarking study of a selection of wave energy converters,” *Renew. Energy*, vol. 41, pp. 44–63, 2012, doi: 10.1016/j.renene.2011.10.002.
[58] A. LiVecchi *et al.*, “Powering the Blue Economy: Exploring Opportunities for Marine Renewable Energy in Maritime Markets,” 2019.
[59] R. G. Coe, S. Ahn, V. S. Neary, P. H. Kobos, and G. Bacelli, “Maybe less is more: Considering capacity factor, saturation, variability, and filtering effects of wave energy devices,” *Appl. Energy*, vol. 291, no. March, p. 116763, 2021, doi: 10.1016/j.apenergy.2021.116763.
[60] T. O. Aderinto, F. Haces-Fernandez, and H. Li, “Design and potential application of small scale wave energy converter,” *ASME Int. Mech. Eng. Congr. Expo. Proc.*, vol. 6, no. June 2018, 2017, doi: 10.1115/IMECE2017-70117.
[61] C. de Abreu D’Aquino, C. Cataldo Scharlau, and L. Casagrande Dalla Vecchia, “Evaluation of the energy extraction of a small-scale wave energy converter,” *Bras. J. Water Resour.*, vol. 24, no. 13, 2019.
[62] T. Johnson, B. Phillips, S. Ringuette, M. Zenouzi, and J. McCusker, “Design and development of a small scale ocean current and wave energy converter,” *ASME Int. Mech. Eng. Congr. Expo. Proc.*, vol. 6B-2016, pp. 1–8, 2016, doi: 10.1115/IMECE2016-66793.
[63] J. Falnes, “A review of wave-energy extraction,” *Mar. Struct.*, vol. 20, no. 4, pp. 185–201, 2007, doi: 10.1016/j.marstruc.2007.09.001.
[64] K. Budal and J. Falnes, “Interacting Point Absorbers with Controlled Motion,” in *Power from Sea Waves*, 1980, pp. 381–399.
[65] J. Falnes and J. Hals, “Heaving buoys, point absorbers and arrays,” *Philos. Trans. R. Soc. A Math. Phys. Eng. Sci.*, vol. 370, no. 1959, pp. 246–277, 2012, doi: 10.1098/rsta.2011.0249.
[66] D. V Evans, “Maximum wave-power absorption under motion constraints,” *Appl. Ocean Res.*, vol. 3, no. 4, pp. 200–203, 1981.
[67] D. J. Pizer, “Maximum wave-power absorption of point absorbers under motion constraints,” *Appl. Ocean Res.*, vol. 15, no. 4, pp. 227–234, 1993.
[68] J. Hals, J. Falnes, and T. Moan, “Constrained optimal control of a heaving buoy wave-energy converter,” *J. Offshore Mech. Arct. Eng.*, vol. 133, no.

1, pp. 1–15, 2010, doi: 10.1115/1.4001431.
[69] K. Budar and J. Falnes, “A resonant point absorber of ocean-wave power,” *Nature*, vol. 256, pp. 478–479, 1975, doi: 10.1038/256478a0.
[70] J. N. Newman, *Marine Hydrodynamics*, 40th Anniv. London: The MIT Press, 2017.
[71] S. J. Beatty, “Self-Reacting Point Absorber Wave Energy Converters,” University of Victoria, 2015.
[72] C. xxx V. K. Prasada Rao, “Spectral width parameter for wind-generated ocean waves,” *Proc. Indian Acad. Sci. - Earth Planet. Sci.*, vol. 97, no. 2, pp. 173–181, 1988, doi: 10.1007/BF02861852.
[73] P. Ruggiero, P. D. Komar, and J. C. Allan, “Increasing wave heights and extreme value projections: The wave climate of the U.S. Pacific Northwest,” *Coast. Eng.*, vol. 57, no. 5, pp. 539–552, 2010, doi: 10.1016/j.coastaleng.2009.12.005.
[74] J. Falnes, “Oscillating-Body Wave-Energy Converters,” in *Ocean waves and oscillating systems: Linear interactions including wave-energy extraction*, pp. 204–241.
[75] M. Nabi Allahdadi, R. He, and V. S. Neary, “Predicting ocean waves along the US east coast during energetic winter storms: Sensitivity to whitecapping parameterizations,” *Ocean Sci.*, vol. 15, no. 3, pp. 691–715, 2019, doi: 10.5194/os-15-691-2019.
[76] S. Ahn, V. S. Neary, M. N. Allahdadi, and R. He, “Nearshore wave energy resource characterization along the East Coast of the United States,” *Renew. Energy*, vol. 172, pp. 1212–1224, 2021, doi: 10.1016/j.renene.2021.03.037.
[77] P. A. Brodtkorb, P. Johannesson, G. Lindgren, I. Rychlik, J. Rydén, and E. Sö, “WAFO - a Matlab toolbox for analysis of random waves and loads,” in *10th International Offshore and Polar Eng. Conf*, 2000, pp. 343–350.
[78] R. Dolan and R. Davis, “Coastal Storm Hazards,” *J. Coast. Res.*, no. Special Issue No. 12, pp. 103–114, 1994.
[79] NOAA, “NOAA National Centers for Environmental Information, State of the Climate: El Niño/Southern Oscillation,” 2004. https://www.ncdc.noaa.gov/sotc/enso/.
[80] R. J. Pasch, “Tropical Cyclone Report: Hurricane Jimena,” 2003.
[81] D. P. Brown, J. L. Beven, J. L. Franklin, and E. S. Blake, “Atlantic hurricane season of 2008,” *Mon. Weather Rev.*, vol. 138, no. 5, pp. 1975–2001, 2010, doi: 10.1175/2009MWR3174.1.
[82] E. Ramudu, “Ocean wave energy-driven desalination systems for off-grid coastal communities in developing countries,” *Proc. - 2011 IEEE Glob. Humanit. Technol. Conf. GHTC 2011*, pp. 287–289, 2011, doi: 10.1109/GHTC.2011.38.

[83] “PacWave,” 2021. .
[84] R. Hahnel, “Economy and Environment,” *Radic. Polit. Econ.*, pp. 65–77, 2018, doi: 10.4324/9781315169149-6.
[85] L. A. C. E. D. Corporation, “The Ocean Economy in Los Angeles County: Economic Impact Analysis,” 2020. doi: 10.1787/9789264251724-en.
[86] “Hawai’i: ho’i i ke kai momona: Return to an abundant ocean,” *Conservation International*, 2021. .
[87] D. Silva, E. Rusu, and C. G. Soares, “The effect of a wave energy farm protecting an aquaculture installation,” *Energies*, vol. 11, no. 8, pp. 1–17, 2018, doi: 10.3390/en11082109.
[88] D. of Business and and T. Economic Development, “Feasibility of Developing Wave Power as a Renewable Energy Resource for Hawaii,” *Report*, vol. 8, no. 8, 2002.
[89] J. Kumagai, “The U.S. Finally Goes Big on Offshore Wind,” *IEEE Spectr.*, vol. 56, pp. 25–26, 2019.
[90] “Cape Cod Blue Economy Foundation,” 2020. https://www.bluecapecod.org.
[91] F. O. Alliance, “Securing Florida’s Blue Economy Strategic Policy Plan for Florida’s Oceans and Coasts,” no. June, 2020.
[92] “Florida Ocean Alliance,” 2019. https://www.floridaoceanalliance.org.
[93] B. Robertson, J. Bekker, and B. Buckham, “Renewable integration for remote communities: Comparative allowable cost analyses for hydro, solar and wave energy,” *Appl. Energy*, vol. 264, 2020, doi: 10.1016/j.apenergy.2020.114677.
[94] D. J. Bednar and T. G. Reames, “Recognition of and response to energy poverty in the United States,” *Nat. Energy*, vol. 5, no. 6, pp. 432–439, 2020, doi: 10.1038/s41560-020-0582-0.
[95] A. Drehobl and L. Ross, “Lifting the High Energy Burden in America’s Largest Cities: How Energy Efficiency Can Improve Low Income and Underserved Communities About the Authors Ariel Drehobl joined ACEEE in 2015. She conducts research and analysis on local-level energy efficiency ,” no. April, 2016, [Online]. Available: http://energyefficiencyforall.org/sites/default/files/Lifting the High Energy Burden_0.pdf.
[96] D. Hernández, “Sacrifice Along the Energy Continuum: A Call for Energy Justice HHS Public Access Author manuscript,” *Environ. Justice*, vol. 8, no. 4, pp. 151–156, 2015, doi: 10.1089/env.2015.0015.Sacrifice.
[97] J. J. Birchler, P. S. Dalyander, H. F. Stockdon, and K. S. Doran, “National assessment of nor’easter-induced coastal erosion hazards: Mid- and northeast Atlantic coast,” p. 34, 2015.

APPENDICES

Appendix A: Wave resource assessment results

Appendix A contains the continued results from the wave resource assessments.

A.1 Traditional wave resource assessment results

Figure 30 shows that significant wave height varies greatly according to the seasons at the PacWave site, with average winter (Nov.-Mar.) values ranging between 2.8m and 3.5m. Summer month (May-Sept.) values fluctuate between 1.5m and 1.8m. The mean significant wave height is greater than the 50th percentile, or median, throughout the year most notably in the winter months, indicating that the dataset is skewed.

Keeping with the seasonal trend, energy period at PacWave in the winter months ranges from 10.5s to 11.5s, while summer months stay between 8s and 9.5s. The mean is about equal to the median throughout the average year, as seen in Figure 31.

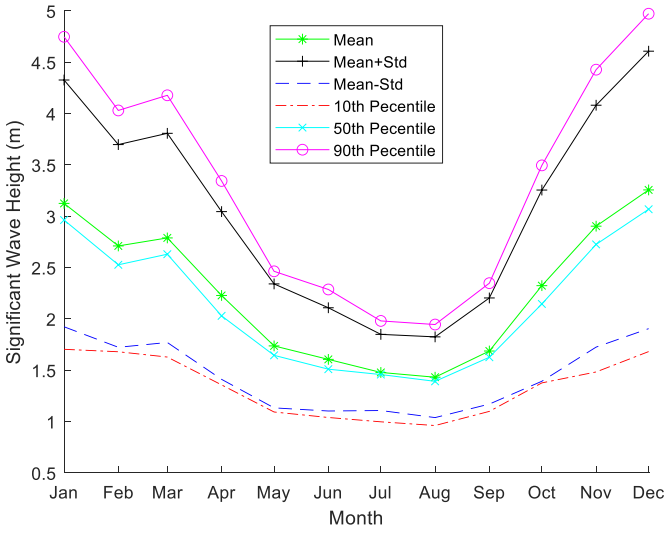

Figure 30: Monthly statistics for significant wave height at PacWave South from 2000-2010

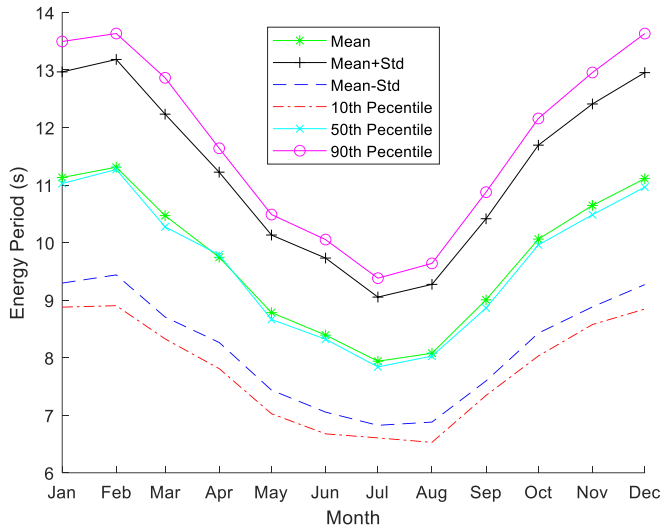

Figure 31: Monthly statistics for wave energy period at PacWave South from 2000-2010

In Figure 32, significant wave height varies minimally throughout the year, with all average and corresponding statistical values remaining below 2m. Average significant wave height varies between 0.9m and 1.2m throughout the year, with slight skewness according to the median values apparent in winter and spring months.

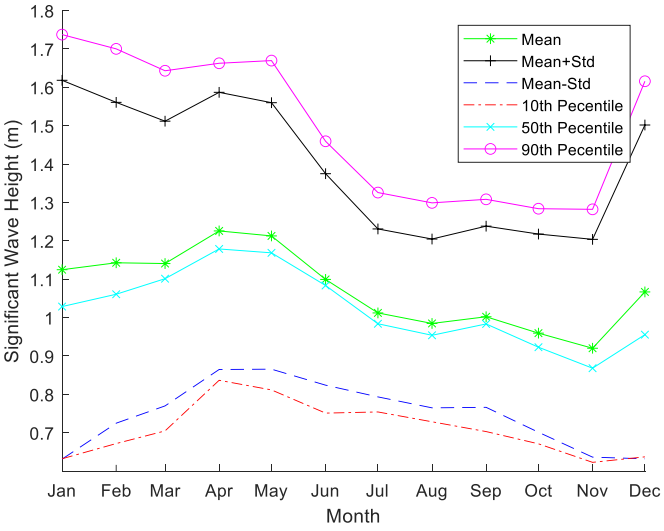

Figure 32: Monthly statistics for significant wave height at Los Angeles from 2000-2010

Energy period remains even less varied throughout the year, averaging between 9s and 9.7s depending on the month. Medians for this parameter are close to the mean values throughout the year, shown in Figure 33.

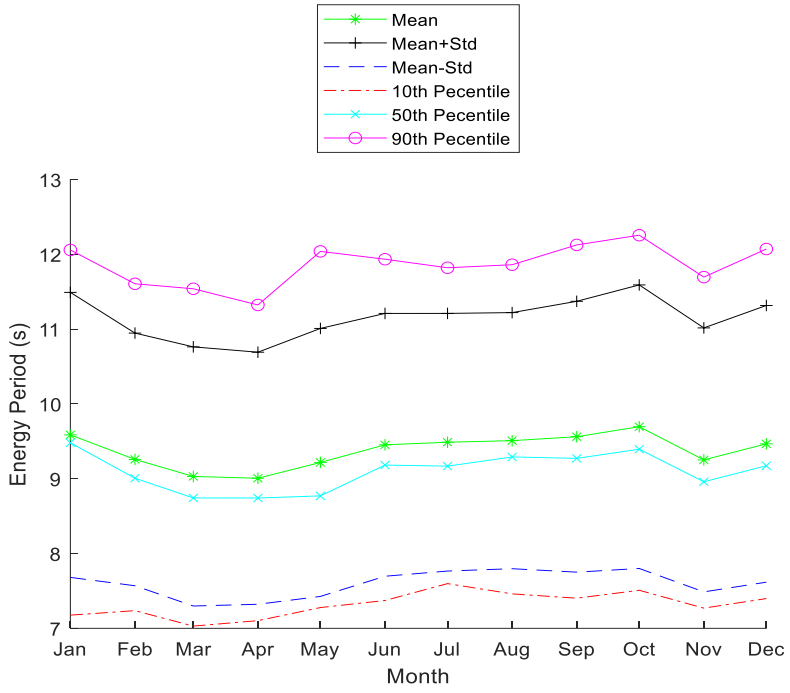

Figure 33: Monthly statistics for wave energy period at Los Angeles from 2000-2010

For significant wave height at WETS, HI, winter months range between 1.75m and 1.9m H_{m0} while summer months drop down to 1.4m to 1.5m. The median is about equal to the mean values, seen in Figure 34.

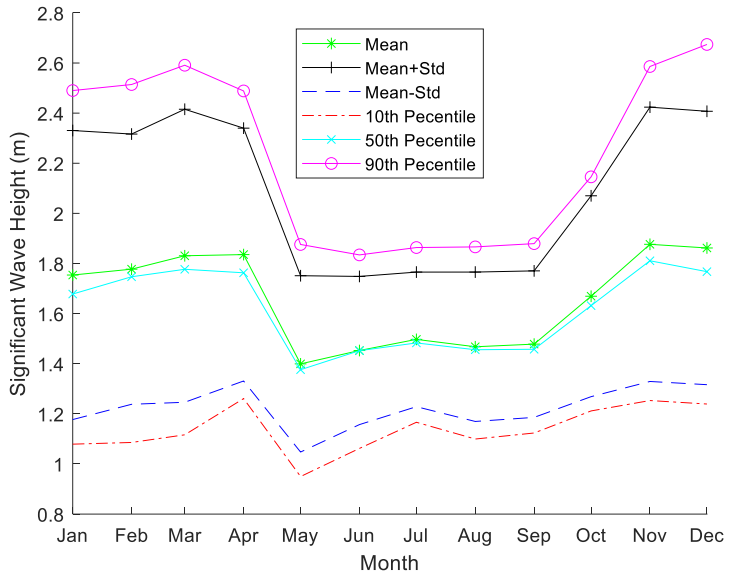

Figure 34: Monthly statistics for significant wave height at WETS from 2000-2010

Energy period at WETS ranges between 6 s and 9 s throughout the year, with the minimums occurring in summer months and maximums in winter months. The average energy period values are about equal to the median values throughout the months of the year, shown in Figure 35.

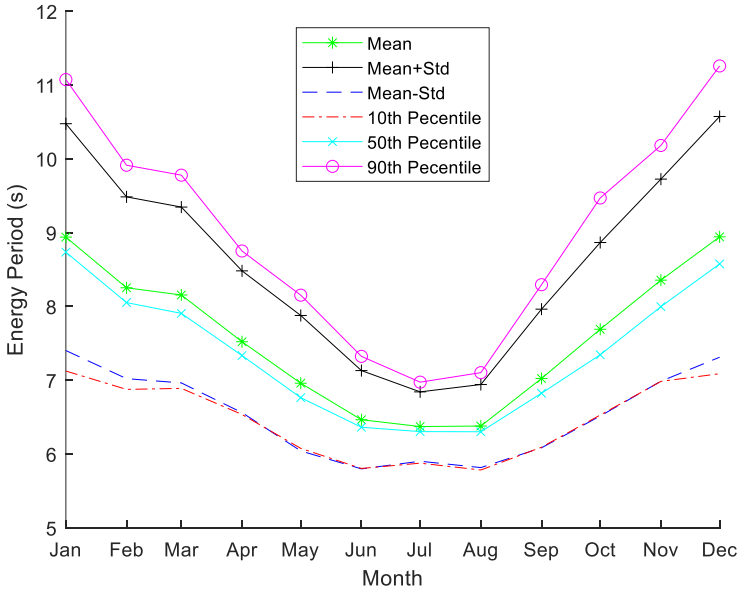

Figure 35: Monthly statistics for wave energy period at WETS from 2000-2010

Figure 36 shows that the mean significant wave height south of Cape Cod varies slightly by month on average, between a maximum of 1.9 m (December) and 1.2 m (August) significant wave height. Positive skewness is apparent in the dataset as the mean is greater than the median, with wider variation of the two in the winter months. This is caused by hurricanes and regional winter storms known as nor'easters [97].

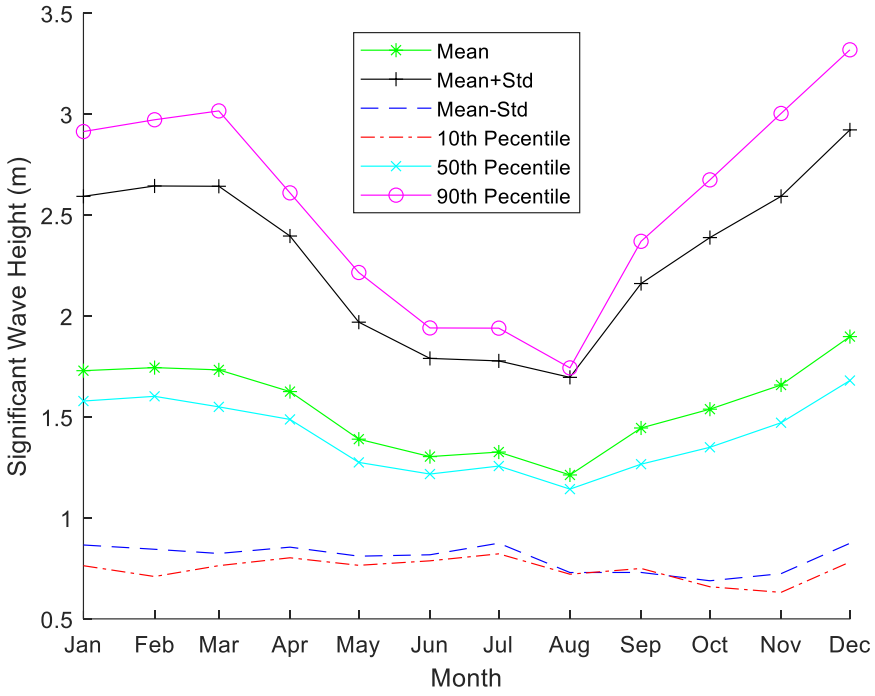

Figure 36: Monthly statistics for significant wave height at Cape Cod from 2000-2010

Energy period at Cape Cod ranges little throughout the months on average, between 6.4 s (June) and 7.3 s (September), as seen in Figure 39. Some positive skewness is present in the fall and winter months, again due to storm events like hurricanes and nor'easters [97].

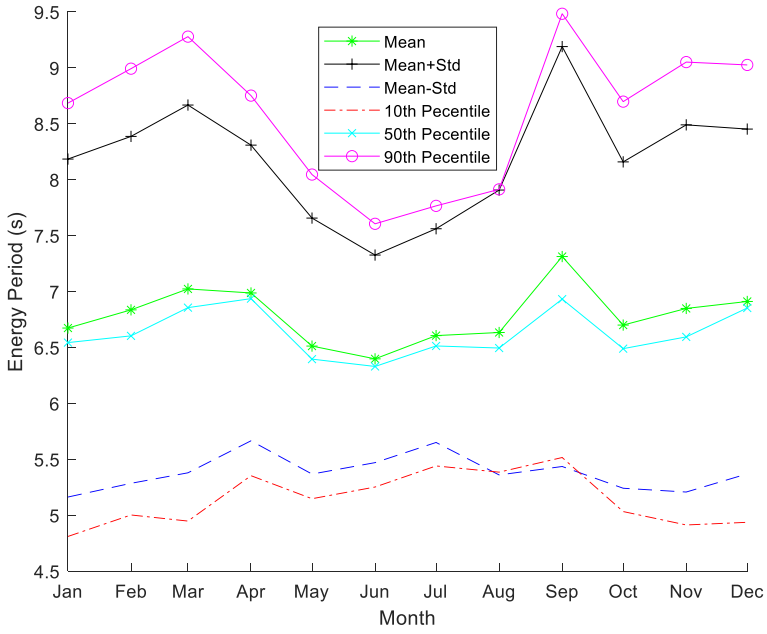

Figure 37: Monthly statistics for wave energy period at Cape Cod from 2000-2010

In Miami, significant wave height varies seasonally, with maximum average H_{m0} in November at 1.1m and minimum in July at 0.5m as seen in Figure 38. The mean significant wave height is greater than the median throughout the entire year, with more variation occurring between October and November, which correlates to hurricane season [78]. During this time, offshore storms will create larger sea states.

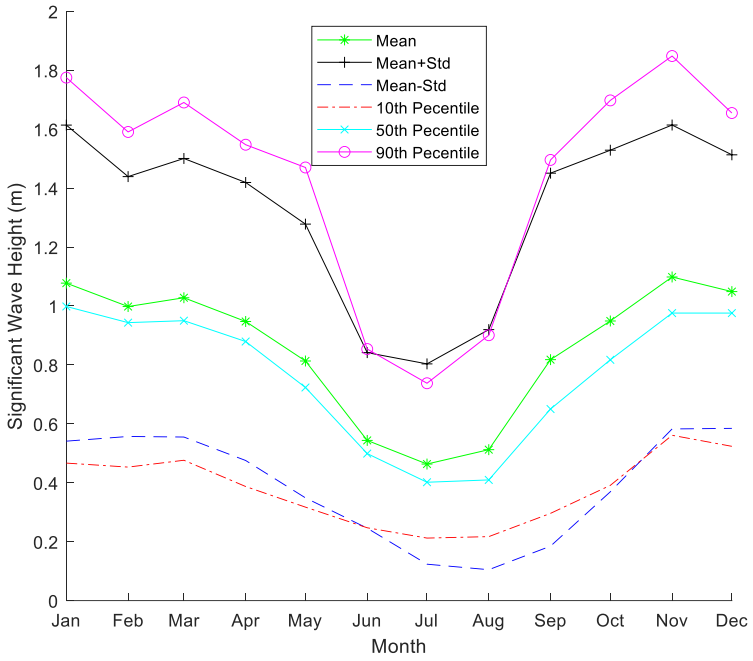

Figure 38: Monthly statistics for significant wave height at Miami from 2000-2010

Energy period also varies seasonally, seen in Figure 39, with a maximum mean of 6s in Nov. and minimum of 4s in July. Again, this is in line with expectations due to hurricane season during the fall and winter in the Atlantic. The mean energy period is consistently greater than the median indicating a slight positive skewness for the dataset due to larger energy periods in the record.

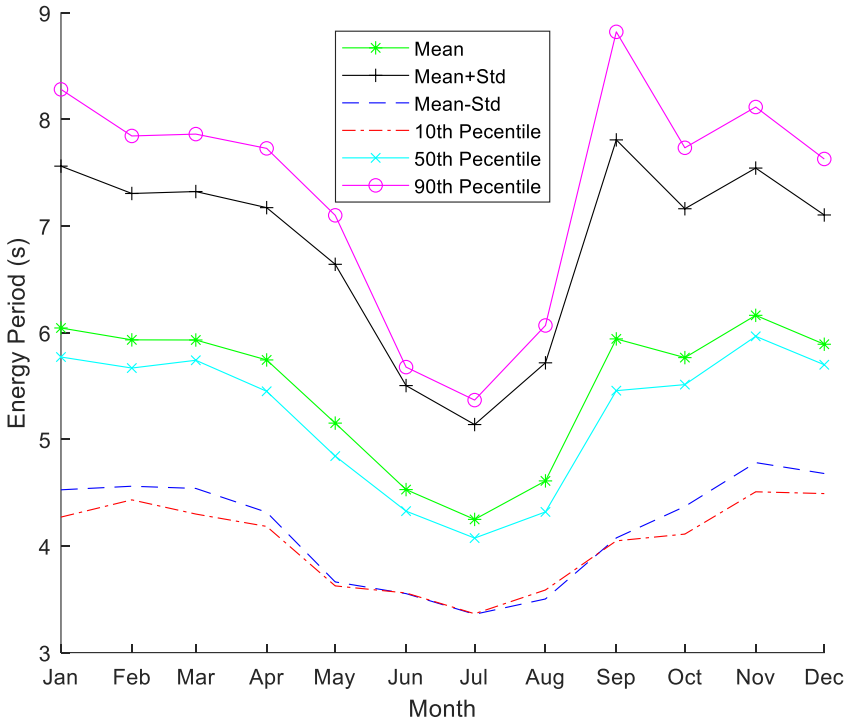

Figure 39: Monthly statistics for wave energy period at Miami from 2000-2010

A.2 Small WEC resource assessment results

As with the 1m WEC, the IEC power available for production is much greater than what was found for absorbable net power by the two cases, shown in Figure 40. Both the 1m and 2m analyses have similar orders of magnitude differences between the IEC power and the net power found for the cases.

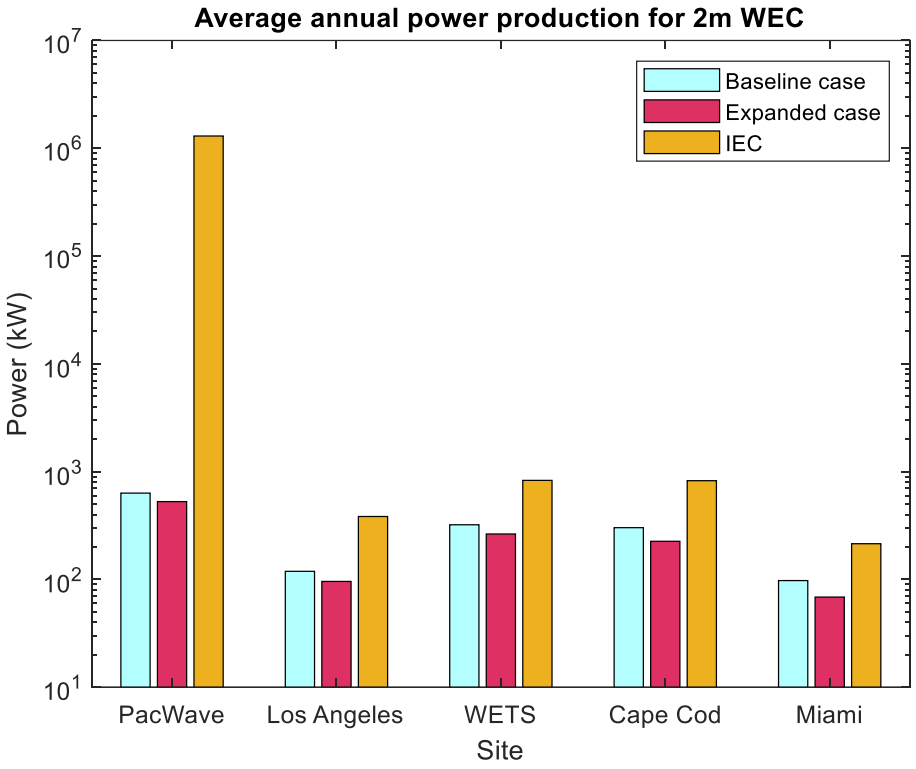

Figure 40: Total average annual power production for a 2m WEC from 2000-2010 for the baseline case and expanded case compared to the average annual gross power available according to the IEC assessment (y-axis is in logarithmic scale)

Figure 41 again shows that PacWave has the greatest amount of gross and net power, with about a three-magnitude difference between the IEC gross power and the baseline and expanded cases for a 5m WEC. At all locations, the baseline case yields more annual power than the expanded case.

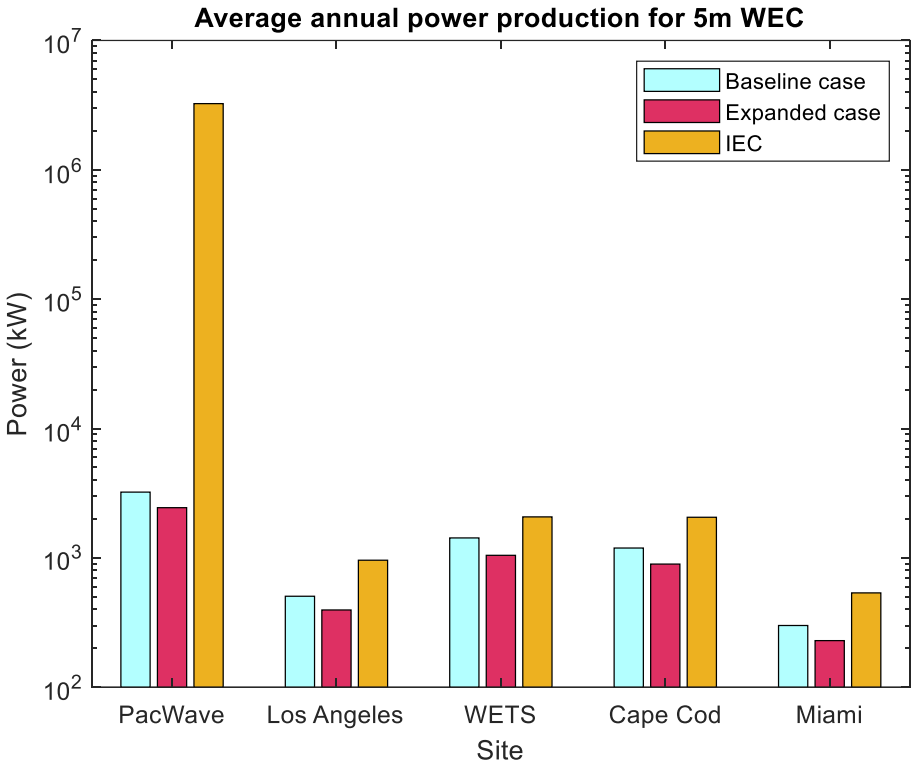

Figure 41: Total average annual power production for a 5m WEC from 2000-2010 for the baseline case and expanded case compared to the average annual gross power available according to the IEC assessment (y-axis is in logarithmic scale)

Figure 42 shows the average annual power production for a 10m WEC. The IEC gross power is consistently larger by multiple magnitudes compared to the baseline and expanded cases for net power. The baseline case is also greater than the expanded case at all locations.

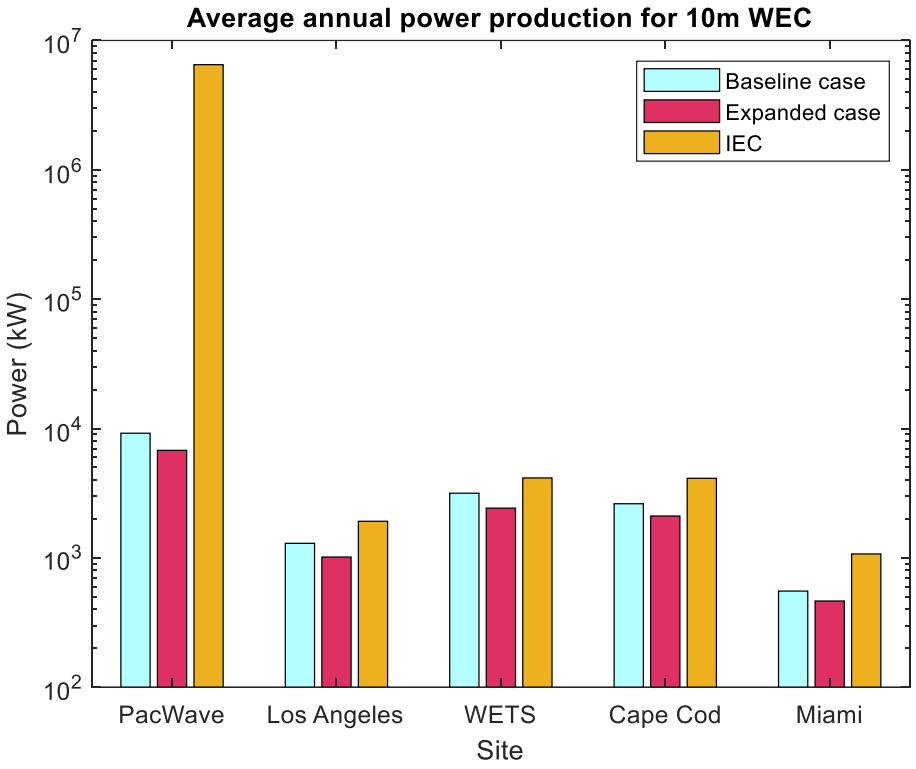

Figure 42: Total average annual power production for a 10m WEC from 2000-2010 for the baseline case and expanded case compared to the average annual gross power available according to the IEC assessment (y-axis is in logarithmic scale)

Looking closer at the baseline and expanded cases, Figure 43 through Figure 46 display the results for the comparison between the two cases for all WEC sizes and the remaining study locations. At each site and for each WEC the baseline case yields more average annual power than the expanded case. Again, this is due to the additional use of the gross power by the expanded case to filter out absorbable power.

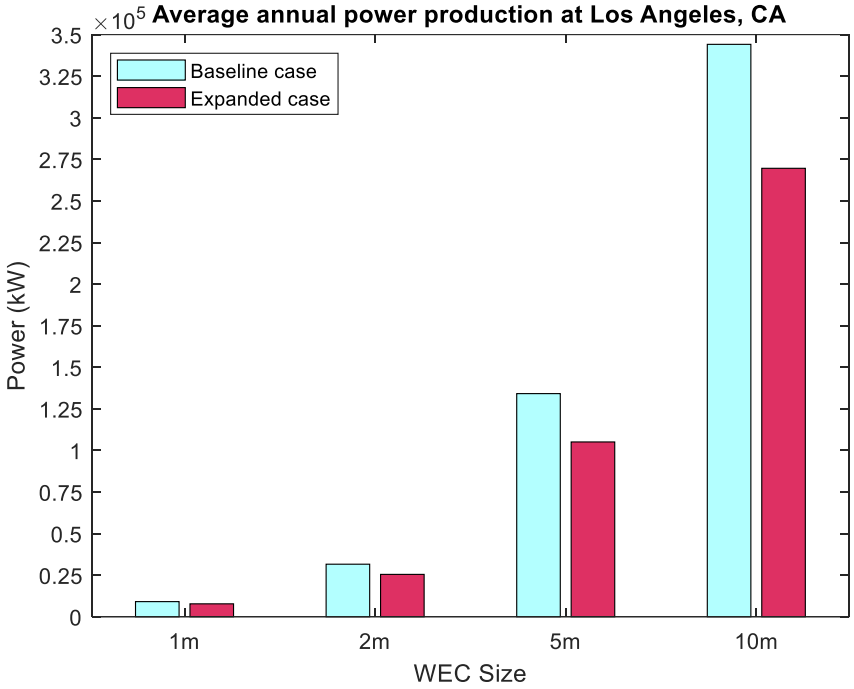

Figure 43: Total average annual power production for all WECs from 2000-2010 for the baseline case and expanded case at Los Angeles, CA

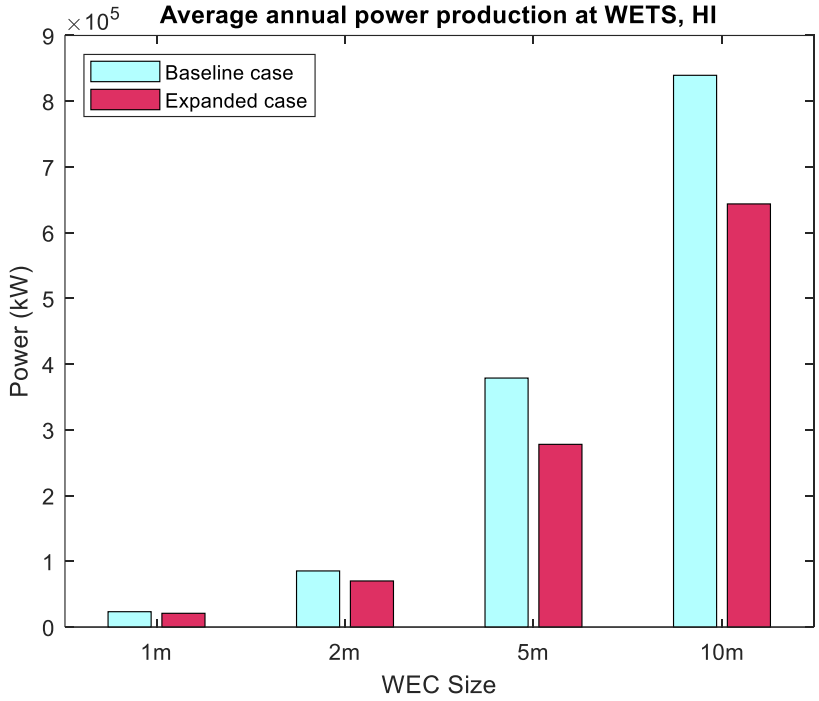

Figure 44: Total average annual power production for all WECs from 2000-2010 for the baseline case and expanded case at WETS, HI

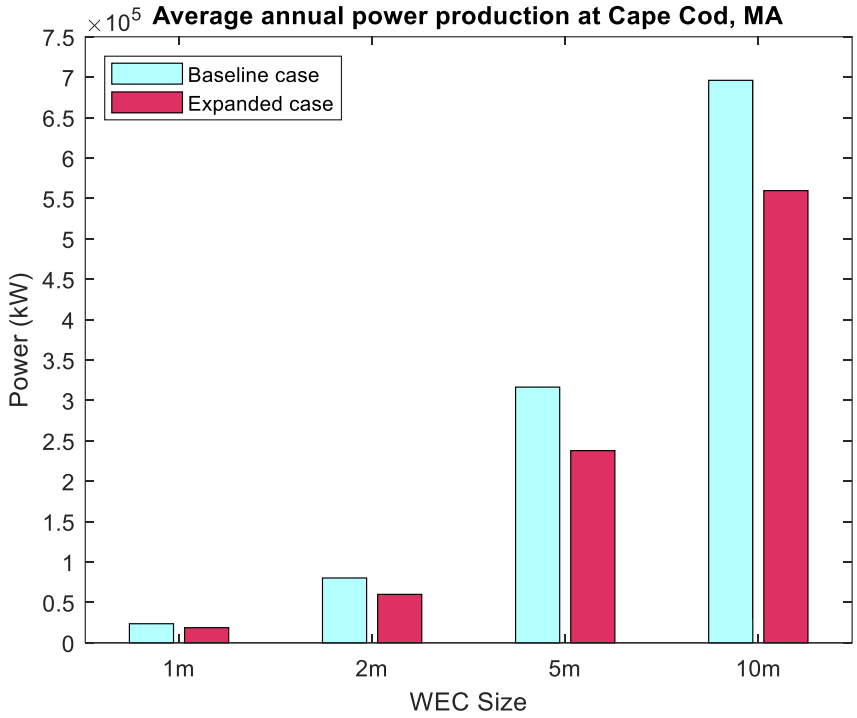

Figure 45: Total average annual power production for all WECs from 2000-2010 for the baseline case and expanded case at Cape Cod, MA

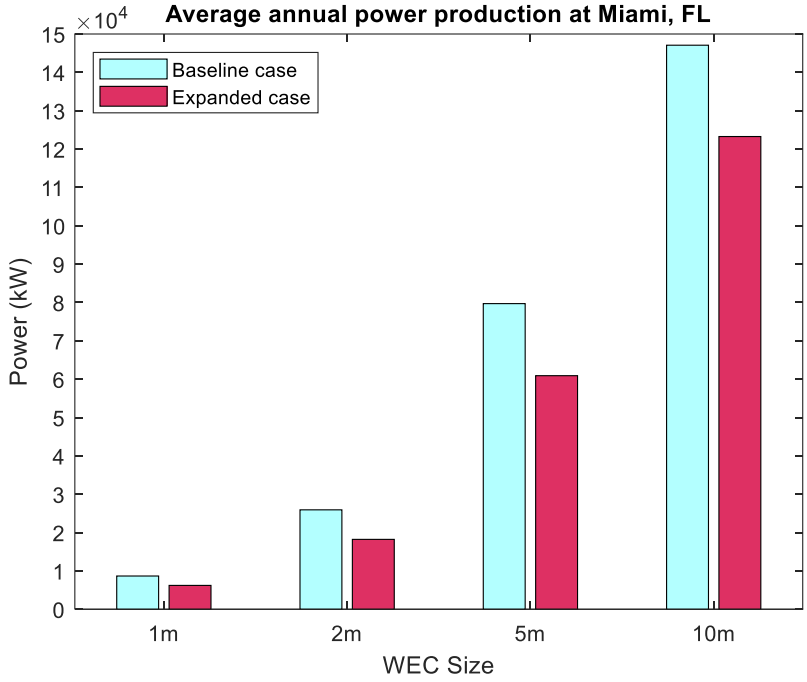

Figure 46: Total average annual power production for all WECs from 2000-2010 for the baseline case and expanded case at Miami, FL

The results for monthly average net power and COV for WEC sizes 2m, 5m, and 10m are shown below. Figure 47 shows the average P_{net} for each month at each site and the associated COV values for a 2m WEC.

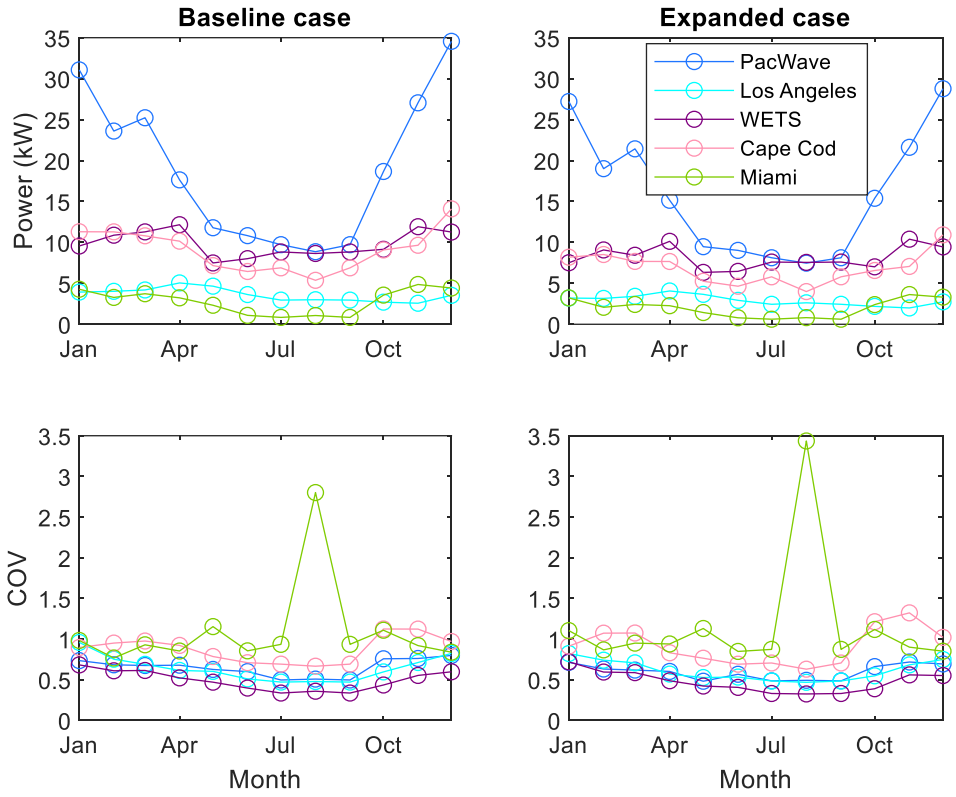

Figure 47: Monthly average power and COV for the baseline and expanded cases applied to a 2m WEC from 2000-2010

As with the 1m device, the 2m WEC sees the greatest P_{net} at PacWave in the winter months and the lowest P_{net} at Miami in the summer. Overall, the net power available to the device is greater for the 2m device than the 1m device since it interacts with more incident waves. For the baseline case, the maximum P_{net} in an average year at PacWave is 34.5 kW in December, at Los Angeles is 5 kW in April, at WETS is 12 kW in April, at Cape Cod is 14 kW in December, and at Miami is 5 kW in November. For the expanded case, a lesser overall P_{net} was calculated, with maximums in an average year at PacWave of 29 kW in December, at Los Angeles of 4 kW in November, at WETS of 10 kW in April, at Cape Cod of 11 kW in December, and at Miami of 4 kW in November.

The COV of P_{net} for a 2m device for both cases follows the same patterns as those of the 1m device. Miami possesses the highest COV in August, followed by Cape Cod, Los Angeles and PacWave, and finally WETS. The expanded case sees a higher COV on average for all locations than the baseline case.

Figure 48 illustrates the mean P_{net} and COV of P_{net} per average year for a 5m WEC for all study locations and both the baseline and expanded cases.

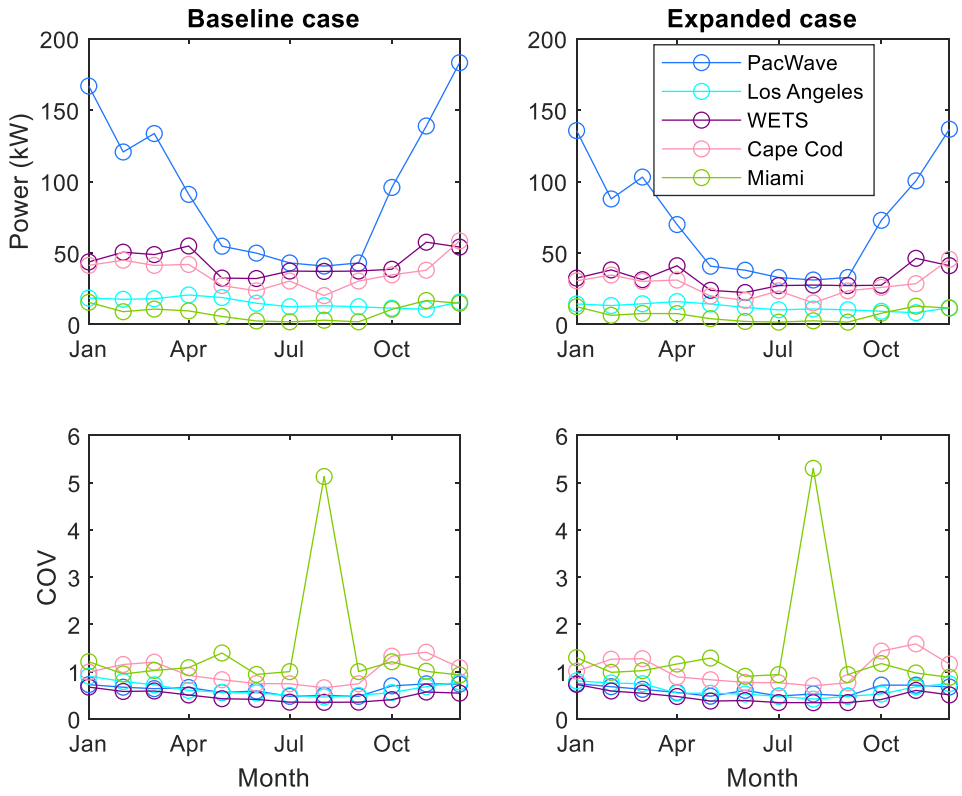

Figure 48: Monthly average power and COV for the baseline and expanded cases applied to a 5m WEC from 2000-2010

Again, the overall P_{net} for each month and case increased for the 5m device compared to the 1m and 2m WECs. For the baseline case, PacWave has the largest amount of P_{net} with 183 kW in December. Further down the West Coast, Los Angeles has a maximum P_{net} of 20 kW in April, WETS is maximum

with 58 kW in November, Cape Cod is 58 kW in December, and Miami 17 kW in November. The expanded case has less overall P_{net}, with PacWave's maximum of 137 kW in December, Los Angeles's 16 kW in April, WETS's 46 kW in November, Cape Cod's 46 kW in December, and Miami's 13 kW in November.

The COVs for the 5m device adhere to the same patterns as the 1m and 2m WECs, but the values are overall larger. WETS still has the lowest COV for both cases, staying under 1. Miami overall has the highest COV for both cases, reaching a maximum of 5.

Figure 49 shows the mean P_{net} and COV of P_{net} in an average year for a 10m device at all locations.

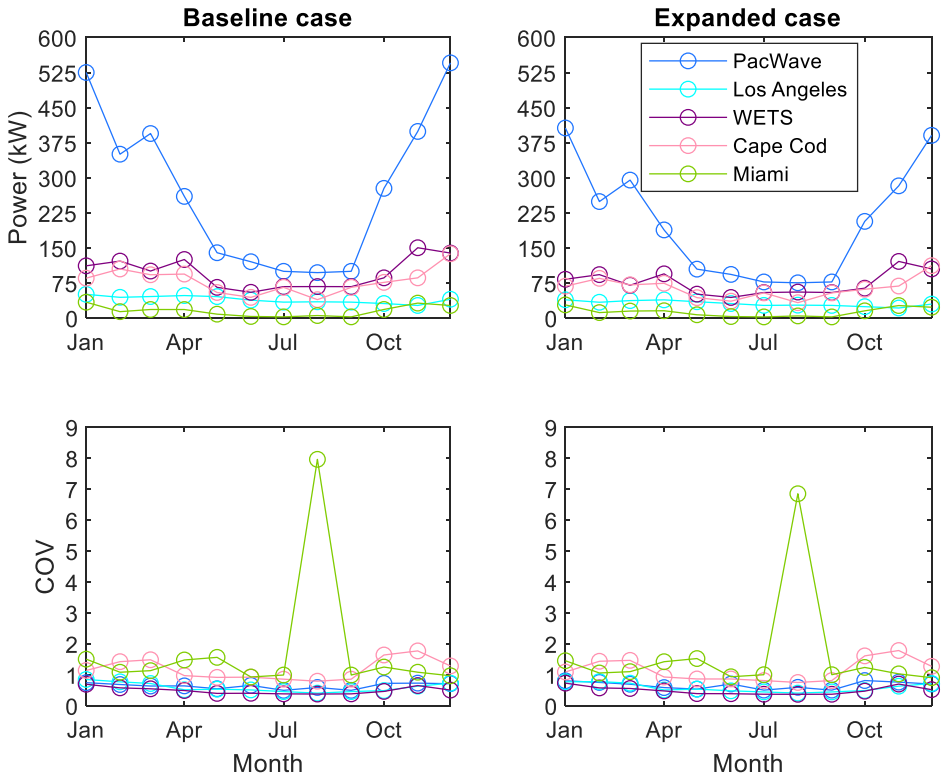

Figure 49: Monthly average power and COV for the baseline and expanded cases applied to a 10m WEC from 2000-2010

In Figure 49, the mean P_{net} in an average year for a 10m WEC for both cases is shown. This device encounters the most incident wave power out of all the WECs studied in this thesis, and therefore has the greatest amount of P_{net} available. In the baseline case, PacWave has the greatest amount of P_{net} with 546 kW in December. Los Angeles has a maximum average P_{net} of 48 kW in April, WETS has 150 kW in November, Cape Cod has 137 kW in December, and Miami has the lowest maximum average P_{net} with 32 kW in November. The expanded case sees significantly less amount of average P_{net}, with PacWave's maximum mean P_{net} of 406 kW in January, Los Angeles's maximum mean P_{net} of 38 kW in April, WETS's of 121 kW in November, Cape Cod's 112 kW in December, and Miami's 27 kW in November.

COVs in Figure 49 remain relatively close to those of the 2m and 5m devices, yet Miami's COV increases to 8 for the baseline case and 7 for the expanded case in August, indicating a great variation of net power from the mean value during that month. WETS continues to have the lowest COV, meaning the site has the steadiest resource.

Annual maximum measurements of net power were found for the expanded case at all locations. Figure 50 shows the maximum net power measurements per year at PacWave for the baseline case. While the 1m and 2m device maximums for the expanded case are comparable to the baseline case, the maximums for the all devices are generally larger for the baseline case.

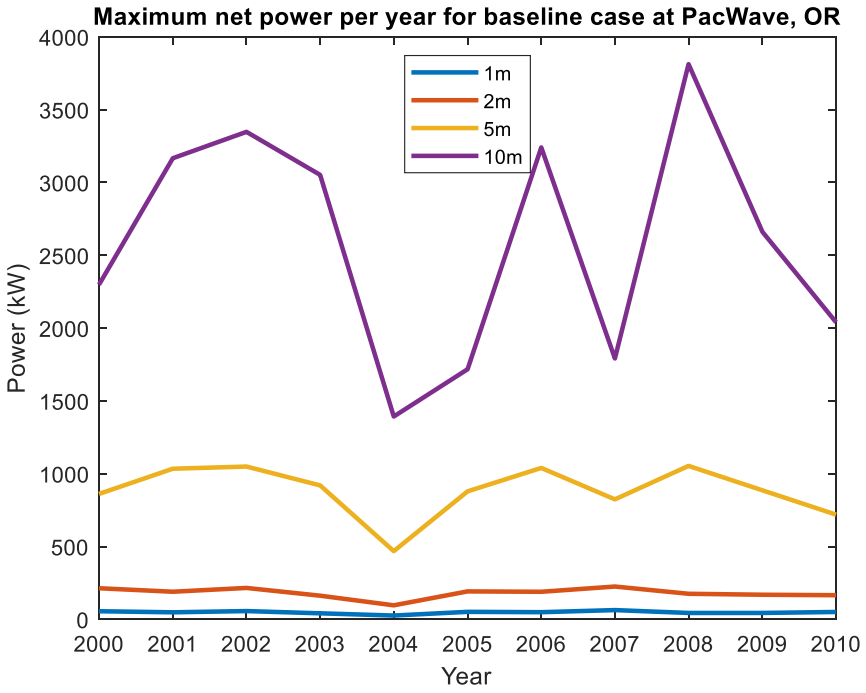

Figure 50: Annual maximum net power for the baseline case at PacWave from 2000-2010

In Figure 51 are the maximum net power values per year at Los Angeles. As with the expanded case, peaks for the maximum net power are seen in 2001, 2002, 2003, 2006, and 2008.

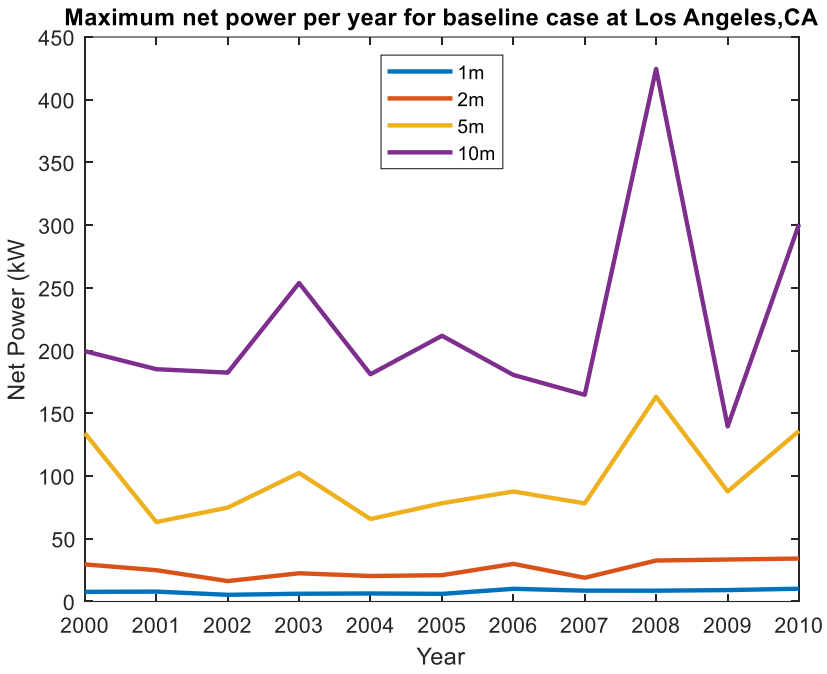

Figure 51: Annual maximum net power for the baseline case at Los Angeles from 2000-2010

Figure 52 shows the maximum net power values per year at WETS for the baseline case.

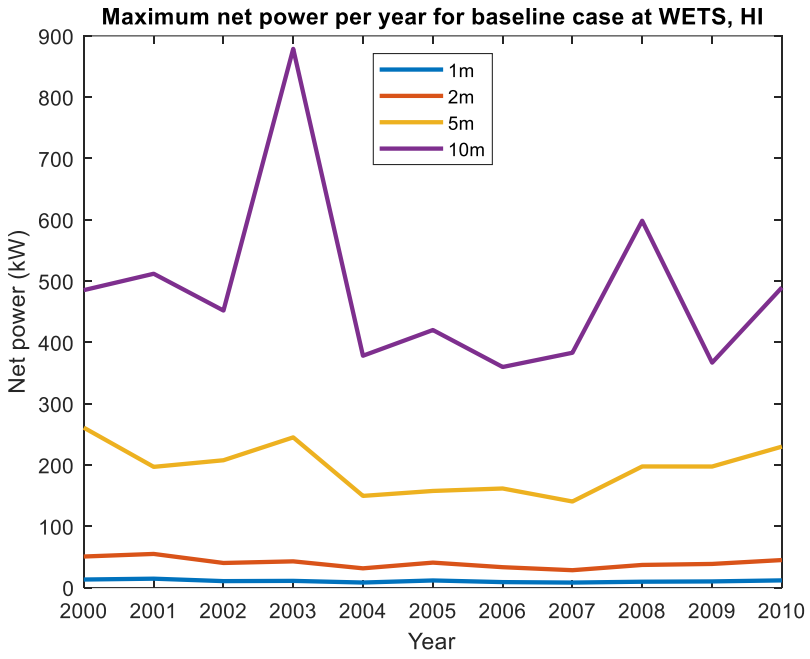

Figure 52: Annual maximum net power for the baseline case at WETS from 2000-2010

Figure 53 describes the maximum net power per year at Cape Cod for all four different WEC sizes for the baseline case.

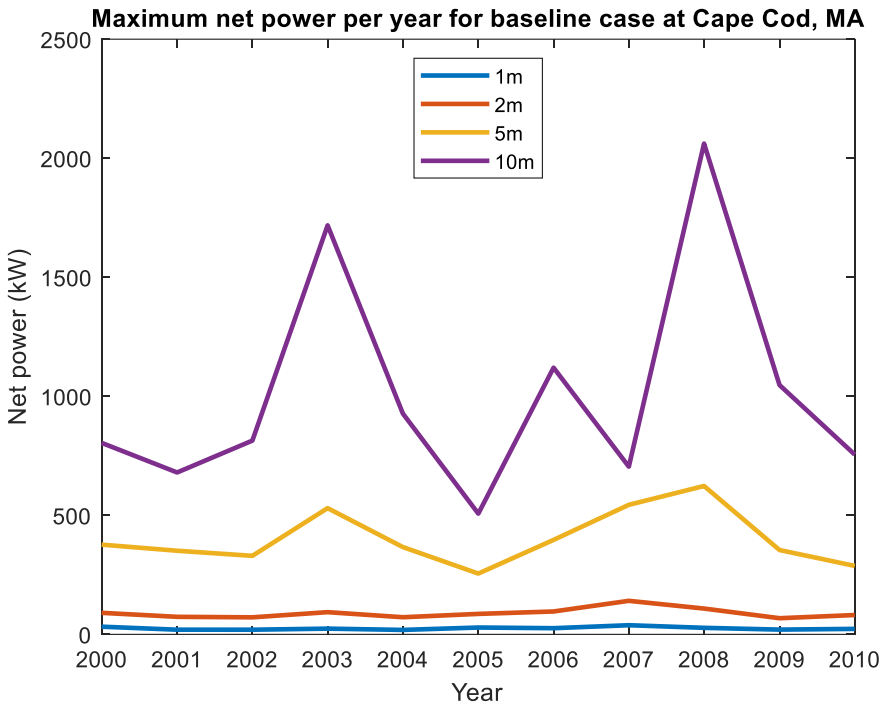

Figure 53: Annual maximum net power for the baseline case at Cape Cod from 2000-2010

In Figure 54 are the maximum net power values per year at Miami for the baseline case.

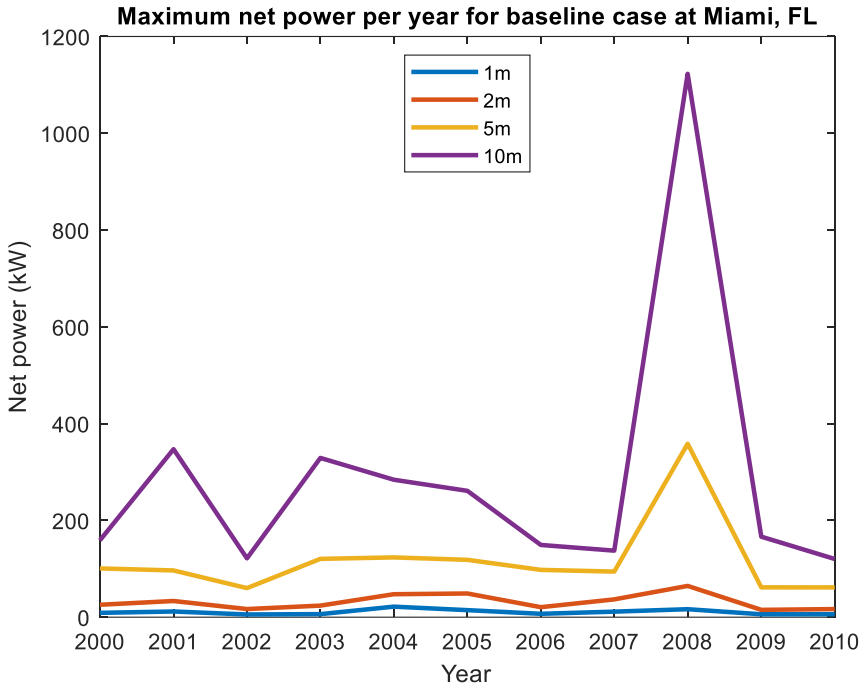

Figure 54: Annual maximum net power for the baseline case at Miami from 2000-2010

Appendix B: PacWave Wave Resource Assessment

Following is a published report completed by the author in Summer 2020. The PacWave Wave Resource Assessment was completed to give industry and WEC developers an idea of the resource available specifically at PacWave North and South. The PDF of the document begins on the next page.

PACWAVE WAVE RESOURCE ASSESSMENT

Prepared by:
Gabrielle Dunkle,
Oregon State
University Bryson
Robertson, Oregon
State University*
Gabriel García-Medina, Pacific Northwest
National LaboratoryZhaoqing Yang, Pacific
Northwest National Laboratory
*bryson.robertson@oregonstate.edu

PMEC
Pacific Marine Energy Center

Oregon State
University

TABLE OF CONTENTS

Note: Document has been updated (Nov. 2020) to reflect wave energy resource at centroid of PacWave South test site and northeast corner of PacWave North test site. The previous edition described wave energy at a location ~1 mile east of PWS centroid. New results prove the resource has not changed significantly between the two locations, and all conclusions from the previous edition still stand.

1 INTRODUCTION

The Pacific Northwest of the United States is characterized by one of the greatest annual mean wave power resources in the world [1]. As a result, the wave energy resource offshore of Oregon has been characterized, through hindcast models and physical buoy data, throughout the past decade [2]–[4]. Over the past 8 years, Oregon State University (OSU) has been developing an open-ocean wave energy test facility, PacWave, which is affiliated with the Pacific Marine Energy Center (PMEC). The facility consists of north and south test sites off the coast of Newport, Oregon.

This report contains detailed analysis of wave characteristics at both the north and south sites based on a newly available 32-year SWAN hindcast simulation [5] and follows the recommendations issued by the International Electrotechnical Commission (IEC) technical specification (TS) 62600-101 for wave energy resource assessments [6]. This assessment aims to build upon the previous wave energy characterizations in the region and provide the most up-to-date characterization of the wave energy resource at PacWave.

2 NEWPORT BUOYS AND SWAN HINDCAST MODEL

There are various sources for physically observed sea state data in the PacWave region. PMEC measured meteorological, wind, wave, current, and ocean surface salinity andtemperature data at PacWave South from November 2014 through January 2015, and again fromMay 2015 through December 2015. Additionally, the Ocean Observatories Initiative of the National Science Foundation has collected physical wave data spanning from January 2015 through April 2019; located at 44°38’21”N 124°18’15”W and 80 m depth. In the general vicinity are multiple National Oceanographic and Atmospheric Administration (NOAA) National Data Buoy Center (NDBC) stations as well, from which various data are highlighted in this report.

The specific location of the model for the purpose of this assessment is the PacWave North site at 44.7021°N, 124.146°W and the PacWave South site at 44.557°N, 124.229°W, which are about 10 miles (16 km) apart and off the coast of Newport, Oregon, demonstrated in Figure 1. The point chosen for PacWave North is 0.3 miles north of the northeast corner of the test site while the point for PacWave South is almost in the exact center of the site. The mean depth at the PacWave North point is 53.0 m and 67.4 m for PacWave South. PacWave South results are examined in the main text of this report; corresponding PacWave North results can be found in the Appendix.

This wave resource assessment was conducted from the years 1980-2010, part of a 32-year hindcast conducted by the Pacific Northwest National Laboratory (PNNL) [5], which operates within the U.S. Department of Energy. The hindcast model constructed by PNNL used nested-grid WaveWatch III (WW3) wave model on both global and regional scales [5]. The WW3 model was paired with a high-resolution, unstructured-grid Simulating WAves Nearshore (SWAN) model via traditional one-way nesting. Both models are forced by Climate Forecast System Reanalysis (CFSR) wind fields [5]. These models are classified as in between a Class 1 Reconnaissance study and a Class 2 Feasibility study by the IEC standard due to their temporal and spatial resolutions [4][5], therefore this IEC specification assessment can generally be classified as a Class 1 Reconnaissance study [6].

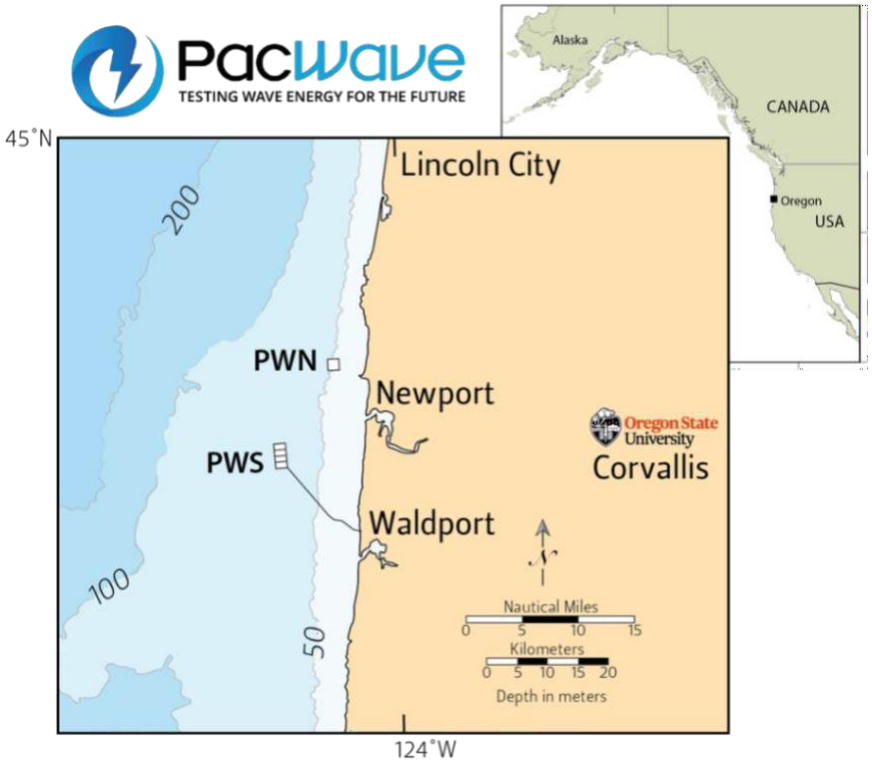

Figure 1: PacWave North (PWN) and South (PWS) locations off the coast of central Oregon (PacWave, 2020)

The use of SWAN with CFSR winds simulates nearshore wave processes along the U.S. West Coast, and was validated by observed buoy data from 28 wave buoys in the region. Wu et al. (2020) demonstrated the congruence between the PNNL model's prediction of IEC wave energy parameters and those recorded at physical buoy stations, accurately providing a reliable wave climate model in the nearshore region of interest [5]. Satisfactory accuracy was also achieved when comparing the spectra distributions in both frequency and directional domains at sites with extreme values, i.e. regions with maximum and minimum wave energy [4]. For detailed model validation methods and results, please see Wu et al., 2020 [5].

The IEC standard states that a minimum of 10 years of data should be used for this type of assessment, however according to both the IEC specification and Yang et al. [4], a longer period of data may be necessary to quantify the low frequency climate variability and its effect on a wave energy resource assessment. This is highlighted in the wave resource results section of this assessment, where the long-term mean and its seasonal variability of each IEC wave energy resource parameters are analyzed.

3 WAVE RESOURCE CHARACTERISTIC PARAMETERS

The sea states are characterized with directional wave spectra, which are described below and sourced from the IEC TS 62600-101 [6]. The variance density described over the i^{th}discrete frequency and j^{th}discrete direction is S_{ij}.

To calculate directionally unresolved (omni-directional) characteristic quantities, the two-dimensional frequency-directional variance densities are transformed into one-dimensional frequency resolved variance densities of θ increments such that:

$$S_i = \sum_j S_{ij} \Delta\theta_j \quad (1)$$

Spectral moments of the n^{th} order, m_n, are calculated from the frequency variance density by:

$$m_n = \sum_i f_i^n S_i \Delta f_i \quad (2)$$

where f_i is the ith discrete frequency. Omni-directional wave power J is the time averaged energy flux through a vertical cross section of unit diameter that extends from the seafloor to the surface, calculated by:

$$J = \rho g \sum_{i,j} c_{g,i} S_{ij} \Delta f_i \Delta\theta_j \quad (3)$$

where

$$c_{g,i} = \frac{\pi f_i}{k_i}\left(1 + \frac{2k_i h}{sinh 2k_i h}\right) \quad (4)$$

where k_i is the wave number at the i^{th} frequency and h is the mean sea level.

The time-averaged energy flux across a plane normalized to direction θ is defined as the directionally resolved wave power. This directionally resolved wave energy transport is the sum of the contributions of each component with a positive component in direction θ, calculated by:

$$J = \rho g \sum \quad c \quad S \quad \Delta f \quad \cos(\theta - \theta) \delta \qquad \begin{cases} \delta = 1, & \cos(\theta - \theta_j) \geq 0 \end{cases} \quad (5)$$

θ $\boldsymbol{j}$ g,i ij i j j $\delta = 0, \quad \cos(\theta - \theta_j) < 0$

The maximum value of J_θ represents the maximum time averaged wave power propagating in a single direction and is denoted by $J_{\theta_{Jmax}}$. Angles in SWAN were calculated in Cartesian with east being the zero-degree bearing [7], and are adjusted such that North is the zero-degree bearing where necessary.

A characteristic wave height of the given sea state is calculated using the zeroth spectral moment by:

$$H_{m0} = 4\sqrt{m_0} \tag{6}$$

This is referred to as the significant wave height calculated from the wave spectrum, which is not the same value as the significant wave height calculated from a wave-by-wave analysis, $H_{1/3}$. $H_{1/3}$, commonly referred to as H_s, is a direct measure of significant wave height whereas H_{m0} is estimated based on the spectrum via (6).

The preferred characteristic wave period for wave resource assessments is the energy period. Energy period is calculated using moments of the wave spectrum by:

$$T_e \equiv T_{-10} = \frac{m_{-1}}{m_o} \tag{7}$$

The directionality coefficient is a characteristic measure of the directional spreading of wave power. It is the ratio of the maximum directionally resolved wave energy transport to the omni-directional wave energy transport:

$$d = \frac{J_{\theta_{Jmax}}}{J} \tag{8}$$

Spectral width characterizes the relative spreading of the energy along the wave spectrum, and provides an idea of the makeup of the sea state [8]. This parameter is defined using the moments of the wave spectrum as:

$$\epsilon_0 = \sqrt{\frac{m_0 m_{-2}}{m_{-1}^2} - 1} \tag{9}$$

The preceding variables were outputs from the SWAN model used in the PNNL hindcast, whose wave parameters are computed from the wave spectrum [7]. These spectral quantities were used in the following analysis of the wave energy resource at PacWave.

4 WAVE RESOURCE RESULTS

4.1 Annual histogram of sea state occurrences

Figure 2 shows the annual frequency of occurrence of sea states parameterized in terms of the significant wave heights, H_{m0}, with a resolution of 0.5 m and energy period, T_e, with a resolution of 1 s as per the IEC specification recommendation. The numbers in each cell represent mean annual hours recorded in each specific H_{m0} - T_e sea state combination. The shading of the cells is an energy flux weighted representation; with the output of particular sea state occurrence calculated by $0.5 \cdot H_{m0}^2 \; T_e$ multiplied by the hours of occurrence. Figure 2 shows the annual mean bivariate histogram from 1980-2010 at PacWave South.

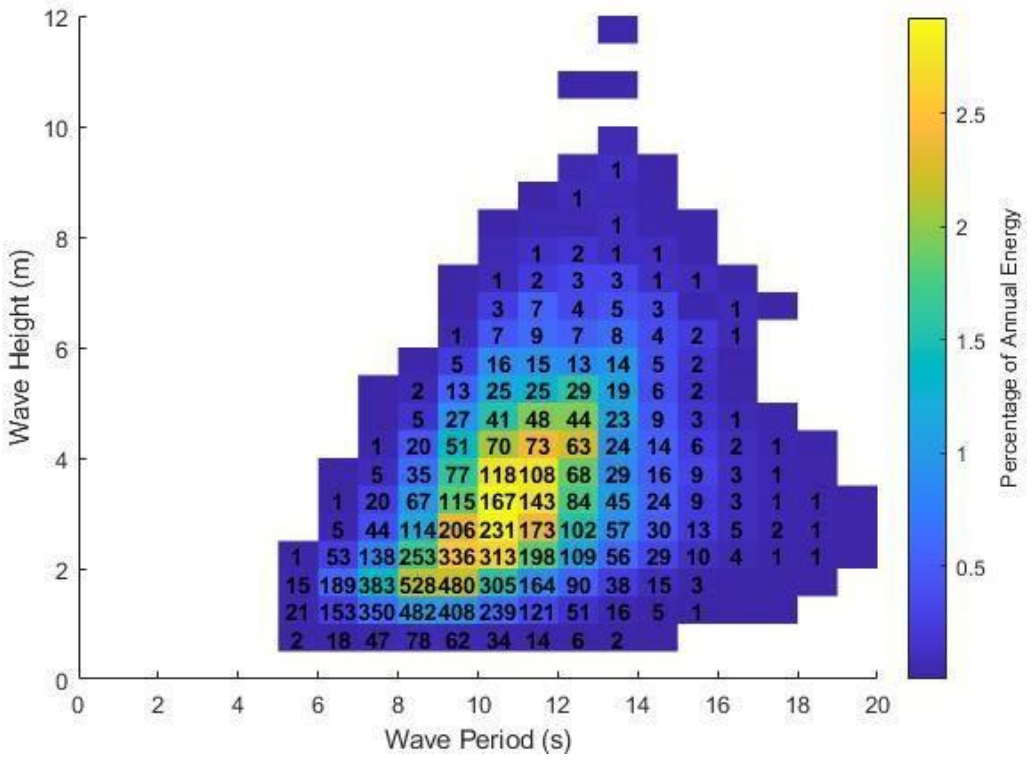

Figure 2: Omni-directional SWAN sea-state histogram from 1980-2010 at PacWave South (annual mean conditions)

At PacWave South, the most commonly occurring seas occur for 528 hours per year with a significant wave height of 1.75 m and an energy period of 8.5 s, while the highest annualized

wave energy sea state occurs for 231 hours per year at a significant wave height of 2.75 m and at an energy period of 10.5 s.

4.2 Annual wave rose

An annual wave rose depicts the long-term joint distribution of the maximum directionally resolved wave energy transport ($J_{\theta_{Jmax}}$) along the direction of maximum directionally resolved energy transport (θ_{Jmax}). Each sea state is represented by a single directionally resolved wave power and associated direction. Figure 3 shows the distributions of the total maximum directionally resolved wave energy transport in W/m. Each bar combines wave headings in a 15° bin, and the length of each color segment represents the annual wave energy transport in a given direction.

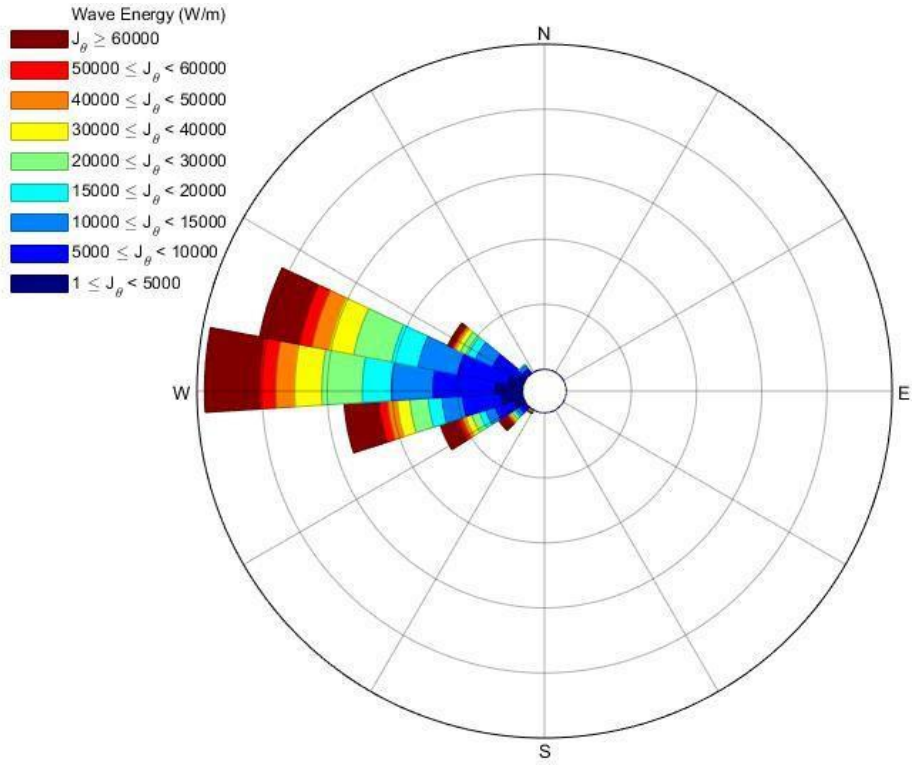

Figure 3: Directionally resolved SWAN wave rose distribution of wave energy from 1980-2010 at PacWave South

The waves come predominately from the west-northwest directions at PacWave South, accounting for the majority of the direction of directionally resolved wave energy throughout the hindcast.

4.3 Annual variation of long-term monthly mean

The long-term monthly mean of wave resource characteristic parameters required by the IEC and are analyzed in the following section. Monthly averages over the years, variations of the mean, variation of one standard deviation above and below the mean, and 10th, 50th, and 90th percentiles are plotted in order to show the statistical monthly variations. The percentile analysis is completed in order to show the limits of the datasets and identify the median. The 10th and 90th percentiles are used to show the upper and lower limits of the data, and the 50th percentile is equivalent to the median of the dataset.

In a normal distribution, the curve of a dataset is symmetric about the mean, earning the common reference of a "bell curve." If a dataset is skewed, the shape of the distribution has asymmetric qualities. Figure 4 offers a visual perspective of skewness in a dataset by comparing variously skewed distributions. By comparing the mean and the median of the distribution, it is possible to assess the degree of skewness. If the mean value is greater than the median, the dataset is positively skewed, meaning that the distribution has the majority of occurrences on the lower end of the curve. This is typical of sea state distributions, as more extreme events are less frequent. For a detailed review of the extreme wave climate and storms on the Oregon coast, refer to Ruggiero et al. (2009) [9].

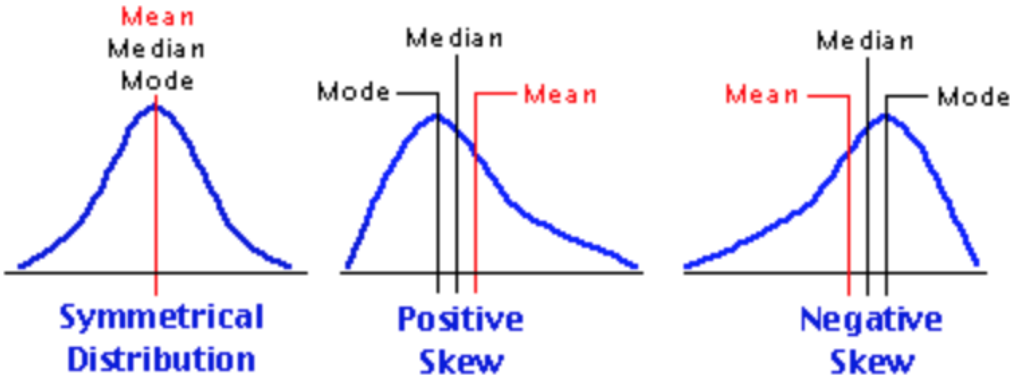

Figure 4: Skewness can be indicated by the difference of the median (50th percentile) and the mean. Larger differences between percentiles and the mean determine the degree to which the distribution is skewed. (CFA, 2020)

Figure 5 depicts the trend of significant wave height at PacWave South, demonstrating the pattern of seasonal change of the wave characteristics. The mean wave height at the site peaks in December at 3.5 m, and steadily falls to a minimum value of 1.75 m in August. In the winter, between November and March, the average wave height varies between 3 and 3.5 m, and the distribution is more positively skewed as the 90th percentile values correspond to more extreme wave height conditions. The summer months, between May and September, stay between 1.5 and 2 m, signifying a more normally distributed range of wave heights as the percentile values range closer to the mean value. This effect can be described as seasonality, where wave heights vary according to different seasons throughout year. Wave heights increase as frequency of extreme sea states increases in the winter, while summer months see smaller sea states.

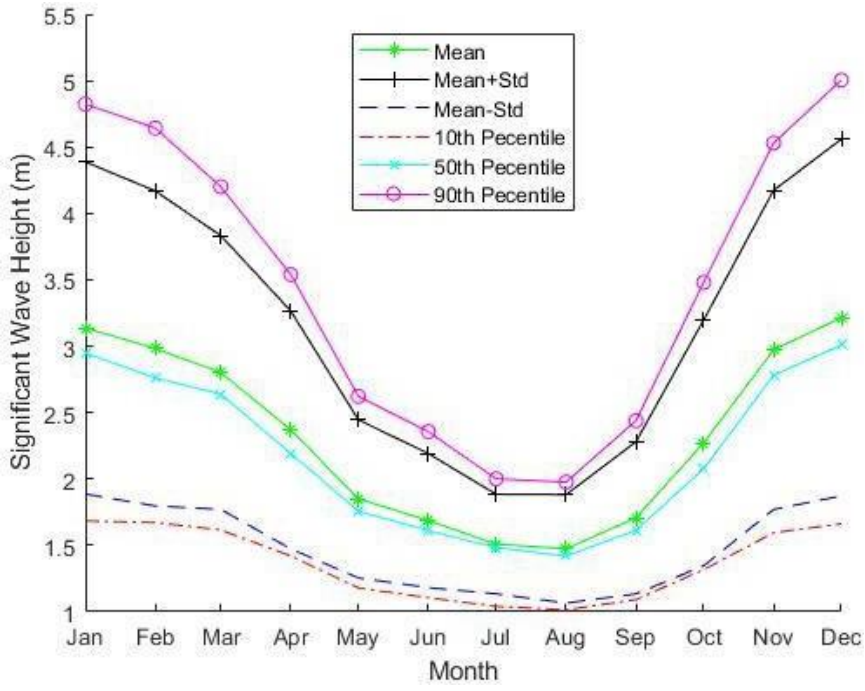

Figure 5: Monthly mean of SWAN significant wave height from 1980-2010 at PacWave South

As shown in Figure 6, the mean energy period is minimum in the summer months with values around 9 s compared to the maximum seen in winter months ranging from 11-12 s. In the summer, waves are forced primarily by local winds, inducing high frequency waves indicated by the lower wave periods. Energy period peaks in February at 11.3 s and is lowest in July at 8.5 s. Wave period is generally normally distributed, which is reflected in Figure 6.

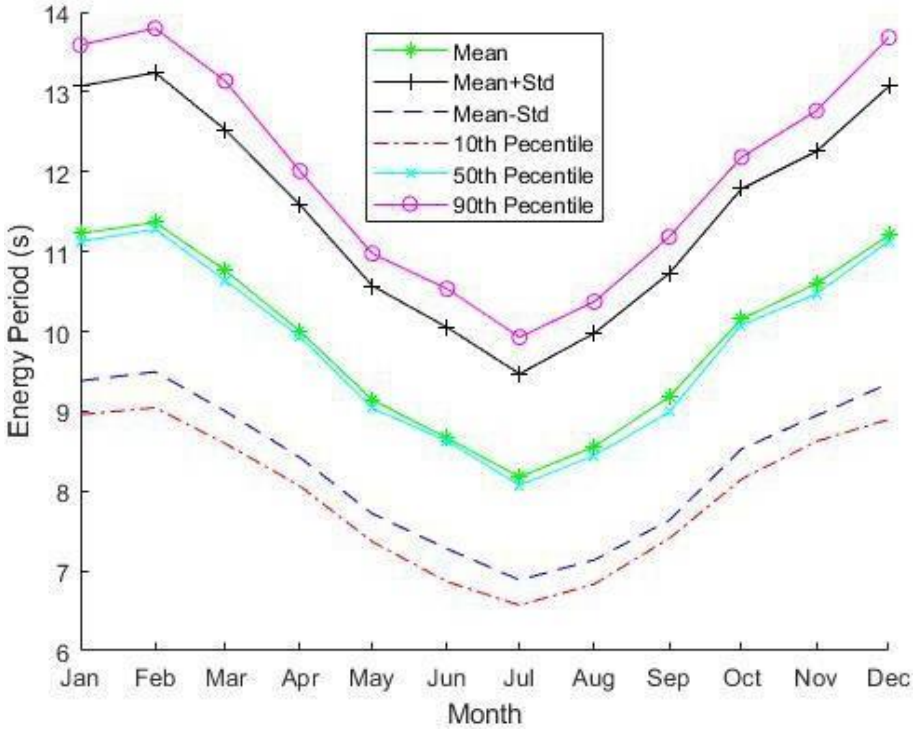

Figure 6: Monthly mean of SWAN wave energy period from 1980-2010 at PacWave South

The omni-directional wave energy transport is shown in Figure 7. The greatest average wave energy occurs in the winter months from 70-80 kW/m and stays in this range from November through February. This is expected, as winter months have more energetic seas due to storms [9]. With storms come extreme sea state events, which cause the large deviations from the mean during these months. Summer months see less variation from the mean due to less energetic sea states. This is another instance in which the data is positively skewed: the 90th percentile values are significantly larger in the winter months and stray from the mean value line, whereas summer months have percentile values that are more normally distributed about the mean.

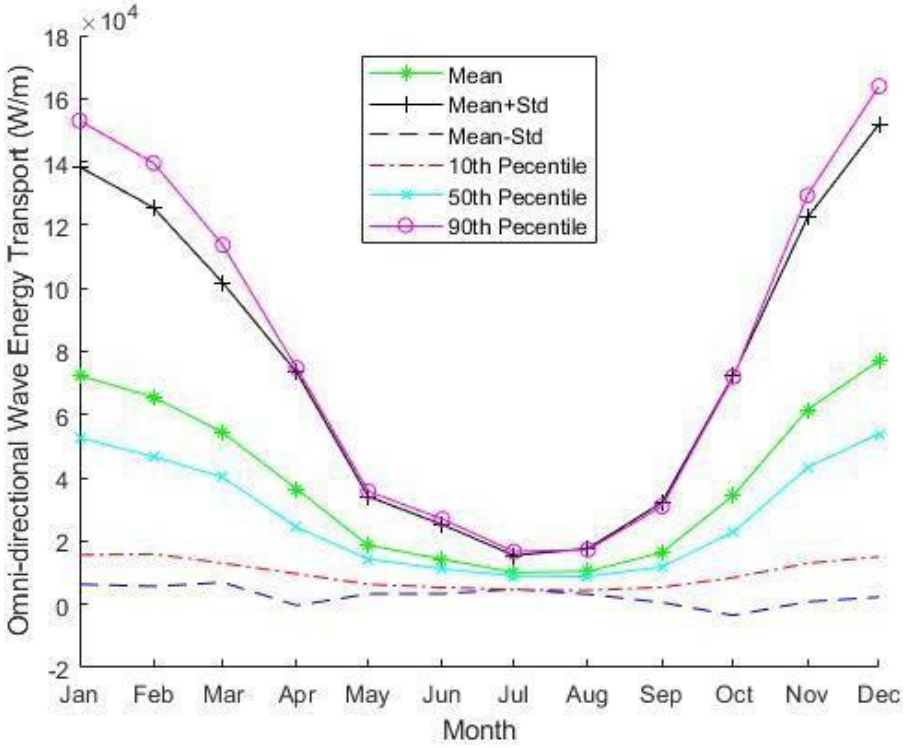

Figure 7: Monthly mean of SWAN omni-directional wave energy transport from 1980-2010 at PacWave South

Figure 8 shows the maximum directionally resolved wave energy transport. As expected, the directionally resolved wave energy transport peaks in the winter months at 75 kW/m and has a minimum in the summer at under 20 kW/m. As with the omni-directional wave energy transport, the directionally resolved wave energy transport also shows positive skewness in the winter and more normally distributed values in the summer.

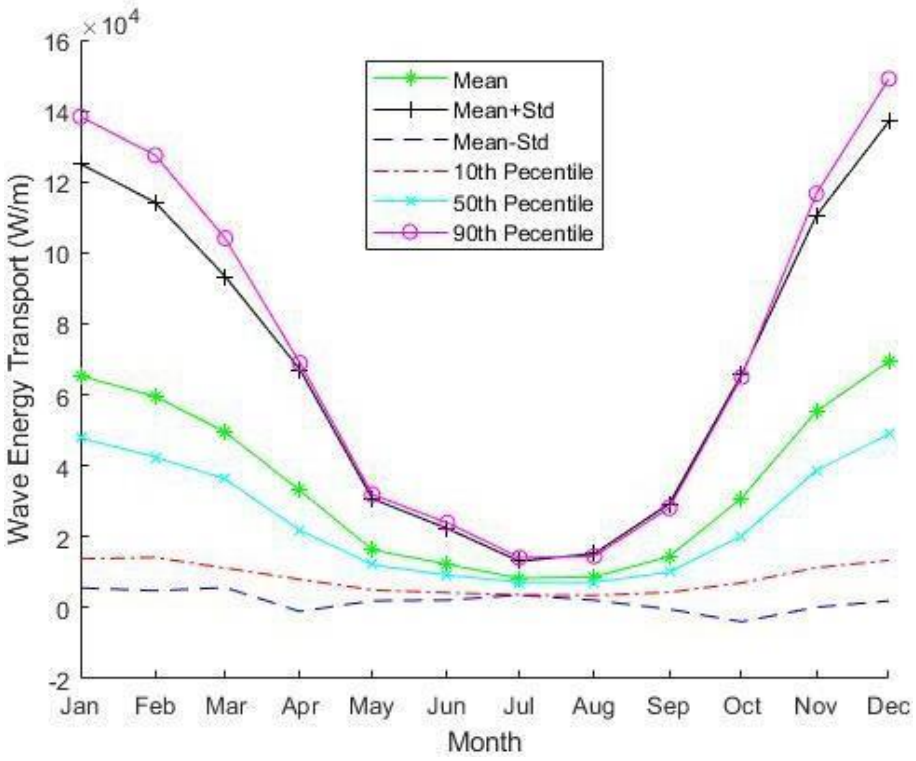

Figure 8: Monthly mean of maximum directionally resolved SWAN wave energy transport from 1980-2010 at PacWave South

Figure 9 describes the mean direction of the maximum directionally resolved wave energy transport. The direction values were adjusted such that the datum was 0° North, and all values were measured clockwise (i.e. Nautical direction convention). In doing so, all output values per 90° section of the circle were adjusted to the correct range as if they were originally measured from the 0° North datum. For example: 180 + (90° - θ) places measurements as though they were taken from 0° North. This method ensured that minimal wave values were recorded as if they originated from the coast and propagated offshore.

The slight variation in mean direction over time indicates that the wave field has a narrow directional change. The directional data is normally distributed about the mean, with average values ranging between 270 and 300 degrees as expected, which can be confirmed by the wave rose in Figure 3.

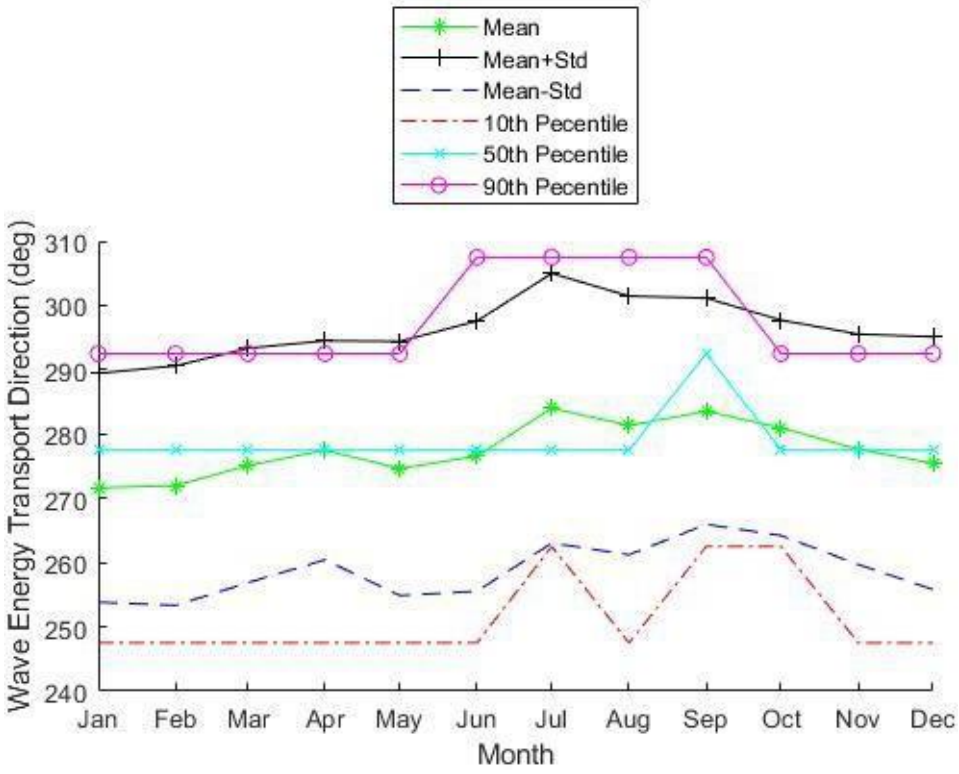

Figure 9: Monthly mean of direction of SWAN directional wave energy transport from 1980-2010 at PacWave South

Figure 10 shows that the average directionality coefficient at PacWave South varies according to season, similar to the majority of previously evaluated wave characteristics. Recall that this plot describes the ratio of J and $J_{\theta_{Jmax}}$. Higher values of directionality coefficient relate to a narrow spread of wave directions in that J and $J_{\theta_{Jmax}}$ are closer in value; approaching a value of 1 indicates that the majority of omni-directional wave energy transport is resolved to a narrow-band of directions. Since the maximum values of the directionality coefficient are seen in winter months, it can be inferred that these months see convergence to a narrower field of directions, mainly due to storm dominated sea states. In the summer, the wave field is comprised of both wind waves, that propagate in a greater variety of directions, and ocean swells. This is indicated by lower values of directionality coefficient from May through September. Overall, the mean directionality varies by less than 0.1 throughout the year, indicating a relatively constant directional bandwidth.

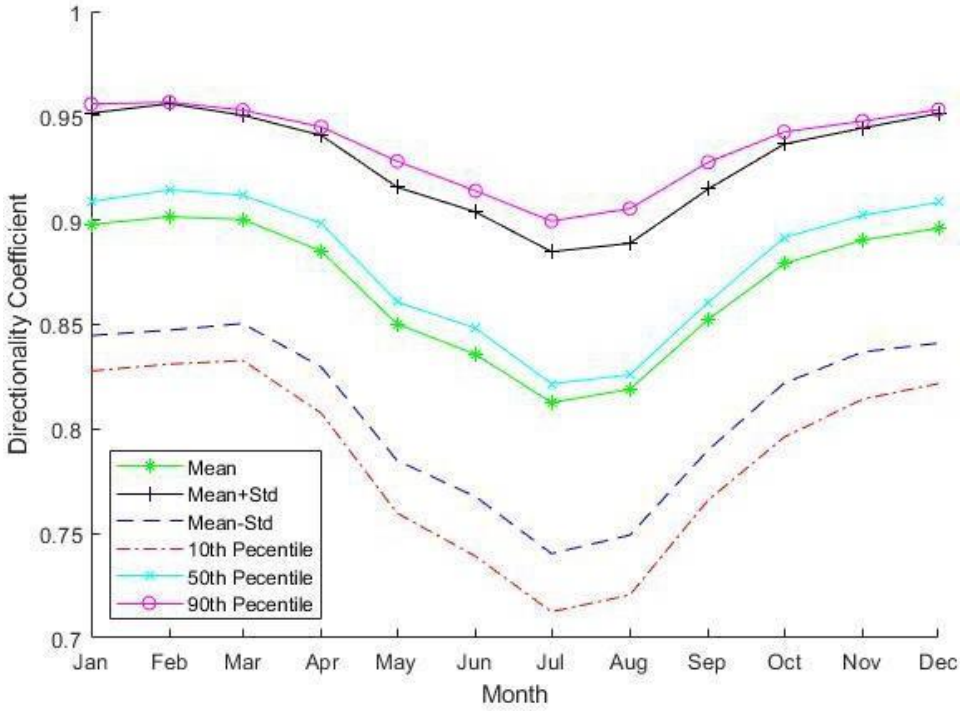

Figure 10: Monthly mean of SWAN directionality coefficient from 1980-2010 at PacWave South

When completing an IEC specification for wave energy resource, it is important to distinguish the definitions of certain attributes of a wave spectrum. Wave spreading and spectral width are similar in that they describe spreading, but these attributes can often become confused with one another. Wave spreading itself describes the directional spread of variance density in a wave energy spectrum, while spectral width describes the frequency spread of variance density. An example of wave energy spreading is shown in Figure 11, where an arbitrary spectrum's

energy is dispersed across a range of directions – which is wider than often found in nature and is purely illustrative. The directional spread of a wave energy spectrum can also be observed in wave rose figures similar to that of Figure 3, which details the main directions from which directionally resolved wave energy arrives at PacWave South. Directional bandwidth is described by directionality coefficient, as explained previously.

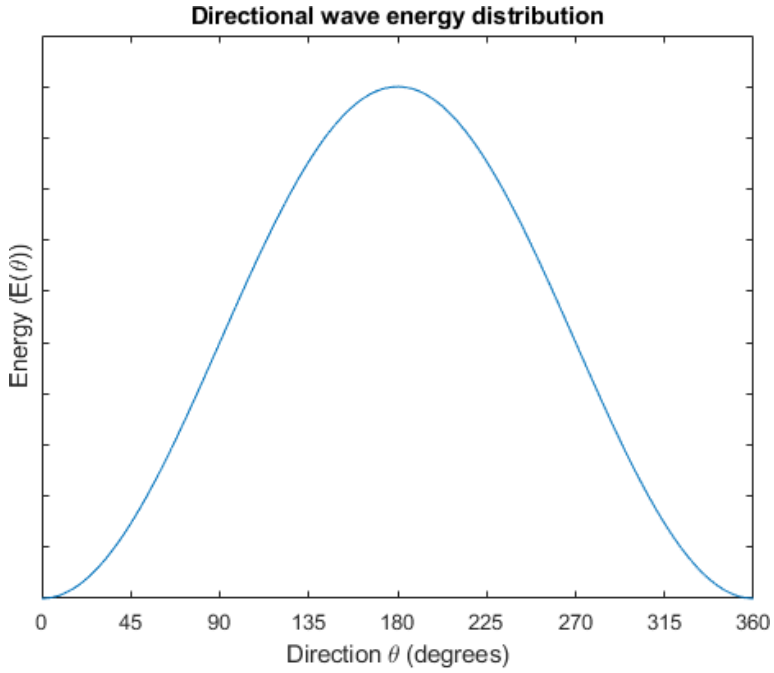

Figure 11: Spread of direction of wave energy for an arbitrary spectrum.

Spectral width is its own parameter recommended for analysis by the IEC, and it varies between 0 and 1 based on the sea state most dominant in the spectrum of interest. A swell-dominated spectrum has a spectral width value that approaches 0, in that its shape has a small width at its peak [8]. Wind-wave dominated spectra tend to have a broader range of wave conditions, with comparatively large widths at their peaks [8]. Figure 12 aims to lend a visual describing spectral width and how the parameter may vary.

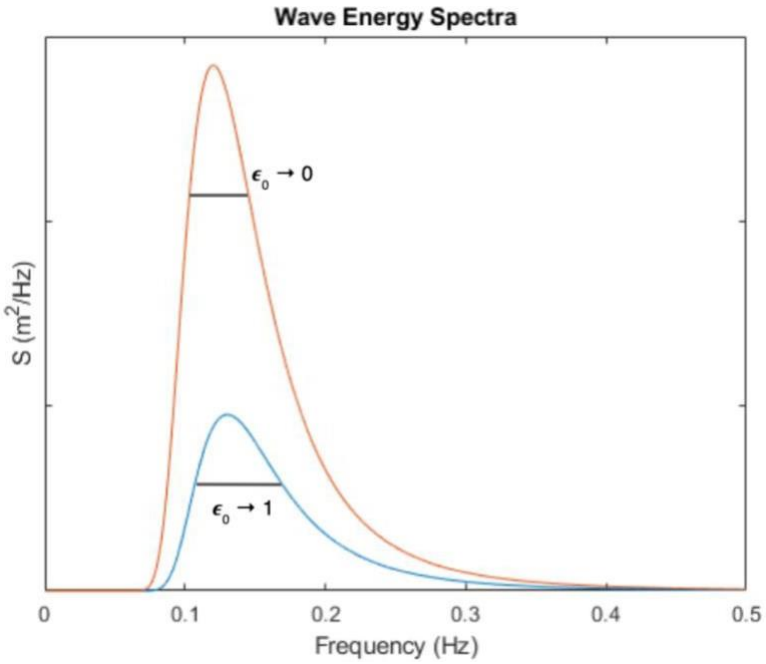

Figure 12: Comparison between two arbitrary wave energy spectra. The orange line is representative of a swell-dominated spectrum, with a spectral width approaching 0. The blue line represents a wind-wave dominated spectrum where its spectral width goes to 1.

The average spectral width over the hindcast at PacWave South is shown in Figure 13. Low spectral width values in the winter months are due to a swell dominated energy spectrum, where the parameter is expected to go to 0. Spectral width increases and goes toward a value of 1 as the wave field variation increases in the summer months, when waves are primarily wind driven.

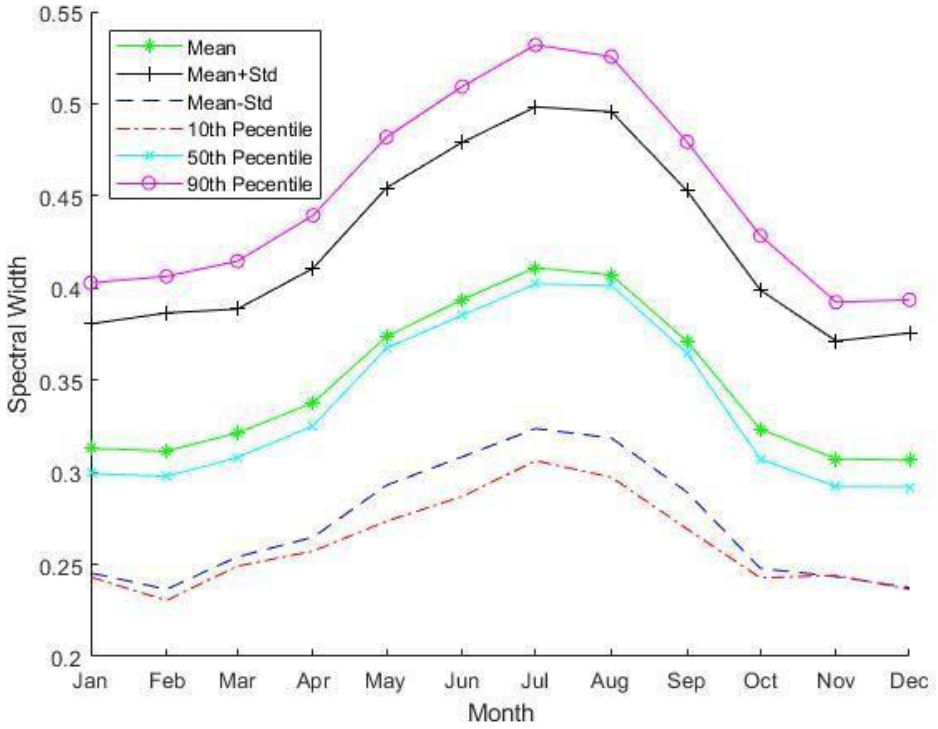

Figure 13: Monthly mean of SWAN spectral width from 1980-2010 at PacWave South

4.4 Monthly cumulative distributions

Monthly cumulative distributions are shown for the characterization parameters to detail the monthly wave resource. A cumulative probability distribution function (CDF) $f(x)$ must equal 0 when the line describing the CDF is at negative infinity, indicating a 0% chance occurrence, and must approach 1 as the line approached positive infinity, indicating a 100% chance occurrence. The steepness of the line indicates the deviations of the data, where a steep curve is indicative of a low deviation.

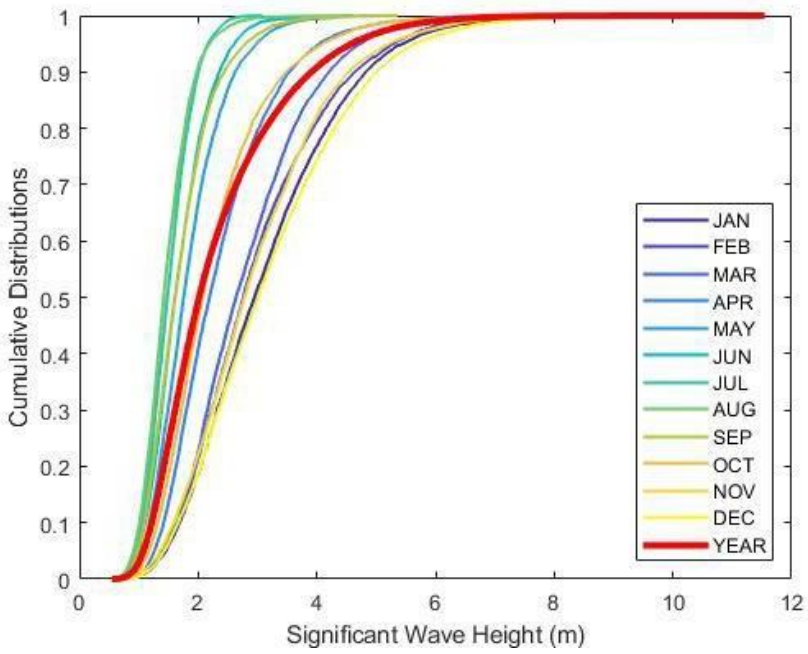

Figure 14: Monthly cumulative distributions of SWAN significant wave height from 1980-2010 at PacWave South

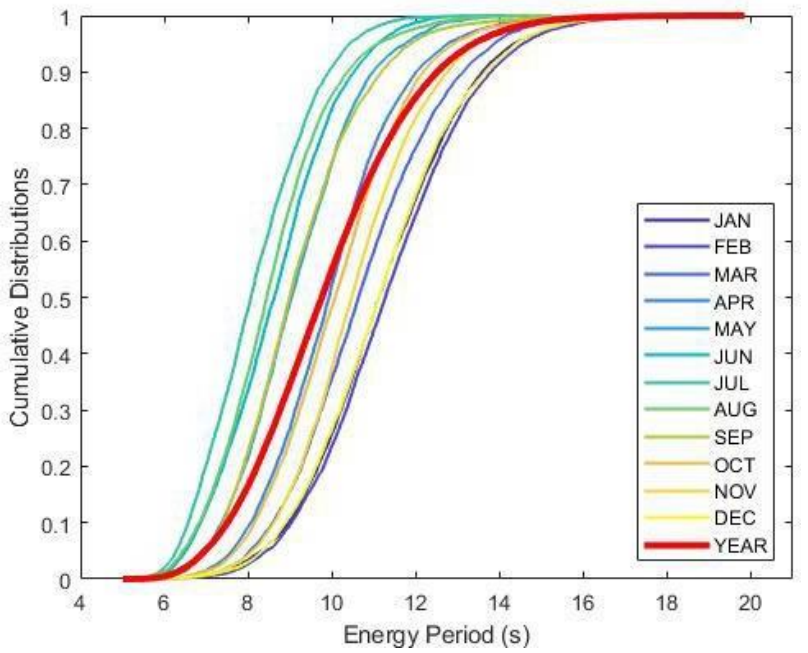

Figure 15: Monthly cumulative distributions of SWAN energy period from 1980-2010 at PacWave South

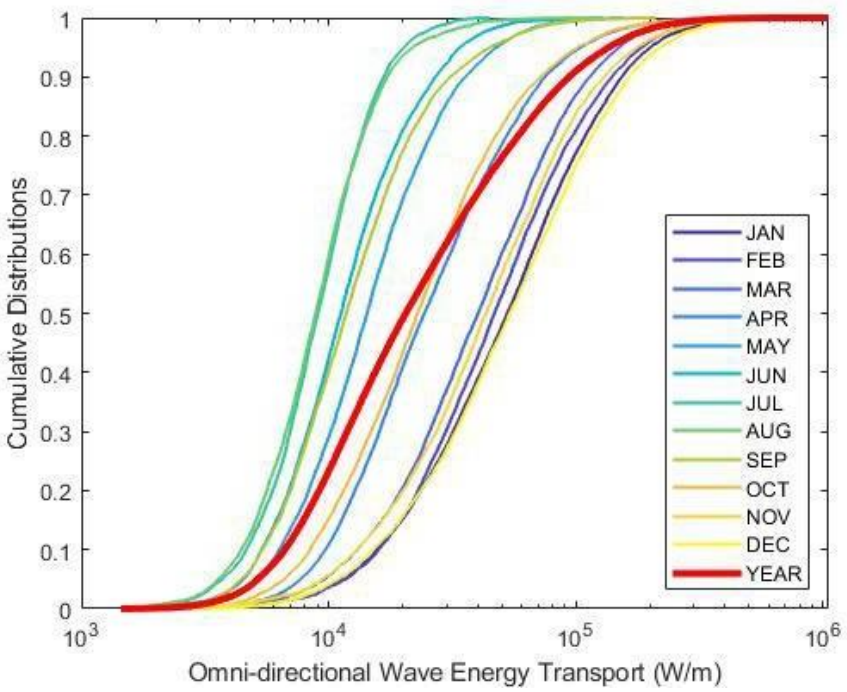

Figure 16: Monthly cumulative distributions of SWAN omni-directional wave energy transport from 1980-2010 at PacWave South. The x-axis is plotted on a logarithmic scale in order to better exhibit the cumulative distribution.

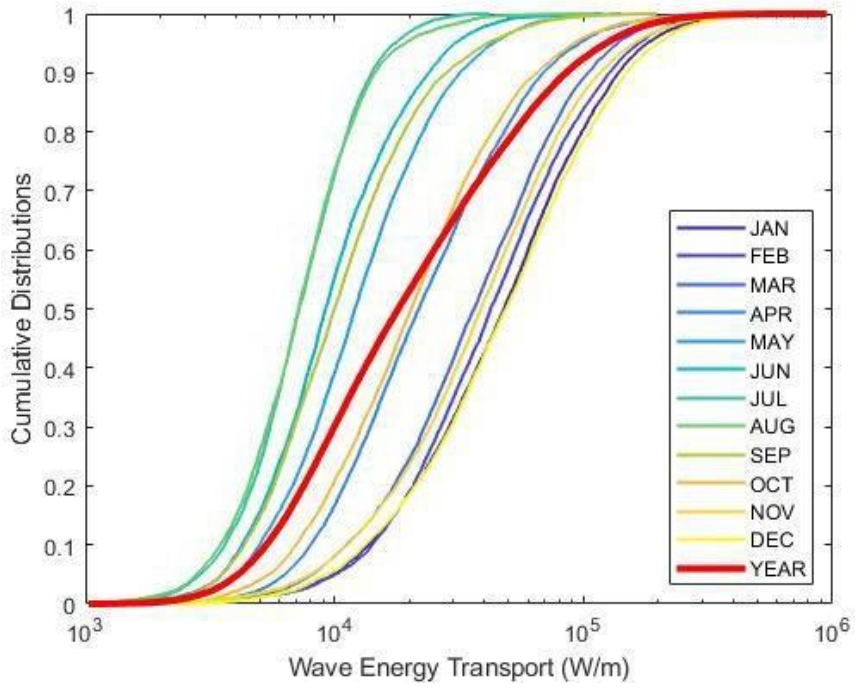

Figure 17: Monthly cumulative distributions of SWAN maximum directionally resolved wave energy transport from 1980-2010 at PacWave South. The x-axis is plotted on a logarithmic scale in order to better exhibit the cumulative distribution.

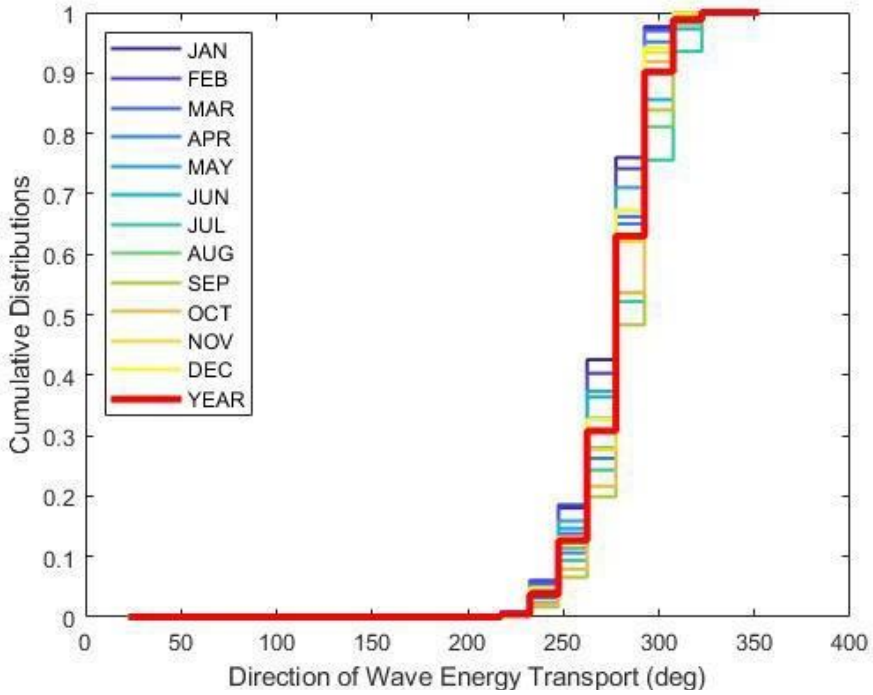

Figure 18: Monthly cumulative distributions of SWAN direction of directionally resolved wave energy transport from 1980-2010 at PacWave South

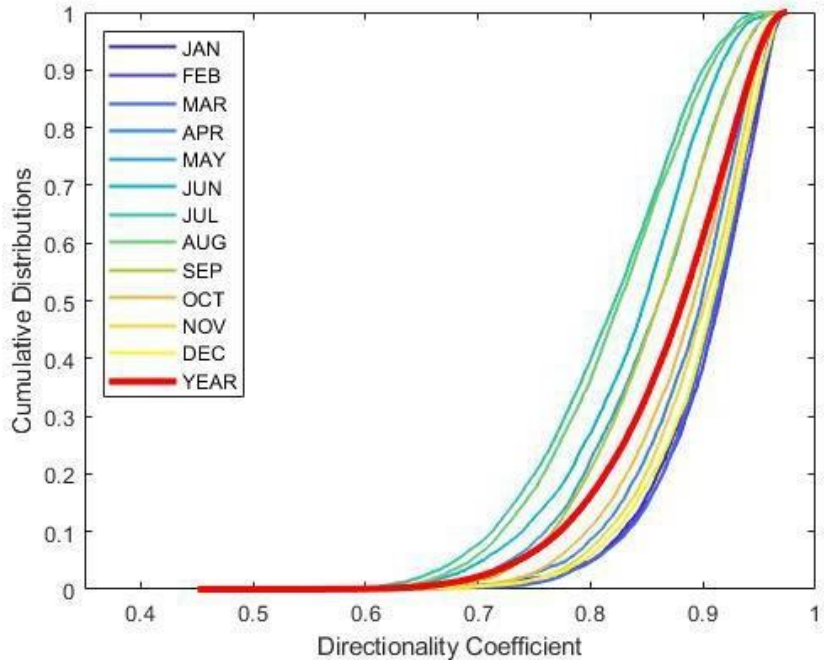

Figure 19: Monthly cumulative distributions of SWAN directionality coefficient from 1980-2010 at PacWave South

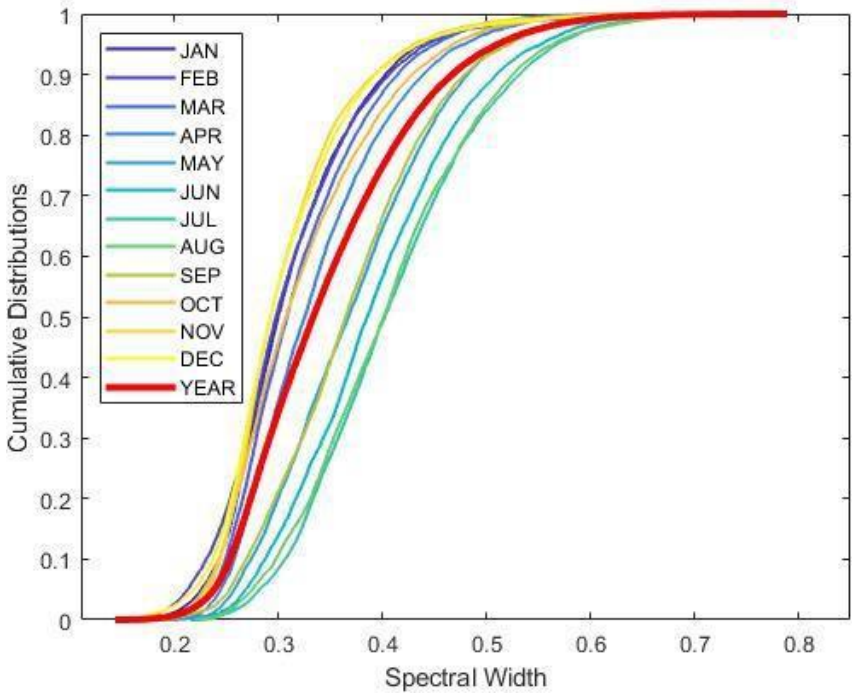

Figure 20: Monthly cumulative distributions of SWAN spectral width from 1980-2010 at PacWave South

5 TEMPORAL FLUCTUATION OF IEC PARAMETERS

Temporal fluctuations of wave parameters are included to highlight the interannual variability of the variables as well as to demonstrate the agreement between the modeled and physically observed data. All plots in Figure 21 show the SWAN calculated parameters from the PNNL hindcast at PacWave South in 2010 compared to the physically observed data at NDBC station 46050 in 2010 (location described in Section 6). This comparison is also included according to the recommendations set by the IEC specification for wave energy resource assessments. For a detailed validation of the SWAN hindcast, please see Wu et al., 2020 [5].

In general, the physically observed data at NDBC 46050 agrees with the modeled data form the PNNL hindcast. There are instances in the direction of maximum directionally resolved wave energy transport plot where NDBC 46050 drops to 0° while the directions in the hindcast vary between 250 ° and 300°. Additionally, directionality coefficient for the model varies between 1 and 0.6 while physically observed directionality coefficient varies between 0.8 and 0.4. Despite this, all IEC parameters showed good error statistics in model validation [5], indicating that the model has good skill in estimating the IEC parameters.

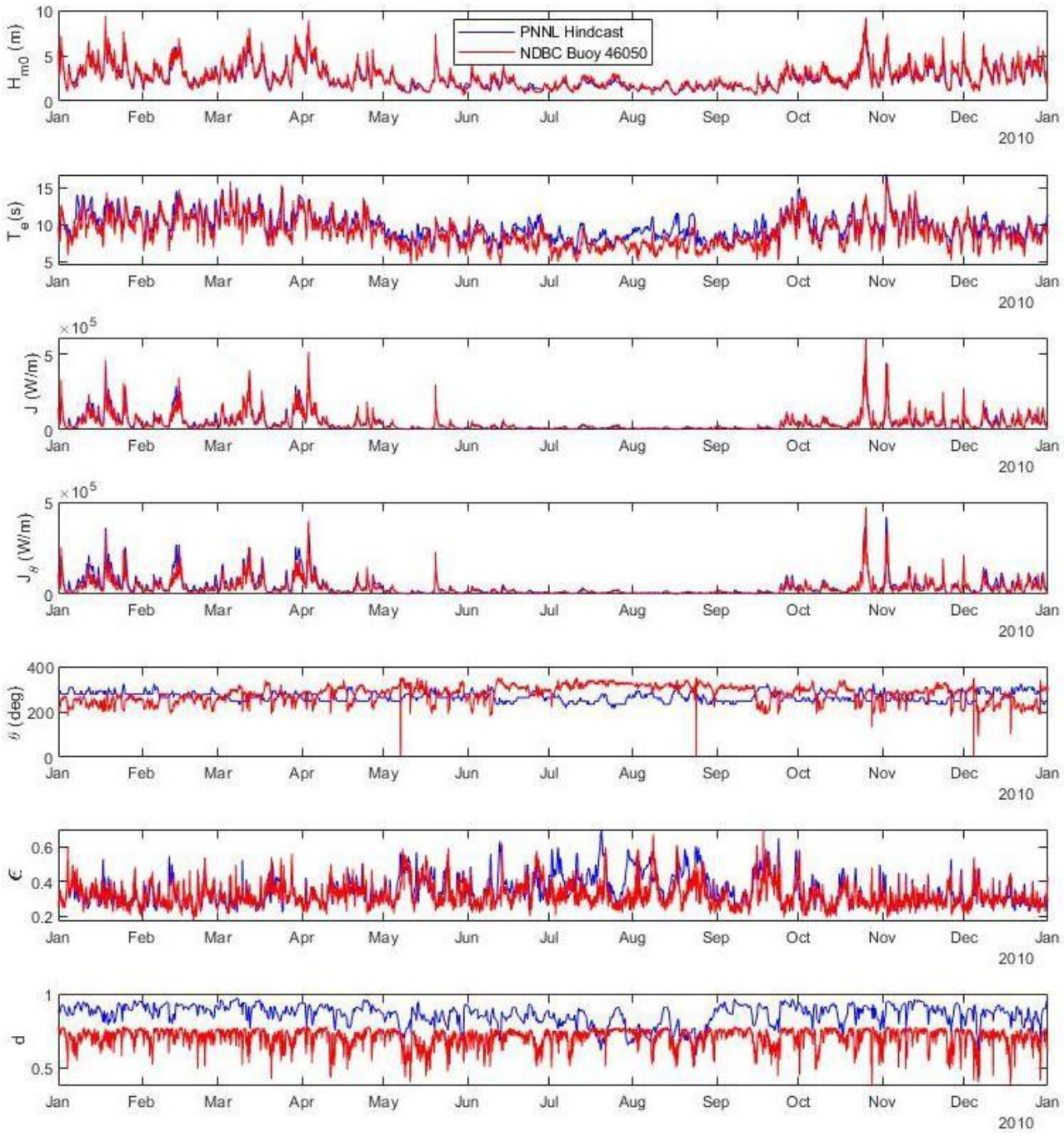

Figure 21: Temporal fluctuation of IEC wave energy parameters for the year 2010. The PNNL hindcast values are representative of the values at PacWave South while the NDBC 46050 values were recorded at its associated location.

6 WIND EFFECT AT PACWAVE

The IEC specification notes that reviewing wind speed and wind direction in the area of interest for wave energy conversion is a valuable addition to a wave resource assessment. The following section offers a general description of the wind field in the PacWave region.

While reporting the seven IEC-required spectral wave quantities for a wave energy resource assessment is descriptive, uncertainty is introduced in wave power predictions when environmental conditions are not adequately taken into account [10]. This effect is under investigation, with researchers attempting to provide additional metrics with which to accurately describe wave energy resource. Robertson et al. has identified wind speed as an additional essential parameter that should be included for a more accurate estimation of wave power [10]. Wave theory describes how waves are affected by wind: wave height grows proportionally to wind speed and duration, thus affecting the amount of energy available in a sea state (i.e. wind generates waves).

Wind data from National Oceanic and Atmospheric Administration (NOAA) National Buoy Data Center (NDBC) stations was analyzed. Wind speed data at NDBC stations is measured by averaging windspeed over an 8-minute period at the height of the offshore buoy anemometers, which is 4.5 m above sea level – which is a relevant elevation for most WEC systems. Figure 22 shows some of the available regional NDBC buoy data in Oregon, Southern Washington, and Northern California. The boxed area represents the specific PacWave region and associated NDBC stations, further described in Figure 23.

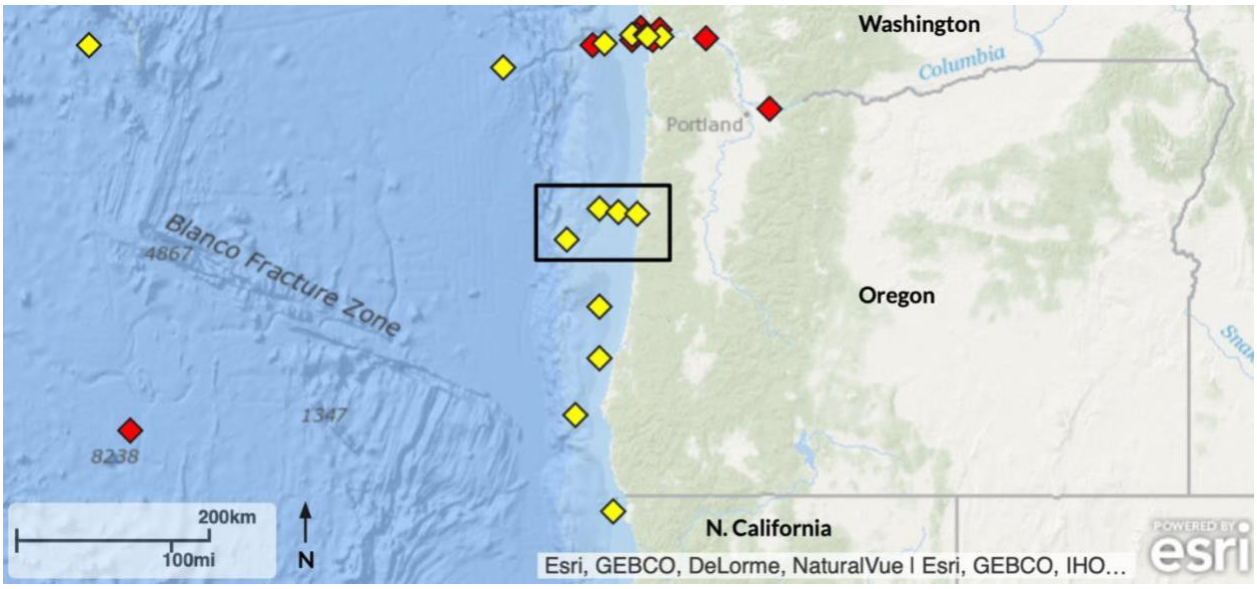

Figure 22: Regional NDBC station locations. Red diamonds indicate stations with no recent data collected, while yellow indicates ongoing data collection at the location. The black box denotes the specific location of the PacWave wave energy test site and associated NDBC stations.

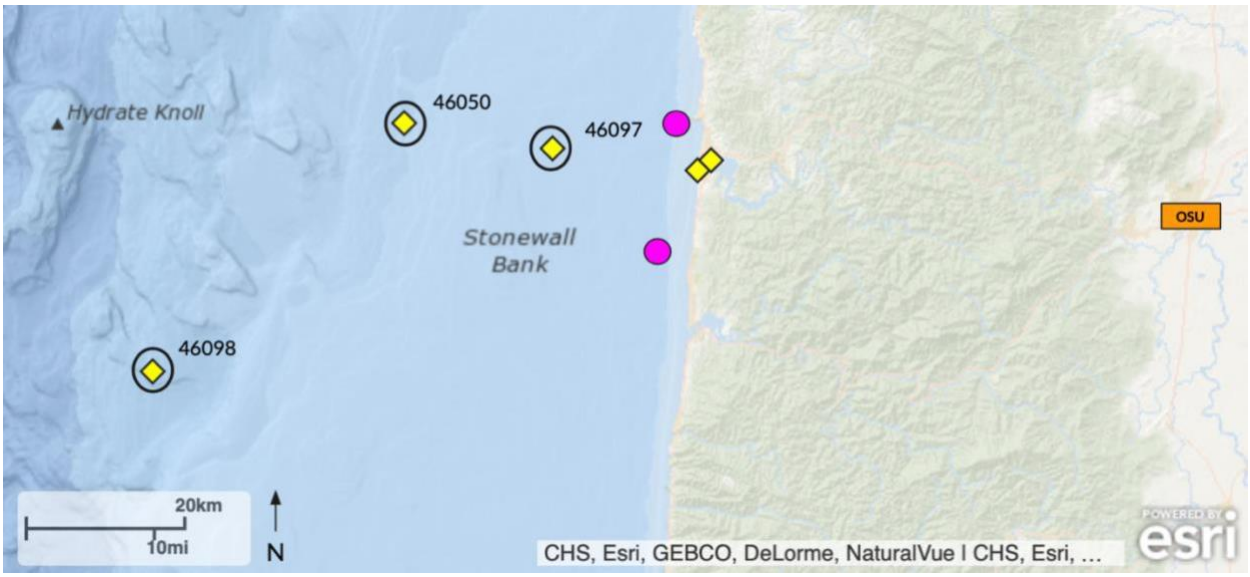

Figure 23: Locations of NDBC buoys from which wind data was analyzed, in reference to the location of PacWave and OSU

In Figure 23, yellow diamonds denote NDBC buoy stations and the red circles indicate the stations used in this report. The pink circles show the approximate locations of PacWave North and South sites from top to bottom respectively, off the coast of Newport. The orange box represents the location of Oregon State University in Corvallis.

The distributions of wind speed and direction were analyzed from NDBC stations 46097, 46098, and 46050 and plotted in Figure 24 through Figure 26. Station 46097 recorded data from 2016 through 2019, station 46098 from 2016 through 2017, and station 46050 from 2014 through 2016. Each distribution was fitted with a Weibull distribution, which is the expected distribution for wind speed since it proves to be a good approximation for this type of measurement [11].

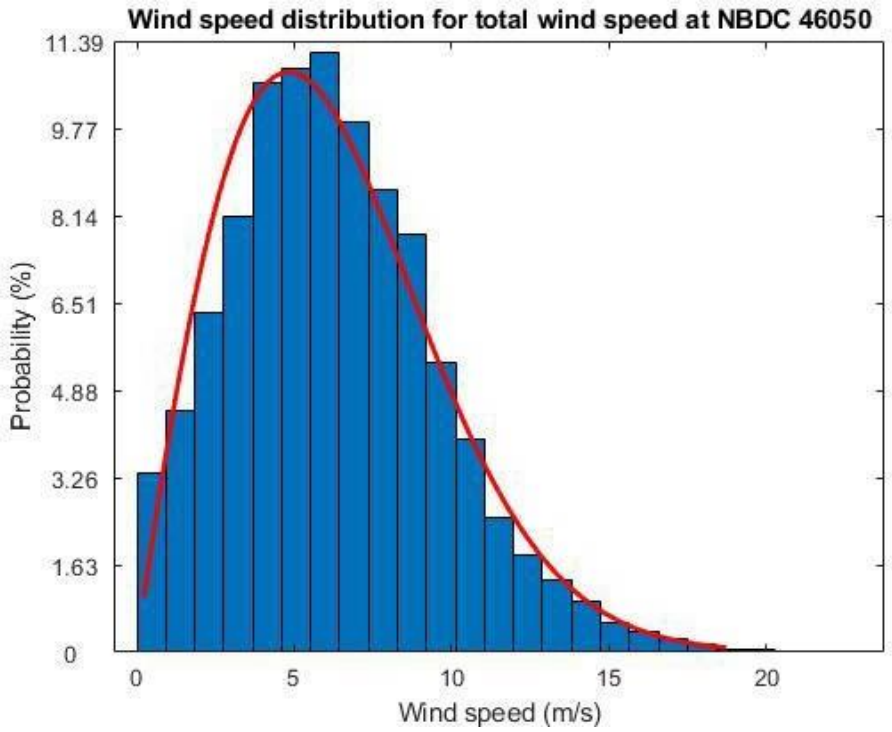

Figure 24: Distribution of wind speed at NDBC 46050 with a Weibull distribution fit

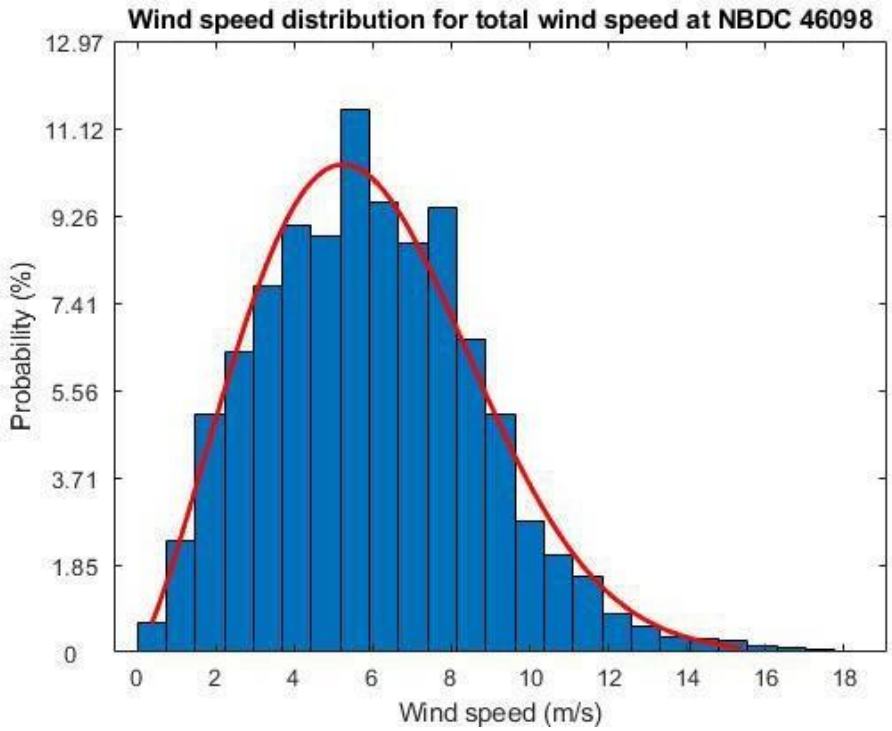

Figure 25: Distribution of wind speed at NDBC 46098 with a Weibull distribution fit

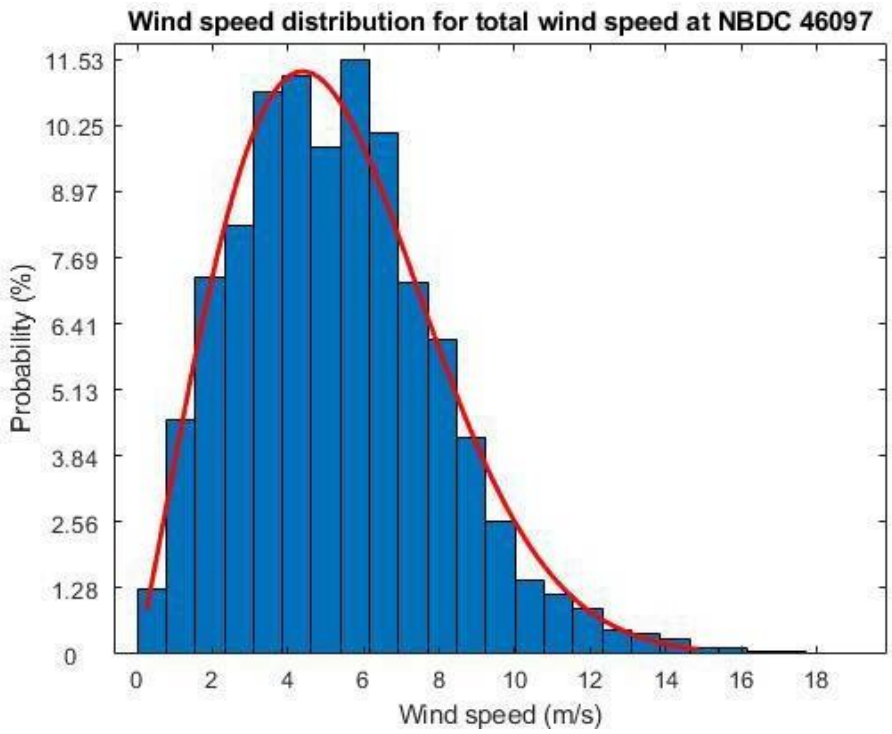

Figure 26: Distribution of wind speed at NDBC 46097 fitted with a Weibull distribution fit

Across the three NDBC stations, the majority of wind speeds are in the 4-8 m/s range, accounting for the highest probability of occurrence. Maximum values of wind speed are 18 m/s per each of the stations. The average wind speed at NDBC 46050 is 6.27 m/s; average windspeed at NDBC 46097 is 5.32 m/s; and average windspeed at NDBC 46098 is 5.98 m/s. The boxplot in Figure 27 describes the range of values measured at the NDBC stations.

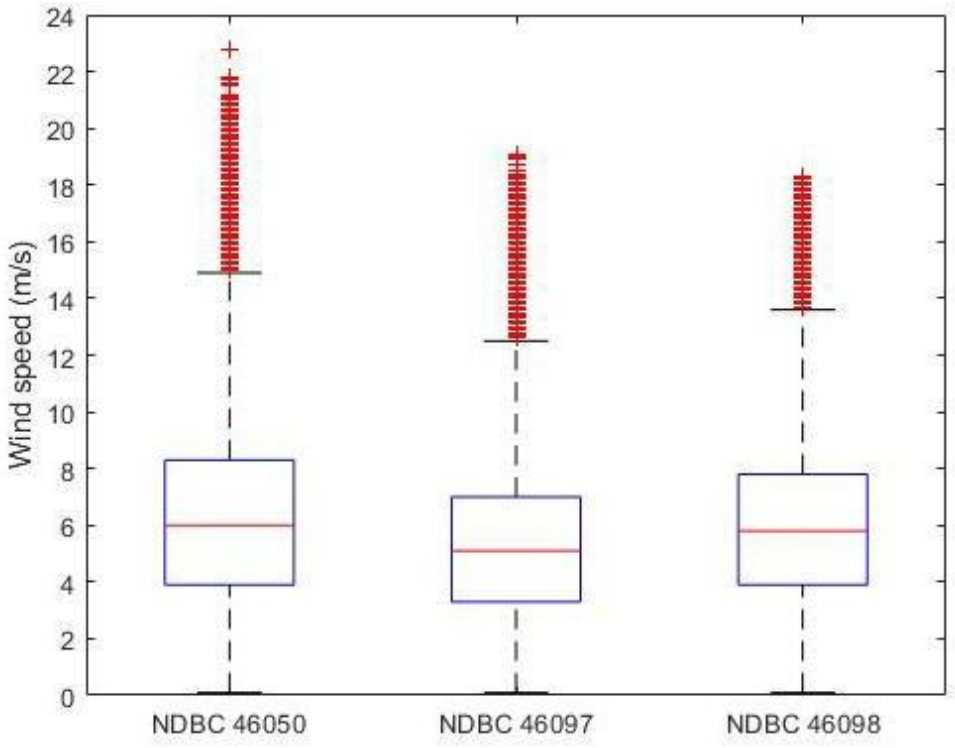

Figure 27: Box and whisker plot describing the wind speeds at NDBC stations near PacWave. Shown in the plot are extreme outlier values, non-extreme minima and maxima, median values (50th percentiles), and 25th and 75th percentile values.

The lower and upper limits of the interquartile range (IQR) denote the 25th and 75th percentiles respectively. Whiskers lead to the most extreme, non-outlier values, and crosses are outlier values. The red line indicates the median value of the dataset, which will fall somewhere within the IQR; at least half of the data is less than or equal to the median and at least half is greater than or equal to it.

The median wind speeds at NDBC 46050, 46097, and 46098 are 6 m/s, 5.1 m/s, and 5.8 m/s respectively; maximum non-outlier wind speeds are 15 m/s, 12.5 m/s, and 13.6 m/s respectively; minimum non-outlier wind speeds are 0.1 m/s at each station. Outliers range from 18 m/s to 23 m/s between the three sites. Figure 27 provides an extensive description of the wind speeds measured near the PacWave sites.

NDBC 46097 has wind data collected from 2016 through 2019 and is closest to the PacWave sites, therefore the station's data was used for representing the directional distribution of the wind speed, as shown in Figure 28. NDBC 46097 measured wind speed and direction measurements from 2016 through 2019 and is located closest to the PacWave sites, as demonstrated in Figure 23. The percentages indicate the frequency at which each bin occurs.

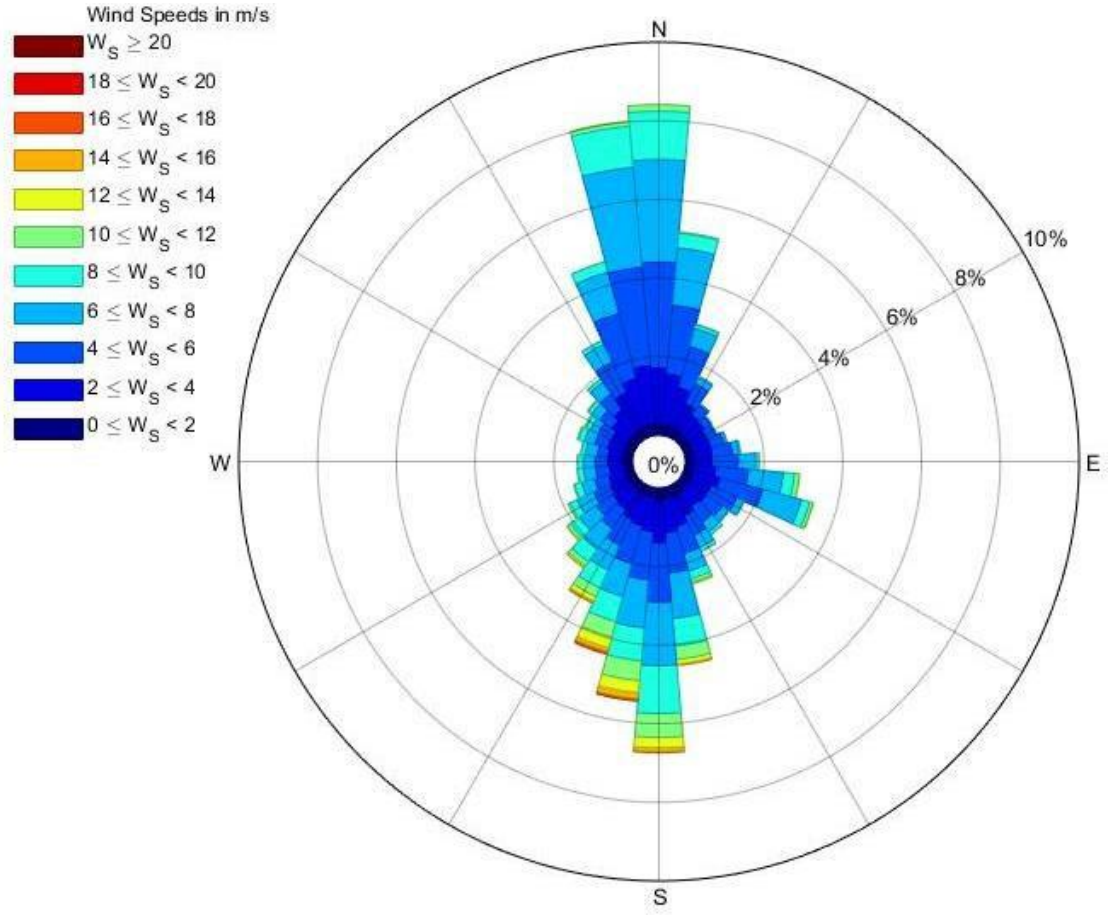

Figure 28: Wind rose distribution for wind speed at NDBC 46097 from 2016-2019

Wind direction at the NDBC stations is measured as the wind is coming from degrees clockwise from 0° North. As expected, the winds come predominately from the north and south. The inclusion of wind speed, among other environmental conditions, decreases uncertainty when comparing modeled data to physically observed sea state data [10].

7 EXTREME ENVIRONMENTAL CONTOURS

When determining the site characteristics for potential wave energy conversion, it is recommended by the IEC to take into consideration extreme sea state conditions. 50-year and 100-year environmental contours were used in this section to describe potential extreme sea states at the PacWave sites. WEC developers may run into issues at the PacWave site due to large waves that occur in the winter months, highlighting the need to ensure survivability of WEC devices.

100-year storm events have a likelihood of 1% per year occurrence, whereas 50-year events have a 2% likelihood of occurrence per year. The analysis corresponding to extreme wave

events in this section is based on Yang et al. (2020), and should be explored for further detail [4]; the environmental contour data used in this report is from PNNL.

Figure 29 and Figure 30 detail the extreme environmental contours in the PacWave region compared to the hindcast predictions. Extreme values at 44°36'7.56"N and 124°13'55.2"W were chosen to compare to the PacWave hindcast measurements, as this location was closest to the actual PacWave South longitude and latitude (i.e. 1.5 miles northwest of PacWave South).

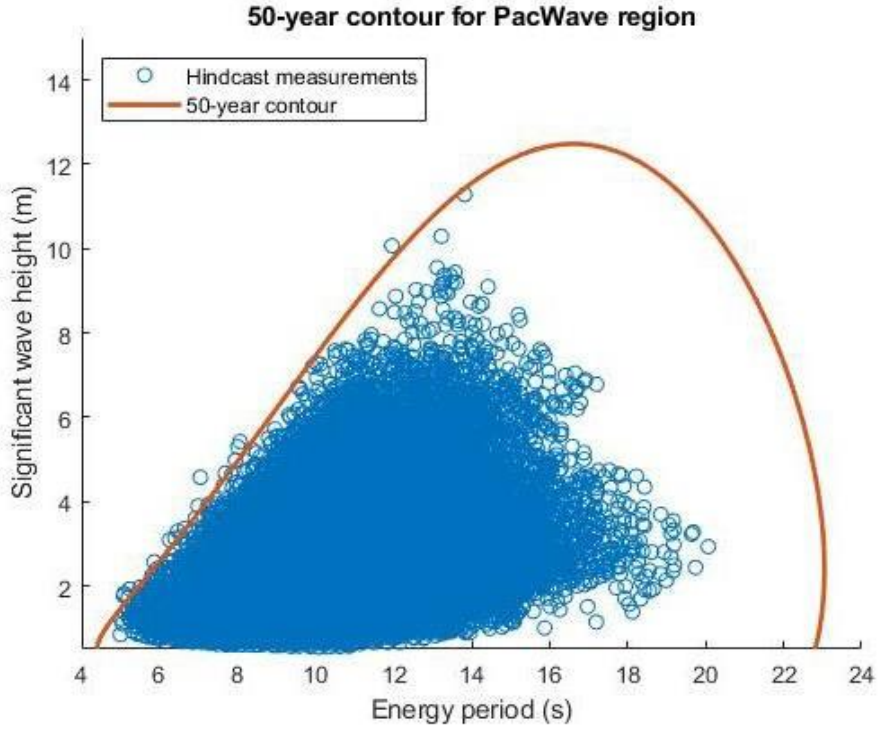

Figure 29: 50-year extreme environmental contour for the PacWave region compared to hindcast measurements recorded for PacWave South from 1980-2010

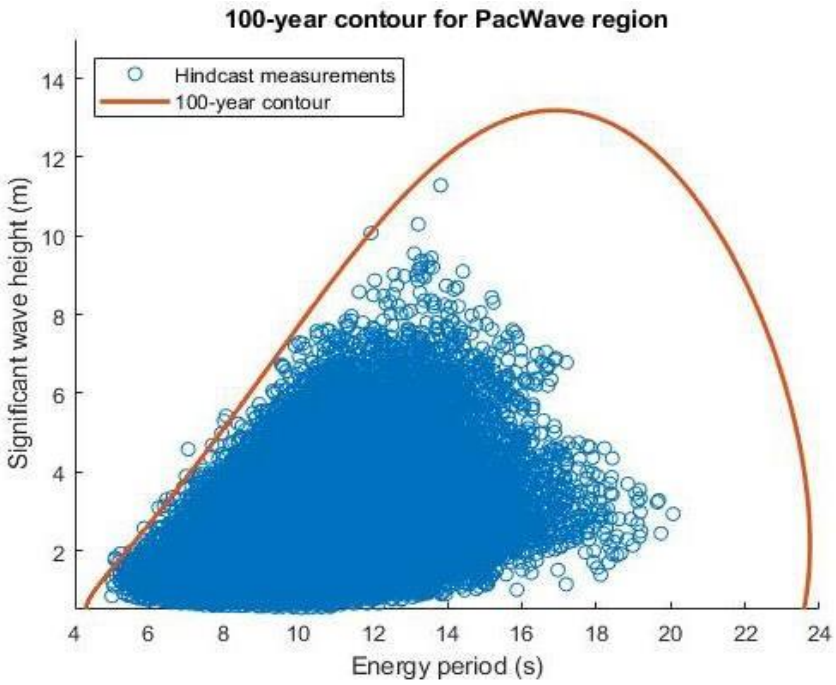

Figure 30: 100-year environmental contour for the PacWave region compared to hindcast measurements recorded for PacWave South from 1980-2010

In both Figure 29 and Figure 30 there are hindcast values that are aligned on the contour lines, which was expected since the dataset analyzed in this report encompasses 31 years, throughout which extreme sea states are statistically bound to occur. This reinforces the advantage of using a long-term dataset. The right-hand portions of each plot lack measurements because the hindcast dataset is not 50 nor 100 years long, during which times the more extreme values would be more likely to occur.

The maximum wave height – energy period combination is about the same for both the 100-year and 50-year contours. The peak of the 50-year contour occurs at a wave height of 12.49 m and energy period of 16.68 s while the 100-year contour peaks at a wave height of 13.19 m and energy period of 16.85 s. From 1980-2010, the hindcast did not measure any values possessing this combination of extreme values.

Extreme environmental analysis is included in this report in order to describe the sea state conditions that may occur at the PacWave sites. Survivability is of concern for WEC developers as high, steep, and breaking waves tend to damage WEC devices, especially at increased frequencies [11].

8 OPERATION & MAINTENANCE WINDOWS

Figure 31 characterizes the average number of single-day weather windows per year available for developers to access and perform operation and maintenance (O&M) at PacWave South. The cumulative amount of days with significant wave height less than 1.5 meters and peak period above 8 s from 1980-2010 are totaled on the plot [12] — these threshold operations windows are based on data from the Navy Wave Energy Test Site in Hawaii and are vessel specific. As expected, throughout this analysis, the summer months yield more optimal conditions for O&M than winter months. The peak for average individual day windows for O&M at PacWave South is 4.6 days in August per year between 1980 and 2010. The months from November through March see less than one full day on average per year available for O&M.

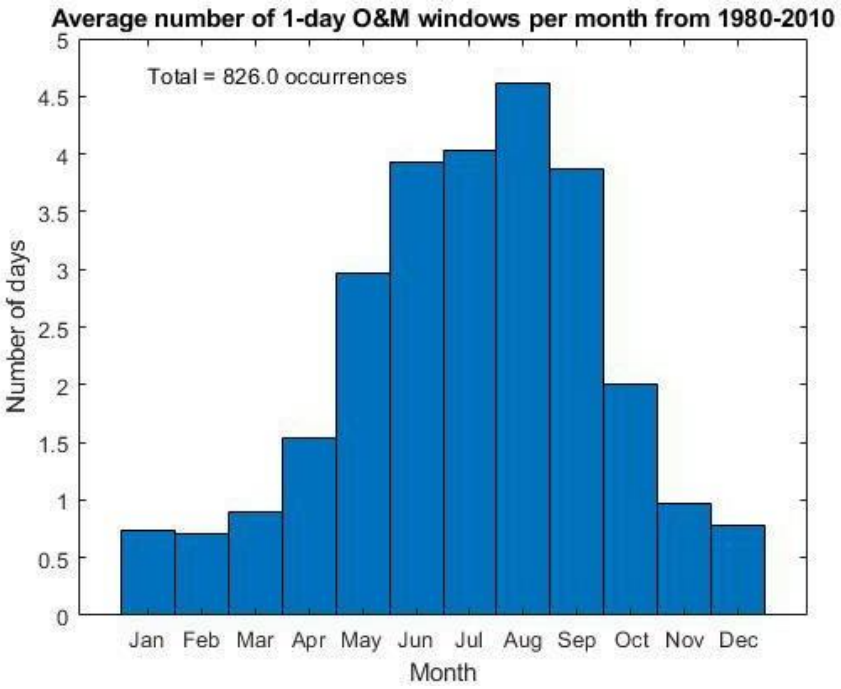

Figure 31: Average number of days with wave height less than 1.5 m and peak period above 8 s available for O&M from 1980-2010 at PacWave South

The average number of 2-day, 3-day, and 5-day weather windows available per year for O&M are shown in Figure 32, Figure 33, and Figure 34 respectively. As expected, summer months June, July, and August allow more opportunity for O&M than winter months. The peak number of 2-day, 3-day, and 5-day windows at PacWave South is 2.4, 1.3, and 0.5 occurrences respectively, all taking place in August. Table 1 and Table 2 describe the average amount of window occurrences per year and month respectively.

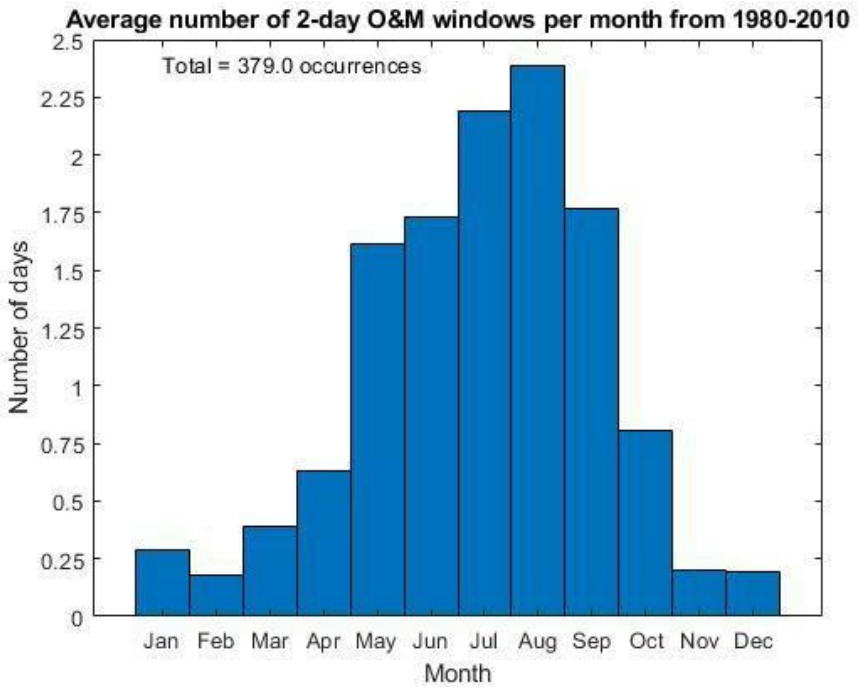

Figure 32: Average number of 2-day windows with wave height less than 1.5 m and peak period above 8 s for O&M from 1980-2010 at PacWave South

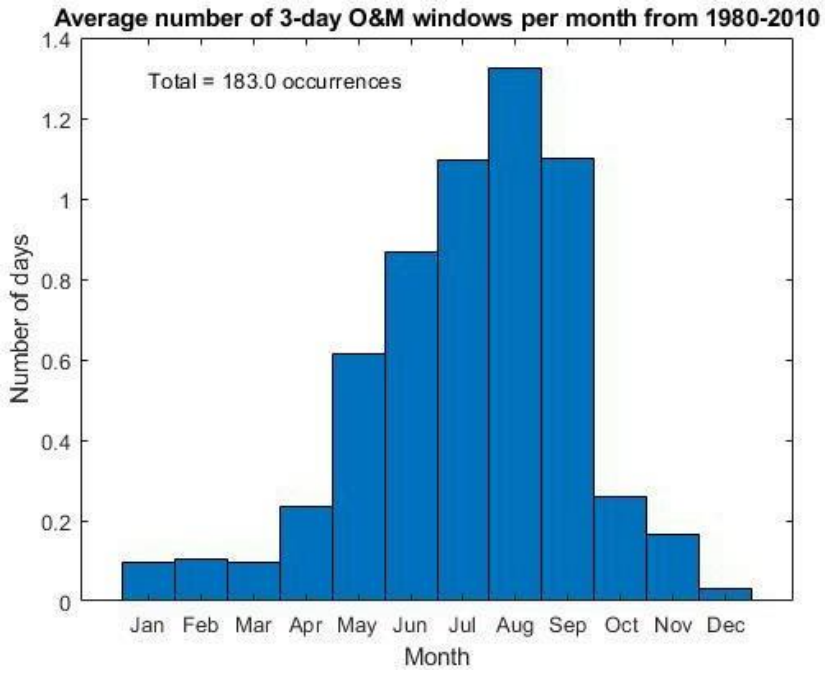

Figure 33: Average number of 3-day windows with wave height less than 1.5 m and peak period above 8 s for O&M windows from 1980-2010 at PacWave South

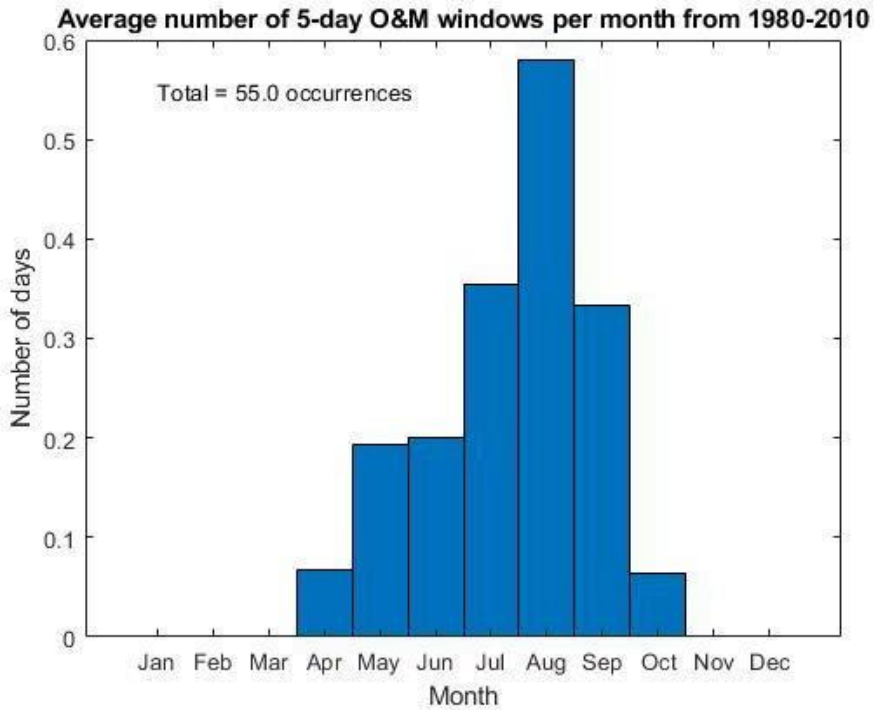

Figure 34: Average number of 5-day windows with wave height less than 1.5 m and peak period above 8 s for O&M from 1980-2010 at PacWave South

	1-day windows	2-day windows	3-day windows	5-day windows
North	28	13	6.5	2
South	27	12	6	2

Table 1: Average O&M windows per year from 1980-2010

	Jan	Feb	Mar	Apr	May	Jun	Jul	Aug	Sep	Oct	Nov	Dec
1-day windows	0.7	0.7	0.9	1.5	3.0	4.0	4.0	4.6	3.8	2	1.0	0.8
2-day windows	0.3	0.2	0.4	0.6	1.6	1.7	2.2	2.4	1.8	0.8	0.2	0.2
3-day windows	0.1	0.1	0.1	0.2	0.6	0.9	1.1	1.3	1.1	0.3	0.2	0
5-day windows	0	0	0	0.1	0.2	0.2	0.4	0.6	0.3	0.1	0	0

Table 2: Average number of O&M windows per month from 1980-2010 at PacWave South

Box and whisker plots were created for the various O&M window durations in order to provide a comprehensive look at the probability of occurrence of satisfactory sea state conditions. The number of days available per month within the O&M conditions were recorded for the time period. Figure 35 through Figure 38 describe the interannual variability of O&M on a monthly basis from 1980-2010.

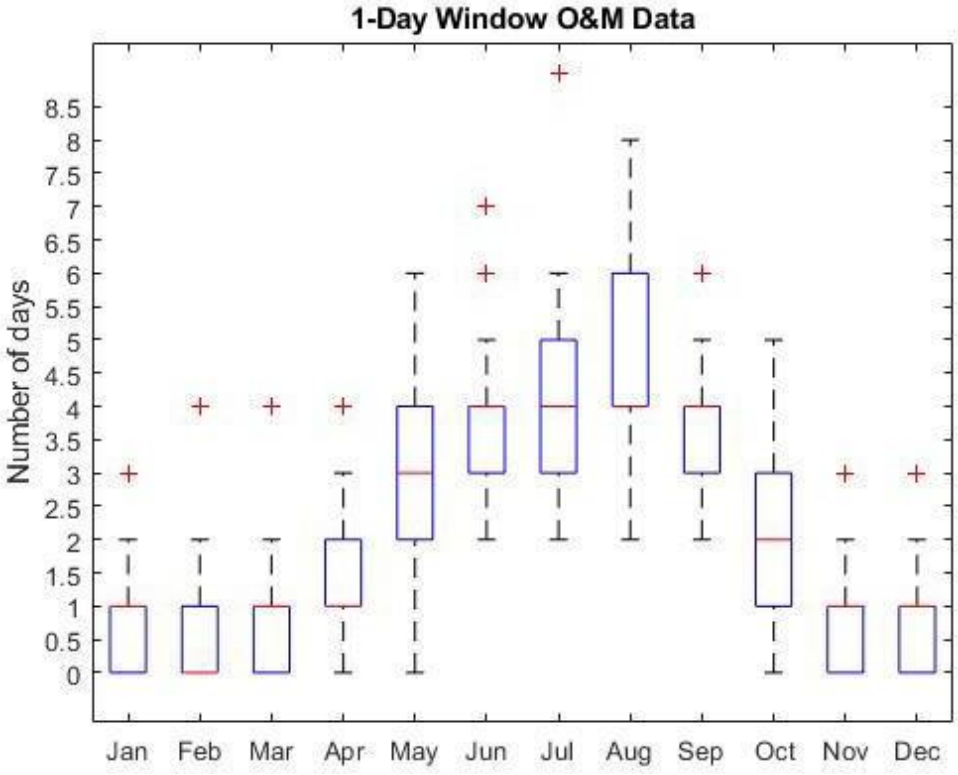

Figure 35: Box and whisker plot describing the 1-day window O&M data at PacWave South. Shown in the plot are extreme outlier values, non-extreme minima and maxima, median values (50th percentile values), and 25th and 75th percentile values.

Figure 35 shows the range of occurrences of 1-day O&M windows from 1980-2010. The winter months from November through March consistently have median values that align with either the 25th or 75th percentile, indicated by a red line marking the outside of the IQR box. This result is due to increased occurrence of such values in the middle of the monthly dataset. There is a non-outlier maximum of two days which occurred during these months in certain years. The summer months have non-outlier maxima of at least two days greater than the 75th percentile and centered median values in the IQR, except for August. Again, this is due to the fact that 4 days was recorded the most frequently in the middle of the August dataset.

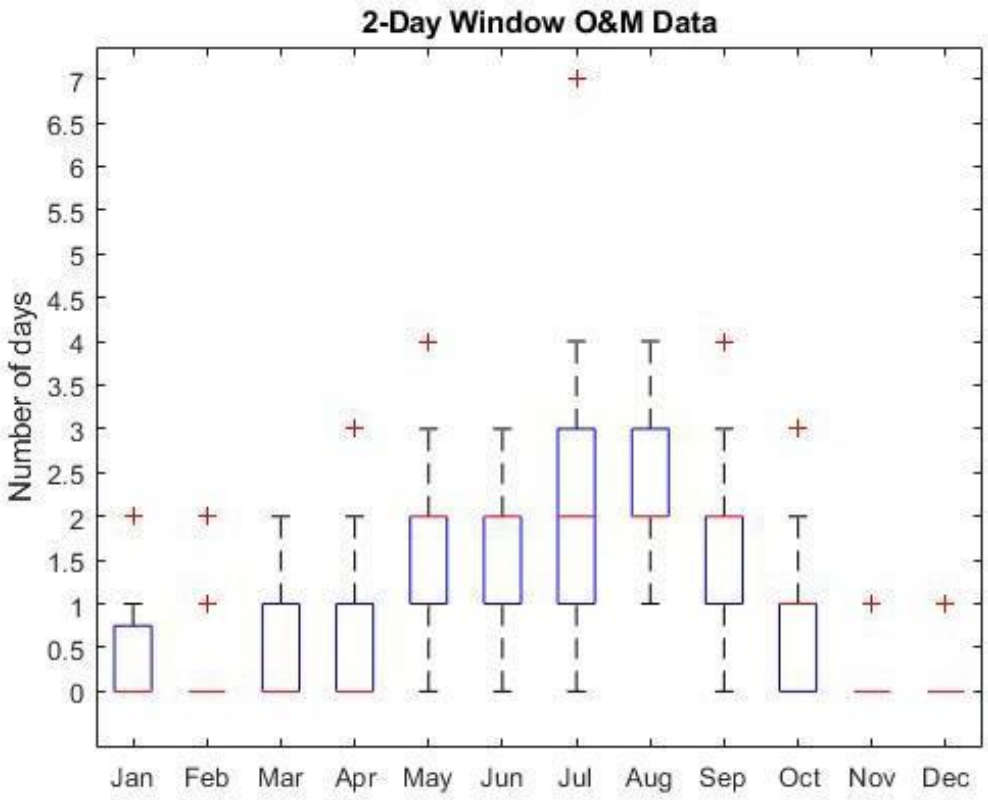

Figure 36: Box and whisker plot describing the 2-day window O&M data at PacWave South. Shown in the plot are extreme outlier values, non-extreme minima and maxima, median values (50th percentile values), and 25th and 75th percentile values.

Figure 36 describes the box and whisker plot data associated with the spread of occurrences of 2-day windows for O&M at PacWave South. As expected, there are fewer occurrences of this window type across the months. Winter months February, November, and December lack an IQR box as 0 is the most recorded window occurrence, with outliers occurring at 1 and 2 days depending on the month. From May through September, the median value for occurrences of 2-day windows is 2, with non-outlier maxima ranging from 3 to 4 occurrences and non-outlier minima between 0 and 1 occurrences. From 1980-2010, there is always at least one 2-day O&M window occurring in August according to the hindcast.

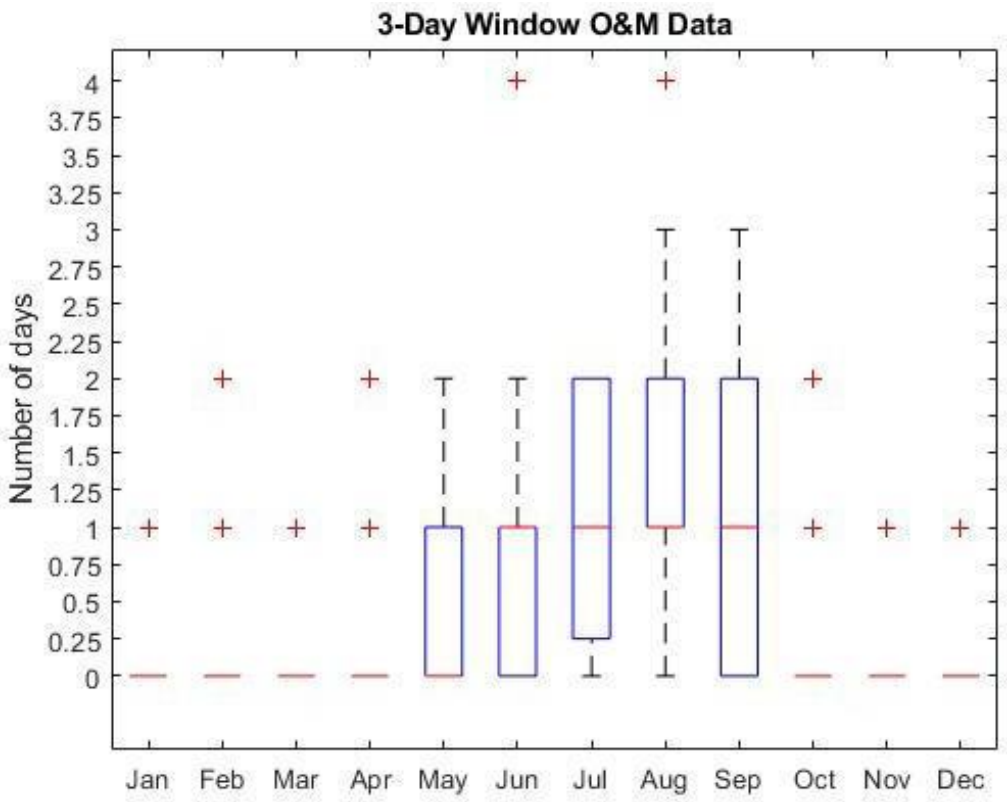

Figure 37: Box and whisker plot describing the 3-day window O&M data at PacWave South. Shown in the plot are extreme outlier values, non-extreme minima and maxima, median values (50th percentile values), and 25th and 75th percentile values.

3-day windows for O&M purposes are sparser from 1980-2010 according to the hindcast. Figure 37 indicates that half the months in a year rarely see an opportunity for 3-day windows with favorable sea state conditions. Months between November and April have outliers ranging from 1 to 2 occurrences and medians of 0 occurrences, lacking an IQR box. From months May through September, the median value of 3-day window occurrences is 1. May and June have non-outlier maxima of 2 occurrences; July and August have non-outlier minima of 0 occurrences. Additionally, August has a non-outlier maximum of 3 and an outlier of 4 occurrences, with a 75th percentile value of 2 occurrences. According to Figure 37, September has an equal probability of window occurrence as July. October has a median of 0 occurrences and an 75th percentile value of 1 occurrence and a non-outlier maximum of 2 occurrences. In summary, 3-day windows are more likely to occur between July and September.

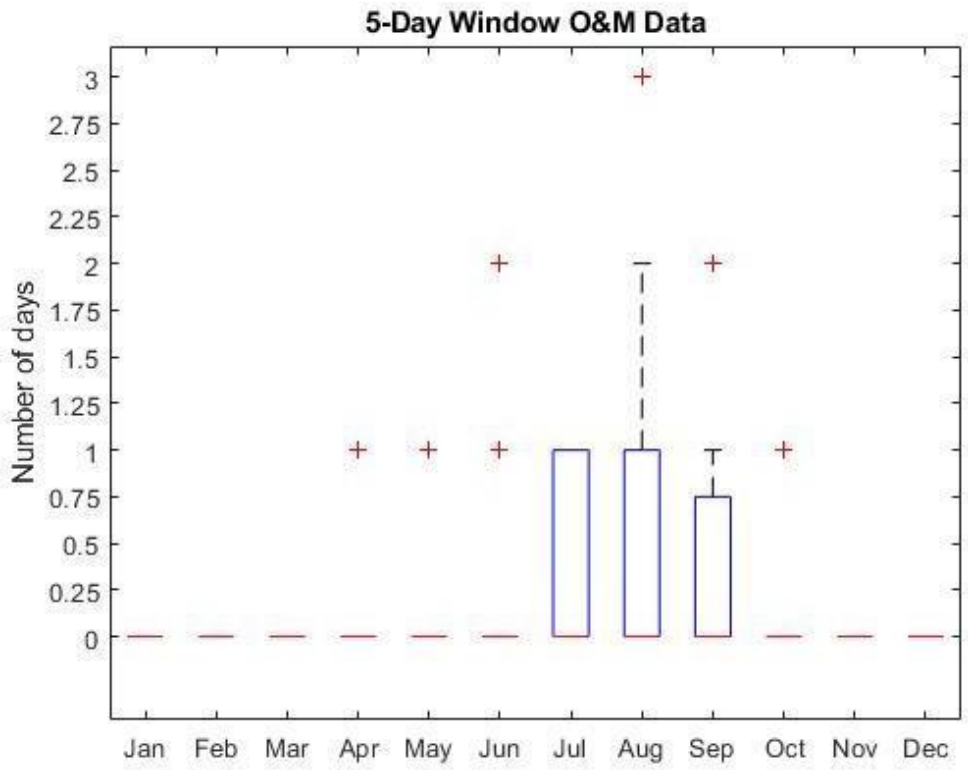

Figure 38: Box and whisker plot describing the 5-day window O&M data at PacWave South. Shown in the plot are extreme outlier values, non-extreme minima and maxima, median values (50th percentiles), and 25th and 75th percentile values.

As expected, Figure 38 demonstrates there are few likely occurrences of 5-day windows available from 1980-2010 in any given month. November through March do not have a recording of a 5-day window, indicated by medians equal to 0 and a lack of outlier values. April, May, June, and October also have medians equal to 0 with outliers between 1 and 2 occurrences. Months July through September also have median values equal to 0 occurrences, with 75th percentile values of 1 and 0.75 respectively. August has a non-outlier maximum of 2 occurrences and an outlier of 3 occurrences of this window type.

The analysis of box and whisker plots for O&M purposes allows for deeper look at potential favorable sea state window opportunities. The range of occurrences available per window type per month, maximum and minimum, median, and outlier occurrences were investigated and presented in this report in order to allow for better assessment and planning for O&M on WEC devices at PacWave.

9 CONCLUSIONS

This report contains a detailed analysis of wave energy resource at the PacWave South and North (shown in Appendix) sites off the coast of Newport, Oregon, utilizing on a 32-year (1980-2010) hindcast developed by the PNNL and based on the International Electronical Commission technical specifications. Bivariate histograms of significant wave height and energy provide a visual description of the variety of sea states occurring at the PacWave sites. The highest mean annualized wave energy transport sea state occurred a total of 231 hours with a significant wave height of 2.75 m and an energy period of 10.5 s at PacWave South. The wave rose illustrates the major directions from which the directionally resolved wave energy transport propagates at PacWave South; the majority of directionally resolved wave energy transport comes from the west.

The monthly means, standard deviations, 10^{th}, 50^{th}, and 90^{th} percentiles of the IEC recommended wave characteristics were calculated and plotted to display the variation, upper and lower limits, and potential skewness of the dataset. It was confirmed that the dataset used in this analysis is skewed, as the mean value of each parameter (except for directionality coefficient) is greater than the median, or the 50^{th} percentile line throughout most of the year. This is typical for sea states as extreme events do not frequently occur throughout the year, but rather are concentrated in the winter months. In the analysis of significant wave height, energy period, and omni-directional and maximum directionally resolved wave energy transports the values increase in the winter months and decrease in the summer, which is attributed to an increase in storms during the winter. The interannual variability is apparent and easily visible in the plots in this section.

In addition to the monthly statistics representation, monthly cumulative distributions were shown to provide greater detail of the wave resource parameters per month throughout the hindcast. Temporal fluctuations were shown for the year 2010 of the PNNL hindcast and were compared to physically observed data recorded at NDBC 46050. The purpose of this assessment was to give a better idea of inter-annual variability of wave resource parameters, and to demonstrate the agreeance between physically observed data and the modeled data.

Wind effects at PacWave were investigated in order to demonstrate the necessity of broadening the basis from which a complete wave energy resource assessment is made. A boxplot was created to show the range of measurements recorded at the NDBC stations. Wind direction and speed data from NDBC 46097 was analyzed to show a profile of the winds dominating the field in the PacWave region.

Extreme environmental contours were shown based on the IEC recommendation to include extreme sea state information in a wave energy resource assessment. Doing so is valuable to a wave energy resource assessment as WEC developers must consider extreme sea states when necessarily preparing WECs for survival in potentially harsh ocean environment. The value of

analyzing a long-term dataset is reinforced in this section, as the hindcast period from 1980-2010 is considered long-term. The plots in this section infer that wave height and energy period values corresponding to 50- and 100-year extreme sea state values would occur during the 30 years. The maximum extreme wave height and energy period for the 50-year contour are predicted to be 12.49 m and 16.68 s respectively. The 100-year contour yields a maximum wave height of 13.19 m and energy period of 16.85 s.

To provide operation and maintenance (O&M) information for the PacWave sites to parties of interest, the significant wave height and peak period data were filtered to only include complete days of measurements where H_{m0} was less than 1.5 m and T_p was greater than 8 s. The number of full days providing these conditions were normalized on a yearly basis to give an idea of the typical availability throughout a year. Tables were created to show the specific breakdown of days available per year and per month by window length. August was overwhelmingly found to be the optimal month to conduct O&M, as it had the maximum amountof window availability per year. Box and whisker plots were also provided to allow a greater understanding of window availability at PacWave. As expected, 5-day windows have the least likelihood of occurrence, followed by 3-day, 2-day, and single day windows respectively. July, August, and September consistently prove to be the most favorable months in terms of appropriate sea state conditions for O&M.

7 REFERENCES

[1] A. Cornett, "A global wave energy resource assessment," *Sea Technol.*, vol. 50, no. 4, pp. 59–64, 2008.

[2] P. Lenee-Bluhm, R. Paasch, and H. T. Özkan-Haller, "Characterizing the wave energy resource of the US Pacific Northwest," *Renew. Energy*, vol. 36, no. 8, 2011, doi: 10.1016/j.renene.2011.01.016.

[3] G. García-Medina, H. T. Özkan-Haller, and P. Ruggiero, "Wave resource assessment in Oregon and southwest Washington, USA," *Renew. Energy*, vol. 64, 2014, doi: 10.1016/j.renene.2013.11.014.

[4] Z. Yang, G. García-Medina, W.-C. Wu, and T. Wang, "Characteristics and variability of the nearshore wave resource on the U.S. West Coast," *Energy*, vol. 203, p. 117818, 2020, doi: 10.1016/j.energy.2020.117818.

[5] W. C. Wu, T. Wang, Z. Yang, and G. García-Medina, "Development and validation of a high-resolution regional wave hindcast model for U.S. West Coast wave resource characterization," *Renew. Energy*, vol. 152, 2020, doi: 10.1016/j.renene.2020.01.077.

[6] International Electrotechnical Commission, *Marine energy : wave, tidal and other water current converters. Part 101, Wave energy resource assessment and characterization.* .

[7] Delft, "USER MANUAL SWAN - Cycle III version 40.72AB," *Cycle*, p. 125, 2009.

[8] C. xxx V. K. Prasada Rao, "Spectral width parameter for wind-generated ocean waves," *Proc. Indian Acad. Sci. - Earth Planet. Sci.*, vol. 97, no. 2, pp. 173–181, 1988, doi: 10.1007/BF02861852.

[9] P. Ruggiero, P. D. Komar, and J. C. Allan, "Increasing wave heights and extreme value projections: The wave climate of the U.S. Pacific Northwest," *Coast. Eng.*, vol. 57, no. 5, pp. 539–552, 2010, doi: 10.1016/j.coastaleng.2009.12.005.

[10] B. Robertson, H. Bailey, and B. Buckham, "Resource assessment parameterization impact on wave energy converter power production and mooring loads," *Appl. Energy*, vol. 244, 2019, doi: 10.1016/j.apenergy.2019.03.208.

[11] M. R. Hashemi and S. P. Neill, *Fundamentals of Ocean Renewable Energy*, 1st ed. Joe Hayton, 2018.

[12] N. Li, "WETS Program Review and Workshop," in *Numerical Wave Modeling and Data Analysis for WETS*, 2020.

APPENDIX A: PACWAVE NORTH WAVE RESULTS

A.1 Annual histogram of sea state occurrences

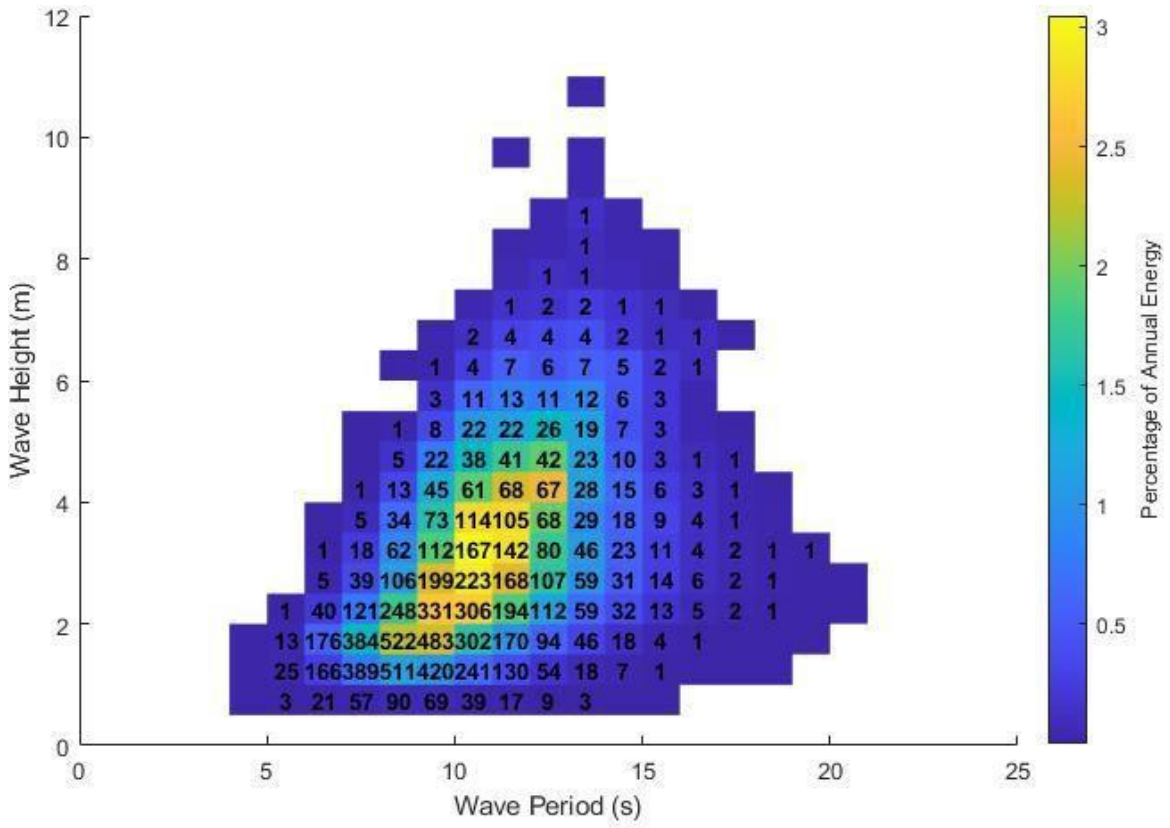

Figure 39: Omni-directional SWAN sea-state histogram from 1980-2010 at PacWave North (annual mean condition)

A.2 Annual wave rose

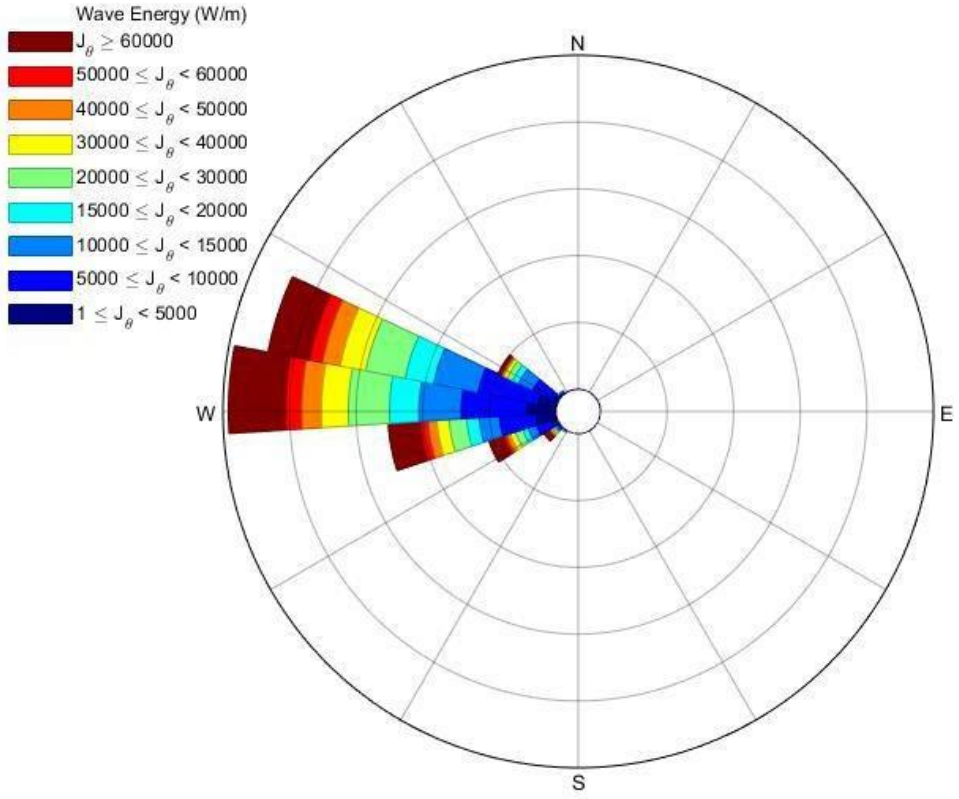

Figure 40: Directionally resolved SWAN wave rose distribution of wave energy from 1980-2010 at PacWave North

A.3 Annual variation of long-term monthly mean

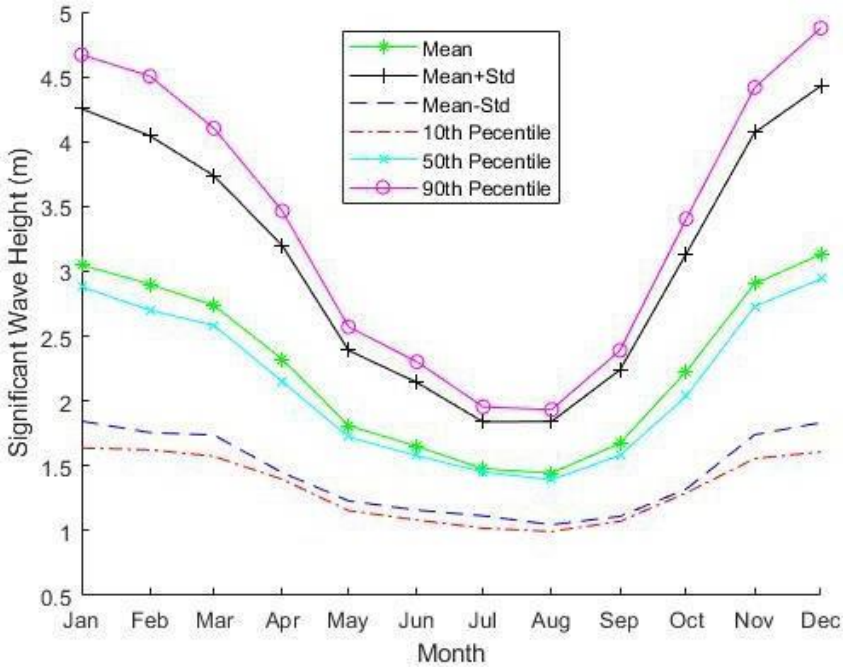

Figure 41: Monthly mean of SWAN significant wave height from 1980-2010 at PacWave North

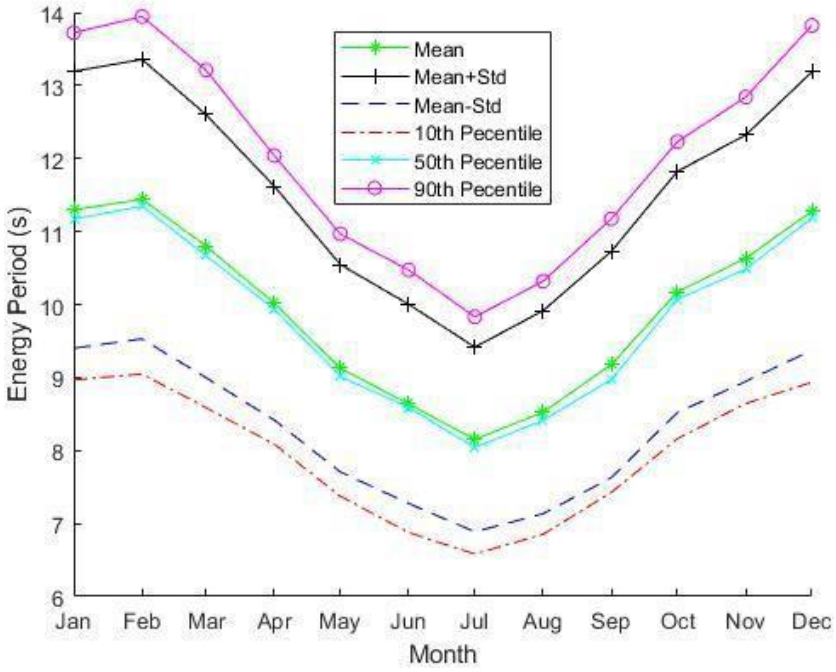

Figure 42: Monthly mean of SWAN energy period from 1980-2010 at PacWave North

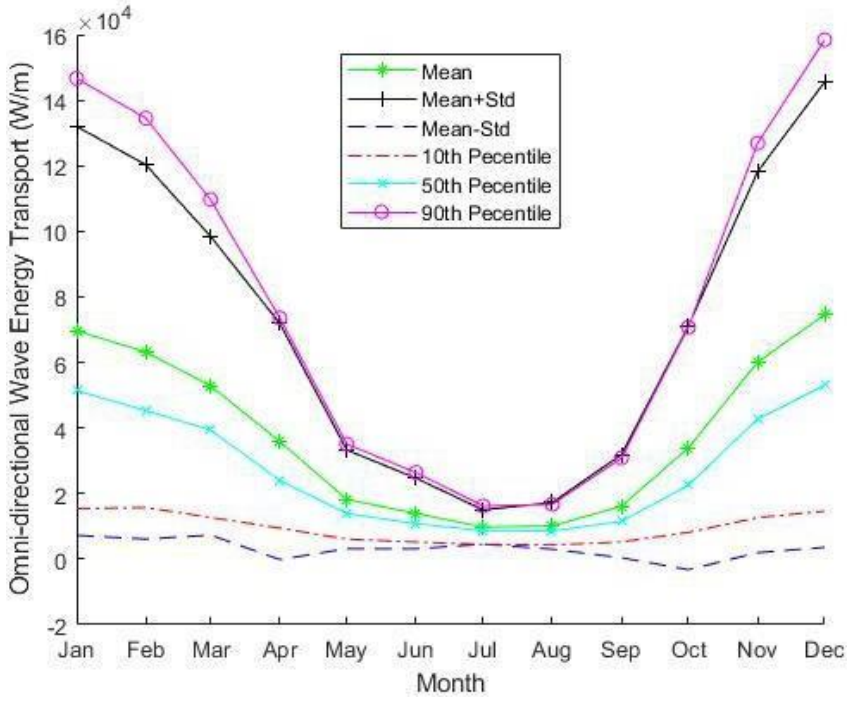

Figure 43: Monthly mean of SWAN omni-directional wave energy transport from 1980-2010 at PacWave North

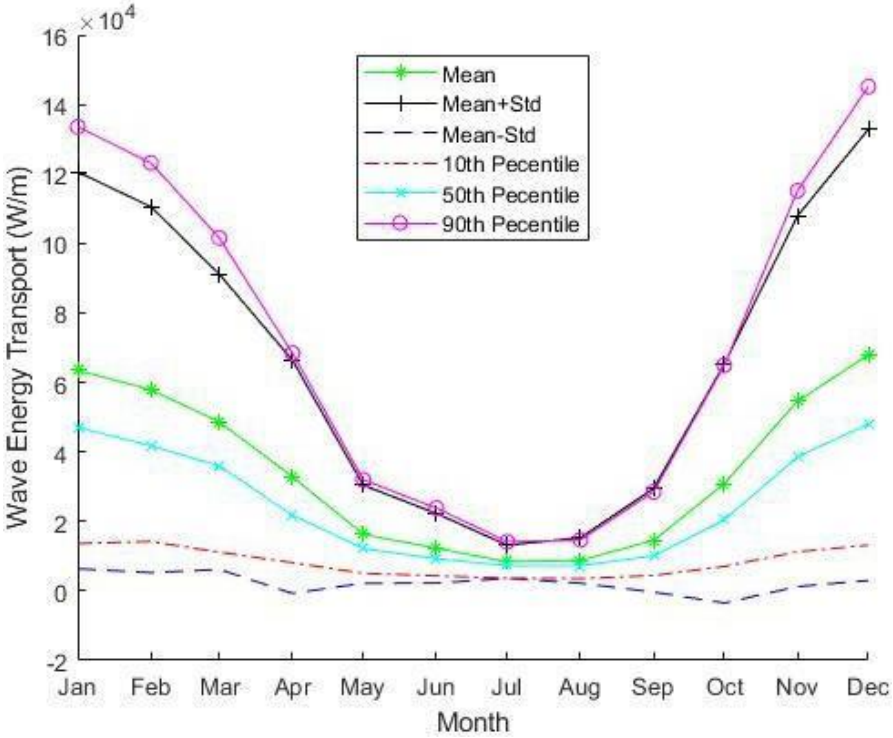

Figure 44: Monthly mean of SWAN directionally resolved wave energy transport from 1980-2010 at PacWave North

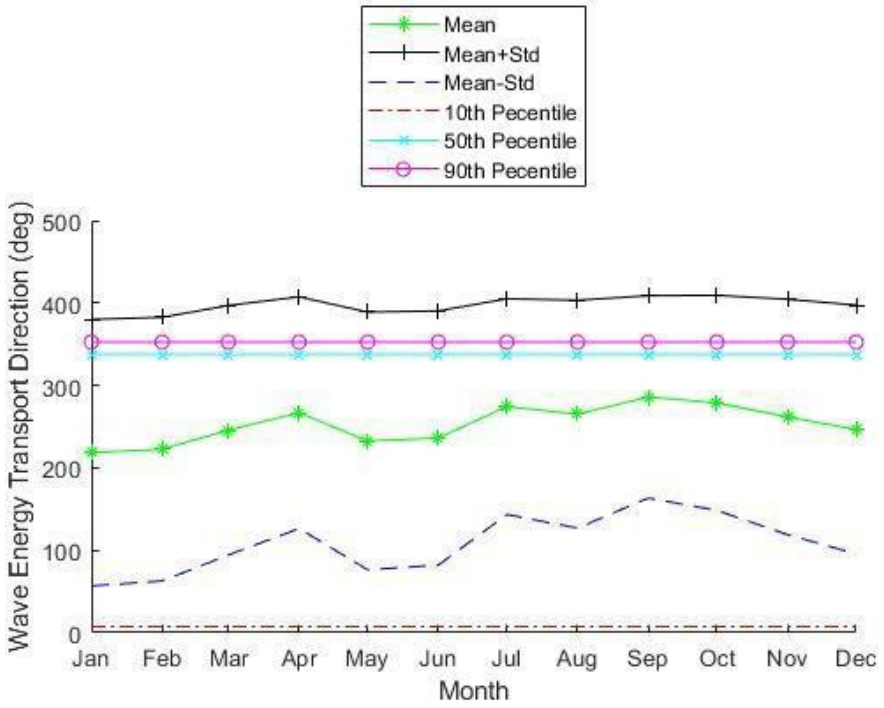

Figure 45: Monthly mean of SWAN direction of maximum directionally resolved wave energy transport from 1980-2010 at PacWave North

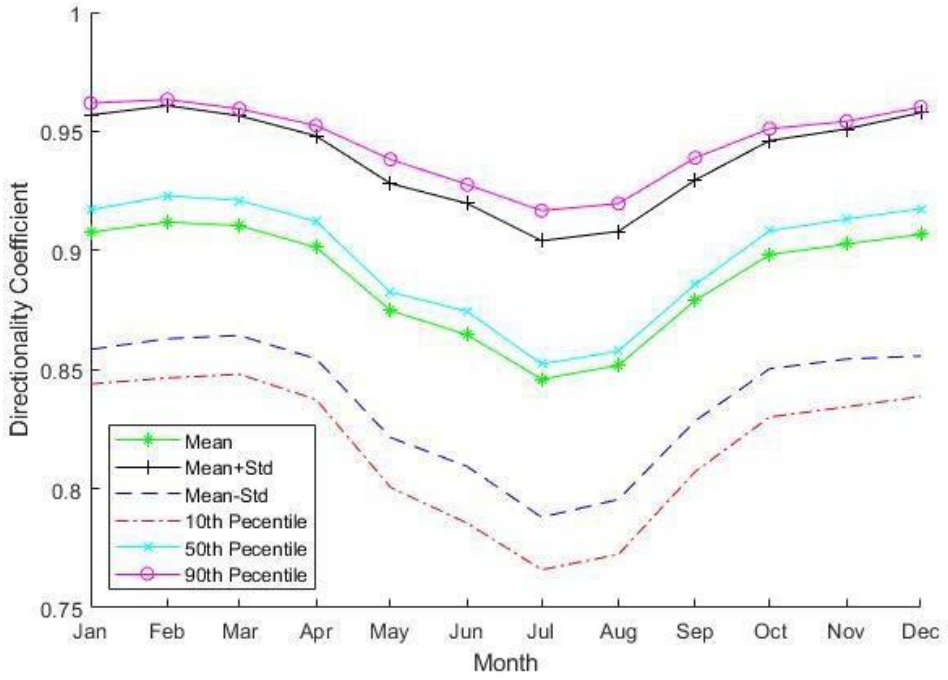

Figure 46: Monthly mean of SWAN directionality coefficient from 1980-2010 at PacWave North

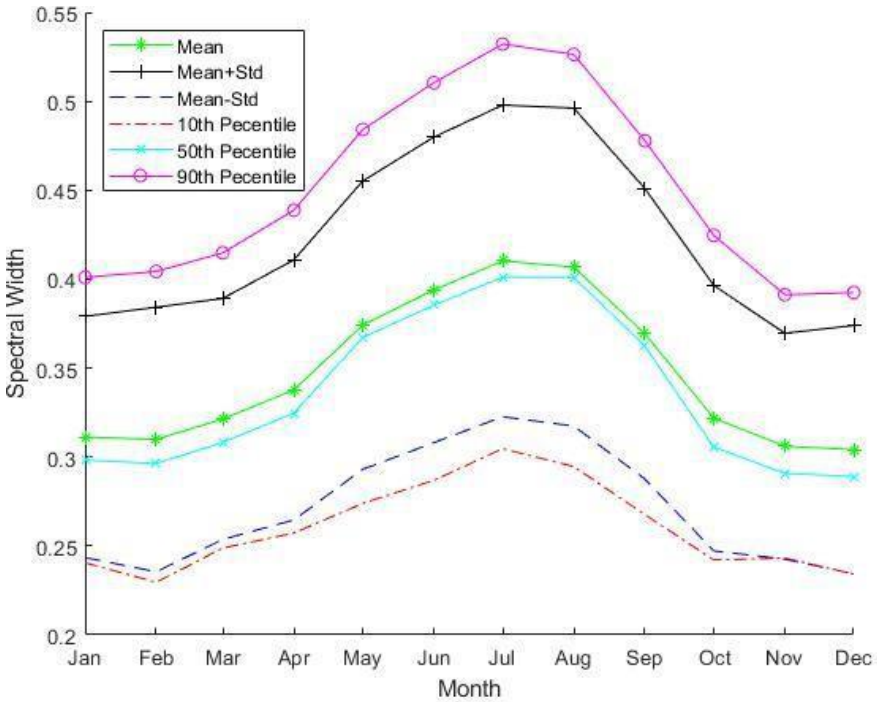

Figure 47: Monthly mean of SWAN spectral width from 1980-2010 at PacWave North

A.4 Monthly cumulative distributions

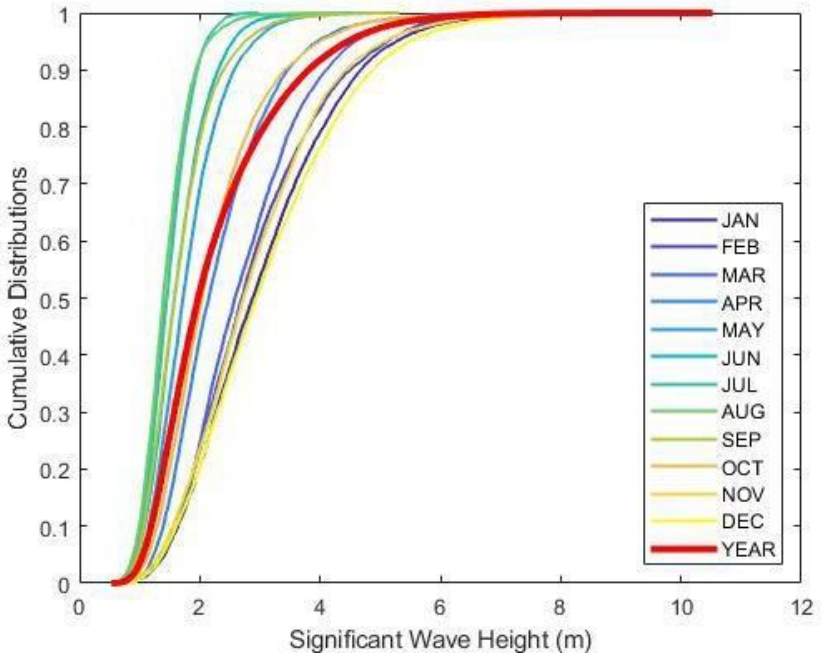

Figure 48: Monthly cumulative distributions of SWAN significant wave height from 1980-2010 at PacWave North

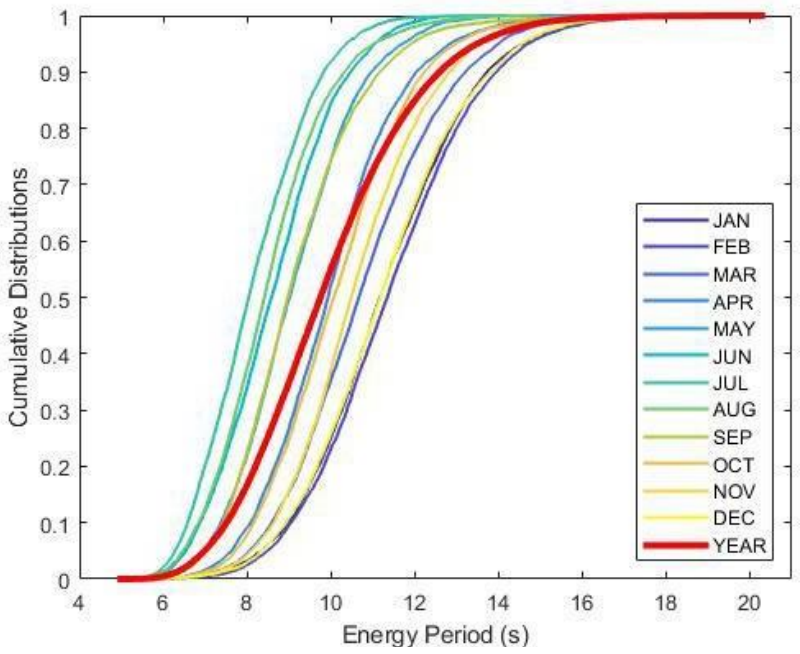

Figure 49: Monthly cumulative distributions of SWAN energy period from 1980-2010 at PacWave North

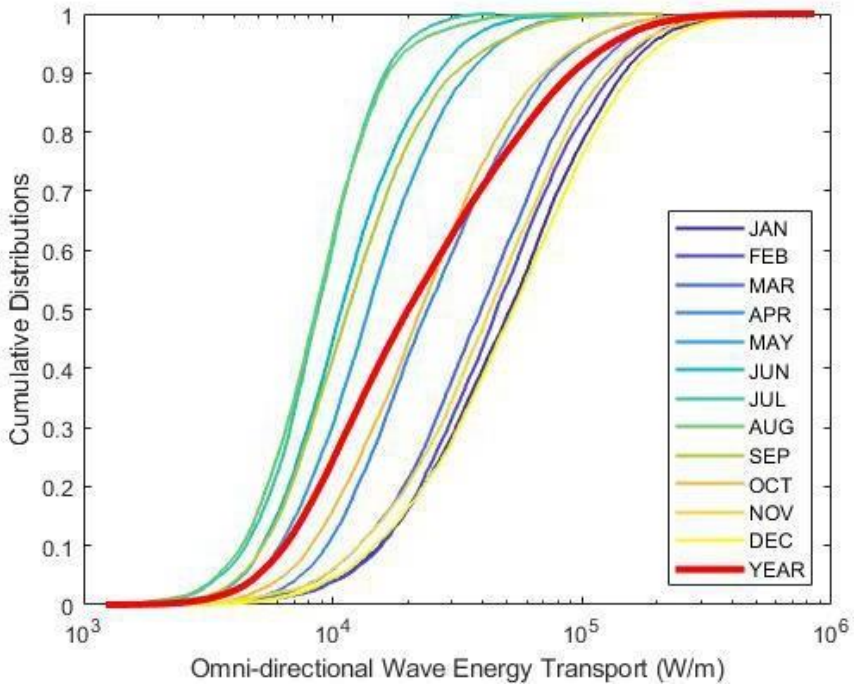

Figure 50: Monthly cumulative distributions of SWAN omni-directional wave energy plotted on a log-scale from 1980-2010 at PacWave North

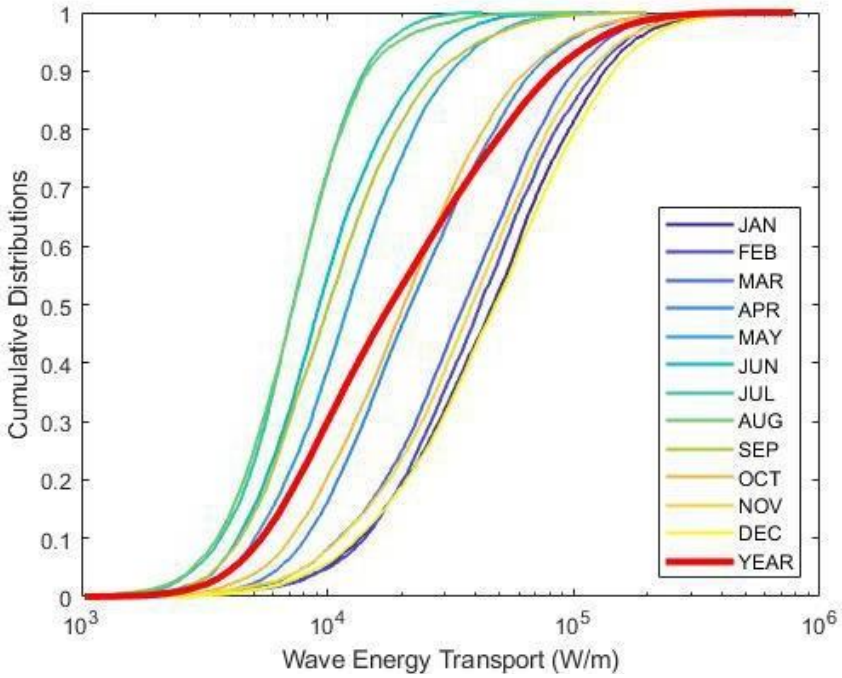

Figure 51: Monthly cumulative distributions of SWAN maximum directionally resolved wave energy transport plotted on a log-scale from 1980-2010 at PacWave North

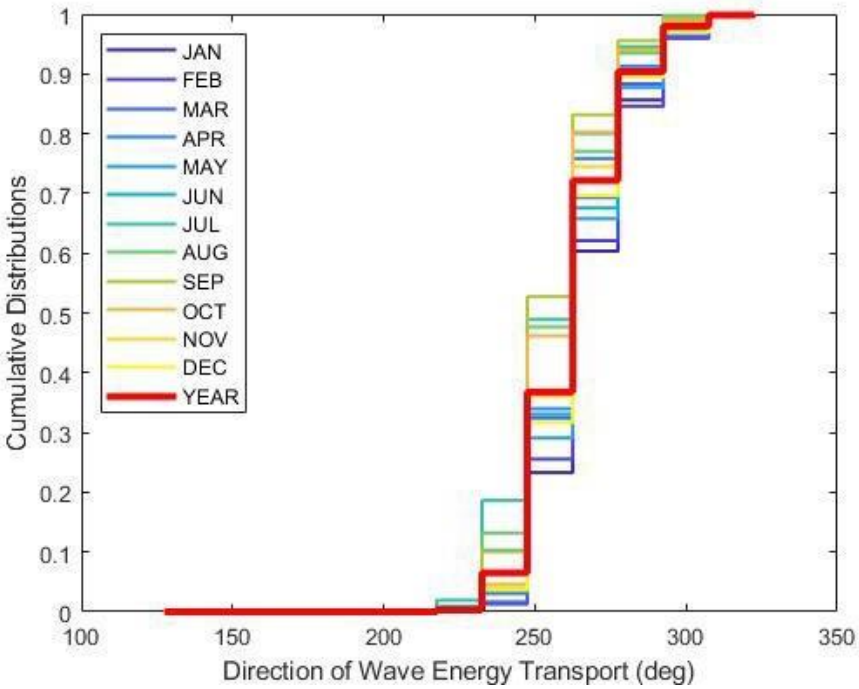

Figure 52: Monthly cumulative distributions of SWAN direction of maximum directionally resolved wave energy transport from 1980-2010 at PacWave North

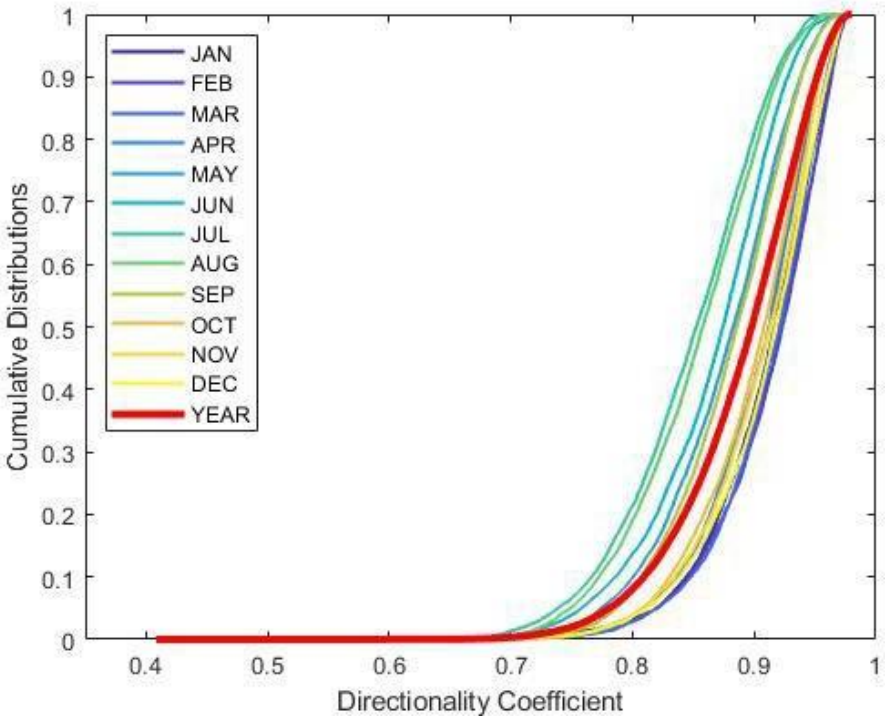

Figure 53: Monthly cumulative distributions of SWAN directionality coefficient from 1980-2010 at PacWave North

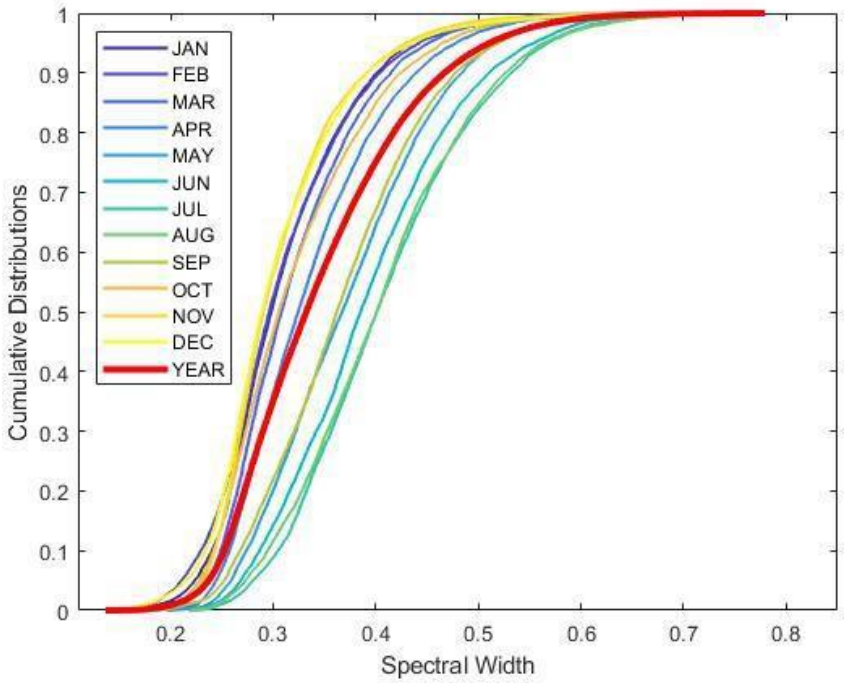

Figure 54**: Monthly cumulative distributions of SWAN spectral width from 1980-2010 at PacWave North**

A.6 Extreme Environmental Contours

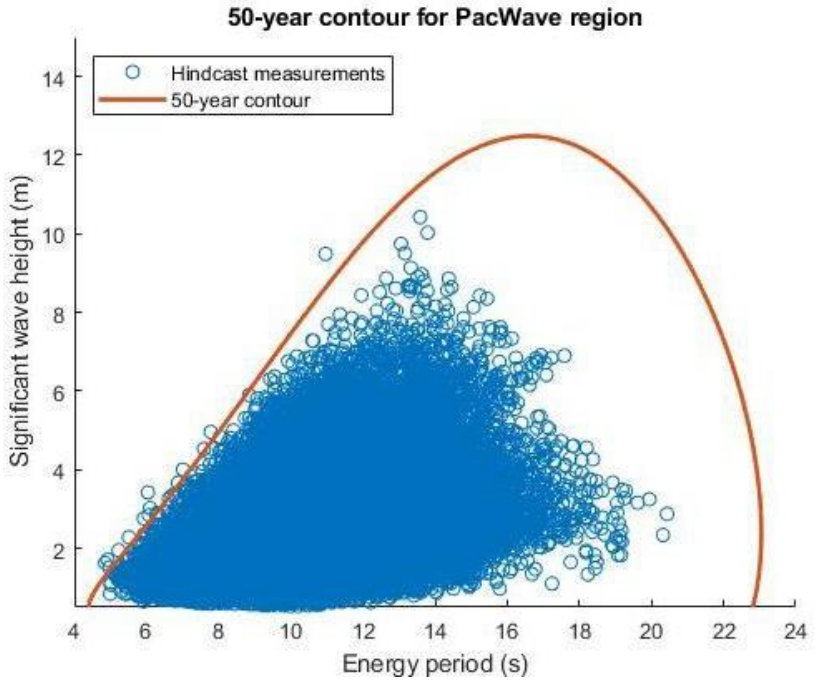

Figure 55: 50-year environmental contour for the PacWave region compared to hindcast measurements recorded for PacWave North from 1980-2010

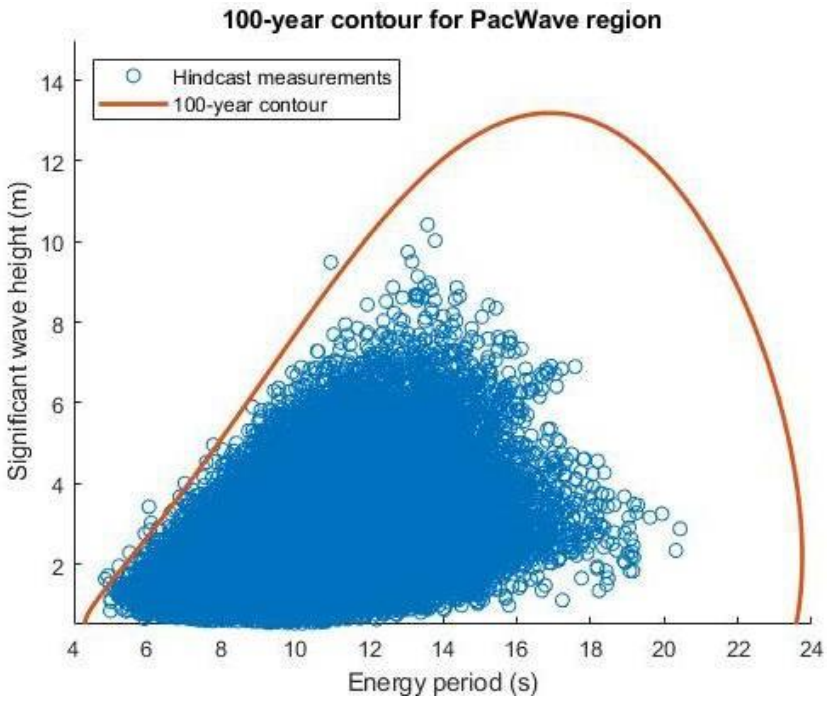

Figure 56: 100-year environmental contour for the PacWave region compared to hindcast measurements recorded for PacWave North from 1980-2010

A.7 Operation & Maintenance Windows

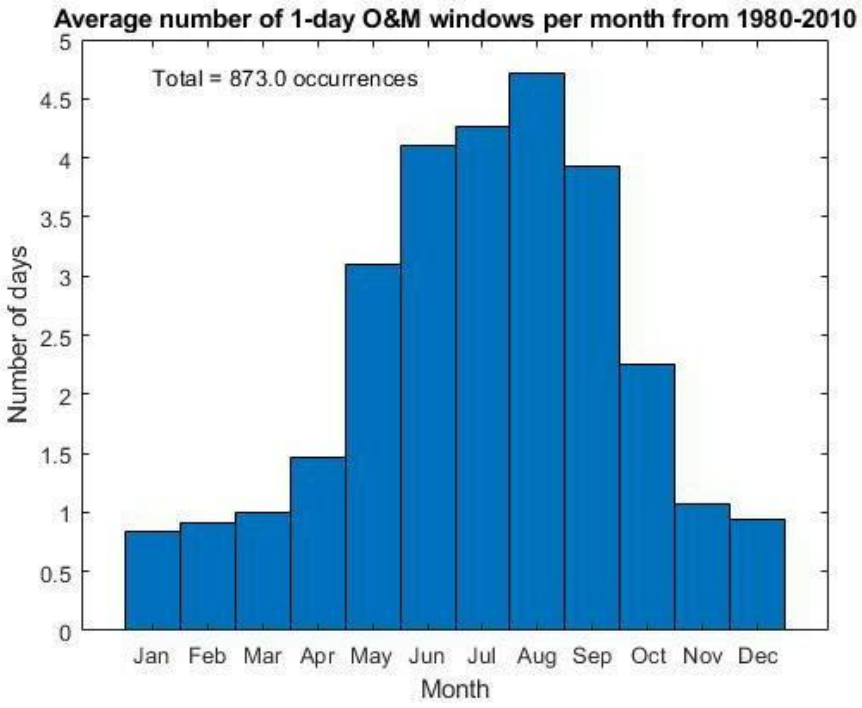

Figure 57: Number of days available for O&M from 1980-2010 at PacWave North

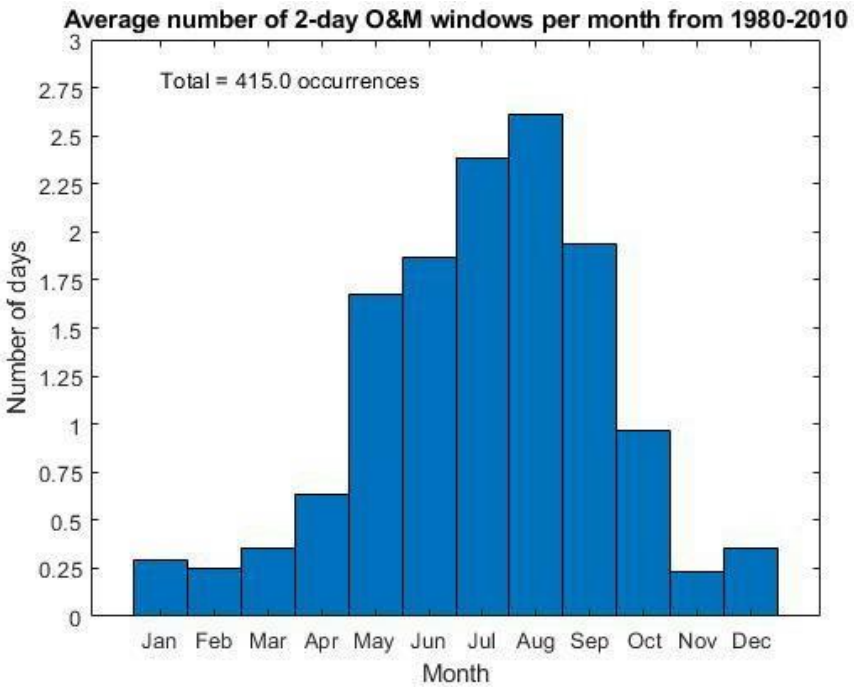

Figure 58: Number of 2-day windows for O&M from 1980-2010 at PacWave North

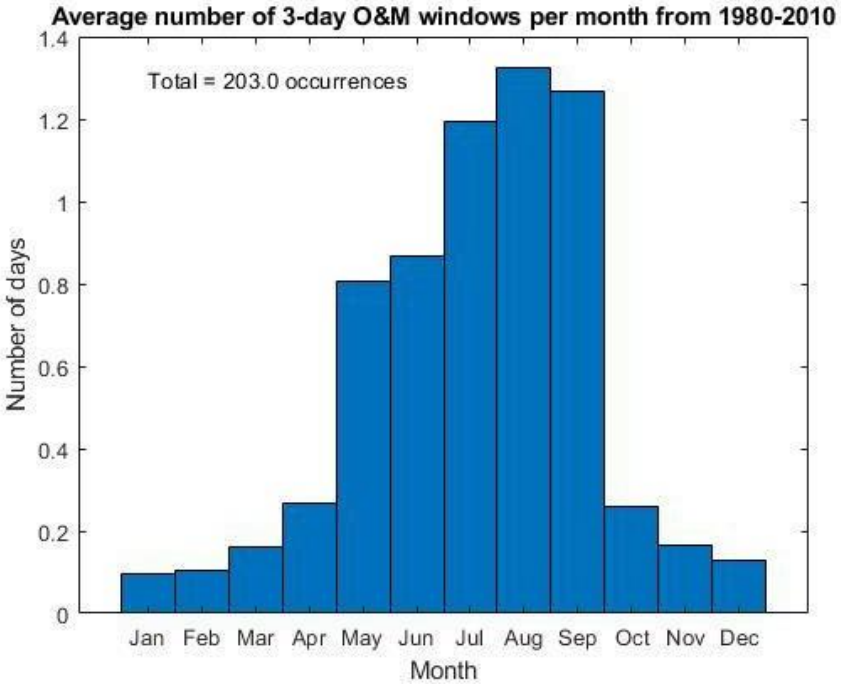

Figure 59: Number of 3-day windows for O&M from 1980-2010 at PacWave North

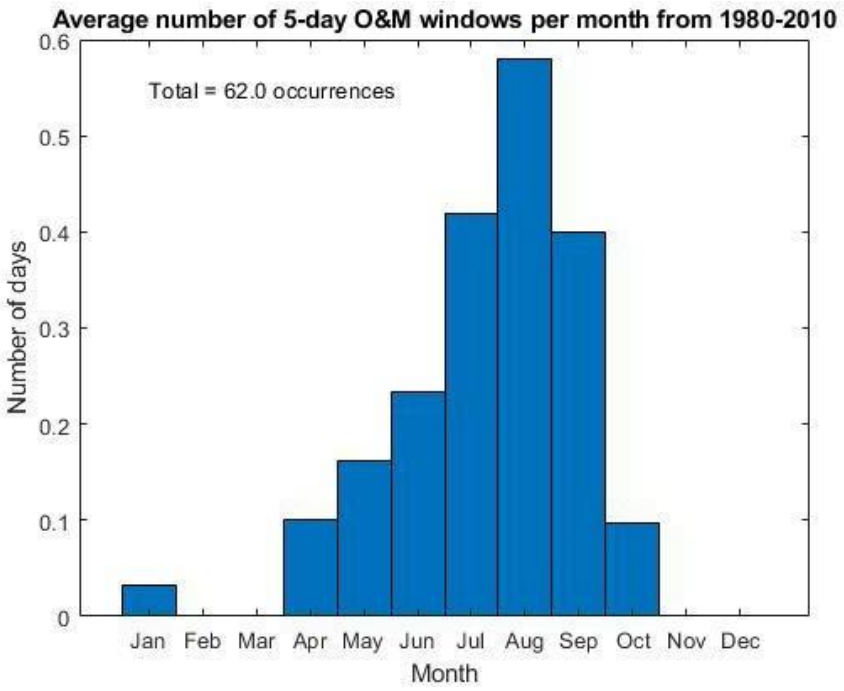

Figure 60: Number of 5-day windows for O&M from 1980-2010 at PacWave North

	Jan	Feb	Mar	Apr	May	Jun	Jul	Aug	Sep	Oct	Nov	Dec
1-day windows	0.8	0.9	1	1.5	3.1	4.0	4.3	4.7	3.8	2.2	1.0	0.9
2-day windows	0.3	0.2	0.4	0.6	1.7	1.8	2.4	2.6	1.9	1.0	0.2	0.3
3-day windows	0.1	0.1	0.2	0.3	0.8	0.9	1.2	1.3	1.3	0.3	0.2	0.1
5-day windows	0	0	0	0.1	0.2	0.2	0.4	0.6	0.4	0.1	0	0

Table 3: Average number O&M windows per month from 1980-2010 at PacWave North

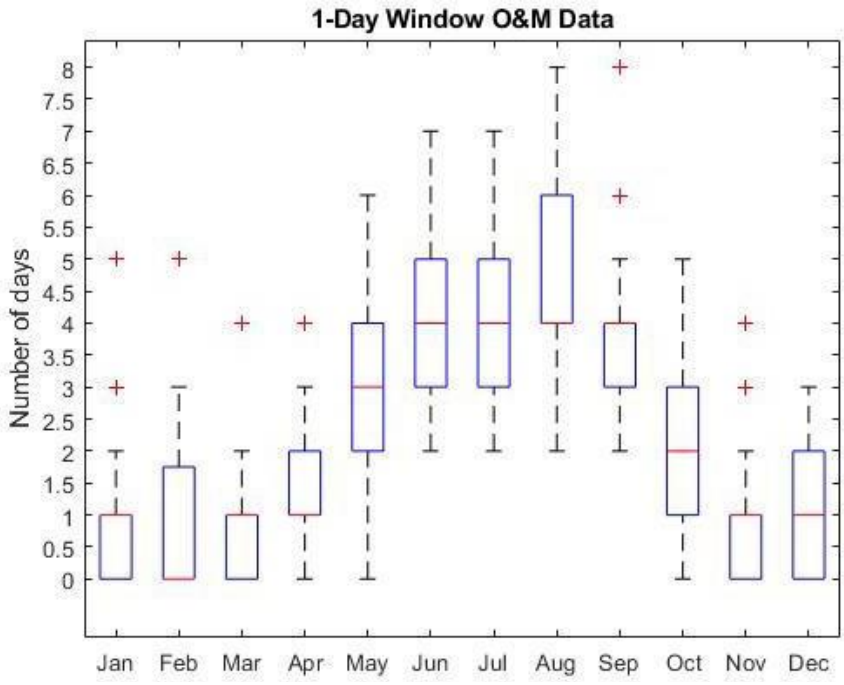

Figure 61: Box and whisker plot describing the 1-day window O&M data at PacWave North. Shown in the plot are extreme outlier values, non-extreme minima and maxima, median values (50th percentiles), and 25th and 75th percentile values.

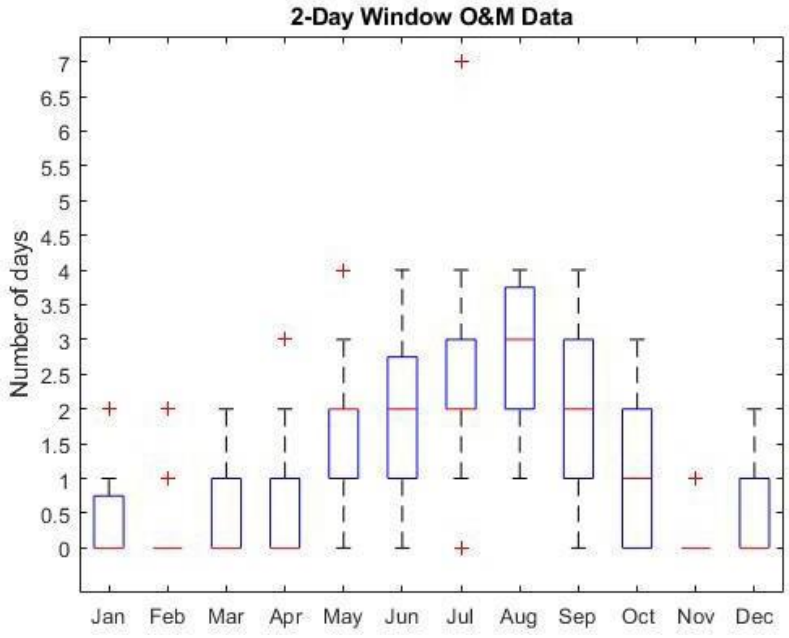

Figure 62: Box and whisker plot describing the 2-day window O&M data at PacWave North. Shown in the plot are extreme outlier values, non-extreme minima and maxima, median values (50th percentiles), and 25th and 75th percentile values.

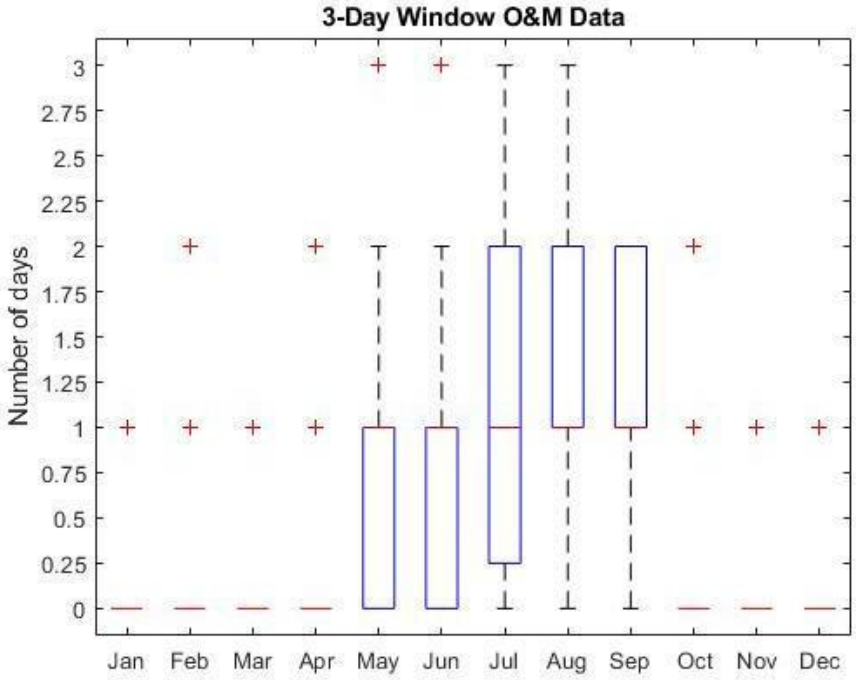

Figure 63: Box and whisker plot describing the 3-day window O&M data at PacWave North. Shown in the plot are extremeoutlier values, non-extreme minima and maxima, median values (50th percentiles), and 25th and 75th percentile values.

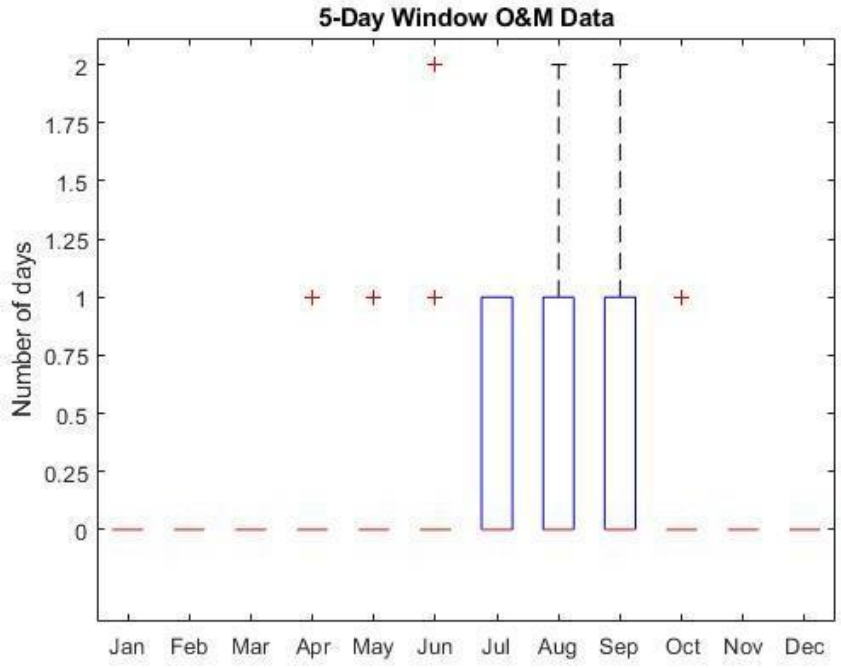

Figure 64: Box and whisker plot describing the 5-day window O&M data at PacWave North. Shown in the plot are extremeoutlier values, non-extreme minima and maxima, median values (50th percentiles), and 25th and 75th percentile values.

Appendix C: Holistic Marine Energy Resource Assessments: A Wave and Offshore Wind Perspective of Metocean Conditions

The following text is the manuscript published in Renewable Energy by the author's advisor and herself along with other researchers. The author completed the wave resource assessment along with the tidal and extreme wave assessments.

Holistic Marine Energy Resource Assessments: A Wave and Offshore Wind Perspective of Metocean Conditions

Bryson Robertson[a,b,*], Gabrielle Dunkle[a], Jonah Gadasi[a], Gabriel Garcia-Medina[b], Zhaoqing Yang[b]

[a] Pacific Marine Energy Center, Oregon State University, USA
[b] Pacific Northwest National Laboratory, USA
[*] Corresponding author

Abstract

Offshore wind and wave energy resources are possibly the last significantly untapped renewable energy resource, and could play a significant role in mitigating the worst impacts of climate change via the generation of renewable electricity. However, offshore wind and wave energy resource assessments have been conducted as independent parallel processes, with little interaction with regard to best practices, lessons learnt, or opportunities to create compatible methodologies for future utilization by the broader marine energy sector. Based on the latest technical specifications from the International Electrotechnical Commission, and the highest fidelity publicly available datasets, the offshore wind and wave conditions at the PacWave site off Oregon, USA were quantified. The results clearly show a significant untapped energy resource an annual average wave energy flux of ~35kW/m and a mean average wind speed of 7.8m/s. The offshore wind and wave energy resources both show significant seasonal variation, with offshore wind also featuring a consistent daily profile during summer. Finally, opportunities and challenges associated with developing a holistic assessment of offshore marine energy resources were discussed and recommendations provided.

Keywords: wave resource; offshore wind resource; wave energy; wind energy; extreme conditions; clustering analyses; ocean currents

1 Introduction and Background

In order to mitigate the worst impacts of climate change, nations around the world are increasingly turning to renewable energy to power their economies, industries and lifestyles. The transition from fossil fuels to renewables is driving new economic opportunities and growth. It is expected that renewables, primarily wind and solar, and batteries will capture 80% of the total $15.1 trillion invested in new power capacity between now and 2050 [1]. This is partially due to the fact that the development of new terrestrial wind and solar projects are increasingly becoming cheaper than generating electricity from existing coal and natural gas facilities. However, the development opportunity for terrestrial wind and solar is not boundless. Presently, the best resources and associated project sites have already been developed, or are facing significant opposition from local stakeholders [2].

In response, many nations and project developers are looking towards the ocean for new opportunities for carbon-free electricity generation and economic growth. Offshore marine energy resources may well be the last significantly untapped renewable energy resource and could play a linchpin role in decarbonizing our energy systems. While our oceans have a wide variety of renewable resources, wave and offshore wind resources are widely acknowledged for global availability and tremendous raw scale [3][4].

Traditionally, wave energy and wind energy resource assessments have been conducted as independent processes, with little interaction between the two communities with regard to best practices, lessons learnt, or opportunities to create compatible methodologies for future utilization by the broader marine energy sector.

In 2008, Cornett et al. [3] completed one of the most widely utilized global assessments of wave parameters and associated energy resources. As shown in Figure 55 from [3], Cornett et al. showed that wave energy resource is predominantly located in high-latitudes, and had significant seasonal variability between summer and winter. This research sparked a slew of follow-on studies to quantify the spatial and temporal aspects of the wave resources in these locations: Northern Europe [5,6][7], North Africa [8] Australia [9,10], South Africa [11], Canada [12,13]. While there were commonalities amongst the approaches used, there was also significant divergence and the need to create standard processes to ensure comparability between research efforts.

Building off the work of Lenee-Bluhm et al. [14] for the Oregon coast of the USA, a set of guidelines were developed [15] which began an International

Electrotechnical Commission (IEC) effort to create a technical specification for a proper wave resource assessment. The IEC convenes international marine energy experts to develop consensus-based standards to help guide the development of a wide variety of sectors. The IEC standards cover all necessary aspects of the development process to mitigate risks and increase the opportunities for successful technology and project development. First released in 2015, the IEC TS 62600-101 has become the de facto standard specification for assessing wave energy resources [16]. The Technical Specification (TS) is currently undergoing international review and a revised version should be available in 2021.

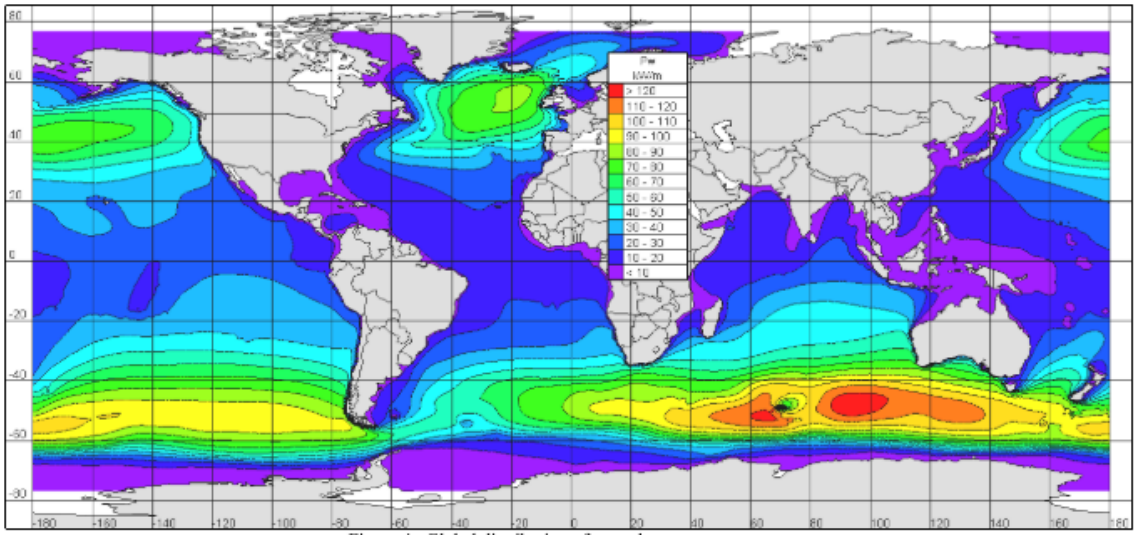

Figure 55: Global distribution of mean annual wave energy flux [3].

In 2012, Arent et al. [4] focused on developing a robust assessment of the scale and quality of wind energy resources globally, based on NOAA's Blended Sea Winds offshore wind dataset [17]. As with the wave energy resources, Arent et al. showed that offshore wind resource is predominantly located in high-latitudes and had significant seasonal variability between summer and winter. This and other leading efforts built on a number of existing studies to quantify the spatial and temporal aspects of the offshore wind resources in a wide variety of locations; for example, Northern Europe [18][19], North America[20][21], China [22][23], the Persian Gulf [24] and Thailand [25]. Unlike wave energy efforts, the international wind energy community has traditionally focused standards development around the technology and associated requirements for classifying the gross resource, rather than the resource in isolation. However, a new technical specification (IEC 61400-15-2 ED1) is currently focused on

providing robust and consistent methodologies to quantifying offshore wind resources.

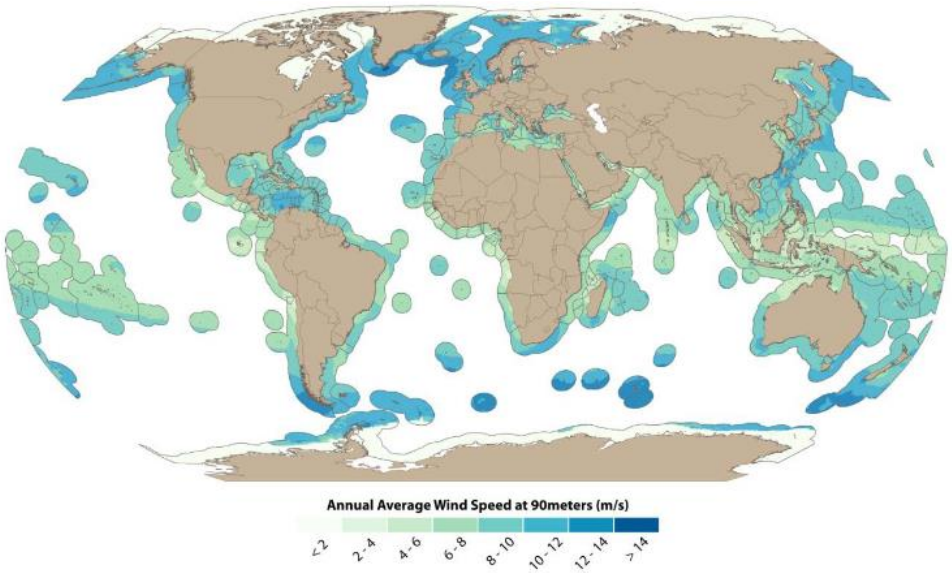

Figure 56: Global distribution of mean annual wind speeds [4]

While the majority of published literature has focused purely on wind or wave resources, a few studies have identified the need for holistic wind and wave assessments. Kalogeri et al. [26] worked to identify the gross wind and wave resources for Western Europe using hindcast data from the SKIRON atmospheric model and a European WAM wave model. They investigated the spacio-temporal impacts of these combined resources at 3 hourly resolution and identified potential locations for technology deployment. Ferrari et al. [27] utilized hourly outputs from a WEF wind model and a WaveWatch III wave model to identify optimal locations for deployments within the Mediterranean Sea. Weiss et al. [28] utilized hourly global numerical model outputs, and a variety of technology deployment and maintenance metrics, to identify Brazil and New Zealand as priority locations for offshore renewable energy deployments. However, each of the aforementioned studies completed their assessments via unique metrics and parameters, thus limiting their applicability when compared against global efforts under the IEC technical specifications. This paper assesses the recommended IEC resource assessment frameworks, and a case study of PacWave, USA, to quantify the opportunities and challenges when developing a holistic assessment of offshore marine energy resources. PacWave is a 20MW, grid connected, test facility for full scale WEC technologies approximately 10 km off the Oregon, USA, coast.

This paper is structured as follows: Section 2 introduces wave and offshore wind resource assessment methodologies, as suggested by the International Electrotechnical Commission, and methods to identify a reduced order condition set for experimental testing. Section 6 applies the presented methodologies to the case study of PacWave in Oregon, USA and provides contextual analyses of the results. Section 14 discusses the compatibility and limitations of the IEC-Specifications to develop a holistic assessment of wave and offshore wind energy resources. Section 15 provides a concluding synthesis of research findings.

2 Resource Assessment Methodology

The following section provides an overview of the methodologies, datasets, resource parameters and the resolutions specified by the IEC. Given the rather complex naming structures of the associated technical specifications, we provide a quick review of those mentioned within the following section.

On the wave side, TS 62600-101 is focused on wave energy resource and characterization while TS 62600-100 is focused on the power performance assessment for a specific wave energy converter (WEC). On the wind side, TS 61400-1 is focused on the development of terrestrial wind turbines and identification of necessary parameters suitable for classifying the wind resource. TS 61400-3-1 and TS 61400-3-2 expand upon information within TS 61400-1 to include fixed and floating offshore wind turbines, respectively.

3 IEC Wave Resource Assessment

When assessing the wave energy resources for a potential project, IEC Technical Specification 62600:101 (TS 62600-101) provides a consistent and robust methodology for wave energy resource characterization. The required wave parameters include significant wave height H_{m0}, energy period T_e, omni-directional wave power J, the directionally resolved wave power and its direction (J_θ and $\theta_{J\theta max}$), directionality coefficient (d), spectral width (ϵ_0), and mean water depth. These wave parameters are calculated from on the directional wave spectrum; obtained via numerical modeling or physically observed measurements. To calculate omni-directional parameters, the two-dimensional frequency-directional variance density spectrum are transformed into one-dimensional frequency-domain spectrum via Eq. (1):

$$S_i = \sum_j S_{ij} \Delta\theta_j \quad (1)$$

where S_{ij} is the variance density in the i^{th} frequency and j^{th} direction bin. Spectral moments of the n^{th} order, m_n, are calculated from frequency variance density by:

$$m_n = \Sigma_i f_i^n S_i \Delta f_i \quad (2)$$

where f_i is frequency. Using the moments of the spectrum, the characteristic wave height is calculated using the zeroth spectral moment:

$$H_{m0} = 4\sqrt{m_0} \quad (3)$$

which is generically referred to as the significant wave height calculated from the wave spectrum. This value is different from H_s, which is directly measured via wave-by-wave analysis by averaging the largest 1/3 waves in a record. The preferred characteristic wave period for wave resource assessments is the energy period – Eq. (4).

$$T_e = T_{-10} = \frac{m_{-1}}{m_o} \quad (4)$$

Omni-directional, or directionally unresolved, wave power J is the time averaged energy flux through a vertical cross section of unit diameter that extends from the seafloor to the surface, calculated by:

$$J = \rho g \sum_{i,j} c_{g,i} S_{ij} \Delta f_i \Delta\theta_j \quad (5)$$

where $c_{g,i}$ is the group celerity, ρ is the water density, and g is the gravitational constant. The time-averaged energy flux across a plane normalized to direction θ is defined as the directionally resolved wave power. This directionally resolved wave energy transport is the sum of the contributions of each component with a positive component in direction θ, calculated by:

$$J_\theta = \rho g \sum_{i,j} c_{g,i} S_{ij} \Delta f_i \Delta\theta_j \cos(\theta - \theta_j)\, \delta \qquad \begin{cases} \delta = 1, & \cos(\theta - \theta_j) \geq 0 \\ \delta = 0, & \cos(\theta - \theta_j) < 0 \end{cases} \quad (6)$$

The maximum value of J_θ represents the maximum time averaged wave power propagating in a single direction and is denoted by $J_{\theta_{Jmax}}$. The directionality coefficient is a characteristic measure of the directional spreading of wave power. It is the ratio of the maximum directionally resolved wave energy transport to the omni-directional wave energy transport:

$$d = \frac{J_{\theta_{Jmax}}}{J} \quad (7)$$

Spectral width, ϵ_0, characterizes the frequency-domain spreading of variance density [29]. This parameter is defined using:

$$\epsilon_0 = \sqrt{\frac{m_0 m_{-2}}{m_{-1}^2} - 1} \quad (8)$$

Annual monthly means, standard deviations, percentiles, and variations of all wave parameters are required, in addition to annual mean bivariate histogram and wave rose. The bivariate histogram shows the annual frequency

of occurrence of sea states, parameterized in terms of H_{m0} and T_e with a resolution of 0.5 m and 1 s respectively, while the wave rose shows the joint distribution of maximum directionally resolved wave power and its direction is also required for inclusion across all classes.

The standards require a minimum of 10 years of sea state data for assessments, and acknowledge that a longer period of data may be necessary to quantify the low frequency climate variability and its effect on a wave energy resource assessment; such as ENSO and El Nino-type events [30]. The specification identifies three classes of resource assessment and associated project application: Class 1 – Reconnaissance, Class 2 – Feasibility, and Class 3 – Design. The spatial and temporal fidelity of the required data increases with Class; with Class 1 being the lowest allowable resolution and Class 3 the highest resolution [30]. A Class 1 assessment may be conducted by analyzing existing, archived sea state parameters, or analyzing directional spectra generated via a numerical wave propagation model, while Class 2 and 3 data should be based on either directly measured directional wave spectra or an Measure-Correlate-Predict method [30].

The wave resource assessment also classifies the wind speed and direction data required and classifies it accordingly. Class 1 wind data has a 3-hour temporal resolution and 100 km spatial resolution, Class 2 data has a 3-hour temporal and 50 km spatial resolution, Class 3 data has a 1-hour temporal and 25 km spatial resolution respectively. Tidal current data and its potential effect on the wave resource is also a required IEC specification output. If the depth-averaged current speed exceeds 1.5 m/s, its effect on the wave climate should be investigated and included in wave modeling [30].

4 IEC Wind Resource Assessment

Wind speed and direction are the two primary parameters essential to a wind resource assessment. IEC TS 61400-1 for wind energy generation systems states that meteorological data must be directly measured and extrapolated or calculated using appropriate methods. These methods include site specific measurements, long-term records from nearby meteorological stations, simulation models validated against representative data, or local codes and standards [31]. Measurements for wind speed and direction shall be measured for a minimum period of 12 months with a temporal resolution of 1 Hz, and span a range of heights within the rotor's swept area. A separation of at least a third of the rotor diameter should be used to enable a robust analysis of vertical wind shear. This ensures the inclusion of seasonal effects on wind conditions and capture of necessary turbulence parameters. Many of the subsequent required

parameters are evaluated using wind utilize 10-minute averaged wind speed [31]. Wind direction distributions are generated for each sampled elevation [32].

If there are no measurements collected at hub height of a specific turbine of interest, information on wind speed is calculated using the wind profile. Wind measurements should be taken at a sufficient range of heights in order to develop a wind elevation profile using the power law in Eq. (9):

$$v_2 = v_1 \cdot \left(\frac{z_2}{z_1}\right)^{\alpha} \tag{9}$$

where v_1 and v_2 are the wind speeds at heights z_1 and z_2, respectively. The parameters denoted by the subscript 1 are typically located at a lower elevation, while the parameters denoted by the subscript 2 are at the elevation where wind speed is extrapolated. The wind shear coefficient, α, is a constant relating wind speeds at different elevations. A wind shear coefficient of 0.14 is initially appropriate for normal wind profiles in the marine environment [33].

Following wind speed and direction, turbulence intensity and air density have been identified as essential parameters for any turbine power performance estimate (by an analytic hierarchy process from professionals and researchers in the field, and a sensitivity analysis performed in the National Renewable Energy Laboratories 'FAST' software [34]). Turbulence intensity is defined as the ratio between wind speed and its standard deviation over a 10-minute period. It is inversely proportional to wind speed. Turbulence intensity and the turbulent standard deviation are utilized to calculate many extreme conditions, and calculated via:

$$\sigma_1 = I_{ref}(0.75V_{hub} + b) \tag{10}$$

where σ_1 is the turbulence standard deviation, I_{ref} is the turbulence intensity corresponding to the 70% quantile for a 15 m/s wind speed, V_{hub} is the hub height wind speed, and b is constant (5.6 m/s) [31]. Generally, air density is calculated from temperature and pressure using the ideal gas law.

Either a steady and turbulent extreme wind models (EWM) is necessary for understanding a site's extreme wind conditions. Each model involves computing the 50-year and 1-year return period for extreme wind speeds as a function of elevation. For the steady EWM, 3-second averaged wind speeds are utilized. The equations below are used to calculate the steady EWM 50- and 1-year extreme wind speeds

$$V_{e50}(z) = 1.4\, V_{ref}\left(\frac{z}{z_{hub}}\right)^{0.11} \text{ and } \; V_{e1}(z) = 0.8\, V_{e50}(z)$$

where V_{e50}, V_{e1} are the 50 and 1 year wind speeds, respectively; z, z_{hub} are the height in question and the hub height, respectively; and V_{ref} is the reference

wind speed [31]. The turbulent EWM 50- and 1-year extreme wind speeds, which utilize 10-minute averaged wind speeds, are given by:

$$V_{50}(z) = V_{ref}\left(\frac{z}{z_{hub}}\right)^{0.11} \text{ and } V_1(z) = 0.8\,V_{50}(z)$$

5 Identification of Reduced Order Representative Conditions

Given the wide-ranging variability in wave and wind conditions, developing a strategy to reduce the order of general wind and wave resource conditions for experimental testing (numerical or physical) and design studies is paramount. In order to identify the reduced order conditions to holistically represent the marine energy resource, a k-means clustering analysis is valuable[35–37]. A k-means clustering algorithm identifies a number of clusters, k, for a dataset, whose centers are representative of the data they contain. Cluster centroid locations are chosen such that the squared Euclidean distance between a centroid and each datapoint in its cluster is at a minimum. The appropriate number of clusters is evaluated via through Elbow and Silhouette tests.

The elbow test plots the sum of the distances of each point to its cluster's centroid (intra-cluster sum) against the number of clusters for a range of cluster numbers. The plot will take on an elbow shape, where the optimal range of clusters is roughly located from the beginning of the elbow to where the addition of more clusters no longer has any significant effect on the intra-cluster sum [37].

The silhouette test determines how similar a data point is to its own cluster versus other clusters. The datapoint is assigned a value between +1 and -1, where +1 indicates the datapoint definitely belongs in that cluster and -1 indicates it definitely does not. The cluster configuration with the highest sum of these values is the one with the most appropriate number of clusters [38]. By applying the Silhouette test to the range of k's obtained through the Elbow test, the optimal number of clusters for the dataset is identified.

6 Methodology Case Study FOR PacWave

The Pacific Northwest of the United States has one of the most active wave energy climates in the world [3] and is frequently noted as a primary location for future development of the wave energy sector. In order to facilitate this development, Oregon State University is developing the PacWave site. PacWave is a grid-connected 20MW, 5-berth open-ocean wave energy test facility, funded by the U.S Department of Energy, and is located at 44°35'04"N 124°12'45"W,

which is 11 km (~7 miles) off the coast of Newport, Oregon, as shown in Figure 57.

Prior research efforts have focused on assessing the wave energy resource offshore Oregon via hindcast models and physical buoy data [14,39,40], yet have not focused on the specific characteristics at the PacWave site. In order to be certified by the IEC for WEC testing, the PacWave site requires a dedicated high-resolution and long-term resource assessment following the methodology in Section 3.

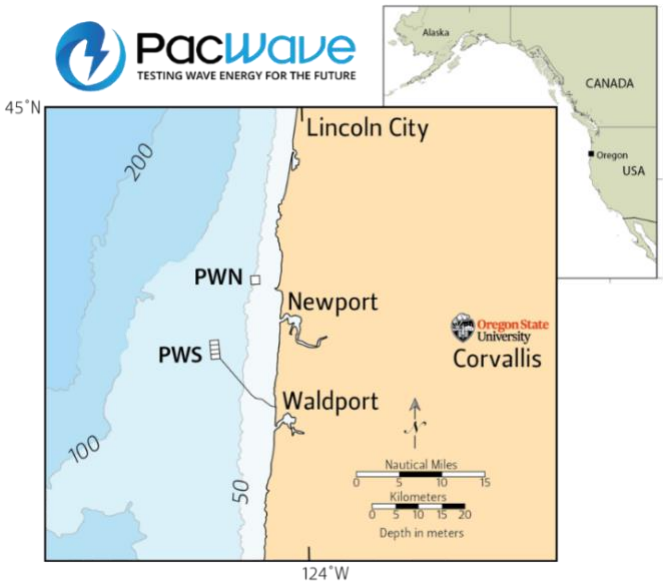

Figure 57: PacWave South (PWS) location off the coast of central Oregon (PacWave, 2020)

7 IEC Wave Resource Assessment Results

The Pacific Northwest National Laboratory (PNNL) recently released a 32-year Simulating WAves Nearshore (SWAN) wave hindcast for the US west coast [41]. Wu et al. utilized WaveWatch III (WW3) boundary conditions and Climate Forecast System Reanalysis (CFSR) wind forcing to resolve wave conditions across this region at 3 hourly and ~200m resolution. In aggregate, these models are classified as a Class 1, yet the majority of the spatial and temporal resolution would be sufficient for Class 2 [41].

The primary method of representing the annual mean wave resource characteristics is via a bivariate histogram of the significant wave height H_{m0} and energy period T_e, as shown in Figure 58. The numbers in each cell represent mean annual hours recorded in each specific H_{m0} - T_e sea state combination. The shading of the cells is an energy flux weighted representation; with the

output of particular sea state occurrence calculated by $0.5 \cdot H_{m0}^2 T_e$ multiplied by the hours of occurrence.

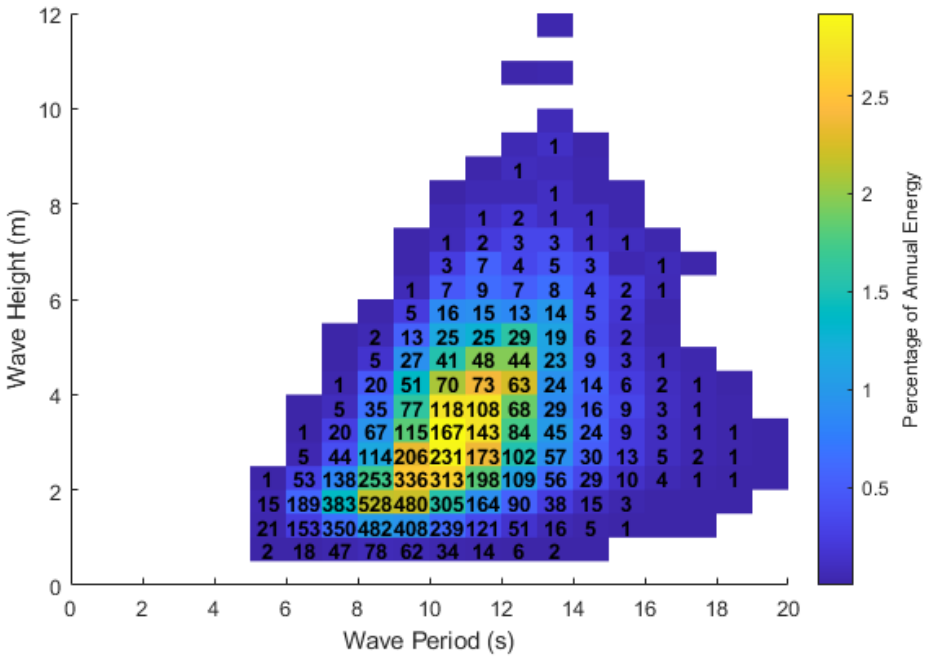

Figure 58: Omni-directional SWAN sea-state histogram from 1980-2010 at PacWave (annual mean conditions)

The most commonly occurring sea state has a significant wave height of 1.75 m and an energy period of 8.5 s and occurs for 528 hours per year. Conversely, the conditions with the highest annualized contribution to the overall wave energy flux (~3%) only occurs for only 231 hours per year and features a significant wave height of 2.75 m and at an energy period of 10.5 s.

A wave rose is required by IEC standards to describe the directional distribution of wave conditions. Figure 59 shows the mean annual directional and energy flux conditions at PacWave over the 32-year period. Note that direction is defined as the direction which waves are travelling from, and the energy flux within each sea state assumes deep-water conditions. Every bar combines wave headings into a 15° bin, and the length of each color segment represents annual wave energy transport in a given direction.

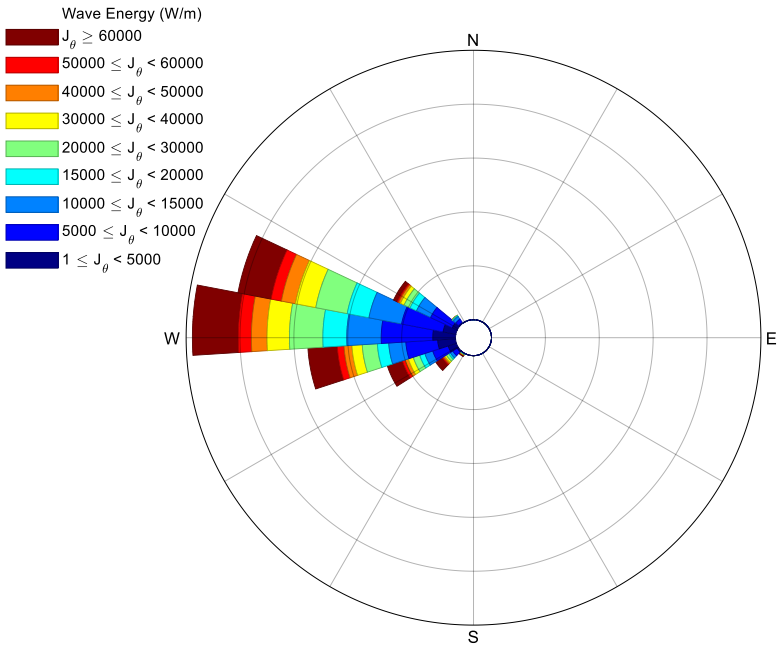

Figure 59: Directionally resolved SWAN wave rose distribution of wave energy from 1979-2010 at PacWave South

As shown, the most frequent waves arrive at PacWave from a predominantly westerly direction; with slight variability between the northwest and southwest directions. Additionally, the distribution of wave intensity events (in W/m) is evenly distributed across the dominant directions. Given the depth at PacWave varies between 50m-70m, depth-based wave refraction is undoubtedly playing a role in the reduction of incoming wave directions to those predominantly shore perpendicular.

As required, Figure 60 - Figure 63 shows the mean annual monthly statistics for the spectral parameters at PacWave. In order to clearly show the temporal and seasonal shifts in wave parameters, the following figures show the monthly mean (+/- one standard deviation), the median (50th percentile), and 10th / 90th percentiles for each parameter.

The significant wave height, shown in Figure 60, varies greatly with the seasons at PacWave. The average value for the parameter in winter months (November through March) varies between 3 and 3.5 m while summer months (May through September) range between 1.5 and 2 m. Figure 61 indicates that energy period also varies significantly with the seasons, with average values at a minimum in summer and at a maximum in winter. Average winter values range from 11 – 12 s while average summer values vary between 8 and 9 s. Both the

significant wave height and energy period statistics are generally evenly distributed about the mean for the entire year; with a slight positive skew in the winter due to large storm events.

Also following the seasonal pattern are omni-directional and directionally resolved wave powers shown in Figure 62 and Figure 63: maximum wave power values are observed in winter while minimums are seen in summer. According to Figure 62, average omni-directional wave power is greatest in December at 80 kW/m and continues to remain above 60 kW/m for the other winter months. Minimum values tend to remain below 20 kW/m during summer months. Figure 63 shows that average maximum directionally resolved wave power occur in winter months and range between 50 and 70 kW/m. Summer months see minimum directionally resolved power values also tending below 20 kW/m.

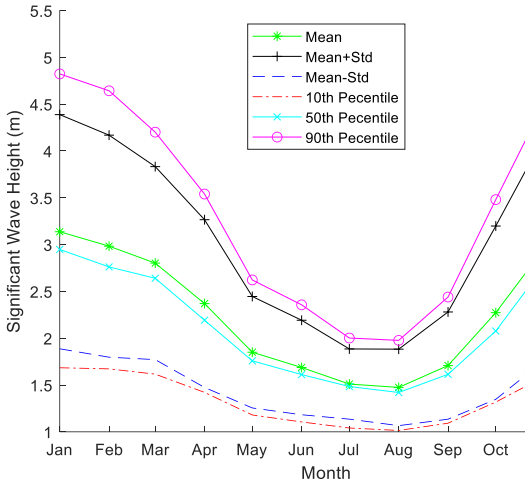

Figure 60: Significant wave height at PacWave

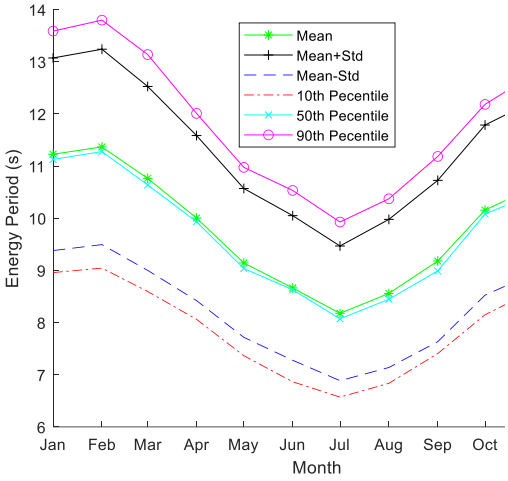

Figure 61: Energy period at PacWave

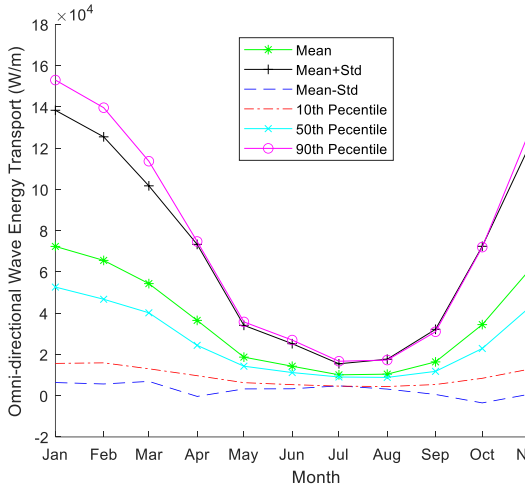

Figure 62: Omni-directional wave power at PacWave

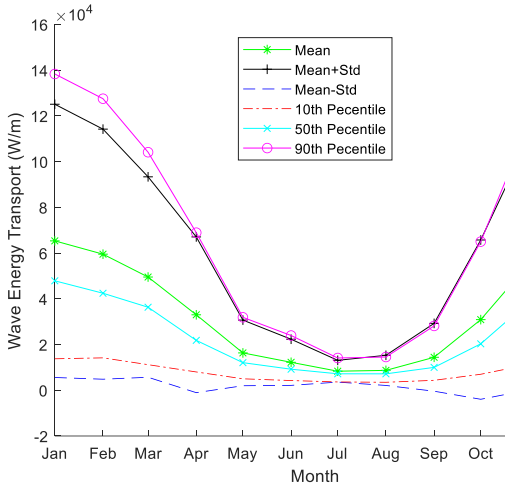

Figure 63: Maximum directionally resolved wave power

Both of these parameters are positively skewed, with extreme conditions playing an important role in the annualized conditions. This confirms prior work by Ruggiero et al. (2009) [42]. Annual variation of monthly mean of the remaining parameters along with annual and monthly cumulative distribution of all seven parameters are optional for a Class 1 resource assessment, and such detailed results can be found in Dunkle et al. [43].

8 IEC Wind Resource Assessment Results

The wind resource assessment at PacWave utilized data from the National Renewable Energy Laboratory (NREL) Wind Integration National Dataset (WIND) toolkit [44]. The meteorological dataset is currently classified as the most comprehensive publicly available wind dataset, running on a 2 km grid at a 5-minute temporal resolution [44]. It uses the Weather Research and Forecasting (WRF) model [45], a type of Numerical Weather Prediction model, to generate site specific meteorological data between 2007 and 2013. Model output parameters of interest include wind speed, wind direction, air temperature (at 10 m, 40 m, 60 m, 80 m, 100 m, 120 m, 140 m, 160 m, and 200 m elevation); air pressure (at the sea surface, 100 m, and 200 m elevation); relative humidity at 2 m; and precipitation rate at the sea surface. For more information on the WIND toolkit and its validation, please see [44].

IEC 61400-1 states that wind speed measurements shall have a temporal resolution of 1 Hz. This ensures that the sample resolution is fine enough to evaluate accurate values for parameters involving turbulence and steady/turbulent extreme wind speeds. Given that NREL's WIND toolkit's 5-minute temporal resolution contains the highest-temporal resolution of any publicly available dataset, it is clear that the resolution of current publicly available datasets are much too low to capture these finer resolution parameters. As such, information on turbulent and extreme wind parameters at PacWave South was beyond the scope of this study.

When reporting the wind measurements as per IEC specifications, wind roses and probability density functions are required. For the wind rose, the wind speed bin width must be less than 2 m/s and 10°. The offshore environment has little wind speed directional variation compared to the onshore environment, so utilizing omnidirectional information for the wind parameters is acceptable for offshore sites [33]. For the remainder of the analyses, the required parameters were evaluated using wind speed utilized 10-minute averaged wind speed [31].

As per [31–33], details on wind turbine nacelle hub height are required to identify the target elevation for the wind resource study. The turbine used in this study was the NREL 5MW reference turbine due to its extensive validation and publicly available specifications. The turbine has a 90 m hub height, which was used in all relevant proceeding calculations [46]. Figure 64 below provides information on PacWave's long-term wind speed at all available elevations. The median wind speed ranges from 6 m/s to 7.6 m/s, non-outlier maximum ranges from 16 m/s to 21.5 m/s, and the maximum outlier ranges from 29.4 m/s to 41.24 m/s. These stochastic values increase as elevation increases. Outliers

account for roughly 1.4% to 1.7% of each elevation's data, and are related to wind gust events.

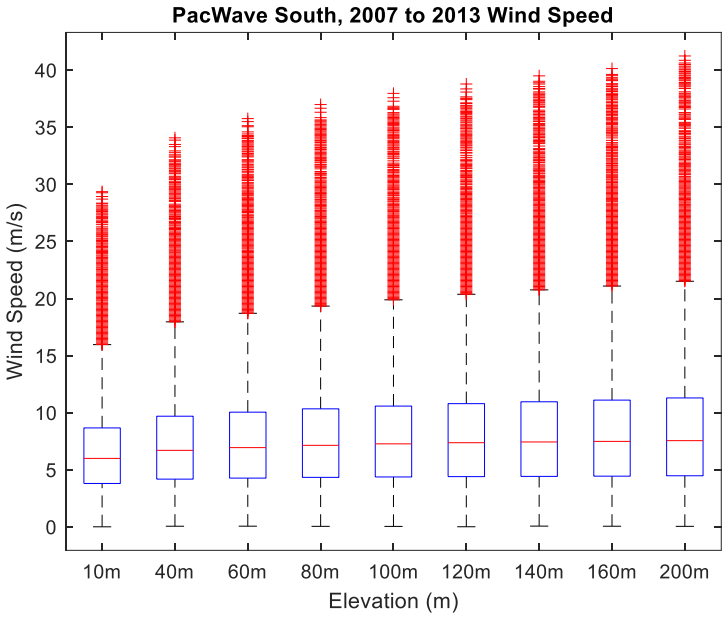

Figure 64: Long-term wind speed for PacWave South, 2007-2013.

Given that the NREL WIND toolkit does not provide outputs at 90m elevation, the wind shear and outputs from Eq. (9) are important. Wind shear coefficients between each sampled elevation were needed to create an accurate wind profile using the power law, then the mean of all elevations' long-term wind shear coefficients was used as a site's wind shear coefficient (WSC). Table 10 below contains the long-term wind shear coefficients between the elevations above and below the 90m nacelle. The final average wind shear coefficient for PacWave was calculated to be 0.087.

WSC BETWEEN	WSC VALUE	WSC BETWEEN	WSC VALUE	WSC BETWEEN	WSC VALUE
α_7 10m to 100m	0.083	α_{11} 10m to 120m	0.084	α_{23} 40m to 160m	0.088
α_8 40m to 100m	0.087	α_{12} 40m to 120m	0.088	α_{24} 60m to 160m	0.090
α_9 60m to 100m	0.091	α_{19} 80m to 140m	0.091	α_{31} 60m to 200m	0.088
α_{10} 80m to 100m	0.090	α_{22} 10m to 160m	0.084	α_{32} 80m to 200m	0.087

Table 10: PacWave's long-term wind shear coefficients, calculated using Eq. (9)

Interestingly, IEC 61400-3-1 suggests the use of a wind shear coefficient of 0.14 for offshore wind turbines [33]. Musial et al. [47] utilized 0.10 wind shear co-efficient for Oregon opportunities, yet did not provide reasoning for this choice. This confirms prior work which has shown that wind shears from site to site can vary significantly and are dependent on seasonality, temperature, surface roughness length and other environmental conditions [48,49][50]. As such, wind shear coefficients should be evaluated for every site in question.

The hub height wind speed was calculated using the power law between 80 m and 100 m and the reference wind at an elevation of 80 m. The probability distribution and stochastic information are shown in Figure 65 and The best fit probability distribution for PacWave's hub height wind speed was a Weibull distribution with a scale parameter of 8.77 and a shape parameter of 1.84. The confidence intervals for the scale and shape parameters were 8.75 to 8.78 and 1.835 to 1.844, respectively. The mean wind speed at hub height was 7.78 m/s with a standard deviation of 4.41 m/s. Outliers account for 1.5 % of hub height wind speeds.

Table 11 below.

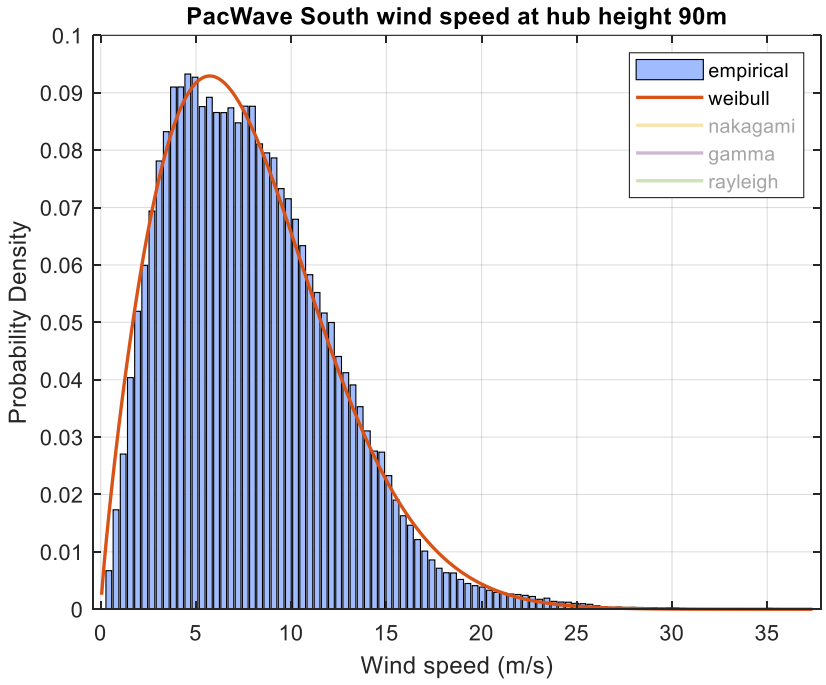

Figure 65: Hub height (90m) wind speed distribution for PacWave South fitted with a Weibull distribution.

The best fit probability distribution for PacWave's hub height wind speed was a Weibull distribution with a scale parameter of 8.77 and a shape parameter

of 1.84. The confidence intervals for the scale and shape parameters were 8.75 to 8.78 and 1.835 to 1.844, respectively. The mean wind speed at hub height was 7.78 m/s with a standard deviation of 4.41 m/s. Outliers account for 1.5 % of hub height wind speeds.

Table 11: PacWave hub height (90m) stochastic information

PacWave Hub Height (90 m) Statistics			
Mean	7.78	25^{th} percentile	4.38
Std	4.41	75^{th} percentile	10.45
Min	0.046	Max outlier	37.38

The wind rose in Figure 66 shows the wind speed directional distribution at 100 m. The raw wind direction data had a 0.01° resolution, but was aggregated to thirty-six 10° bins, as per IEC requirements. similar to wave directionality, directions shown are the direction the wind is coming from. As shown, wind blows predominantly north-south, with an occasional easterly wind. These easterly winds are the response to uneven surface heating of land masses compared to the ocean, resulting in land and sea breezes at various points of the day. As elevation increases, wind speed magnitude increases, and direction becomes increasingly dominated by north-south flow. High wind speeds (>30m/s) are predominantly from the south, despite the most energetic wave conditions being from the west, thus creating perpendicular wind and wave forces on energy conversion technologies. PacWave's mean wind speed and directional distribution closely align with information from a NREL study of a neighboring site [47].

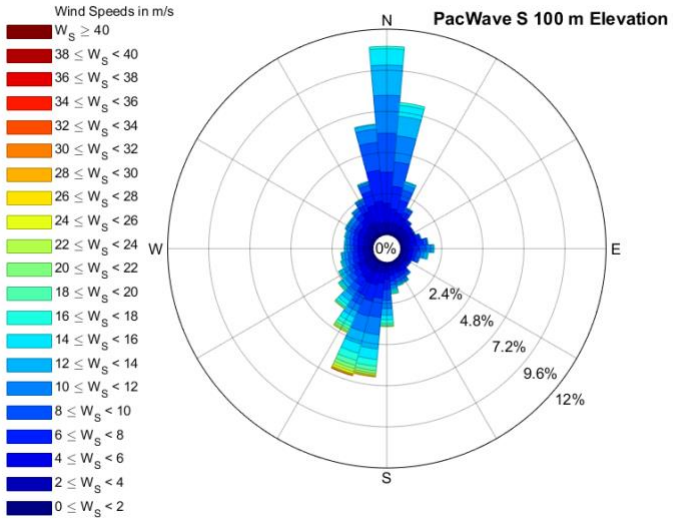

Figure 66: Wind direction distribution of wind speed at an elevation of 100m for PacWave South.

Seasonal and diurnal effects of mean wind speed are shown in Figure 67 and Figure 68. Several observations can be made from the figures. Initially, it is immediately evident that winter wind speeds are greater (90th percentiles of ~16m/s in winter and ~14m/s in summer), and are positively skewed (corroborating the wave findings). Additionally, there is limited diurnal variability in wind speeds in the winter. In contrast, the summer sees significant diurnal variability with wind speeds. The wind speeds are lowest in the morning hours (0500 – 1000 hrs) and average 25% increase in 90th percentile winds by late afternoon/evening (1600 – 2000hrs). This is solar/heat driven effect with on-shore winds dominating the late afternoon summer.

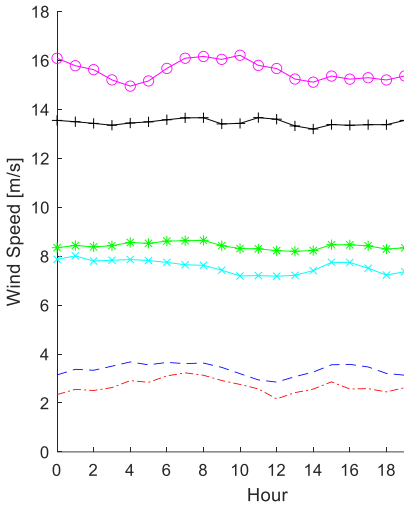

Figure 67: PacWave average diurnal wind speed for January at 90 m.

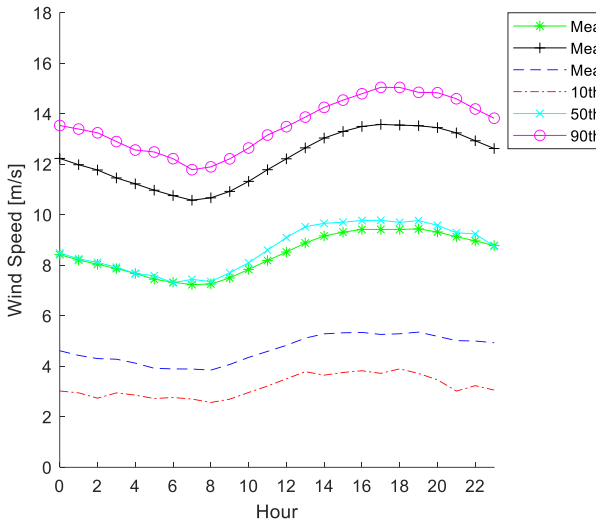

Figure 68: PacWave average diurnal wind speed for July at 90 m.

Final the air density for elevations 0 m, 100 m, and 200 m were calculated using the ideal gas law and are shown in Table 12. Due to a lack of temperature data at the sea surface, the temperature at 10 m was used in conjunction with sea surface pressure to calculate sea surface density.

Elevation $[m]$	Density $[kg/m^3]$
0	1.250
100	1.237
200	1.224

Table 12: PacWave air density at 0m, 100m, and 200m.

9 Additional Environmental Conditions of Importance

10 Extreme Wave Conditions

Knowledge of extreme wave and wind conditions is a key component of technology design, project design, and associated economics. While extreme conditions are not required for analysis by the IEC TS 62600-101 for wave resource assessments, it is required by the IEC TS 62600-2 for marine energy converter design. Additionally, floating offshore wind turbine design (IEC TS 61400-3-2) specifications call for quantification of extreme conditions [32][51].

Environmental contours represent the joint-probability of conditions within certain return periods. Many methods to develop contours exist, yet arguably the most common is the Inverse First Order Reliability Method (IFORM). Hiles et al. provide an overview of the methodology and associated nuances for

the Pacific Northwest in [52]. Environmental contours detailing significant wave height and energy period combinations for 50- and 100-year return periods are shown in Figure 69.

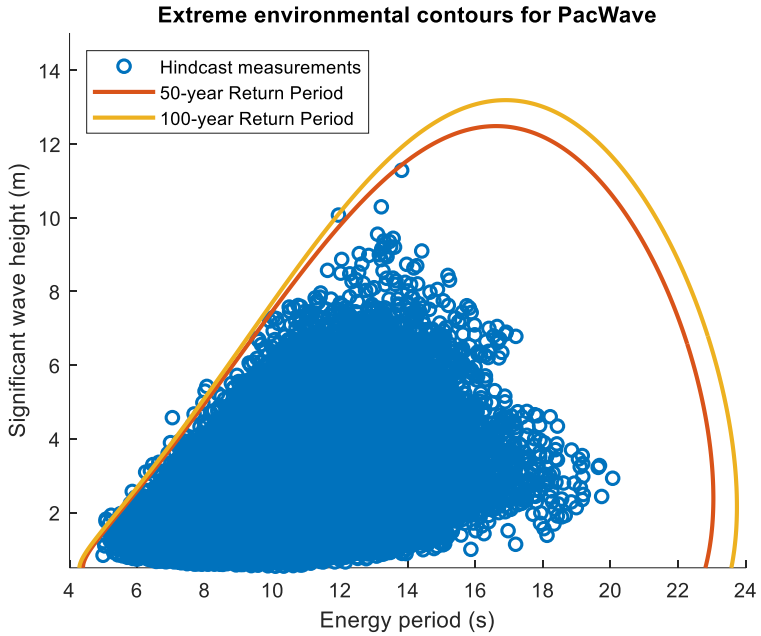

Figure 69: Extreme environmental contours associated with 50- and 100-year return periods of sea states represented by significant wave height and energy period. Hindcast measurements include data from 1979-2020 in the PacWave region.

As shown, the 32-yr hindcast results fall within the 50- and 100-year environmental contours. One measurement falls completely out of the estimated H_{m0} - T_e range, with a wave height of 4.6 m and period of 7 s. The maximum significant wave height – energy period combination for the 50-year return period occurs at 12.49 m and 16.68 s respectively; 100-year return period maximum significant wave height – energy period occurs at 13.19 m and 16.85 s respectively. Long-term hindcast models, forced by course temporal resolutions winds, are well recognized for under-estimating extreme conditions. As a result, the maximum predicted significant wave height would be considered a conservative estimate of possible largest waves [53].

Interestingly, extreme sea states are not required by the IEC TS 62600-101 for wave energy resource assessments; in fact the TS states that it is not intended for extreme anaysis [30]. Instead, analysis of extreme sea state conditions is required by the IEC TS 62600-2 and IEC TS 61400-3-2 for marine energy technology design and floating offshore wind turbine design respectively [32,51].

11 Ocean Currents

The IEC TS for wave resource assessments [30] recommends providing a description of ocean surface current speed, due to its possible effect on wave conditions. If the depth-averaged current speed exceeds 1.5 m/s, its effect on the wave climate shall be investigated and included in wave modeling. On the wind side, the IEC TS for floating offshore wind turbine design [32] requires the analysis of extreme sea surface current values corresponding to one- and five-year return periods if relevant.

Seven years of ocean surface current data measured at an hourly resolution was obtained from the U.S. Integrated Ocean Observing System (IOOS) High Frequency Radar Network (HFRNet) and accessed through the Coastal Observing R&D Center (CORDC), encompassing 2012 through 2019. Eastward current velocity, where positive values equal shoreward propagation, and northward current velocity, where positive values correspond to northern propagation, were obtained and evaluated in order to align with a holistic environmental review of conditions at PacWave.

As shown in Figure 70, both datasets are relatively normally distributed and possess median velocities near 0 m/s. In Figure 70, January and December are the only months that see a slight prevailing direction of current, toward the shore. During the summer months, the slight negative mean velocity confirms coastal upwelling activities and associated flow away from the coast.

Figure 70 shows the predominant surface current speed at PacWave is northward from January through April and again from August through December. In June and July, currents are predominately flowing in the southward direction, as the minimum northward values prevail in these months. This was expected, since alongshore current flow off the Oregon coast in generally northward in the winter, while surface current in the summer is generally southward [54].

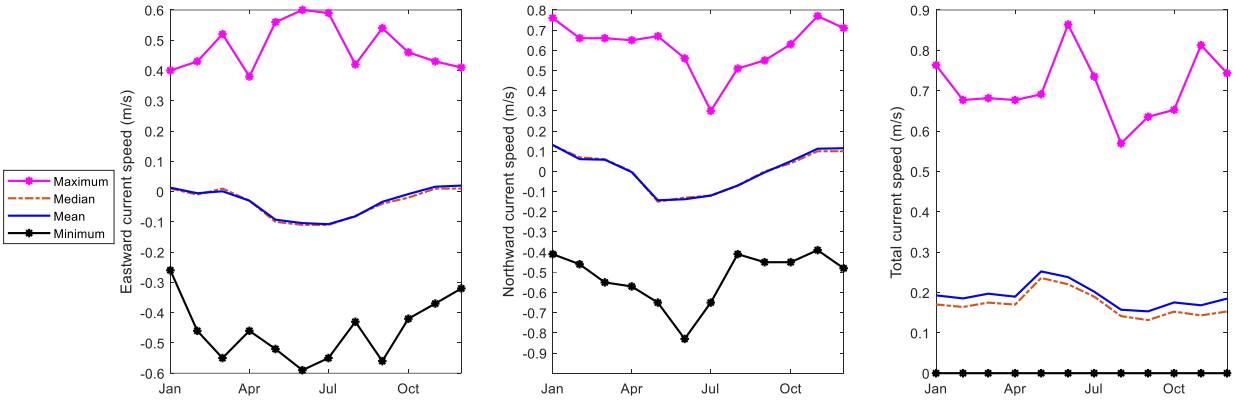

Figure 70: Variation of mean, median, maximum, and minimum of eastward, northward, and total current speeds at PacWave

Minimum and maximum current velocities are shown in order to indicate the total current variability. No measured values approach 1.5 m/s, dismissing the need to include ocean current effects in the wave propagation model and indicating that the current speeds at PacWave do not have a great effect on the wave resource available.

12 Tidal Elevation

Water level and tidal variation information are recommended by the IEC TS 61400-3-2 for design requirements for offshore floating wind turbines [32]. The IEC TS for wave resource assessments states that the tidal variation and water level data may be excluded if their influences on the wave resource are negligible.

Tidal data from the NOAA Tides and Currents station at South Beach, OR near Newport was obtained and evaluated, based on the mean sea level (MSL) datum. The variation of tide during 2016 is shown in Figure 71. Maximum high tide onshore of PacWave reaches just over 2 m while maximum low tide reaches just below -2 m. Oregon has a mixed semi-diurnal tide, with two high tide and low tide events per day occurring at different magnitudes. This is highlighted in Figure 71 as there are visible low-high and low tide values marked by the overlapping, dark blue lines, whereas high-high and low tide values are shown by the lighter, less frequently occurring lines.

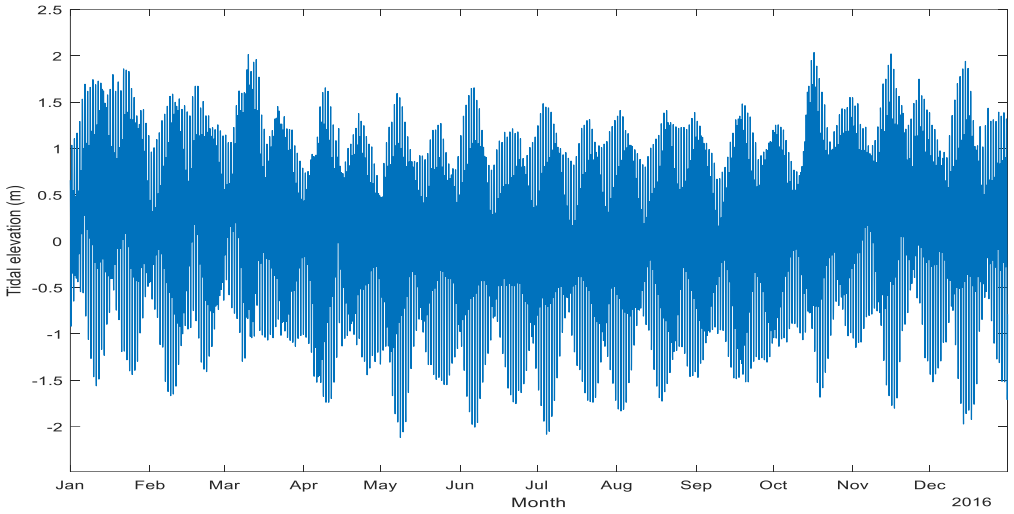

Figure 71: Tidal elevation variation in 2016 measured at MSL

In order to provide a rough estimate of the impact of tidal water elevation on wave conditions at PacWave, the most frequency sea state is used as an example (1.75m and 8.5s). For the baseline PacWave water depth of 60m, and assuming linear wave theory, the shoaling related wave height changes would be less than 1% for the +2m and -2m tidal variation. As a result, the impact of tidal variation at PacWave are deemed negligible.

13 Reduced-Order Representation

Utilizing the same wind and wave data, from NREL's WIND toolkit and PNNL's 32-yr wave hindcast respectively, a temporally overlapping dataset between 2007 through 2010 was utilized. The 5-minute WIND toolkit data was averaged to create an hourly mean value, while the 3-hour PNNL wave data was linearly interpolated to create a time synchronous, 1-hour temporal resolution, dataset.

From the master dataset, the parameters significant wave height, peak energy period, direction of maximumly resolved wave power, spectral width, and wind speed and direction at 100 meters were identified as key parameters necessary for developing comprehensive numerical models. As such, they were the resource parameters chosen for k-means clustering analysis.

Based on the results of the Elbow and Silhouette tests, eight clusters were chosen to represent wind-wave conditions at PacWave. Table 13 below lists the parameter values associated with the center of each cluster. Note that the reduced order representation is focused on representing the bulk of conditions, not the range of conditions.

H_{m0} $[m]$	T_e $[s]$	$J_{\theta_{Jmax}}$ [°]	Spectral Width	Wind speed 100m	Wind direction 100m
3.35	9.67	247.93	0.3142	13.45	201.80
2.21	9.34	290.12	0.3185	6.91	327.18
1.69	8.06	291.48	0.4166	9.44	16.05
2.37	11.40	279.64	0.2795	5.92	58.66
2.24	10.59	282.44	0.2844	6.78	191.52
4.40	11.83	278.95	0.2984	10.69	234.46
1.44	8.67	270.31	0.4256	6.56	336.66
1.59	8.70	262.57	0.4197	7.35	209.85

Table 13: PacWave cluster centroid parameter values

14 Discussion of Compatiblity between Wave and Wind Assessment Standards

The development of a holistic assessment methodology for marine energy resources is necessary to assist the sustainable development of marine energy resources; however, it is rife with complications and compromises. As we move towards increasing the utilization of oceanic resources to generate renewable energy, we need to ensure that there is equitable distribution of opportunity and risk between current and future projects – based on a complete understanding of all resource opportunities present. As floating offshore wind turbines and integrated marine energy conversion devices gain traction, it is important to ensure that resource assessment studies provide the necessary details of a site and, at a minimum, do not provide conflicting assessments.

First, it is important to reiterate the inherent connection between resource assessment and the associated technologies used to harness the resources. The requirements for characterizing the energy resource at a single site for wind and wave conversion technologies are understandably different. Wave energy and associated technology deployments will be at sea level and increasingly focused on assessing wave conditions, whereas wind turbines will be at 90+ m above the sea surface and concerned with wind conditions. While this fundamental difference is unavoidable, there are various rectifiable discrepancies that prevent a sound holistic analysis between offshore wind and wave energy conversion, which become apparent when comparing the IEC TS for the two types of resources.

Regarding baseline wave conditions, IEC TS 61400-3-2 for floating offshore turbine technology design requires a greater depth of metocean

knowledge than the TS 62600-101 for wave resource assessment itself. TS 61400 3-2 requires the following marine conditions (based on a 3-hour reference period): tidal variation and/or storm surge, extreme tides, extreme sea state conditions and characteristics (e.g. H_{m0} and T_p combinations for 1- and 50-year return periods), extreme sea surface currents for 1- and 50-year return periods, and wind and wave joint distribution, among other parameters [32]. This level of detail is not congruent with the recommendations on the wave resource assessment side, as environmental conditions are required for description 'where relevant', yet little information is disclosed regarding the level of detail to discuss. In contrast, the reporting required by TS 62600-101 for the required spectral wave quantities is descriptive and uncertainty analyses are required when environmental conditions are not adequately considered. This requirement reinforces prior work by Robertson et al. whom identified wind speed, current speed, and wave groupiness as additional parameters that should be included for a more accurate estimation of wave power [55].

With regards to extreme and additional environmental conditions, these are outlined as a requirement by the wave resource assessment specification (IEC TS 62600-101), yet are required as an input into wave technology design specifications (IEC TS 62600-2) [51]. For example, the impacts of surface currents are required in both the IEC TS 62600-2 for wave/tidal energy technology and 61400-3-2 for wind technology design. It is suggested that for true convergence and holistic resource assessments, such metocean conditions should be outlined in the energy resource assessment documents themselves.

Finally, there exists a discrepancy between resource assessment for wind and wave energy devices in resolution requirements and classifications for assessment types. The wave resource TS clearly outlines different assessment classes with spatial resolutions from 25 km to 500+ km and temporal resolutions between 1 and 3 hours. It is yet to be determined in the forthcoming IEC TS for wind resource assessment if the data will be classified by Class for required resolution and uncertainty. Currently, the wind resource is not categorized by Class in the wind resource assessment TS, but rather in the turbine design TS (classifications of turbines based on a priori determined reference wind speeds and turbulence intensities). Agreement across the IEC marine energy TS with regard to technology versus resource Class structure is crucial and a missing part in creating a holistic resource classification process.

15 Conclusions and Recommendations

In order to mitigate the worst impacts of climate change, nations around the world are increasingly turning to renewable wind and solar energy to power

their economies, industries and lifestyles. However, the development opportunity for terrestrial wind and solar is not boundless and many nations are looking towards the ocean for new opportunities for carbon-free electricity generation and economic growth. While our oceans have a wide variety of renewable resources, wave and offshore wind resources are widely acknowledged as having the greatest opportunity for development due to their global availability and tremendous magnitude of the raw resources [3][4].

Traditionally, wave energy and wind energy resource assessments have been conducted as independent parallel processes, with little interaction with regards to best practices, lessons learnt, or opportunities to create compatible methodologies for future utilization by the broader marine energy sector. At best, this resulted in duplicative and non-compatible assessments of marine resources. At worst, this has delayed the development of the marine energy sector and created a competitive approach towards site identification. This paper assessed the recommended IEC resource assessment frameworks for offshore wind and wave resources, utilizing the case study of PacWave USA, to identify the opportunities and challenges when developing a holistic assessment of offshore marine energy resources.

Utilizing a publicly available 32-yr SWAN hindcast of wave conditions [40], a Class 1 wave resource assessment was conducted for PacWave. The analyses highlighted a number of important attributes with regards to the magnitude of the resource, the distribution of wave conditions and the seasonality of these parameters. The PacWave site has an annual average energy flux of ~35kW/m, with the most frequently occurring wave conditions having a significant wave height of 1.75m and an energy period of 8.5s (528hrs./yr.). However, the sea state which provided the greatest percentage of the overall energy flux was 2.75m and 10.5s (231 hrs./yr.). The seasonal variation in significant wave height and energy period was 1.5m to 3.5m, and 8s – 12s for summer and winter respectively. Given the relatively shallow nature of the PacWave site (60m), the majority of the energy flux was from a westerly (270°) direction with only +/- 40° variation over the year.

A publicly available 5-yr WRF hindcast of wind from the NREL Wind Toolkit [44], with 5-min resolution, was utilized to assess offshore wind resources at PacWave. Based on the assumption of a 90m nacelle and hub height, the analyses identified the location-specific wind shear co-efficient, the wave perpendicular wind flow, and the significant seasonal and daily fluctuations. The mean wind speed was determined to be 7.78m/s, with 4.38m/s and 10.45m/s speed representing the 25^{th} and 75^{th} percentiles respectively. The calculated wind shear co-efficient of 0.087 was markedly lower the prior used values and

those suggested by the IEC. The wind flow followed a north-south flow for the majority of the year. Interesting, this is perpendicular to the incoming wave directions. Significant daily variability in the wind speed and direction was shown for summer months, while winter conditions remained stable over the daily cycle.

A comparison of the internationally recognized IEC TS for offshore wind and wave resource conditions highlighted a number of incongruent methodologies and opportunities for increased compatibility for holistic resource assessments. Firstly, a coherent Class structure for assessing both wave and wind conditions would provide a common framework and perspective on the fidelity of the assessments. Secondly, identification of important resource parameters was distributed between resource and technology focused specifications, and resulted in incompatibility within a single renewable energy resource. It is recommended that all needed parameters should be detailed within the associated resource specification, rather than a more technology specific specification. While a number of parameters used to characterize the wind or wave conditions were consistent, discrepancies in definitions, resolution, and necessity limit the opportunity for cross utilization between the two sectors.

In conclusion, this paper presented a detailed assessment of offshore wind and wave conditions for PacWave, based on the latest International Electrotechnical Commission Technical Specifications (IES TS) and the highest resolution, publicly available datasets. The assessment illustrates the significant untapped renewable energy resources available in our oceans and the opportunity to responsibly develop these resources to mitigate the worst impacts of climate change.

For the acknowledgements: Wave hindcast data can be downloaded from a web-service database
maintained by the National Renewable Energy Laboratory
(https://registry.opendata.aws/wpto-pds-uswave/).

16 References

[1] Bloomberg. New Energy Outlook 2020 2020.

[2] Boudet HS. Public perceptions of and responses to new energy technologies. Nat Energy 2019;4:446–55. https://doi.org/10.1038/s41560-019-0399-x.

[3] Cornett AM. A global wave energy resource assessment. Proc. 18th Int. offshore polar Eng. Conf., Vancouver, Canada: 2008.

[4] Arent D, Sullivan P, Heimiller D, Lopez A, Eurek K, Badger J, et al. Improved Offshore Wind Resource Assessment in Global Climate Stabilization Scenarios. Natl Renew Energy Lab 2012:29.

[5] Guedes Soares C, Bento AR, Gonçalves M, Silva D, Martinho P. Numerical evaluation of the wave energy resource along the Atlantic European coast. Comput Geosci 2014;71:37–49. https://doi.org/10.1016/j.cageo.2014.03.008.

[6] Pilar P, Soares CG, Carretero JC. 44-year wave hindcast for the North East Atlantic European coast. Coast Eng 2008;55:861–71.

[7] Neill SP, Hashemi MR. Wave power variability over the northwest European shelf seas. Appl Energy 2013;106:31–46. https://doi.org/10.1016/j.apenergy.2013.01.026.

[8] Sierra JP, Martín C, Mösso C, Mestres M, Jebbad R. Wave energy potential along the Atlantic coast of Morocco. Renew Energy 2016;96:20–32. https://doi.org/10.1016/j.renene.2016.04.071.

[9] Hemer MA, Griffin DA. The wave energy resource along Australia's Southern margin. J Renew Sustain Energy 2010;2. https://doi.org/10.1063/1.3464753.

[10] Behrens S, Hayward J, Hemer M, Osman P. Assessing the wave energy converter potential for Australian coastal regions. Renew Energy 2012;43:210–7. https://doi.org/10.1016/j.renene.2011.11.031.

[11] Lavidas G, Venugopal V. Prospects and applicability of wave energy for South Africa. Int J Sustain Energy 2018;37:230–48. https://doi.org/10.1080/14786451.2016.1254216.

[12] Robertson BRD, Hiles CE, Buckham BJ. Characterizing the near shore wave energy resource on the west coast of Vancouver Island, Canada. Renew Energy 2014;71. https://doi.org/10.1016/j.renene.2014.06.006.

[13] Robertson B, Bailey H, Clancy D, Ortiz J, Buckham B. Influence of wave resource assessment methodology on wave energy production estimates. Renew Energy 2016;86. https://doi.org/10.1016/j.renene.2015.09.020.

[14] Lenee-Bluhm P, Paasch R, Özkan-Haller HT. Characterizing the wave energy resource of the US Pacific Northwest. Renew Energy 2011;36:2106–19. https://doi.org/10.1016/j.renene.2011.01.016.
[15] Folley M, Cornett AM, Holmes B, Lenee-Bluhm P, Liria P. Standardising resource assessment for wave energy converters. 4th Int. Conf. Ocean Energy, 2012, p. 1–7.
[16] International Electrotechnical Commission T C 114. IEC TS 62600-101 Technicial Specification - Part 101: Wave energy resource assessment and characterization. 2015.
[17] Zhang H-M, Reynolds RW, Bates JJ. P2. 23 BLENDED AND GRIDDED HIGH RESOLUTION GLOBAL SEA SURFACE WIND SPEED AND CLIMATOLOGY FROM MULTIPLE SATELLITES: 1987-PRESENT 2006.
[18] Sempreviva AM, Barthelmie RJ, Pryor SC. Review of methodologies for offshore wind resource assessment in European seas. Surv Geophys 2008;29:471–97. https://doi.org/10.1007/s10712-008-9050-2.
[19] Jimenez B, Durante F, Lange B, Kreutzer T, Tambke J. Offshore wind resource assessment with WAsP and MM5: Comparative study for the German bight. Wind Energy 2007;10:121–34. https://doi.org/10.1002/we.212.
[20] Manwell JF, Rogers AL, McGowan JG, Bailey BH. An offshore wind resource assessment study for New England. Renew Energy 2002;27:175–87. https://doi.org/10.1016/S0960-1481(01)00183-5.
[21] Doubrawa P, Barthelmie RJ, Pryor SC, Hasager CB, Badger M, Karagali I. Satellite winds as a tool for offshore wind resource assessment: The Great Lakes Wind Atlas. Remote Sens Environ 2015;168:349–59. https://doi.org/10.1016/j.rse.2015.07.008.
[22] He G, Kammen DM. Where, when and how much wind is available? A provincial-scale wind resource assessment for China. Energy Policy 2014;85:74–82. https://doi.org/10.1016/j.enpol.2014.07.003.
[23] Jiang D, Zhuang D, Huang Y, Wang J, Fu J. Evaluating the spatio-temporal variation of China's offshore wind resources based on remotely sensed wind field data. Renew Sustain Energy Rev 2013;24:142–8. https://doi.org/10.1016/j.rser.2013.03.058.
[24] Amirinia G, Mafi S, Mazaheri S. Offshore wind resource assessment of Persian Gulf using uncertainty analysis and GIS. Renew Energy 2017;113:915–29. https://doi.org/10.1016/j.renene.2017.06.070.
[25] Chancham C, Waewsak J, Gagnon Y. Offshore wind resource assessment and wind power plant optimization in the Gulf of Thailand. Energy 2017;139:706–31. https://doi.org/10.1016/j.energy.2017.08.026.

[26] Kalogeri C, Galanis G, Spyrou C, Diamantis D, Baladima F, Koukoula M, et al. Assessing the European offshore wind and wave energy resource for combined exploitation. Renew Energy 2017;101:244–64. https://doi.org/10.1016/j.renene.2016.08.010.
[27] Ferrari F, Besio G, Cassola F, Mazzino A. Optimized wind and wave energy resource assessment and offshore exploitability in the Mediterranean Sea. Energy 2020;190:116447. https://doi.org/10.1016/j.energy.2019.116447.
[28] Weiss CVC, Guanche R, Ondiviela B, Castellanos OF, Juanes J. Marine renewable energy potential: A global perspective for offshore wind and wave exploitation. Energy Convers Manag 2018;177:43–54. https://doi.org/10.1016/j.enconman.2018.09.059.
[29] Prasada Rao C xxx VK. Spectral width parameter for wind-generated ocean waves. Proc Indian Acad Sci - Earth Planet Sci 1988;97:173–81. https://doi.org/10.1007/BF02861852.
[30] International Electrotechnical Commission. Marine energy : wave, tidal and other water current converters. Part 101, Wave energy resource assessment and characterization. n.d.
[31] IEC. IEC 61400-1 Wind energy generation systems - Part 1: Design requirments. 61010-1 © Iec2001 2006;2006:13.
[32] IEC, Commission IE. IEC 61400-3-2 Ed 1.0 Wind turbines Part 3-2: Design requirements for floating offshore wind turbines. 2014.
[33] 61400-3-1:2019 I. IEC 61400-3-1:2019 Wind energy generation systems - Part 3-1: Design requirements for fixed offshore wind turbines. Int Stand 2019.
[34] Tinnesand H, Sethuraman L, Tinnesand H, Sethuraman L. Distributed Wind Resource Assessment Framework : Functional Requirements and Metrics for Performance and Reliability Modeling Distributed Wind Resource Assessment Framework : Functional Requirements and Metrics for Performance and Reliability Modeling 2019.
[35] Camus P, Vidal C, Méndez FJ, Espejo A, Izaguirre C, Gutiérrez JM, et al. A methodology to evaluate wave energy resources in shallow waters. Proc. 7th Eur. Wave Tidal Energy Conf., 2007.
[36] Camus P, Mendez FJ, Medina R, Cofiño AS. Analysis of clustering and selection algorithms for the study of multivariate wave climate. Coast Eng 2011;58:453–62. https://doi.org/10.1016/j.coastaleng.2011.02.003.
[37] Fairley I, Lewis M, Robertson B, Hemer M, Masters I, Horrillo-Caraballo J, et al. A classification system for global wave energy resources based on multivariate clustering. Appl Energy 2020;262:114515. https://doi.org/10.1016/j.apenergy.2020.114515.

[38] Rousseeuw PJ. Silhouettes: A graphical aid to the interpretation and validation of cluster analysis. J Comput Appl Math 1987;20:53–65. https://doi.org/10.1016/0377-0427(87)90125-7.
[39] García-Medina G, Özkan-Haller HT, Ruggiero P. Wave resource assessment in Oregon and southwest Washington, USA. Renew Energy 2014;64:203–14. https://doi.org/10.1016/j.renene.2013.11.014.
[40] Yang Z, García-Medina G, Wu W-C, Wang T. Characteristics and variability of the nearshore wave resource on the U.S. West Coast. Energy 2020;203:117818. https://doi.org/10.1016/j.energy.2020.117818.
[41] Wu WC, Wang T, Yang Z, García-Medina G. Development and validation of a high-resolution regional wave hindcast model for U.S. West Coast wave resource characterization. Renew Energy 2020;152. https://doi.org/10.1016/j.renene.2020.01.077.
[42] Ruggiero P, Komar PD, Allan JC. Increasing wave heights and extreme value projections: The wave climate of the U.S. Pacific Northwest. Coast Eng 2010;57:539–52. https://doi.org/10.1016/j.coastaleng.2009.12.005.
[43] Dunkle G, Robertson B, Garcia-Medina G, Yang Z. PacWave Wave Resource Assessment. 2020.
[44] Draxl C, Clifton A, Hodge BM, McCaa J. The Wind Integration National Dataset (WIND) Toolkit. Appl Energy 2015;151:355–66. https://doi.org/10.1016/j.apenergy.2015.03.121.
[45] Skamarock WC, Klemp JB. A time-split nonhydrostatic atmospheric model for weather research and forecasting applications. J Comput Phys 2008;227:3465–85. https://doi.org/10.1016/j.jcp.2007.01.037.
[46] Jonkman J, Butterfield S, Musial W, Scott G. Definition of a 5-MW Reference Wind Turbine for Offshore System Development. 2009.
[47] Musial WD, Beiter PC, Nunemaker J, Heimiller DM, Ahmann J, Busch J. Oregon Offshore Wind Site Feasibility and Cost Study 2019.
[48] Farrugia RN. The wind shear exponent in a Mediterranean island climate. Renew Energy 2003;28:647–53. https://doi.org/10.1016/S0960-1481(02)00066-6.
[49] Rehman S, Al-Abbadi NM. Wind shear coefficient, turbulence intensity and wind power potential assessment for Dhulom, Saudi Arabia. Renew Energy 2008;33:2653–60. https://doi.org/10.1016/j.renene.2008.02.012.
[50] Hsu SA, Meindl EA, Gilhousen DB. Determineing the Power-Law Wind-Profile Exponent under Near-Neutral Stability Conditions at Sea. J Appl Meteorol Climatol 2008;7:1–16.
[51] Ts IEC. IEC TS 62600-2 TECHNICAL. 2019.
[52] Hiles CE, Robertson B, Buckham BJ. Extreme Wave Statistics of the British

Columbia Coast. J Estuarine, Coast Shelf Sci 2019.
[53] Hiles CE, Robertson B, Buckham BJ. Extreme Wave Statistical Methods and Implications for Coastal Analyses. J Estuarine, Coast Shelf Sci 2019.
[54] Mazzini PLF, Barth JA, Kipp Shearman R, Erofeev A. Buoyancy-driven coastal currents off oregon during fall and winter. J Phys Oceanogr 2014;44:2854–76. https://doi.org/10.1175/JPO-D-14-0012.1.
[55] Robertson B, Bailey H, Buckham B. Resource assessment parameterization impact on wave energy converter power production and mooring loads. Appl Energy 2019;244:1–15. https://doi.org/10.1016/j.apenergy.2019.03.208.